Volatiles in the Outer Solar System:

I. Thermodynamics of Clathrate Hydrates

II. Ethane Ocean on Titan

III. Evolution of Primordial Titan Atmosphere

Thesis by

Jonathan Irving Lunine

In Partial Fulfillment of the Requirements

for the Degree of

Doctor of Philosophy

California Institute of Technology, Pasadena, California

1985

(Submitted June 18, 1984)

To my family

and

To the memory of my father.

Acknowledgements

It is my greatest pleasure to thank my adviser, Prof. David J. Stevenson, for his invaluable guidance in the pursuit of research and preparation of this thesis. His careful aid and criticism on research problems and the philosophy of doing science in general, along with his friendship, were instrumental in the successful completion of my graduate student career. I shall miss our extensive discussions on science as well as a multitude of other matters. Dave also deserves the thanks of this city boy for demonstrating that the beauty and grandeur of the California wilderness far exceed that of the canyonlands of midtown Manhattan.

I want to thank Prof. Yuk L. Yung for the extensive discussions and collaborations we have had. The intertwining of photochemistry and physical chemistry reflected in some of the pages to follow could not have been possible without his enthusiasm for pursuing ''the big picture'' on Titan. I am grateful to Prof. Dewey Muhleman for his guidance as my academic adviser, as well as for discussions on Titan radio observations. Prof. Andrew Ingersoll also advised me on course selection, and has given me much helpful scientific assistance. Dr. Mark Allen of JPL has insisted on asking me the questions about my research which I neglected to ask myself; for this I am grateful. Also, Mark and his wife Emily, in opening their home and place of worship to me time after time, have given me that element of emotional support which cannot be quantified and yet is of such great value.

Prof. Robert P. Sharp has enriched my education at Caltech immeasurably through a series of field trips in the southwest United States and Hawaii. I hope I never forget, while pursuing planetary science, the beauty and complexity with which physical processes manifest themselves in terrestrial landforms.

Prof. Hugh M. Van Horn, University of Rochester, galvanized my interest in planetary science. His broad knowledge of the fields of theoretical astrophysics, observational astronomy, and planetary science, coupled with his patient and thoughtful advice, guided me into this graduate program and nascent career. My stepfather, Norman Jacobs, was crucial in nurturing my interest in science as early as my high school years, and has the amazing ability to come up with experimental counterexamples to the behavior of any chemical system which I may describe to him. I am grateful for all his help.

Donna Lathrop, with skill, patience, and good-humor has produced revision after revision of papers and abstracts from her magic word-processor; that skill is evident here. Kay Campbell has provided aid and assistance to me many times, and tolerated my repeated incursions into the planetary science office for coffee.

Donald Rudy deserves my thanks as a willing ear during times of siege in Pasadena; to all my fellow graduate students for valuable conversations, advice, and companionship I will always be in debt.

This work has been supported by NASA grant NAGW-185.

Preface

This thesis examines the role of volatiles in the origin, evolution, and present state of outer solar system objects, with strong emphasis on Saturn's satellite Titan. The first portion is a study of the thermodynamics and kinetics of clathrate hydrate, a phase of water ice in which the lattice of H_2O molecules forms cages which can enclose molecules of other chemical species. The clathrate is of interest because of its ability to trap large quantities of volatiles such as methane, carbon monoxide, and molecular nitrogen, under conditions in which the pure condensed forms of these species are not stable. Clathrate has thus been suggested as the most plausible phase in which highly volatile species were accreted onto forming satellites, giant planets and comets (Delsemme and Swings, 1952; Lewis, 1971). The scope and detail of Part 1 exceed that of previous studies of clathrate in the planetary literature; in particular, the stability of clathrate at high pressure and effect of ammonia have not previously been modeled or tested experimentally. Despite this, a great debt is owed to the pioneering work of Stanley Miller (most notably Miller, 1961) as described in the literature review of Part 1. It is expected that the present work will be incorporated into models of planet and satellite formation, evolution of satellite interiors, and atmospheres. It is also hoped that the work will serve as a stimulus to future experiments, notably in the tens of kilobar pressure range. Such experiments,

proposed in the final section of Part 1, are crucial if we are to understand the evolution and present configuration of icy satellite interiors, as well as the origin of volatile materials seen on the present surfaces of Titan, Triton, and Pluto (Stevenson et al., 1984; Cruikshank and Brown, 1984).

Part 2 presents a model for a global ocean on the surface of Titan, composed primarily of methane and its photochemical by-product ethane, and consistent with spacecraft and ground-based data on the atmosphere. The implications of such a reservoir of methane and its by-products are profound, not only in determining the total quantity and composition of volatiles in the surface/atmosphere environment, but also in affecting the evolution of the atmosphere above and bedrock beneath. The second portion of Part 2 examines the interaction of the proposed ocean with the bedrock (most likely primarily water ice) and atmosphere. It is concluded that (1) significant degradation of cratering topography, detectable with radar, could have occurred by solution and mechanical erosion in the ocean, and (2) chemical properties of the ocean, along with photolytic processes in the upper atmosphere are apparently primary controls on the present temperature and pressure of the lowermost atmosphere.

The final part of the thesis is a more speculative study of the earliest evolution of Titan's atmosphere. Processes examined include accretion, which provided sufficient energy to devolatilize planetesimals and thus build up a massive primordial atmosphere, and escape of gas and cooling of such an atmosphere toward the present state. This

work is part of a broader ongoing effort with D.J. Stevenson to constrain physical processes operating in the early solar system based on the present properties of large icy satellites.

A number of spacecraft and earth-based measurements ongoing, planned, or contemplated are capable of testing aspects of the modeling done in this thesis. An important prediction of Part 1 is that the noble gas abundances in a body comprised of, or substantially contaminated with, volatiles brought in as clathrate will be strongly nonsolar, enriched in heavier, and depleted in lighter noble species. Although further chemical partitioning of the noble gases during planetary or satellite evolution would be expected, measurements are still of value in inferring the origin of volatiles. A strongly non-solar noble gas abundance in the Jovian atmosphere could be indicative of post-formation contamination by clathrate-laden debris; the Galileo probe will make such measurements in 1989. The noble gas abundances in Titan's atmosphere are almost completely unconstrained (Lindal et al., 1983); measurements by an atmospheric probe of the abundances are needed to guide modeling of the origin and evolution of the atmosphere. Some of the processes affecting noble gas abundances in Titan's atmosphere are analyzed in the thesis; further work is needed to make specific predictions of abundances for different evolution scenarios.

Characterization of the nature of Titan's surface should be of high priority for ground- or space-based observing programs. Radio brightness measurements of Titan at centimeter wavelengths (Muhleman et al., 1984) can potentially test for the presence of an ocean. Radar

mapping of the surface, preferably at close range by spacecraft, would detect the presence of an ocean as well as do altimetry sounding (D. Stevenson, personal communication, 1984) to test for degradation of craterforms immersed in the liquid. Probe measurements of lower atmospheric hydrocarbon abundances and cloud structure would also distinguish between a wet and dry surface. Also, the importance of conducting an extensive set of observations of Triton using Voyager 2, comparable to that of Titan from Voyager 1, cannot be overemphasized.

The past ten years have seen tremendous advances in our knowledge of physical and chemical make-up of outer solar system bodies, thanks to extensive ground- and space-based observations. Modeling of properties of materials relevant to these bodies, as well as of the properties of the bodies themselves, must keep pace to provide a theoretical framework within which to interpret and extend the observations. It is hoped that the present work can make a contribution to such an effort.

References

Cruikshank, D.P. and Brown, R.H. (1984). In Natural Satellites, J. Burns and D. Morrison, eds. (Tucson: University of Arizona Press), submitted.

Delsemme, A.H. and Swings, P. (1952). Ann. Astrophys., **15**, 1.

Lewis, J.S. (1971). Icarus, **15**, 174.

Lindal, G.F., Wood, G.E., Hotz, H.B., Sweetnam, D.N., Eshleman, V.R., and Tyler, G.L. (1983). Icarus, **53**, 348.

Miller, S.L. (1961). Proc. Natl. Acad. of Sci. USA, **47**, 1798.

Muhleman, D.O., Berge, G.L., and Clancy, R.T. (1984). Science, **223**, 393.

Stevenson, D.J., Harris, A.W., and Lunine, J.I. (1984). In Natural Satellites, J. Burns and D. Morrison, eds. (Tucson: University of Arizona Press), submitted.

Abstract

Three investigations are conducted into the physical chemistry of volatiles in the outer solar system and the role of volatiles in icy satellite evolution.

Part I:

The thermodynamic stability of clathrate hydrate is calculated under a wide range of temperature and pressure conditions applicable to solar system problems, using a statistical mechanical theory developed by Van der Waals and Platteeuw (1959) and existing experimental data on properties of clathrate hydrates and their components. At low pressure, dissociation pressures and partition functions (Langmuir constants) for CO clathrate (hydrate) have been predicted using the properties of clathrate containing, as guests, molecules similar to CO. The comparable or higher propensity of CO to incorporate in clathrate relative to N_2 is used to argue for high CO to N_2 ratios in primordial Titan if N_2 were accreted as clathrate. The relative incorporation of noble gases in clathrate from a solar composition gas at low temperatures is calculated, and applied to the case of giant planet atmospheres and icy satellites. It is argued that non-solar but well-constrained noble gas abundances would be measured by Galileo in the Jovian atmosphere if the observed carbon enhancement were due to bombardment of the atmosphere by

clathrate-bearing planetesimals sometime after planetary formation. The noble gas abundances of Titan's atmosphere are also predicted under the hypothesis that much of the satellite's methane accreted as clathrate. Double occupancy of clathrate cages by H_2 and CH_4 in contact with a solar composition gas is examined, and it is concluded that potentially important amounts of H_2 may have incorporated in satellites as clathrate. The kinetics of clathrate formation is also examined, and it is suggested that, under thermodynamically appropriate conditions, essentially complete clathration of water ice could have occurred in high pressure nebulae around giant planets but probably not in the outer solar nebula; comets probably did not aggregate as clathrate. At moderate pressures, the phase diagram for methane clathrate hydrate in the presence of 15% ammonia (relative to water) is constructed, and application to the early Titan atmospheric composition is described. The high pressure stability of CH_4, N_2, and mixed CH_4-N_2 clathrate hydrate is calculated; conversion back to water and CH_4 and/or N_2 fluids or solids is predicted for pressures $\gtrsim$12 kilobars and/or temperatures $\gtrsim$320 K. The effect of ammonia is to shrink the T-P stability field of clathrate with increasing ammonia concentration. A preliminary phase diagram for the high pressure ammonia-water system is constructed using new data of Johnson et al. (1984). These results imply that 1) clathrate is stable throughout the interior of Oberon- and Rhea-sized icy satellites, and 2) clathrate incorporated in the inner-most icy regions of Titan would have decomposed, perhaps allowing buoyant methane to rise. Brief speculation on the implications of this conclusion for

the origin of surficial methane on Titan is given. A list of suggested experiments and observations to test the theory and its predictions is presented.

Part II:

We propose a global Titanic ocean, one to several kilometers deep, the modern composition of which is predominantly ethane. If the ocean is in thermodynamic equilibrium with an atmosphere of 3% (mole fraction) methane then its composition is roughly 70% C_2H_6, 25% CH_4, and 5% N_2. Photochemical models predict that C_2H_6 is the dominant end-product of CH_4 photolysis so that the evolving ocean is both the source and sink for ongoing photolysis. The coexisting atmosphere is compatible with Voyager data. Two consequences are pursued: the interaction of such an ocean with the underlying ''bedrock'' of Titan (assumed to be water-ice or ammonia hydrate) and with the primarily nitrogen atmosphere. It is concluded that although modest exchange of oceanic hydrocarbons with enclathrated methane in the bedrock can in principle occur, it is unlikely for reasonable regolith depths and probably physically inhibited by the presence of a layer of solid acetylene and complex polymeric hydrocarbons a couple of hundred meters thick at the base of the ocean. However, the surprisingly high solubility of water ice in liquid methane (Rebiai et al., 1983) implies that topographic features on Titan of order 100 meter in height can be eroded away on a time scale $\lesssim 10^9$ years; ''Karst'' topography could be

formed. Finally, the large solubility difference of N_2 in methane versus ethane implies that the ocean composition is a strong determinant of atmospheric pressure; a simple radiative model of the Titan atmosphere is employed to demonstrate that significant surface pressure and temperature changes can occur as the oceanic composition evolves with time. The model suggests that the early methane-rich ocean may have been frozen; scenarios for evolution to the present liquid state are discussed.

Part III:

A simple convective cooling model of a primordial, CH_4-NH_3-N_2 Titan atmosphere is constructed, in an effort to understand the fate of volatiles accreted from a gaseous disk (''nebula'') surrounding Saturn and released from accreting planetesimals during the satellite's formation. Near-surface temperatures are initially $\gtrsim$400 K consistent with the large amount of energy supplied to the atmosphere during accretion. As a consequence of accretional heating, the upper mantle of the satellite consists of an ammonia-water liquid, extending to the surface. This ''magma ocean'' is the primary buffer of atmospheric cooling because it is $\gtrsim$10 times as massive as the atmosphere. The radiative properties of the atmosphere are assumed independent of frequency and the resulting temperature profile is found to be adiabatic; if the atmosphere contains dark particulates surface temperatures could be lower than calculated here. Three major processes drive the cooling:

(1) hydrodynamic escape of gas from the top of the atmosphere, which determines the cooling time scales, (2) atmospheric ablation by high velocity impacts (not modeled in detail here), and (3) formation of clathrate hydrate at the ocean-atmosphere interface, at $T \leq 250$ K. Cooling time scales driven by escape are sufficiently long (10^8–10^9 years) to allow ~10 bars of N_2 to be produced photochemically from NH_3 in the gas phase (Atreya et al., 1978); however, the abundance of NH_3 at temperatures $\lesssim$150 K (where the intermediate photochemical products condense out) is optically thick to the dissociative UV photons. Thus, N_2 formation may proceed primarily by shock heating of the atmosphere during large body impacts, as well as by photochemistry (1) at $T < 150$ K if intermediate products supersaturate, or (2) in a warm stratosphere, with NH_3 abundance fixed by its tropopause value. The clathrate formed during late stages of cooling sequesters primarily CH_4, with some N_2, and forces surface temperatures and pressures to drop rapidly. The clathrate is only marginally buoyant relative to the coexisting ammonia-water liquid. If it sinks, the atmosphere is driven to an N_2-rich state with most of the methane sequestered in clathrate when the ocean surface freezes over at ~180 K. Implications of this scenario for the present surface state of Titan are contrasted with those obtained if the clathrate forms a buoyant crust at the surface.

Table of Contents

List of Figures

Part I:

List of Tables

Part I.

Part III.

PART I

THERMODYNAMICS OF CLATHRATE HYDRATES AND APPLICATION TO THE OUTER SOLAR SYSTEM

Thermodynamics of Clathrate Hydrate at Low and High Pressures with Application to the Outer Solar System

Jonathan I. Lunine and David J. Stevenson

Division of Geological and Planetary Sciences
California Institute of Technology
Pasadena, California 91125

Submitted to Astrophys. J.

Contribution number 4068 of the Division of Geological and Planetary Sciences, California Institute of Technology, Pasadena, California 91125.

ABSTRACT

The thermodynamic stability of clathrate hydrate is calculated under a wide range of temperature and pressure conditions applicable to solar system problems, using a statistical mechanical theory developed by Van der Waals and Platteeuw (1959) and existing experimental data on properties of clathrate hydrates and their components. At low pressure, dissociation pressures and partition functions (Langmuir constants) for CO clathrate (hydrate) have been predicted using the properties of clathrate containing, as guests, molecules similar to CO. The comparable or higher propensity of CO to incorporate in clathrate relative to N_2 is used to argue for high CO to N_2 ratios in primordial Titan if N_2 was accreted as clathrate. The relative incorporation of noble gases in clathrate from a solar composition gas at low temperatures is calculated, and applied to the case of giant planet atmospheres and icy satellites. It is argued that non-solar but well-constrained noble gas abundances would be measured by Galileo in the Jovian atmosphere if the observed carbon enhancement were due to bombardment of the atmosphere by clathrate-bearing planetesimals sometime after planetary formation. The noble gas abundances in Titan's atmosphere are also predicted under the hypothesis that much of the satellite's methane accreted as clathrate. Double occupancy of clathrate cages by H_2 and CH_4 in contact with a solar composition gas is examined, and it is concluded that potentially important amounts of H_2 may have incorporated in satellites as clathrate. The kinetics of clathrate formation is also examined, and it

is suggested that, under thermodynamically appropriate conditions, essentially complete clathration of water ice could have occurred in high pressure nebulae around giant planets but probably not in the outer solar nebula; comets probably did not aggregate as clathrate. At moderate pressures, the phase diagram for methane clathrate hydrate in the presence of 15% ammonia (relative to water) is constructed, and application to the early Titan atmospheric composition is described. The high pressure stability of CH_4, N_2, and mixed CH_4-N_2 clathrate hydrate is calculated; conversion back to water and CH_4 and/or N_2 fluids or solids is predicted for pressures $\gtrsim$12 kilobars and/or temperatures $\gtrsim$320 K. The effect of ammonia is to shrink the T-P stability field of clathrate with increasing ammonia concentration. A preliminary phase diagram for the high pressure ammonia-water system is constructed using new data of Johnson et al. (1984). These results imply that 1) clathrate is stable throughout the interior of Oberon- and Rhea-sized icy satellites, and 2) clathrate incorporated in the inner-most icy regions of Titan would have decomposed, perhaps allowing buoyant methane to rise. Brief speculation on the implications of this conclusion for the origin of surficial methane on Titan is given. A list of suggested experiments and observations to test the theory and its predictions is presented.

1. INTRODUCTION

Clathrate hydrates are water-ice compounds in which a distinctive open lattice structure of the ice forms cages stabilized by the inclusion of molecules of other chemical species. As a means of incorporating large quantities of volatile gases in solid bodies under conditions well outside the stability field of the condensed phases of the volatiles, they have been of great interest in terrestrial and solar system studies. Increasing interest in the possible importance of clathrates in the outer solar system has arisen for two reasons. First, volatiles such as methane may owe their existence on Titan, Triton, and perhaps Pluto, in part because of clathrates. Second, refined observational techniques have, for the first time, made direct observation of these compounds on outer solar system bodies a possibility, renewing interest in their thermodynamic properties.

In this paper we extend a statistical mechanical model of clathrate formation originally developed by Van der Waals and Platteeuw (1959) to predict the formation conditions and composition of clathrate hydrate under a wide range of situations of interest to solar system studies. These include the low pressure (10^{-12}–1 bar) regimes of gaseous nebulae in which the outer planets and their satellites may have formed, intermediate pressures (1–10^2 bars) obtained in the present-day atmosphere of Titan and plausible models for primordial atmospheres, and high ($\gtrsim 10^3$ bars) pressure relevant to the interiors of large icy satellites. The goal of this paper is to treat all of these cases with a single,

physically reasonable model of clathrate formation which is tied as much as possible directly to laboratory data on the stability of the various clathrate compounds or the thermodynamic properties of the pure components themselves. The model allows us to make a prediction for the conditions of formation of clathrate hydrate of CO, an important molecule cosmochemically and one for which no laboratory data on the clathrate yet exists. We also predict substantial double occupancy of clathrate cages by CH_4 and H_2, the latter by itself being a poor clathrate hydrate former. This may have implications for satellite outgassing processes. We also deal, for the first time, with the stability of clathrates at high pressure and the formation of clathrates in the presence of an ammonia-water solution (a probable primordial environment in large icy satellites). The difficult problem of clathrate formation kinetics in a gaseous environment is also analyzed. We find that disequilibrium is likely in many circumstances, including the formation conditions of comets, but that approach to full equilibrium may occur if ice particles or planetesimals undergo extensive collisional gardening. Approach to equilibrium is more probable in the higher density, higher temperature nebulae around proto-giant planets than in the primordial solar nebula. A study of this scope has not been previously attempted in the literature; two areas for which little or no data exist, the high (>5 kilobar) pressure clathrate stability and formation of clathrate in the presence of ammonia-water solution, are dealt with for the first time here. Application to relevant solar system objects will be given to make the results more concrete; however,

our results are intended to be incorporated into models for the properties and evolution of bodies for which additional considerations and constraints must be applied beyond the scope of the present paper. We are working on several of these applications; we hope, also, that the present effort will be useful to other workers in the field who desire to incorporate clathrate thermodynamics in their models.

The plan of the paper is as follows. Section 2 reviews pertinent literature on clathrate properties and occurrence as well as previous applications to solar system problems. Section 3 presents the statistical mechanical model used to predict clathrate formation. In Section 4 we calculate the phase diagram of clathrate hydrate in the presence of ammonia at moderate pressures. Section 5 uses the results given in 3 to calculate the complete stability fields of both methane and molecular nitrogen clathrate hydrate up to tens of kilobars of pressure. Although almost no laboratory data are available at these pressures, the regime is directly relevant to the interiors of large satellites such as Titan and Triton, and perhaps the planet Pluto. Section 6 addresses the problem of kinetics of clathrate formation. Section 7 applies the results of previous sections to calculate the abundance of volatiles incorporated in clathrate formed from a solar composition gas, and explores implications for the current composition and evolution of satellites and giant planet atmospheres. Section 8 reviews our important results and lists the outstanding uncertainties in clathrate thermodynamics and kinetics which have yet to be resolved by experiment and theory.

Because the nomenclature used in the clathrate literature is confusing and not always consistent, we establish some conventions for the paper. We will deal almost exclusively with clathrate compounds for which water ice forms the lattice structure (i.e., the ''host'' molecule). Hence, the term clathrate is here understood to mean clathrate hydrate. The gas molecule occupying a cage site is the ''guest'' molecule. The term methane clathrate is used to denote a clathrate hydrate in which methane is the primary guest molecule. Occasional discussion of clathrates in which a substance other than water ice is the host, for example quinol, will employ the term quinol clathrate, as in the literature, but care will be taken to be sufficiently explicit to avoid confusing the guest and host molecules in the minds of the readers. Finally, a stoichometric compound of water ice, in which molecules bond chemically with the water molecule and do not form a clathrate, will be denoted as a hydrate, i.e. ammonia hydrate. Hence, the use of the term gas hydrate to denote a clathrate hydrate (employed in the geological and geophysical literature) is avoided here.

2. BACKGROUND

The history of synthesis of clathrate hydrate compounds extends back to the preparation of chlorine clathrate hydrate by Davy in 1811 and Faraday in 1823 (Jeffrey and McMullan, 1967). The clathrate hydrate structure consists of open, cage-like voids each formed by 20 to 28 hydrogen-bonded water molecules. Two structural types of clathrate hydrate are known, referred to as I and II; the size of the included guest molecule determines which is formed. Figure 1 from Miller (1973) illustrates the cage geometry of the structure I clathrate, first determined by Pauling and Marsh (1952), which is organized into cells with two small cages and six large. We focus on structure I because most guest molecules of interest to planetary applications will incorporate in this structure in preference to structure II. Data on the geometry of both types of clathrate hydrate structures are tabulated in Davidson (1971).

Several good reviews of the literature up to the late sixties are Davidson (1973), Jeffrey and McMullan (1967), Miller (1974), Hagan (1962), and Van der Waals and Platteeuw (1959). An interesting review from the Russian perspective is Byk and Fomina (1968). Of particular importance to the present study are the Van der Waals and Platteeuw (1959) treatment of the statistical mechanics of clathrate formation, laboratory studies by Barrer and Edge (1967) on inert gas clathrates including dissociation pressures and heats of formation data, and work

Figure 1. Structure I clathrate hydrate lattice. Oxygen atoms are located at vertices; hydrogen atoms are considered to lie on line between two vertices. The small cage (upper center) is a pentagonal dodecahedron with 20 water molecules; 24 water molecules make up the large cage tetrakaidecahedron (after Miller (1973)).

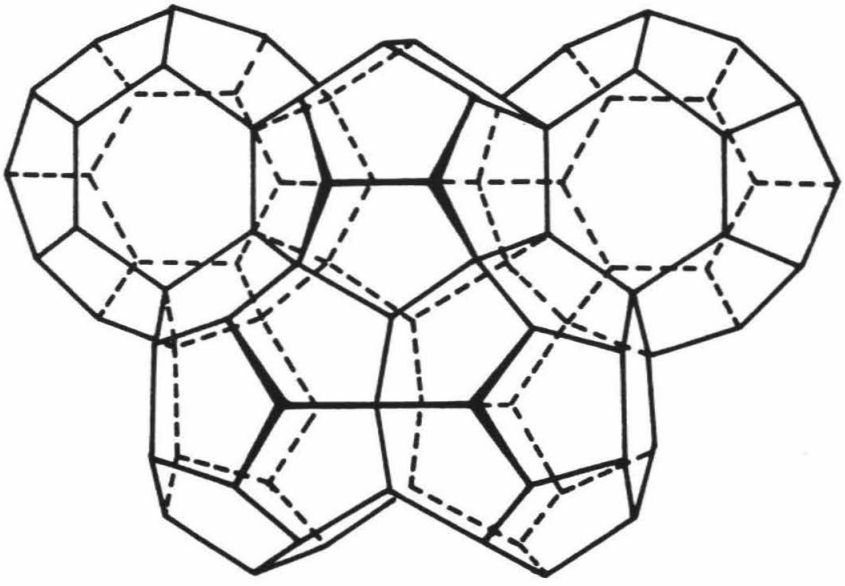

by Marshall et al. (1964) on clathrate stability at pressures up to 4 kilobars.

Clathrates can be ''pure'' (only one kind of guest molecule) or ''mixed'' (more than one kind of guest molecule). In the pure case, a clathrate can be characterized by two parameters: the dissociation pressure, defined empirically as the minimum gas pressure of the guest molecule at a given temperature for which the corresponding clathrate is stable, and the degree of occupancy, defined as the fraction of available cage sites occupied by a guest molecule. In the mixed case, a single dissociation pressure still exists but there are as many parameters characterizing relative occupancy as there are guest molecules. The chemical formula for the structure I clathrate in the usual notation is $(\prod_i X_{i(y_i)}) \cdot 5\ 3/4\ H_2O$ where y_i is the number fraction of all guests that is species X_i. As implied above, not all cages need be filled and one of the guest species can be thought of as a hole, which enters the partition functions appropriately but otherwise does not contribute to the energy. Since the early 1960's much work has centered on using the Van der Waals and Platteeuw model to predict these parameters (McKoy and Sinanoglu (1963), Saito et al. (1964), Nagata and Kobayashi (1966), Parrish and Prausnitz (1972), and Holder et al. (1980)). This type of modeling is employed in section 3 to calculate dissociation pressures and occupancies for guest molecules of cosmochemical interests; details of the calculation will be deferred to that section.

Some work has also been done in understanding explicitly the interaction between guest molecule and the surrounding host cage, theo-

retically by Davidson (1971) and experimentally, using infrared spectroscopy and dielectric measurements, by Bertie and Jacobs (1982, 1978, 1977) and Davidson and Wilson (1963). Other studies involving computer simulation of guest and cage molecule motions have been undertaken by Tester et al. (1972), Plummer and Chen (1983), and Tse et al. (1983). These studies are important in determining the degree of rotational inhibition of the encaged guest molecule, the magnitude of electric fields within the cage, and degree of interaction between guest molecules in adjacent cages (see section 3).

Much less attention has been given to the kinetics of clathrate formation, most likely because of the long duration of experiments required to measure diffusion of gas molecules within grains and along grain boundaries in water ice. Both Barrer and Edge (1967) and Barrer and Ruzicka (1962) achieved nearly complete clathration in a system of water ice and noble gases by agitating the system, apparently exposing fresh ice to the gas. In the absence of shaking an initially rapid uptake of gas by the ice to form clathrate was followed by a very slow uptake suggesting a diffusional process. The problem of kinetics of clathrate formation will be explored in detail in section 6.

A number of studies have been done on physical properties of clathrate which are relevant to identifying clathrate in terrestrial ocean sediments as well as processes in solar system bodies. The thermal conductivity at low to moderate pressures was measured by Cook and Leaist (1983) and Stoll and Bryan (1979); the latter also measured acoustic wave velocity. Dharma-Wardana (1983) attempted to explain the

low thermal conductivity of clathrate (1/5 that of ice I_H) in terms of the large number of molecules per unit clathrate cell. Thermal conductivity and heat capacity studies were undertaken by Ross and Andersson (1982) to explore high-pressure solid compounds of water and tetrahydrofuran (THF), including THF clathrate. Results suggest the possibility of a high density clathrate hydrate phase existing above 11 kilobars; implications for satellites as well as our theoretical high-pressure stability calculations will be presented below. A unique study by Pinder (1964) focused on the time-dependent rheology of a clathrate hydrate slurry, with THF and hydrogen sulfide as guest molecules. Some data on the density of clathrate compounds are available in Byk and Fomina (1968) and Kvenvolden and McDonald (1982).

We turn now to literature describing the predicted or observed occurrence of clathrates in natural environments. Reviews of the terrestrial occurrence of clathrate have been given by Claypool and Kvenvolden (1983) and Kvenvolden and McMenamin (1980). A recent review of properties of natural clathrate deposits is that of Pearson et al. (1983). Although evidence exists for clathrate in permafrost in Western Siberia, Canada, and Alaska, and the existence of an N_2-O_2 clathrate in Antarctic ice has been proposed (Miller, 1969) and tentatively detected (Shoji and Langway, 1982) the best evidence for the existence of naturally formed clathrate comes from bottom-simulating reflectors in a number of ocean sediment areas around the world. The reflectors are apparently due to an abrupt decrease in sound velocity caused by trapped methane gas. The association of the gas with methane clathrate is

supported by (a) calculations showing that the reflectors are in a temperature-pressure regime stable for methane clathrate (Shipley et al., 1979) and (b) the retrieval in drill cores of frozen sediments and water ice evolving primarily methane gas (Shipley and Didyk, 1982; Kvenvolden and McDonald, 1982). The methane is likely of biogenic origin; the existence of the clathrate demonstrates that, in the presence of liquid water at least, clathrate compounds form spontaneously under the appropriate gas pressure and temperature conditions.

Application of clathrate hydrate properties to solar system objects extends over a thirty year period in the literature. The first direct application to solar system studies was probably that of Delsemme and Swings (1952) who proposed the existence of clathrate hydrate in cometary nuclei. This was followed by more detailed work by Delsemme and Wenger (1970), and Delsemme and Miller (1970). The former produced methane clathrate at temperatures as low as 82 K by condensing water vapor onto a cold plate in the presence of methane gas. The stripping of ice grains during dissociation was suggested as a mechanism for cometary halo production. The latter paper modeled clathrate formation as a special case of gas adsorption, and suggested that radicals observed spectroscopically in comets could be emitted from clathrate cages. Although more detailed observations of comets are now available, the existence of clathrate in comets is still hypothetical.

In a pioneering paper, Stanley Miller (1961) utilized the Van der Waals and Platteeuw model and his own experimental data to determine the likelihood of occurrence of clathrate hydrate in a wide range of solar

system objects, including the envelopes of the outer planets, Saturn's rings, satellite interiors, terrestrial planet atmospheres, Mars polar caps, comets, as well as interstellar grains. An updated discussion was later presented by Miller (1973). A somewhat more detailed analysis of the stability of carbon dioxide clathrate in the Martian ice caps was given by Miller and Smythe (1970). Somewhat later Smythe (1975) produced a set of laboratory reflectance spectra of methane and carbon dioxide clathrate frost to determine the detectability of clathrate on surfaces of the outer planet satellites.

The application of clathrate formation in primordial gaseous disks to the present atmospheres of planets and satellites has received sporadic attention over the past decade. A prescient paper by Lewis (1971) suggested incorporation of methane clathrate in Titan, and predicted the resulting argon to methane ratio in Titan's atmosphere derived from the clathrate composition. Hunten (1978) also suggested an atmosphere in equilibrium with a surface of methane-clathrate, which at the time was not ruled out by the data. Sill and Wilkening (1978) used existing laboratory data on clathrate dissociation pressures for a range of guest molecules of cosmochemical interest to calculate the gas composition in clathrate hydrate derived from a solar composition gas. They concluded that addition of one part per million clathrate gases (in comets) to the earth's atmosphere could explain the observed terrestrial noble gas ratios.

More recently, spacecraft missions to the outer solar system have renewed interest in understanding the origin and effect of volatiles in

icy satellites. Stevenson (1982) proposed clathrate hydrate dissociation as a driver for explosive ammonia-water volcanism on Rhea-sized satellites in the Saturn system. Much recent work on clathrate applications has centered on Titan. Owen (1982) renewed the suggestion that Titan's atmosphere is derived from clathrate, and suggested that the N_2 comprising the bulk of the present atmosphere was accreted in clathrate. Lunine and Stevenson (1982a) calculated gas composition in clathrate derived from a circum-Saturnian nebula and concluded that although CH_4 in Titan is likely derived from primordial clathrate, N_2 would not be substantially incorporated and may have been photochemically produced from NH_3 later (Atreya et al., 1978).

It is important to note that no direct evidence exists for clathrate anywhere aside from the earth. In part this may be because clathrate ''hides'' itself very well as ordinary water ice I in reflection spectra (Smythe, 1975). The utility of studying clathrate thermodynamics rests more on indirect evidence that clathrates play a role in determining the composition and evolution of surfaces and atmospheres of satellites (and perhaps giant planet envelopes) in the outer solar system. Striking improvements in spectral resolution in ground based reflection spectroscopy now raise the possibility of distinguishing between water ice I (and its high pressure polymorphs -- Gaffney and Matson (1980)) and clathrate hydrate on surfaces in the outer solar system in the near future.

3. STATISTICAL MECHANICAL MODEL FOR CLATHRATE FORMATION

In this section we describe the thermodynamic model used to predict the stability regimes of clathrate hydrate and the composition of the guest molecule component.

3.1. Thermodynamic and Structural Properties

Clathrate hydrate is a distinct phase in a multicomponent system consisting of water and any number of non-polar, weakly-polar, and more rarely, strongly-polar chemical species. It is non-stoichometric since, although the number of cages is precisely determined, their fractional occupancy is a function of temperature, pressure, and relative abundance of the species. Although the clathrate structure is distinguished from that of other ice phases by containing large open cage structures, the water molecule lattice bonding mechanism is the usual hydrogen bonding (Jeffrey and McMullan, 1967). The guest molecule-cage interaction is primarily the sum of core overlap effects (a strongly repulsive term) and an attractive Van der Waals-like (induced dipole-induced dipole) interaction. The included guest molecule must stabilize the cage structure because of the attractive term, since the empty cage structure is energetically unfavorable relative to the usual (more compact) forms of water ice.

The phase boundary in temperature pressure space of clathrate hydrate is defined by the equality of chemical potentials (or Gibbs energies g, where dg = -SdT + PdV) of each component (guest and water host) in the coexisting phases. The coexisting phases are (a) clathrate hydrate with incorporated guest molecule, and (b) water ice or liquid (with some dissolved molecules of the guest species) plus the pure phase of the guest species stable under ambient conditions T, P. We consider only a single guest species in the present discussion. Figure 2 plots qualitatively the phase boundary as a function of P and T. Consider, first, the low pressure regime in which the system pressure is essentially the vapor pressure of the guest molecule (since the vapor pressure of water is invariably much lower). With increasing gas pressure at a given temperature the Gibbs energy of the gas is increased by decreasing its entropy. The clathrate Gibbs energy is negligibly affected by pressure, since the pressure is much less than the bulk modulus, so it follows that an increase in pressure favors clathrate formation. In this ideal gas regime, the net volume change and entropy change accompanying clathrate formation are clearly both negative and the Clausius Clapeyron equation predicts a positive value of dT/dP. The phase boundary pressure, at a given temperature, for clathrate formation has been referred to in the literature as the dissociation pressure of the clathrate. We use this term only in the low pressure regime. As pressure is increased and the guest is no longer in the ideal gas regime, compressive effects primarily on the guest molecule (and secondarily on the water) become important, and the volume change from

Figure 2. Schematic diagram of stability fields of clathrate hydrate, occupied by guest molecule x, plotted as log P (in bars) versus temperature in degrees Kelvin. Solid line delineates region in which clathrate is thermodynamically preferred relative to water ice or liquid plus coexisting component x. Dashed line is water ice-liquid phase boundary; within the clathrate stable region the existence of water phase separate from clathrate is contingent on the relative amounts of water and x. Superimposed are dotted lines representing the vapor-liquid (A) and liquid-solid (B) phase boundaries of pure component x. The axis values are for x = methane; the diagram is qualitatively similar for N_2, CO, and other volatile, mainly nonpolar species with small molecular diameters. Note change in slope of clathrate stability field in crossing water ice-liquid boundary.

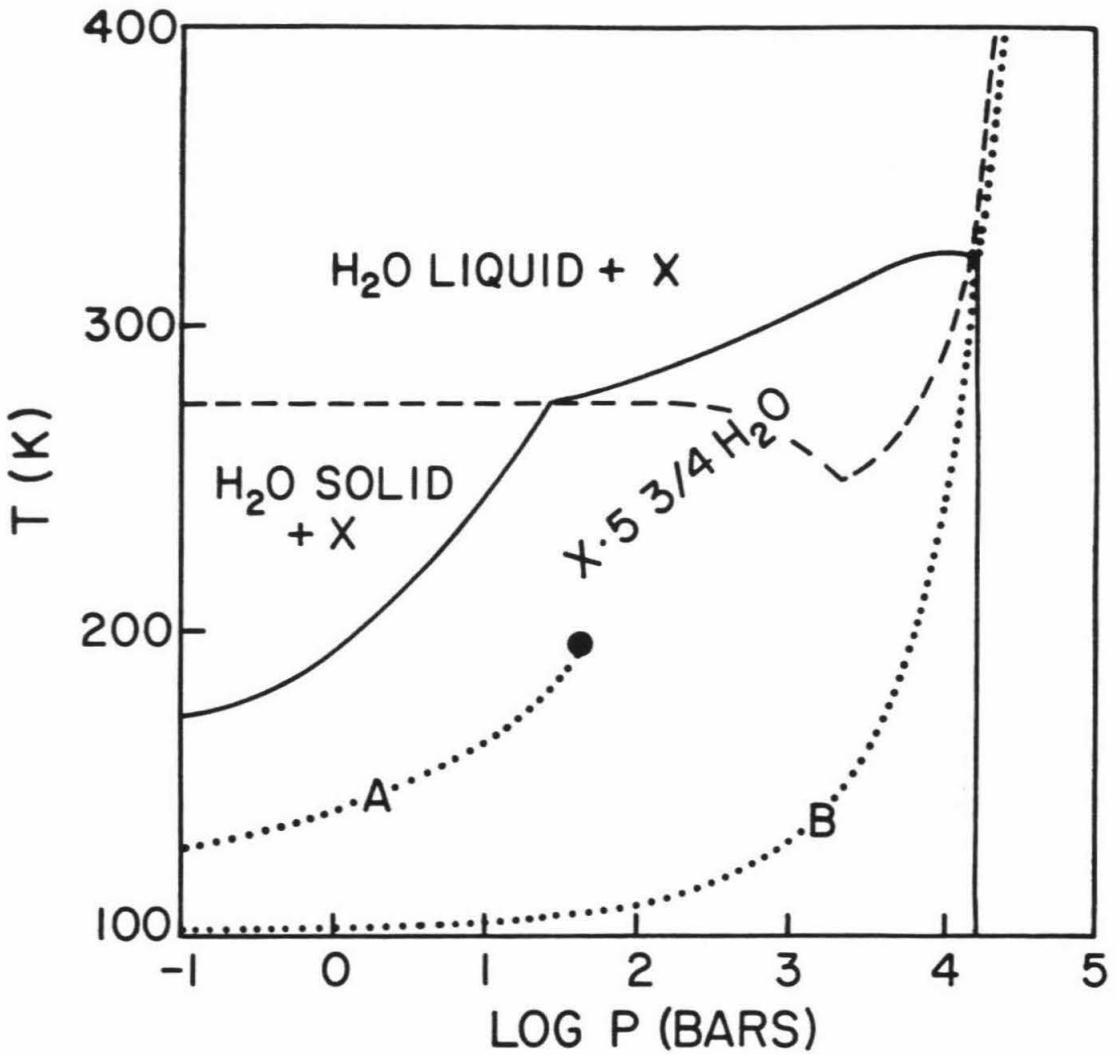
400
300
200
100
T (K)
H2O LIQUID + X
H2O SOLID
+ X
X·5 3/4 H2O
A
B
-1
0
1
2
3
4
5
LOG P (BARS)

phase A (guest + H_2O) to B (clathrate) decreases. At a given temperature, then, a higher system pressure is required to stabilize the clathrate than would be expected in the ideal gas regime, and dT/dP decreases as seen in Figure 2. Eventually the volume change A -> B becomes zero and dT/dP = 0, defining a maximum temperature at which the clathrate is stable. This ''critical point'' T_c is a function of the thermodynamic properties of the particular guest, and, hence, is different for each species. At each temperature below T_c, there exist both maximum and minimum pressures defining the domain of clathrate stability. The minimum pressure exists because at lower pressures the gas entropy is very large (i.e. more favorable) and the maximum pressure exists because the coexisting pure guest phase has reached a low enough specific volume that the <u>volume</u> change (clathrate -> guest + H_2O) is energetically favorable. The precise sign and value of dT/dP at the high pressure end of the clathrate stability field are sensitive functions of the compressibility of the clathrate, water, and guest molecule components, and are calculated for CH_4 and N_2 in section 5. P-T data in the literature are restricted to the low pressure end of Figure 2 ($\lesssim$4 kilobar); one study by Tamman and Krige (1925) appears to have located the critical point for SO_2 clathrate.

Considering in more detail the nature of the guest-host interaction, it is inaccurate to think of the guest molecules as impurities occupying imperfections or substituting for water molecules in the lattice structure. X-ray diffraction studies of clathrates (see Jeffrey and McMullan (1967) for a review of the substantial literature on this

subject) demonstrate a well defined structure in which cages of diameter ~10 Å are present. Calculations by Davidson (1971) indicate substantial cancellation of lattice water molecule dipolar fields within the cage volume. Theoretical and experimental studies of infrared spectra (e.g., Davidson, 1971; Bertie and Jacobs, 1978) and physical properties of clathrate such as sound velocity (Pearson et al., 1983), suggest that these properties are to first order determined by the water molecules and their lattice structure, crudely independent of particular guest species, and the interaction between the guest molecule and host lattice is extremely weak. Even the very low thermal conductivity of the clathrate relative to water ice may be a result of the form of the lattice structure and not due to coupling to the guest molecule (Dharma-Wardana, 1983) although this is controversial. The weak interaction is consistent with London dispersion forces (Fowler and Guggenheim, 1960, p. 278) being responsible for the attractive part of the guest-host interaction, with lesser contribution from induced-dipole-dipole and dipole-dipole interaction with residual fields in the cage. This has long been recognized (Van der Waals and Platteeuw, 1959) since the noble gases are observed as encaged guest molecules; we wish to emphasize the point here since the predominantly ice-like properties are potentially important for evolution models of icy satellites. Strongly dipolar molecules apparently can occupy cage sites (Jeffrey and McMullan, 1967); the possible incorporation of ammonia in clathrate cages is deferred to a later section.

3.2. Model of Clathrate Formation

The statistical mechanical model for clathrate formation developed by Van der Waals and Platteeuw (1959) assumes that the guest molecule incorporation into clathrate cages is physically similar to ideal adsorption onto fixed sites, generalized to three dimensions. Their explicit assumptions are adopted here and are as follows:

(1) The free energy of the H_2O lattice structure is independent of the occupation (and mode of occupation) of the guest molecule.

(2) (a) The guest molecules are confined to the cage volume with one guest molecule per cage. (b) Guest molecules rotate freely within the cage.

(3) Guest molecules do not interact with each other so that the partition function describing the guest molecule motion is independent of the presence and type of other guest molecules.

(4) Classical statistics applies.

Assumption (1) says that the cage structure is relatively undistorted from the presence of the guest molecule, which as noted above seems to be valid based on spectroscopic and other studies for small guest molecules such as CH_4. It is undoubtably in error for large molecules such as CO_2; however, we will see below that our qualitative

conclusions regarding the incorporation of this molecule in ice are probably not sensitive to this assumption. A very interesting possible violation of assumption (2a), with astrophysical implications, is the occupancy of single cages by more than one molecule. Our calculations indicate a finite number of cages occupied by both CH_4 and H_2 when both gases are present. In this circumstance, the ''dimer'' (CH_4, H_2) must be thought of as a separate species from CH_4 and H_2 in the statistical mechanical accounting. (2b) is valid for small spherical molecules but could be in error at low temperatures for rodlike molecules, even small ones such as N_2 and CO. We address this problem further in the context of the calculations. Assumption (3) is verified for moderate-sized guest molecules in Davidson (1971). Assumption (4) is not valid for H_2, He, Ne but for larger molecules on which our quantitative analysis is concentrated, classical statistics is generally valid.

Van der Waals (1956) and Van der Waals and Platteeuw (1959) outline the construction of the configuration partition function for clathrate hydrate in which a fraction y of the cages are occupied by a guest molecule. The condition is then imposed that the chemical potentials of both guest and host molecules in the coexisting phases be equal. Appendix A outlines the derivation. The result is the set of equations

$$\frac{\mu^{i}_{H_2O} - \mu^{\beta}_{H_2O}}{kT} \equiv \frac{-\Delta\mu^{\beta}}{kT} = \frac{1}{23}\ln\left(1 - \sum_j y_{1j}\right) + \frac{3}{23}\ln\left(1 - \sum_j y_{2j}\right) \tag{1}$$

$$y_{ij}(T,P) = \frac{C_{ij}(T,P)\, f_j(T,P)}{1 + \sum_k C_{ik}(T,P)\, f_k(T,P)} \qquad (2)$$

$$C_{ij}(T,P) = \frac{z_{ij}}{k_B T} \int_0^{a_i/2} e^{-\omega_{ij}(r)/k_B T}\, 4\pi r^2\, dr \qquad (3)$$

where

$\mu^{\beta}_{H_2O}$ = chemical potential of unoccupied water ice clathrate structure,

$\mu^{i}_{H_2O}$ = chemical potential of water in coexisting phase.

y_{ij} = fractional occupancy of cage sites i = 1,2 by molecule of species j,

f_j = fugacity of guest molecule j in its pure phase (i.e. μ_j = kT ln f_j),

a_i = cage radius

$\omega_{ij}(r)$ = spherically averaged potential energy of the guest molecule located a distance r from the cage center.

k_B = Boltzmann's constant.

k = gas constant.

The factors 1/23 and 3/23 are the number of cage sites per water molecule for the small and large cages, respectively. The numerical factor z in (3) is the ratio of the rotational and vibrational partition function (volume factor removed) of the guest molecule in the cage to that of the free molecule at the same temperature. If the rotational

and vibrational degrees of freedom of the encaged molecule are the same as for the free molecule $z_{ij} = 1$. In what follows we assume based on the above discussion that $z_{ij} = 1$; exceptions are discussed as they occur.

In general we may compute the fugacity for a single guest species j as

$$f_j(T,P) = \phi_j(T,P_o)\ P_o \exp \frac{1}{kT} \int_{P_o}^{P} V(T,P')\ dP' \qquad (4)$$

where S, V are entropy and volume of the coexisting guest species phase at system temperature T and pressure P, P_o is a reference pressure and $\phi(T, P_o)$ is the fugacity coefficient (Prausnitz, 1969, p. 5) at reference conditions.

$\Delta\mu^\beta$ is computed using an expression from Holder et al. (1980):

$$\frac{\Delta\mu^\beta(T,P)}{kT} = \frac{\Delta\mu^\beta(T_o,P_o)}{kT_o} - \int_{T_o}^{T} \frac{\Delta h^\beta\ (T',P_o)}{kT'^2}\ dT'$$

$$+ \frac{1}{kT} \int_{P_o}^{P} \Delta V^\beta\ (T,P')\ dP' \qquad (5)$$

where Δh^β, ΔV^β are the enthalpy and volume difference between the empty hydrate and coexisting water phase, and T_o is a reference temperature. The pressure dependence of C_{ij} is discussed in section 5. Equations (1) through (5) are the basic equations we will use to determine clathrate stability throughout the paper. In the low pressure (<< a kilobar)

regime considered in sections 3 and 4, three simplifications are made: $C_{ij}(T,P) = C_{ij}(T)$, the last term in equation (5) is neglected, and $f_j = P_j$ = pressure exerted by the guest species vapor (or supercritical fluid) phase.

The C_{ij} are called Langmuir constants and depend on the molecular properties through $\omega(r)$, the spherically averaged interaction between guest and cage. This effective potential depends on the shape as well as size of the molecule. The approximation of spherical cages is adequate for the large cage, where the vertices of the cage as defined by water oxygen atoms vary in distance to center by $\lesssim$14%, and for the small cage, where the variation is $\lesssim$3.5% (Davidson, 1971).

McKoy and Sinanoglu (1963) and Parrish and Prausnitz (1972) derived expressions for the spherically averaged potentials for spherical and rod-like guest molecules using the Kihara potential appropriate for dispersion interactions between guest and host:

$$\Gamma(r) = \varepsilon \left[\left(\frac{\rho_m}{\rho'} \right)^{12} - 2 \left(\frac{\rho_m}{\rho'} \right)^{6} \right] \qquad \rho > 0 \qquad (6)$$

for a single guest molecule interaction, where ρ' = shortest distance between molecular cores, ε = potential minimum, and ρ_m is separation at which $\Gamma = -\varepsilon$ is attained. Note that when the core radius is zero (point-like molecules), we recover the Lennard-Jones 12-6 potential (used in Van der Waals and Platteeuw, 1959), and that $\rho_m/(2)^{1/6} = \sigma$, the distance of closest approach of two molecules which collide with zero initial relative kinetic energy (Hirschfelder et al., 1954, p. 23).

The derivation of the spherically averaged potential is formally the same as in Fowler and Guggenheim (1960, p. 338-9) for models of liquids using the Lennard-Jones (L-J) potential, and consists of keeping the guest molecule fixed at distance r from the center while the host water molecule is moved about a spherical surface of radius a centered on the origin. We will not reproduce the derivation here; rather we give the results from McKoy and Sinanoglu (1963):

$$\omega(r) = \frac{Z\varepsilon}{2} \left[\frac{\rho_m^{12}}{a^{11} r} \left(\delta^{10} + \frac{c}{a} \delta^{11} \right) - \frac{2\rho_m^6}{a^5 r} \left(\delta^4 + \frac{c}{a} \delta^5 \right) \right] \tag{7}$$

$$\delta^N = \frac{1}{N} \left[\left(1 - \frac{r}{a} - \frac{c}{a} \right)^{-N} - \left(1 + \frac{r}{a} - \frac{c}{a} \right)^{-N} \right]$$

for spherical guest molecules and

$$\omega(r) = \frac{Z\varepsilon}{2} \sum_{n=0}^{\infty} \left(\frac{d}{a} \right)^n \left[f_n \frac{\mu_n(y)}{\alpha^4} - \frac{g_n \lambda_n(y)}{\alpha^2} \right]$$

$$\mu_n(y) = \frac{1}{\sqrt{y}} \left[\frac{1}{(1 - \sqrt{y})^{n+10}} - \frac{1}{(1 + \sqrt{y})^{n+10}} \right] \tag{8}$$

$$\lambda_n(y) = \frac{1}{\sqrt{y}} \left[\frac{1}{(1 - \sqrt{y})^{n+4}} - \frac{1}{(1 + \sqrt{y})^{n+4}} \right]$$

for rod-like molecules, where d = rod length, Z = number of nearest neighbor water molecules in a cage of radius a (20 for small, 24 for

large cage), c = core radius of guest molecule, $y = (r/a)^2$, $\alpha = (a/\rho_m)^3$, and we find the constants f_n and g_n to be

$$f_n = \binom{-6}{n} \frac{1}{n+1} \frac{1}{10+n}$$

$$g_n = \binom{-3}{n} \frac{1}{n+1} \frac{1}{4+n}$$

where

$$\binom{-\ell}{n} = \frac{\ell \cdot (\ell+1) \cdot \ldots \cdot (\ell+n-1)}{n!} \cdot (-1)^n$$

(Marion, 1970, pp. 542-3).

For a given choice of parameters ε, ρ_m, c, and temperature T we compute the integral in equation (3) using (7) or (8), terminating the integration at a value r such that the probability of finding the molecule, $\exp[-\omega(r)/kT]$, at r is $\ll\ll 1$. This gives $C_{ij}(T)$, and in the low pressure calculations for a single species j equations (1) and (2) are then solved (using a laboratory value for $\Delta\mu^\beta$; see below) for the dissociation pressure for species j. To solve for several guest species, abundance relations between them must be applied to close the system. Application of equations (1)-(5) to the high pressure regime is discussed in section 5.

3.3. Choice of Molecular Parameters

We now fit the above equations to existing laboratory data on clathrate to derive values for ε, ρ, and where necessary, c. We will then use these parameters to predict the dissociation of clathrate at temperatures below that available in the data, or the dissociation pressure for guest molecules similar to others but for which laboratory data is scant or nonexistent. We use our results in section 7 to predict the composition of the clathrate in plausible nebular models. Our derived parameters also will be used to predict the stability of clathrate under high pressure and in coexistence with an ammonia-water solution.

In evaluating equation (1) a choice of $\Delta\mu^{\beta}$, the difference in chemical potential between the empty clathrate lattice and coexisting liquid water or ice phase must be made. To date no attempt has been made to calculate this from first principles; instead, it has been derived by several laboratory studies. Van der Waals and Platteeuw (1959) suggest 167 cal/mole at 273 K, based on the bromine structure I clathrate. Parrish and Prausnitz (1972) and Holder (1980) derive $\Delta\mu^{\beta} \sim$ 310 cal/mole based on argon, krypton, and methane clathrate. Since the existence of a structure I bromine clathrate has been called into question (Parrish and Prausnitz, 1972) we use the latter value.

Of equal concern is the temperature dependence of $\Delta\mu^{\beta}$ below the ice point, on which authors disagree. Parrish and Prausnitz conclude $\Delta\mu^{\beta}$ decreases by ~6% from 273 to 70 K; Holder et al. (1980) predict an

increase of 27% over that temperature range. Using the Debye model of solids, infrared spectral data on intermolecular translational frequencies in ice I and structure II clathrate (Johari and Chew, 1984), and thermodynamic data in Giauque and Stout (1936), we estimate that $\Delta\mu^{\beta}$ increases ~15% from 273 to 70 K. Unfortunately, data on librational vibrations in the clathrate lattice do not exist. We adopt a constant $\Delta\mu^{\beta}$ in the low pressure ice I regime. In the liquid water field the temperature dependence of $\Delta\mu^{\beta}$ is large and dominated by the ice-to-liquid enthalpy change; this will be important for calculations in sections 4 and 5.

Table I lists the guest molecules included in the present study, along with sources of laboratory data and their temperature range. Molecules listed under ''substantial data'' were studied over a temperature range sufficient to allow fitting of Kihara or Lennard-Jones parameters such that the calculated dissociation pressures should be good to within 10% at moderate temperatures ($\gtrsim$150 K) and probably within a factor of several extrapolated to low ($T < 100$ K) temperatures. Molecules in the ''some data'' category have been studied under restricted temperature ranges and the consequent degree of uncertainty in dissociation pressure at low temperatures increases by about a factor of 10. Those molecules listed under the ''little or no data'' category required special treatment which is outlined later.

Table II lists dissociation pressures derived from the data fits over a range of temperatures, below the low pressure ice point, of interest to solar system studies. Also shown are corresponding data

Table I

Summary of Guest Molecules Analyzed

Species	Reference	Temperature Range (K)
I. Substantial Data		
Ar	1	273
	2	148-90.2
	3	273
Kr	1	273
	2	202-149 ± 1
Xe	1	273
	2	268.3-211.2
CH_4	1	273
	4	207-173
	5	111-82
CO_2	1	273
	4	232-175
C_2H_4	1	273
	4	240-163
	6	272-269
II. Some Data		
N_2	7	272
	8	238
H_2S	9	272-247
	10	273-250
SO_2	1	273
	11	271-265
PH_3	1	273, 267
	12	298, 274

Species	Reference	Temperature Range (K)
III. Little or No Data		
O_2	8	272
CO	--	--
H_2	13 (mixed clathrate)	279
He	--	--
Ne	--	--

1. von Stackelberg and Muller (1954). 2. Barrer and Edge (1967).
3. Van der Waals and Platteeuw (1959). 4. Miller (1961).
5. Delsemme and Wenger (1970). 6. Diepen and Scheffer (1950).
7. Miller (1969). 8. van Cleef and Diepen (1965).
9. Korvezee and Scheffer (1931). 10. Selleck et al. (1952).
11. Tammann and Krige (1925). 12. Byk and Fomina (1968).
13. von Stackelberg and Meinhold (1954).

Table II

Results of Fits to Dissociation Pressures

	T	P (bars)	$P_{experimental}$ (bars)
CH_4	273	24.4	25.2-26.0
	230	5.61	5.65
	180	0.412	0.405
	100	2.60(-5) {1.18(-5)}	2.10(-5)
	82	2.17(-7) {1.45(-8)}	2.10(-7)
N_2	272	141	141.5
	238	62.4	61.9 ± 0.5
	180	7.50	
	100	7.14(-3)	
	60	2.16(-7)	
CO_2	273	12.1	12.5
	200	0.359	0.351
	150	4.40(-3)	4.78(-3)
	100	6.45(-7)	
	80	8.42(-10)	
Ar	273	91.8	92.5-95.5
	230	33.0	33.7
	149	0.973	0.97-1.0
	116	5.74(-2)	5.2-5.5(-2)
	90	1.46(-3)	1.38-1.45(-3)
	60	4.19(-7)	
Kr	273	14.6	14.5-14.7
	203	1.21	1.11
	181	0.371	0.342
	149 ± 1	3.62(-2)	6.30(-2) ± 0.3(-2)
	100	5.94(-5)	
	60	1.49(-10)	
Xe	273	1.44	1.15-1.5
	238	0.306	0.307
	211	6.52(-2)	6.52(-2)
	180	6.17(-3)	
	100	1.59(-8)	
	60	6.39(-17)	

	T	P (bars)	$P_{experimental}$ (bars)
H_2S	273	0.921	0.919
	247	0.299	0.298
	180	3.69(-3)	
	100	9.05(-9)	
	80	6.47(-12)	
C_2H_4	272	5.27	5.25
	269	4.70	4.70-4.72
	180	2.78(-2)	2.04(-2)
	100	9.49(-8)	
	80	7.49(-11)	
SO_2	271	0.291	0.29
	265	0.206	0.21
	180	1.20(-4)	
	100	8.83(-13)	
PH_3	298	16.0	16.0
	273	1.68	1.6
	267	0.945	1.0
	180	1.15(-2)	
	100	1.09(-7)	
	80	1.69(-10)	

Note: $a(-b) = a \times 10^{-b}$. $P_{experimental}$ is data from sources in Table I. Values in brackets for CH_4 assume amorphous water ice as coexisting phase (see text).

points when available from the data sources given in Table I. The ability to fit the data with two or three parameters so well over large temperature ranges gives confidence in the physical significance of the form of the equation, our choice of $\Delta\mu^{\beta}$ = constant, and our ability to use those fits to extrapolate to low temperature, and high pressure. These results may be conveniently utilized by fitting to the approximate form log P = A/T + B, where A, B are constants (Miller, 1961).

Data on Ar, Kr, Xe, and CH_4 clathrate extend to low temperatures, as low as 82 K for the CH_4 clathrate. Below 110 K, condensation of water vapor may produce a metastable amorphous ice phase. Using the maximum estimated enthalpy difference between amorphous ice and ice I of 300 cal/mole (Eisenberg and Kauzmann, 1969, p. 90) we calculate the ratio of $\Delta\mu^{\beta}$ for amorphous ice divided by that for hexagonal ice to be 0.91 at 100 K and 0.65 at 70 K. The dissociation pressure data for methane in Table I strongly suggest no change in $\Delta\mu^{\beta}$ for T as low as 70 K, consistent with laboratory conditions in which ice I itself is cooled below 110 K or the condensing water vapor forms the clathrate phase directly in the presence of methane gas. The existence of amorphous ice under nebular condensation conditions is controversial; in what follows we assume hexagonal water ice but discuss the effect of having amorphous ice where relevant.

We now use our fitted parameters to derive dissociation pressures of clathrate containing guest molecules for which little or no laboratory data are available. We reason in the following manner: the mixed parameters c_m, ε_m, ρ_m, fitted to laboratory data, characterize the

averaged intermolecular potential interaction between guest molecule and the cage comprised of water molecules. Similarly shaped guest molecules will likely experience similar types of interactions with the cage; hence, using mixing rules we can derived Kihara parameters for the unknown molecule from those of a similar type of molecule for which dissociation pressure data exist. We use the so-called geometric mean and hard-sphere mixing rules (Prausnitz, 1969, pp. 63, 104):

$$c_m = c$$

$$\varepsilon_m = (\varepsilon\ \varepsilon_\omega)^{1/2}$$

$$\rho_m = \frac{\rho + \rho_\omega}{2} \qquad (9)$$

where the unsubscripted parameters refer to the pure guest molecules, and ω refers to the water lattice. We take $c_\omega = 0$ as in Holder et al. (1980), since the main guest-water molecule interaction is with the point-like oxygen atom; guest-hydrogen atom interaction has been shown by numerical modeling to be much less important (Tse et al., 1983). Values of ε, ρ, and c are obtained from tables based on virial data (e.g., Hirschfelder et al., 1954, pp. 1110-1112); these coupled with the mixed parameters for the known clathrate are used to derive effective ρ_ω, ε_ω from (9). Using tabulated ε, ρ, c for the unknown molecule, equation (9) gives the mixed parameters for this species from which we derive dissociation pressure in equations (1), (2), and (7) or (8).

Because two-parameter L-J fits to virial data are better established as ''reference data'' in the literature, and our two-parameter fit to the known N_2 dissociation pressures is fairly accurate, we employed the L-J potential for this portion of the study.

We first used argon to derive dissociation pressures for neon and helium, two molecules of cosmochemical interest. To test out our procedure we derived Kr and Xe dissociation pressures from the argon data, and compared with the fits from laboratory data. The results are shown in Figure 3. The correspondence is within a factor of two above 100 K, and does not diverge dramatically unit $T \lesssim 80$ K. Thus, this procedure appears to be satisfactory. When applied to He and Ne, the unusual curves in Figure 4 result. Of course, the pressures shown are far outside the ideal gas regime, so the model is invalid. Nevertheless, it illustrates that these gases are extremely poor clathrate formers, because their interaction with the cage is exceedingly weak. This is also the origin of the unusual shapes of the curves: C is an extremely weak function of T and the term $\Delta\mu^{\beta}/T$ dominates the P(T) dependence. (Note for helium quantum effects would lower the dissociation pressure slightly based on Hirschfelder et al.'s (1954, p. 1110) quantum force constants tabulation; however, this does not change our conclusion.)

We next derive carbon monoxide and molecular hydrogen clathrate dissociation pressures from those of molecular nitrogen. CO may have been the predominant form of carbon in the solar nebula (Lewis and Prinn, 1980); H_2 would be the most abundant constituent in any scenario of satellite or planet formation. Here we use a two parameter L-J fit

Figure 3. Temperature versus log of the dissociation pressure for krypton (top) and xenon (bottom) clathrates. Solid line calculated by adjusting molecular parameters ε and ρ to fit laboratory data for the two clathrates; dotted lines calculated from argon clathrate data, and mixing rules for molecular parameters.

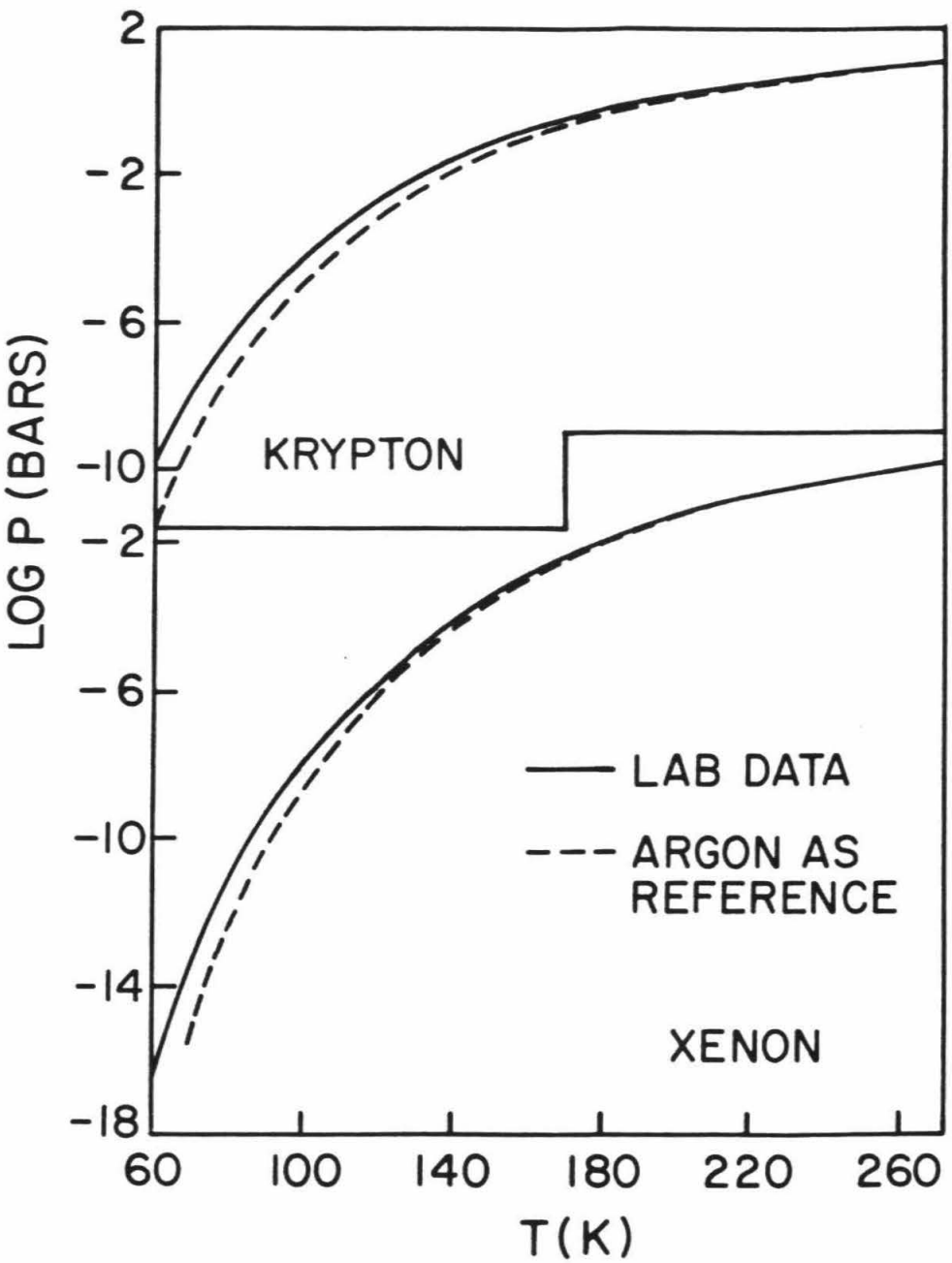
2
-2
-6
-10
-2
-6
-10
-14
-18
LOG P (BARS)
KRYPTON
LAB DATA
ARGON AS
REFERENCE
XENON
60
100
140
180
220
260
T(K)

to the measured N_2 clathrate dissociation pressures; to test our procedure we derive mixed parameters for O_2 as plotted in Figure 5. The agreement with the scant laboratory data (about 30% too low) is not as good as in the noble gas case. We thus have less confidence in these fits; however, the molecular weight of CO and hence pure L-J parameters are closer to N_2 than are those of O_2, so we expect our procedure to be more valid for CO than O_2. The same cannot be said for H_2, and we must consider the derived dissociation pressures to be of qualitative interest only.

Figure 4 shows the result for H_2 and Figure 5 the result for CO clathrate. The similarity in dissociation pressures for N_2 and CO clathrate are striking, within a factor of four even down at T = 60 K. We thus conclude that CO and N_2 are very similar in their ability to incorporate into clathrate, with the tentative suggestion that CO dissociation pressures are slightly lower than those of N_2. H_2 dissociation pressures are extremely high with a temperature dependence expected for a very small molecule with a low value of ε (weak energy of interaction). Thus the derived values of P serve as a qualitative indicator that H_2, by itself, is a poor clathrate ''former.'' The small size of H_2 coupled with its ubiquity in astrophysical settings raises the possibility that H_2 could occupy a cage already occupied by another guest molecule. We present a model for such double occupancy below; before doing so we return to CO and examine the effect of its dipole moment on dissociation pressure.

The weak dipole moment of CO (0.1 Debyes; Prausnitz, 1969, p. 64)

Figure 4. Dissociation pressure versus temperature for helium, H_2, and neon clathrates predicted from the theory. No correction for non-ideality is made; the model is thus strictly invalid but the results are shown to demonstrate that these molecules are poor clathrate formers.

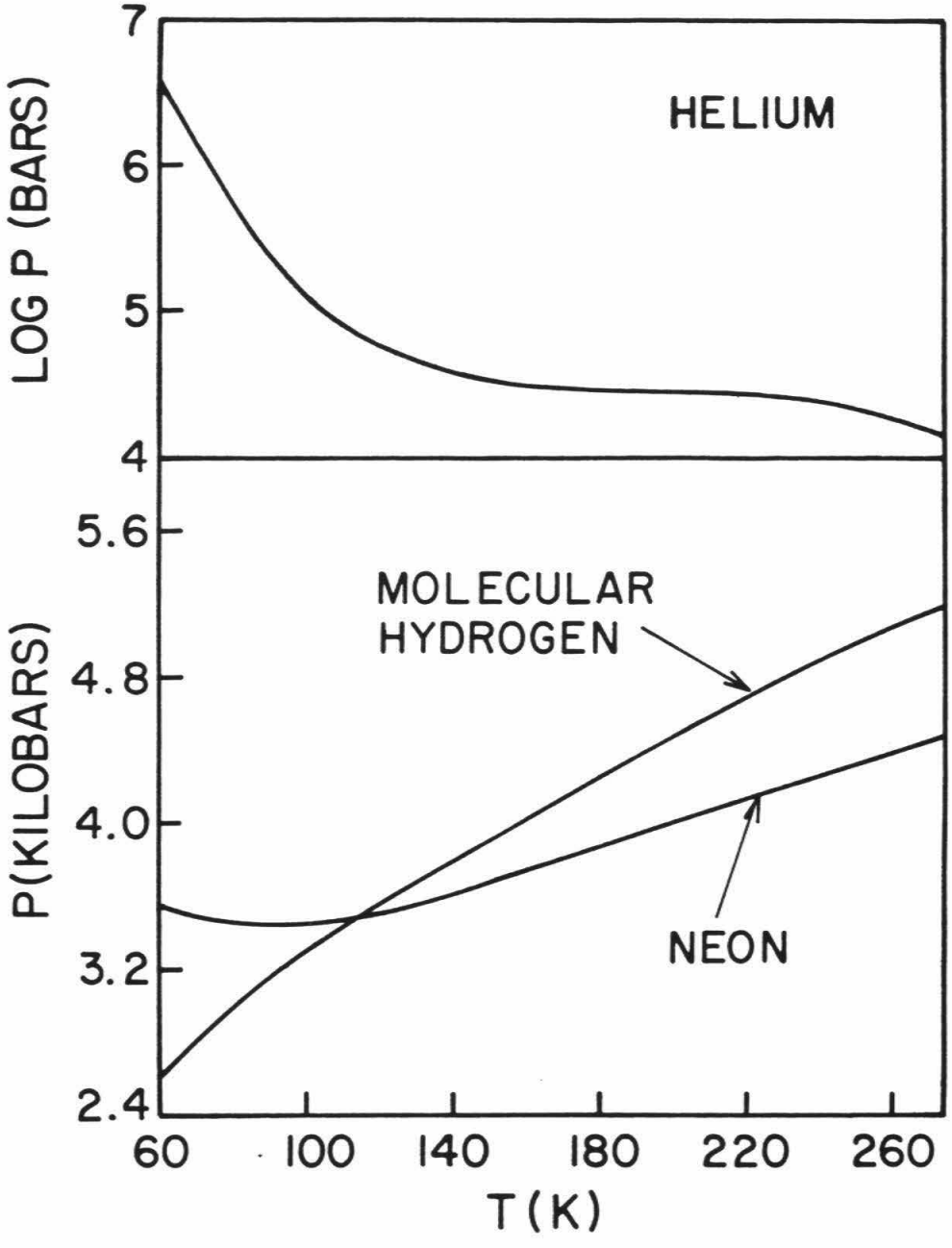
LOG P (BARS)
7
6
5
4
HELIUM
P(KILOBARS)
5.6
4.8
4.0
3.2
2.4
MOLECULAR
HYDROGEN
NEON
60
100
140
180
220
260
T(K)

Figure 5. Dissociation pressure versus temperature for CO and O_2 clathrates predicted from theory. Cross marks O_2 data at ~272 K from van Cleef and Diepen (1965). The N_2 dissociation pressure line would be essentially coincident with that for CO on this scale.

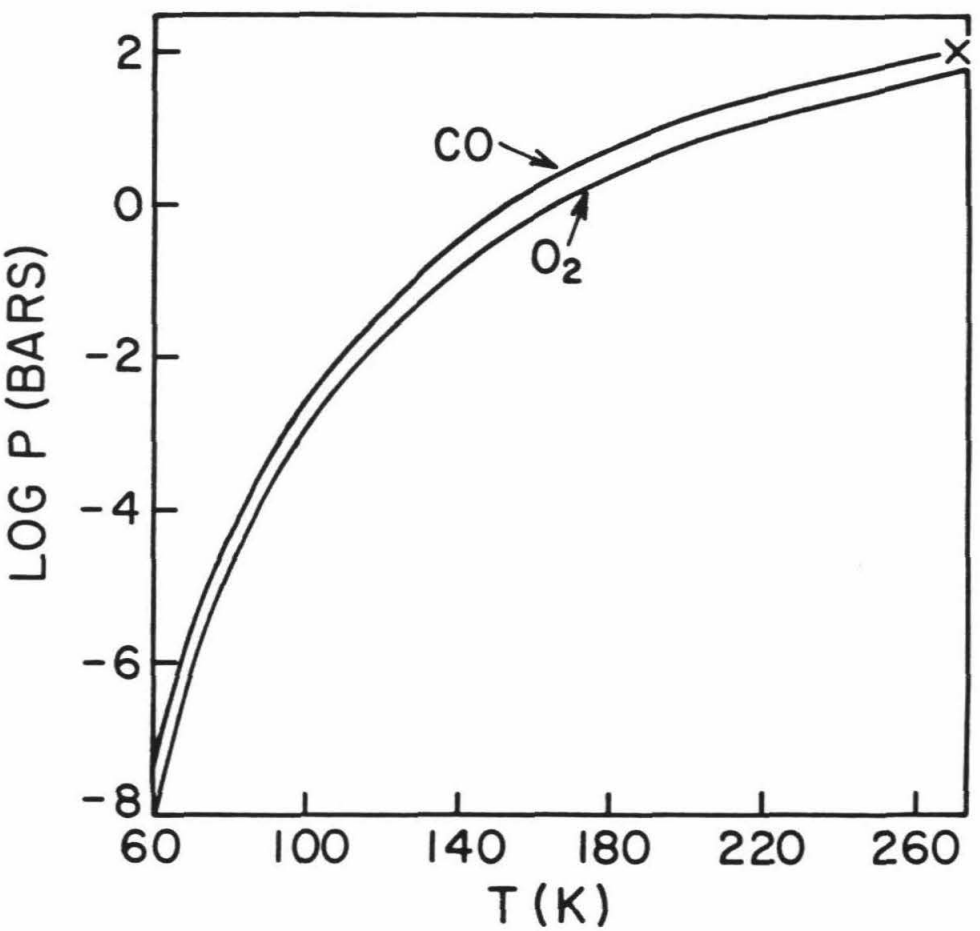
2
0
-2
-4
-6
-8
LOG P (BARS)
CO
O_2
60
100
140
180
220
260
T (K)

distinguishes it from the nonpolar N_2. Although a residual, fluctuating dipole field may be produced by the clathrate cage (Davidson, 1971) the induction force generated on nonpolar guest molecules is accounted for in the force parameters derived from experimental data. The interaction should be similar for similar molecules, hence, our bootstrapping procedure for deriving force constants for one guest species from that of others. Note that the effective L-J parameters for the water molecule derived from argon are similar to those derived from N_2, ε_ω/k_B = 152.7, ρ_ω = 3.72 Å vs. 152.7, 3.84 Å. Hence for nonpolar guest molecules, the nature of the interaction with the cage is the same. The polar nature of CO implies that an additional dipole-dipole interaction between CO and the cage field must be incorporated in the potential. There are two opposing effects: (1) the additional attractive term lowers the dissociation pressure, and (2) at low temperature the CO dipole may orient, restricting the rotational degrees of freedom and raising the dissociation pressure. The first effect is straightforward to calculate. The interaction potential energy between the CO dipole moment ξ_{CO} and that of another dipole ξ_p, averaged over all orientations is (Prausnitz, 1969, p. 57)

$$\bar{\Gamma}_{ij} = \frac{-\frac{2}{3}\,\xi_{CO}^2\,\xi_p^2}{r^6\,k_B T} \qquad (10)$$

The CO molecule interacts with a variable cage-averaged dipolar field estimated by Davidson (1971) to be roughly comparable to that of a

single water molecule. To examine the effect of equation (10) we use a somewhat large value of $\xi_p = 2\xi_{H_2O}$, and plot in Figure 6 P'/P, the ratio of CO clathrate dissociation pressure including the dipolar term to that given in Figure 5. The Boltzmann factor in $\bar{\Gamma}_{ij}$ produces the strong temperature dependence. The weakness of the CO dipole means that P' differs appreciably from P only at $T \lesssim 100$ K. For Davidson's most probable field strength P'/P is nearly unity down to 60 K.

Opposing this stabilization of CO clathrate is the possible loss of one or both rotational degrees of freedom of the CO molecule at low temperatures due to the oriented nature of the cage dipolar field. Infrared spectra of ethylene oxide structure I clathrate suggests reorientation of the guest becomes strongly inhibited at low (~50–100 K) temperatures (Bertie and Jacobs, 1977). If the excitation of rotational degrees of freedom of the encaged molecule is less than that of a free molecule, then $z < 1$ but $\omega(r)$ must necessarily be larger (equation (3)). The net effect should always be increased stability of the clathrate (i.e. lower dissociation pressure) since if it were not more stable, the guest molecule would spontaneously revert to the freely rotating state with a release of energy (c.f. Mazo, 1964). In reality, the situation is somewhat more complex since the parameters in the potential have been adjusted to fit data that may include some of the effects of rotational inhibition. The net effect of hindered rotation can not be accurately calculated, therefore.

However, we can get a rough measure of the possible magnitude of the effect from the Helmholtz free energy difference ΔF between the non-

Figure 6. Ratio of CO clathrate dissociation pressures for two models of the CO-cage interaction, plotted as a function of temperature. P is the dissociation pressure assuming dispersion and cage dipole-CO induced dipole interactions; P′ includes CO dipole interaction with dipole field of cage.

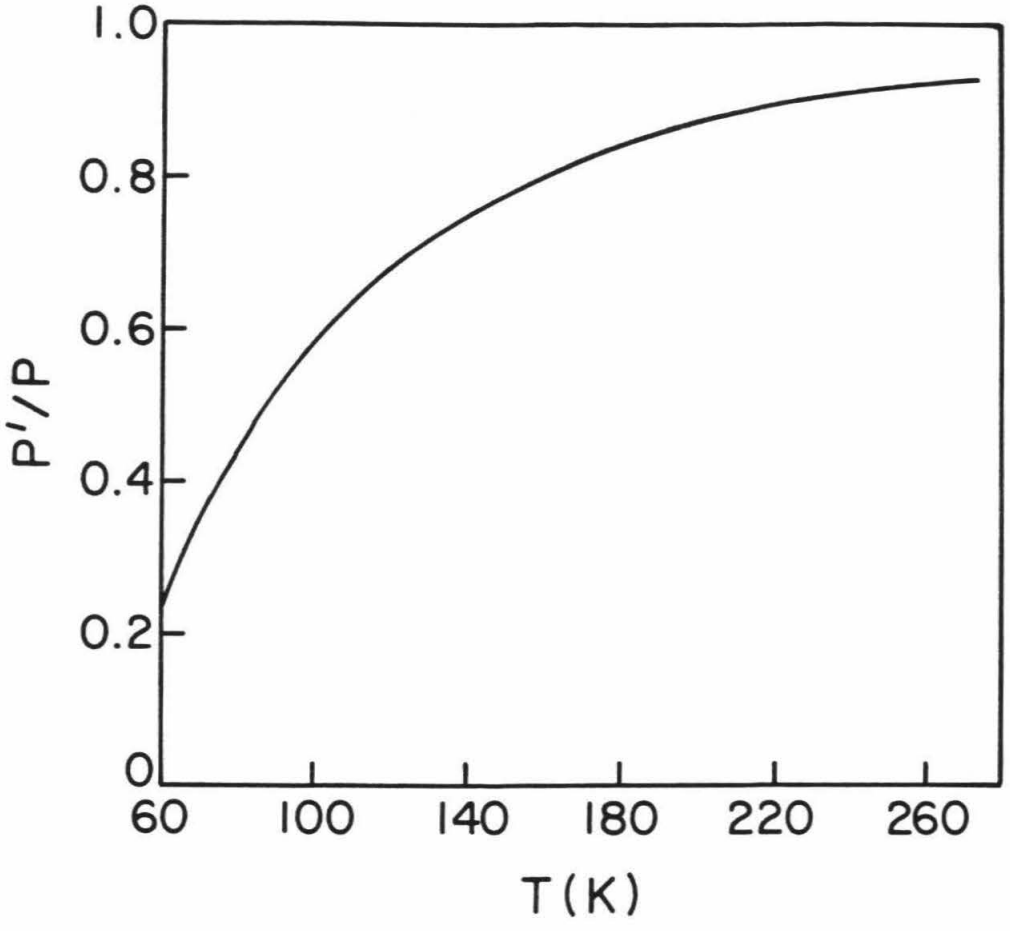
1.0
0.8
0.6
0.4
0.2
0
P'/P
60
100
140
180
220
260
T(K)

rotating molecule and the freely rotating diatomic molecule:

$$\Delta F \simeq RT \ln \left(\frac{i\, I k_B T}{\hbar^2} \right) - \Delta E - RT \ln N \qquad (11)$$

(Landau and Lifshitz, 1969; p. 115 and p. 132), where I = moment of inertia of molecule, $\hbar$ = Planck's constant divided by 2π, N = number of cage sites per unit cell (~8), ΔE = energy gained over spherically averaged state by oriented guest molecule, i = 1 for like, 2 for unlike nuclei. Using ΔE = 180 cal/mole derived for chlorine (Davidson, 1971) we find ΔF is negative (clathrate stabilized by hindrance) for $T \lesssim 110$ K for N_2 and $\lesssim$70 K for CO. Even where ΔF is positive it is small compared to the energy of encagement (Barrer and Edge, 1967) because of cancellation of terms.

We conclude that the dissociation pressure of CO clathrate is similar to, but less than, that of N_2 clathrate. At 60 K the ratio of CO to N_2 clathrate dissociation pressures could be as low as 1/20 but probably closer to 1/4.

3.4. Double Occupancy of Cage sites

We now consider the possibility of double occupancy of cage sites by small molecules (suggested by Van der Waals and Platteeuw, 1959); in particular, methane-molecular hydrogen double occupancy. Neon and helium are only briefly considered, the former because of its low solar abundance relative to hydrogen (Anders and Ebihara, 1982) and the latter

because of its exceedingly low Langmuir constants, even compared to H_2. In calculating the importance of this effect for the situation of a gaseous nebula around the sun or a giant planet, we anticipate somewhat the result that the degree of incorporation of a guest molecule in clathrate relative to other guests is directly proportional to the relative abundance in the coexisting gas. Also, for simplicity, we use a square well cage potential (Prausnitz, 1969, p. 109) in the model which follows. Although the shape of the Lennard-Jones or Kihara potentials is different, the force parameters for the guest-cage interaction are chosen such that the ''width'' of the square well potential is comparable to the average width of the attractive portion of the L-J potential. (Width refers to the value of r for a particular value of the potential $\omega(r)$.)

Consider a molecule with Langmuir constant C_M occupying the large cage of a structure I clathrate, and a second molecule with Langmuir C_H << C_M. Equation (10) can be generalized to read (writing out the large cage term only):

$$\frac{\Delta\mu^{\beta}}{kT} = \frac{3}{23} \ln \left(1 + C_M P_M + C_H P_H + q_{MH} C_M C_H P_M P_H + \frac{1}{2} q_{MM} C_M^2 P_M^2 + \frac{1}{2} q_{HH} C_H^2 P_H^2\right) \quad (12)$$

where P_M, P_H are the partial pressures of M and H in the gas, and q_{ij} gives the probability of double occupancy of a cage site by molecules i and j. Note that in the Van der Waals and Platteeuw theory $q_{ij} = 0$ by assumption. Here it is calculated as

$$q_{ij} = 1 - \frac{V_{E,i}}{V_{cage}} \tag{13}$$

where $V_{cage} = 4\pi/3(a - \sigma_j)^3$ is the volume available for occupation of the cage by molecule j and $V_{E,i}$ is the excluded volume due to occupation by i, given by the common volume of spheres of radius $a - \sigma_j$ and σ_i. σ_j is the square-well collision diameter for molecule j's interaction with H_2O molecules in the cage while σ_i is the value for molecule i's interaction with molecule j. Recall $\sigma^6 = \rho^6/2$. Figure 7 illustrates the intersection. In employing this model we have made the somewhat artificial assumption that one molecule is fixed at the center of the cage while the other is forced to occupy other regions in the cage. This introduces some asymmetry in the results for two different molecules (i.e. $q_{HM} \neq q_{MH}$) but is adequate for our purposes.

Evaluating the volume of the region of intersection of the two spheres we find:

$$V_{E,i} = \pi\{ (a - \sigma_j)^3 \left[\frac{2}{3} - \cos\theta_2 + \frac{1}{3}\cos^3\theta_2 \right]$$

$$+ \sigma_i^3 \left[\frac{2}{3} - \cos\theta_1 + \frac{1}{3}\cos^3\theta_1 \right] \} \tag{14}$$

$$\theta_1 = \pi/2 - \theta_2/2$$

$$\theta_2 = 2\sin^{-1}\frac{\sigma_i}{2(a - \sigma_j)}$$

Using square-well parameters estimated for H_2 (σ_H) and CH_4 (σ_M) from

Figure 7. Geometric construction for clathrate double occupancy calculation. σ_i and σ_j are the collision diameters for molecules i and j, a is cage radius; the shaded region is the cage volume excluded from molecule j given by the common volume of spheres of radius $a - \sigma_j$ and σ_i.

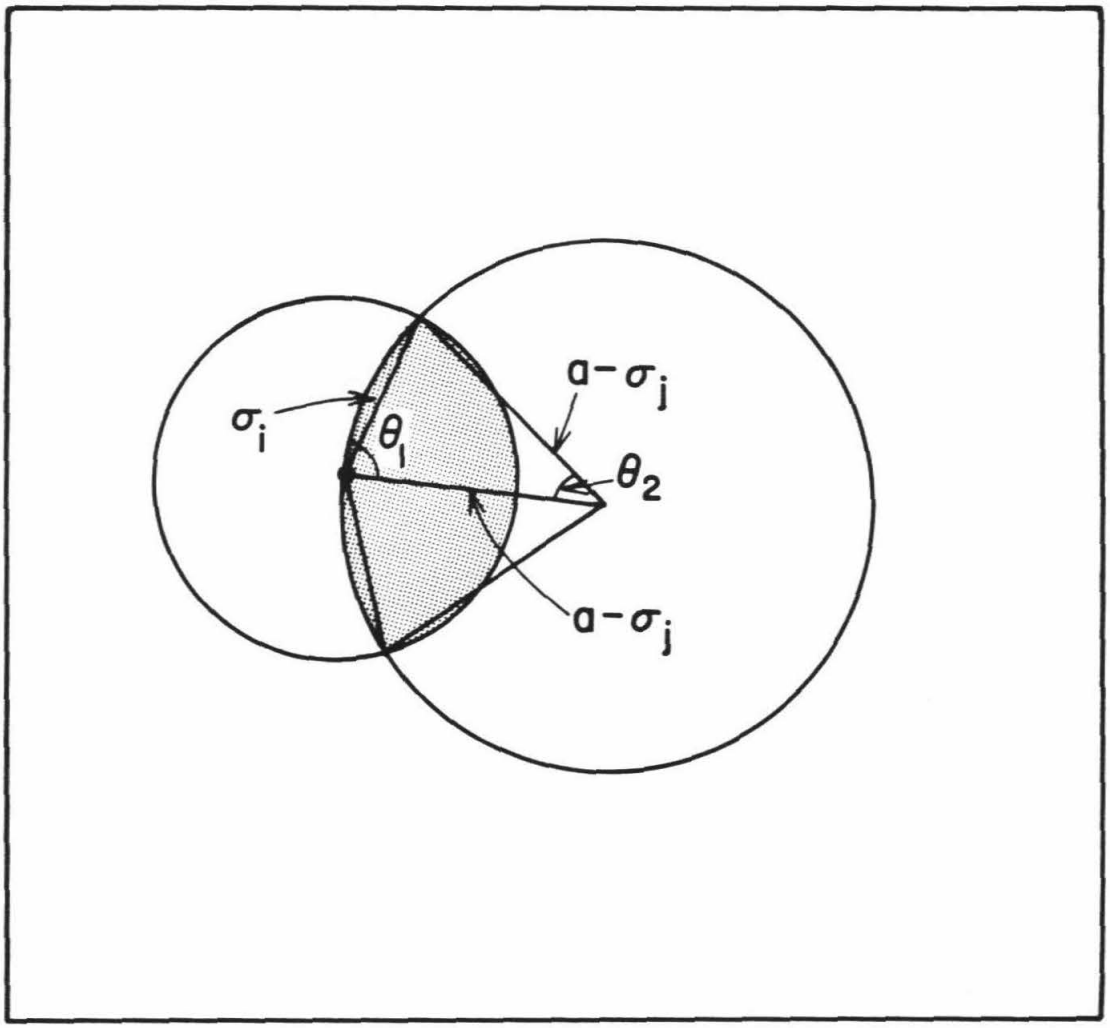
σ_i
θ_1
$a-\sigma_j$
θ_2
$a-\sigma_j$

data in Hirschfelder (1954, pp. 160, 552, 1110) we find $q_{MM} = 0$, $q_{HH} \sim 0.4\text{-}0$, $\bar{q}_{HM} \sim 0.04\text{-}0$, where $\bar{q}_{HM}$ is an average of the two permutations. The range in q reflects uncertainty in the choice of square-well parameters for these molecules; in particular, the value of σ for the guest molecule cage interaction. If the low value of σ_w in McKoy and Sinanoglu (1963) is used, we get the upper value of q. If σ_w derived in our fits is used, we find q = 0. Although we prefer our fits and choice of $\Delta\mu^\beta$ over that of McKoy and Sinanoglu, we cannot a priori rule out their selection in this calculation, nor can we rule out distortion of the cage structure to accommodate H_2. We apply the double occupancy model to clathrate composition in primordial nebulae in section 7.

4. Clathrate Equilibria at Moderate Pressures in the Presence of Ammonia

We now turn to the problem of clathrate equilibria in the presence of ammonia. Prinn and Fegley (1981) concluded that in proto-satellite nebulae, the abundance of NH_3 should be comparable to or much greater than that of N_2. At nebular gas (H_2) pressures of 0.1 bar, if most of the nitrogen is in the form of ammonia, then the latter will condense out as a stoichometric hydrate, $NH_3 \cdot H_2O$, at 130 K. Clearly, then, Titan and perhaps the small Saturnian satellites (Stevenson, 1982a; Ellsworth and Schubert, 1983), may have incorporated large quantities of ammonia, perhaps as much as 15% of the total ice budget. We wish to determine what effect ammonia could have on clathrate formation in nebular and higher pressure environments. In this section we calculate equilibria between the ammonia hydrates and clathrate, and between clathrate, water ice, and an ammonia-water solution. These relationships are displayed on a single slice of an NH_3-H_2O-CH_4 phase diagram (Fig. 8). Here we restrict ourselves to moderate pressures for which pressure corrections to the fugacities of the various components is negligible or of secondary importance; in the next section we present a model for clathrate equilibria (including the presence of ammonia) for pressures in excess of a kilobar.

The phase diagram for the ammonia-water system at moderate pressures is fairly well established (see e.g., Clifford and Hunter, 1933;

Rollet and Vuillard, 1956; Chan and Giauque, 1964; Tsiklis et al., 1965; Lewis, 1969; van Kasteren, 1973; and Miller, 1974). The last reference contains an excellent depiction of the phase diagram which therefore will not be reproduced here. It is characterized by three eutectics, at ~33, 57, and 80 mole percent ammonia, defining minimum melting points between the solids H_2O, $NH_3 \cdot H_2O$, $2NH_3 \cdot H_2O$, and NH_3. Because the solar N to O ratio is ~0.13, the low-ammonia eutectic (at 33%) is particularly relevant to solar system applications; its minimum melting-point is 172 K, the coexisting solids being pure water ice and NH_3-H_2O (''ammonium hydrate''). We neglect the presence of an $NH_3 \cdot 2H_2O$ solid for two reasons. First, its domain of stability in equilibrium with the solution is very small (Rollet and Vuillard, 1956); hence, the chemical potential of the dihydrate is only slightly less than that of the monohydrate plus water. Data on specific heats and entropies of the phases (Giauque and Stout, 1936; Dorsey, 1940; Hildenbrand and Giauque, 1953; Chan and Giauque, 1964) indicate this to be true down to temperatures <100 K. The dihydrate is difficult to make in the laboratory compared to the monohydrate (Fink and Sill, 1982). We conclude that under planetary formation conditions monohydrate + water ice could condense out in preference to dihydrate. Secondly, if dihydrate did condense out in the primordial gas, a roughly two- to four-fold excess in CH_4 gas pressure over the clathrate dissociation pressure would be sufficient to cause conversion to monohydrate plus methane clathrate. This conclusion is based upon a simple calculation analogous to one presented below for the monohydrate in a CH_4 gas, but should be regarded as an estimate

because of the lack of data on the vapor pressure of the dihydrate. Behavior of the $NH_3 \cdot H_2O$ melting curve at high (> kilobar pressures) is under investigation by Johnson et al., 1984).

At low temperatures and pressures in the presence of ammonia, a ''competition'' would be expected to ensue between the methane which seeks water ice so as to form clathrate, and ammonia which would like to form a stoichometric hydrate. At higher temperatures and pressures, the liquid ammonia-water field would also be expected to affect the stability of the coexisting clathrate, since the energy cost in converting liquid water to clathrate hydrate structure differs from that of water ice, and results in a different slope to the dissociation pressure-temperature curve.

In what follows we make the following assumptions: (1) NH_3 does not incorporate as a guest molecule in clathrate, and (2) NH_3 does not incorporate in the cage-forming ice clathrate lattice, nor does it form a clathrate lattice structure of its own. Although no experiments relevant to these assumptions have been made, finite occupancy of cages for (1) by NH_3 molecules is required by statistical mechanics but this is likely to be a small effect in most situations of interest, where the NH_3 partial pressure is very low because of the formation of a stoichometric ammonia hydrate. The Langmuir constant for NH_3 occupancy of the large cage was estimated by including contributions from dispersion forces and dipole interaction between NH_3 and the cage dipole moment (Davidson, 1971). Although the Langmuir constant is large compared to that for CO or CH_4 (because of the dipole interaction) the

fugacity of NH_3 in the NH_3-H_2O solution is low so that even at room temperature NH_3 occupies a small fraction of cages compared to CO or CH_4. (2) is more difficult to justify but the greater dipole moment of H_2O than that of NH_3 and high propensity for water hydrogen bonding suggests cages would be composed primarily of water molecules.

The above assumptions allow us to equate chemical potentials for the ammonia hydrates and clathrate and evaluate them using properties known from laboratory data or calculated from section 3. Since complete clathrate and hydrate formation would exhaust the available water ice in a solar composition nebula, we examine phase equilibria between the following assemblages:

a) NH_3-$H_2O_{(L)}$ + $CH_{4(FL)}$

b) NH_3-$H_2O_{(L)}$ + $CH_4 \cdot 6H_2O$ + $CH_{4(FL)}$

c) NH_3-$H_2O_{(L)}$ + Ice I + $CH_{4(FL)}$

d) $NH_3 \cdot H_2O_{(s)}$ + Ice I + $CH_{4(FL)}$

e) $NH_3 \cdot H_2O_{(s)}$ + $CH_4 \cdot 6H_2O$ + $CH_{4(FL)}$

f) $2NH_3 \cdot H_2O_{(s)}$ + $CH_4 \cdot 6H_2O$ + $CH_{4(FL)}$

Here (s) = solid, (L) = liquid), (FL) refers to vapor, liquid, or supercritical phase as appropriate, $CH_4 \cdot 6H_2O$ indicates methane clathrate, and Ice I is pure hexagonal water ice I. The effect of methane solubility in the liquid ammonia-water is neglected as it is small under these conditions (Culberson, 1951; Wiebe and Gaddy, 1937); it is examined more carefully in section 5.

We deal first with equilibria between (b) and (c), and (d) and (e), and restrict ourselves for the moment to an ammonia mole fraction relative to water of 15% (~solar). In the corresponding water-ammonia system, at T less than 249 K, water ice forms with consequent enrichment of the liquid in ammonia until the eutectic at 172 K is reached, at which point ammonium hydrate freezes out in coexistence with water ice, the ratio of the two being ~0.18. The methane pressure at which clathrate forms is dictated by the equilibria given in equations (1) and (2). Since the ammonia-water solution is in coexistence with pure water ice, the additional condition

$$\mu^{L}_{H_2O} = \mu^{I}_{H_2O} \qquad (15)$$

holds, where $\mu^{L}_{H_2O}$ is the chemical potential of water in the ammonia-water solution and $\mu^{I}_{H_2O}$ that in ice I. With the additional constraint that the solubility of methane in ammonia-water solid or liquid is negligible, the equilibria between clathrate, methane vapor and water ice is identical to the pure water case, and hence the dissociation pressure of methane clathrate is unchanged. The abundance of clathrate is then limited by the amount of water ice in coexistence with the ammonia water solution. The same is true below the 172 K eutectic, where 85% of the water is available for clathration.

Thermodynamics also predicts the formation of clathrate from water in the ammonia-water solution and even from the ammonia hydrate. We deal with the latter case first (i.e. assemblages (e) and (f), no

free water ice present); the equilibrium is essentially:

$$CH_4(FL) + 12(NH_3 \cdot H_2O)(s) \quad \langle = \rangle \quad CH_4 \cdot 6H_2O + 6(2NH_3 \cdot H_2O)(s) + CH_4(FL) \tag{16}$$

In terms of chemical potentials:

$$\mu_{2NH_3-H_2O} + \mu^{cl}_{H_2O} = 2\mu_{NH_3-H_2O} \tag{17}$$

Now

$$\mu_{NH_3-H_2O} = \mu^{v}_{NH_3} + \mu^{v}_{H_2O}$$

$$= kT \left(\ln \frac{P^{NH_3-H_2O}_{NH_3}}{P^{R}_{NH_3}} + \ln \frac{P^{NH_3-H_2O}_{H_2O}}{P^{R}_{H_2O}} \right) \tag{18}$$

and

$$\mu_{2NH_3-H_2O} = kT \left(2 \ln \frac{P^{2NH_3-H_2O}_{NH_3}}{P^{R}_{NH_3}} + \ln \frac{P^{2NH_3-H_2O}_{H_2O}}{P^{R}_{H_2O}} \right) \tag{19}$$

where μ^{v}_{x} = chemical potential in the vapor phase of constituent x, p^{y}_{x} = vapor pressure of constituent x over solid compound y, and P^{R}_{x} is a reference pressure for the pure component x at the system temperature T.

Now let

$$\mu^{cl}_{H_2O} - \mu^{I}_{H_2O} = \Delta\mu^{o} - \nu kT \ln C_{CH_4} P_{CH_4} \qquad (20)$$

where $C_{CH_4} P_{CH_4} >> 1$, $\Delta\mu^{o}$ is the chemical potential difference between the empty clathrate and ice I, and for the purposes of this rough analysis we combine both cages of the clathrate ($\nu = 4/23$) and let C be the Langmuir constant of the large cage. This will give a lower bound to the pressure at which (16) occurs. Also

$$\mu^{I}_{H_2O} = kT \ln \frac{P^{I}_{H_2O}}{P^{R}_{H_2O}} \qquad (21)$$

Combining (17), (18), (19), (20), and (21) and cancelling out the reference pressures:

$$\nu\, kT \ln \frac{P^{o}_{CH_4}}{P_{CH_4}} =$$

$$kT \ln \frac{\left(P^{NH_3-H_2O}_{H_2O} P^{NH_3-H_2O}_{NH_3} \right)^2}{\left(P^{2NH_3-H_2O}_{NH_3} \right)^2} \frac{1}{P^{2NH_3-H_2O}_{H_2O} P^{I}_{H_2O}} \qquad (22)$$

where we have substituted for $\Delta\mu^{o}$ the expression $\nu kT \ln(C_{CH_4} P^{o}_{CH_4})$,

where $P^{o}_{CH_4}$ is the methane clathrate dissociation pressure in coexistence with pure water ice. Note also $C_{CH_4} P^{o}_{CH_4}$ and $C_{CH_4} P_{CH_4} >> 1$ at temperatures of interest.

To evaluate the vapor pressures of the ammonia and water constituents we use the expressions of Haudenschild (1970) who relied on Lewis (1969) as the data source. Evaluating (22) using his expression yields the result

$$P_{CH_4} = P^{o}_{CH_4} \, 10^{(0.618 + 50.54/T)1/\nu} \qquad (23)$$

Above this methane pressure $NH_3 \cdot H_2O$ is converted to methane clathrate and $2NH_3 \cdot H_2O$. The methane pressure as a function of temperature is plotted in Figure 8, for which the ammonia to water ratio is 15%. The line defined by equation (23) separates regions I and II as indicated on the figure. Note that for the given temperature range this pressure is above the saturation vapor pressure for methane (indicated by the line separating regions II and III); P_{CH_4} is thus strictly the <u>fugacity</u> of the CH_4 liquid at which the conversion occurs. An external pressure would have to be applied to raise the fugacity to the appropriate value for the conversion to occur, violating our neglect in this section of PV effects.

Extended to lower temperatures, the phase boundary pressure is 3.1×10^{-3} bar at 60 K. Recalling that this is a lower bound (if we consider only large cage occupancy $P_{CH_4} = 2.0$ bar), we conclude that this transition is not of interest to planetary or satellite formation

Figure 8. Phase diagram for methane clathrate in the presence of ammonia, plotted as methane partial pressure versus temperature. Within regions I and II the ordinate must be redefined as methane fugacity. The NH_3 mole fraction x_a (relative to ammonia + water) is 0.15. Roman numerals correspond to regions in which the following phases are stable: I: $2NH_3 \cdot H_2O_{(s)}$ + $CH_4 \cdot 5.75H_2O$ + $CH_{4(L)}$; II: $NH_3 \cdot H_2O_{(s)}$ + $CH_4 \cdot 5.75H_2O$ + $CH_{4(L)}$; III: $NH_3 \cdot H_2O_{(s)}$ + $CH_4 \cdot 5.75H_2O$ + $CH_{4(v)}$; IV: $NH_3 \cdot H_2O_{(s)}$ + ice I + $CH_{4(v)}$; V: NH_3-$H_2O_{(L)}$ + ice I + $CH_{4(FL)}$; VI: NH_3-$H_2O_{(L)}$ + $CH_{4(FL)}$; VII: NH_3-$H_2O_{(L)}$ + $CH_4 \cdot 5.75H_2O$ + $CH_{4(FL)}$. Here s = solid, v = vapor, L = liquid, FL = fluid, and $CH_4 \cdot 5.75H_2O$ = CH_4 clathrate but does not necessarily imply complete occupancy of cage sites. Point A defines CH_4 critical point and B defines the NH_3-H_2O freezing point for a 40% ammonia-water solution. Dotted lines are phase boundaries between regions VI and VII for ammonia fractions (relative to water + ammonia) other than 0.15.

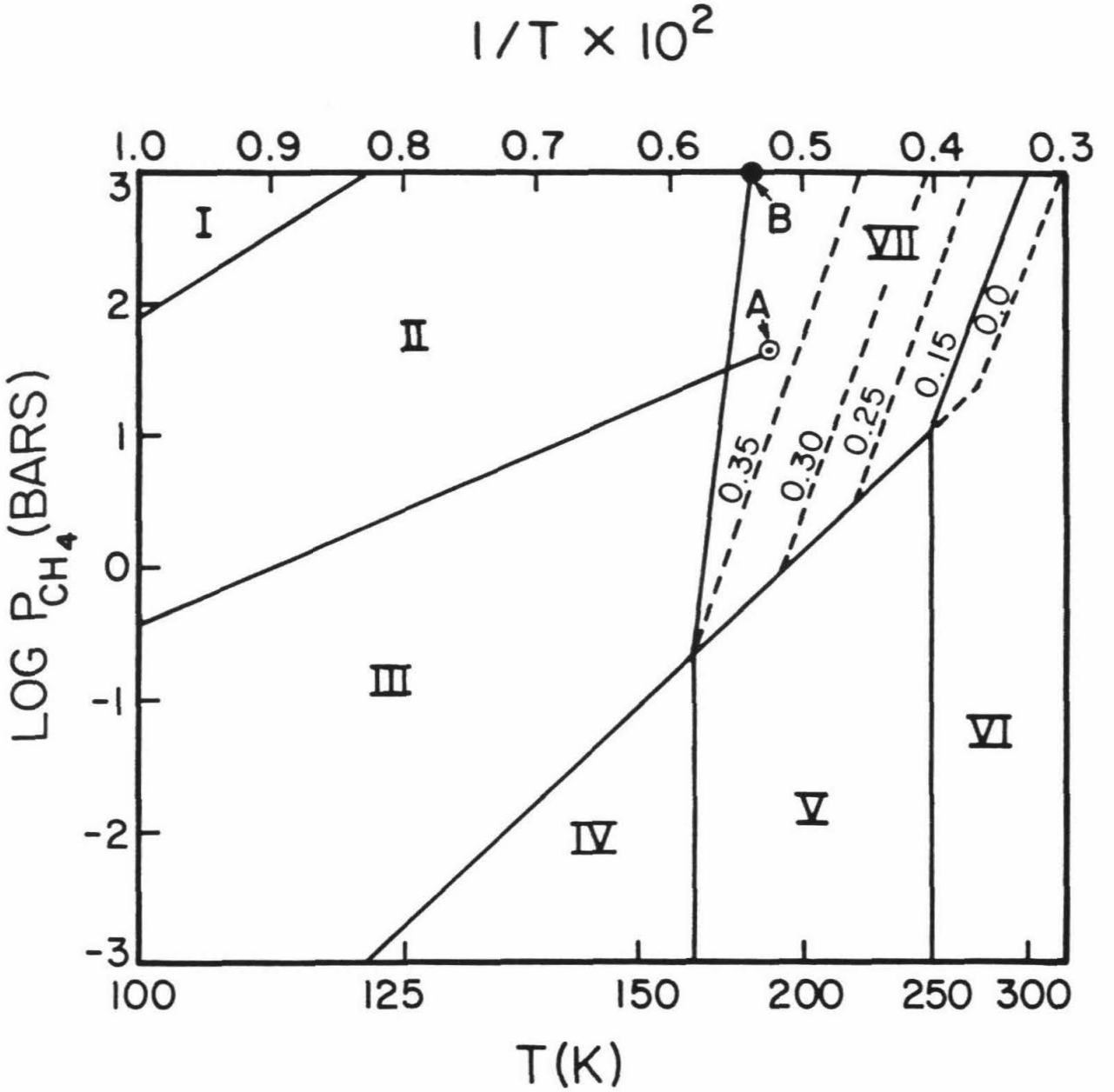
1/T × 10²
1.0
0.9
0.8
0.7
0.6
0.5
0.4
0.3
3
2
1
0
-1
-2
-3
LOG P_CH4 (BARS)
I
II
III
IV
V
VI
VII
A
B
0.35
0.30
0.25
0.15
0.0
100
125
150
200
250
300
T(K)

scenarios, since the methane itself condenses out as a solid at 10^{-4} bars and 60 K. Thus, although the conversion of $NH_3 \cdot H_2O$ to $2NH_3 \cdot H_2O$ in the presence of methane is an interesting possibility which merits laboratory investigation, at present we see no application of this transformation to solar system objects. Also, the transformation

$$6(2NH_3 \cdot H_2O) + CH_{4(g)} \quad \langle = \rangle \quad 12NH_3 + CH_4 \cdot 6H_2O$$

should occur at even higher pressures and hence is not considered here.

We now consider phase equilibrium between assemblages a) and b), i.e., clathrate formation in an ammonia-water solution in coexistence with methane vapor, no free water ice being present. The equilibrium in this case is

$$\mu^{cl}_{H_2O} = \mu^{NH_3-H_2O_{(L)}}_{H_2O}$$

so that $\Delta\mu^{\beta}$, the free energy difference between the empty hydrate cage and the coexisting water phase, is now $\mu^{\beta}_{H_2O} - \mu^{NH_3-H_2O}_{H_2O}$.

Since we are now considering the liquid water field $\Delta h(T)$ in equation (5) is dominated by the enthalpy of freezing, 1440 cal/mole. Using values from Holder et al. (1980), and ignoring the pressure term, equation (5) becomes

$$\Delta\mu^{\beta}(T) = \Delta h^{\beta} + \frac{T}{T_f}\left(\Delta\mu^{\beta}(T_o) - \Delta h^{\beta}\right)$$

$$= -1161 + 1471\,\frac{T}{T_f} \qquad (24)$$

For the ammonia-water case, T_f is the freezing temperature of water ice in the mixture. Freezing points versus ammonia mole fraction is given in Haudenschild (1970). An alternative but equivalent expression for $\Delta\mu^{\beta}$ is

$$\Delta\mu^{\beta}(T) = \Delta h^{\beta} + \frac{T}{T_f^{o}}\left(\Delta\mu^{\beta}(T_o)\right) - \Delta h^{\beta}) - kT \ln \gamma\, X_{H_2O} \qquad (25)$$

where T_f^{o} is now the freezing point of pure water, X_{H_2O} is the mole fraction of water in solution and γ is the activity coefficient of the ammonia-water solution.

Inserting (24) into (1), and using Langmuir constants derived in section 3, the methane clathrate dissociation pressure in equilibrium with a 15% ammonia-water solution is plotted as a function of temperature in Figure 8 as the solid line separating regions VI and VII. This line terminates by intersecting the dissociation pressure curve for the water ice case at the water-ice freezing point of the ammonia water solution, 249 K. A vertical line is drawn downward from this point, separating region V with NH_3-H_2O solution containing water ice from VI with no water ice. Another vertical line is drawn at 172 K where the 33% NH_3 eutectic is reached, below which temperature (IV) ammonia hydrate and water ice exist, and above which (V) water ice coexists with

ammonia-water solution. Since $P < P_{dissociation}$ for regions IV, V, and VI, the methane is a vapor or supercritical fluid.

In region VII we have plotted clathrate dissociation pressures for ammonia mole fractions in excess of 15%. These plotted lines terminate at the dissociation pressure curve for the water ice case at the appropriate water ice freezing line for the labeled concentrations. Also, the pure water case is plotted by extending the dissociation pressure curve for the water-ice case to 273 K, and using equation (24) with $T_F = T_F^o$. These dotted curves may be thought of as projections of the third dimension of the diagram, the X_{H_2O} coordinate, onto the X_{H_2O} = 0.85 slice. They define region VII in their own slice to be smaller ($X_{H_2O} < 0.85$) or larger ($X_{H_2O} > 0.85$) than in the displayed slice. Since in region VII the clathrate is produced at the expense of water in solution with ammonia, for a given temperature and methane partial pressure one may read off the concentration of the ammonia-water solution in equilibrium with the clathrate and, hence, calculate how much clathrate is produced.

Finally, we plot the boundary between regions II and VII, and III and VII, at which $NH_3 \cdot H_2O$ in coexistence with the ammonia-water solution freezes out. The line is constructed by calculating the clathrate dissociation pressure for solutions with $X_{H_2O} < 0.66$, at a temperature corresponding to the $NH_3 \cdot H_2O$ freezing point for the given liquid composition. For our pressure restrictions, the highest practical ammonia concentration is 40% ($X_{H_2O} = 0.6$). To calculate the clathrate dissociation pressure at this composition a hypothetical standard state,

that of water ice freezing out of the solution, was assumed. The use of hypothetical standard states is a common ''trick'' in fluid phase equilibrium studies (see Prausnitz, 1969, pp. 386-387).

$\Delta\mu^{\beta}$ and P_{diss} were evaluated for the solution at the appropriate $NH_3 \cdot H_2O$ freezing point calculated from Haudenschild (1970), to yield 950 bars at T = 185 K, plotted as point B on Figure 8. A line was then drawn from B down to the eutectic at 172 K on the water ice-clathrate dissociation pressure line, to define the entire $NH_3 \cdot H_2O$ freezing boundary. Although we have used low pressure data to define point B, work by Johnson et al. (1984) indicates that the $NH_3 \cdot H_2O$ freezing temperature shifts upwards by only a few degrees from 1 to 1000 bars.

The NH_3-H_2O freezing line so defined must intersect the boundary between I and II at the NH_3-H_2O congruent melting point, i.e. X_{H_2O} = 0.50. Extrapolation of both lines upwards in pressure indicates the intersection occurs at the expected temperature, but at a pressure so high ($\sim 10^5$ bars) that our neglect of low pressure corrections is no longer valid.

The graph is terminated at 10^3 bar to avoid serious modification to the diagram from pressure effects, considered in the next section. Even so, at $\gtrsim 10^2$ bars the dissociation pressure lines in VII and VI should bend slightly toward the left with increasing pressure, i.e., the dissociation pressure increases more rapidly with temperature than the figure indicates.

5. High Pressure Equilibria

Calculation of clathrate stability at high pressures requires consideration of several effects neglected in previous sections: (1) the volume increase in conversion of ice or liquid water to the empty hydrate cage begins to dominate the corresponding free energy change above a few hundred bars; (2) the fugacity of the guest molecule phase in coexistence with the clathrate is no longer the partial pressure and must be explicitly calculated in terms of the system temperature and total pressure; (3) compression of the cage sites at high pressure alters the interaction potential between guest and host molecules. In this section we present our model for incorporating these effects, display the P-T phase diagram for methane (and molecular nitrogen) clathrate stability in coexistence with pure water and water ammonia, and consider the effect of methane solubility in water. Application of our results to satellite interiors is made in section 7.

5.1. Formulation for Pure Water Case

The equations of clathrate equilibrium, valid at high pressure have been given in section 3. In constructing the high-pressure diagram, it is useful to derive a Clausius Clapeyron relation, dP/dT, from equations (1) and (2). Differentiating with respect to T, P:

$$\frac{d\Delta\mu^{\beta}}{dT}\,dT + \frac{d\Delta\mu^{\beta}}{dP}\,dP = k[\,\nu \ln(1 + Cf)$$

$$+ \frac{\nu\, T}{1 + Cf}\left(C\,\frac{df}{dT} + f\,\frac{dC}{dT} \right)]\,dT + \frac{\nu\, kT}{1 + Cf}\,\frac{Cdf}{dP}\,dP \qquad (26)$$

where we consider a single guest species, and for brevity write down terms for only a single cage -- the addition of the second is trivial. We have also assumed $fdC/dP \ll Cdf/dP$; this is justified later in this section. Superscripts on quantities referring to the guest molecule and its bulk phases are implicit; superscript β refers to differences between empty clathrate cage and coexisting water ice or liquid phase. Using standard thermodynamic relations, for the H_2O:

$$d\Delta\mu^{\beta} = \Delta V^{\beta}(P,T)\,dP - \Delta S^{\beta}(P,T)\,dT \qquad (27)$$

and for the guest species:

$$d\left(kT \ln \frac{f}{f^{o}} \right)\Big|_{P} = -(S - S^{o})\,dT = k \ln \frac{f}{f^{o}}\,dT + \frac{kT}{f}\,\frac{df}{dT}\,dT$$

$$d(kT \ln f)\Big|_{T} = VdP = \frac{kT}{f}\,\frac{df}{dP}\,dP \qquad (28)$$

where f^{o}, S^{o} are fugacity and entropy of a reference state, taken to be in the ideal gas regime of the guest molecule. Solving for df/dT and df/dP in (28), plugging these and (27) into (26) and rearranging, we find

$$\frac{dP}{dT} = k[\,\nu \ln(1 + Cf) + T\,\{\,\frac{(\,(S^o - S) - k \ln f/f^o\,)f}{kT}\,\frac{C\nu}{1 + Cf}$$

$$+ \frac{dC}{dT}\,\frac{\nu f}{1 + Cf}\,\} + \frac{\Delta S^\beta}{k}\,]\,/\,(\,\Delta V^\beta - fV\,\frac{C\nu}{1 + Cf}\,) \qquad (29)$$

for all applications in the present section $Cf \gg 1$ so

$$\frac{dP}{dT} = \frac{\nu(\,k \ln Cf + (S^o - S) - k \ln \frac{f}{f^o} + \frac{kT}{C}\frac{dC}{dT}) + \Delta S^\beta}{\Delta V^\beta - V\nu} \qquad (30)$$

Comparing equations (27) and (24) we see

$$\Delta S^\beta = -\frac{\Delta\mu^\beta(T_f, P_o) - \Delta h^\beta(P_o)}{T_f} \qquad (31)$$

$$= \begin{cases} 0 & T < T_f \\ -\dfrac{1471}{T_f}\ \text{cal/mole/K} & T > T_f \end{cases}$$

Examination of equation (30) confirms the qualitative picture given in Figure 2. Consider first the ideal gas regime. Here $(S^o - S) = k \ln f/f^o$, and for $T < T_f$ $\Delta S^\beta = 0$; then the numerator becomes $\nu k \ln CP + \nu(kT/C)(dC/dT)$. With $dC/dT < 0$, inserting values for C, P we find the numerator to be negative. The denominator is the difference (per mole of H_2O) between the volume <u>expansion</u> required to form a cage from the coexisting water phase, and the volume of the coexisting guest phase

weighted by the number of cage sites per water molecule. It is, in effect, the net volume gained or lost by converting one mole of ice (or liquid water) plus gas into clathrate. Since in the ideal gas state $V > \Delta V^{\beta}/\nu$, the denominator is negative, and dP/dT is positive, hence the dissociation pressure increases with temperature. Inserting numerical values for methane reproduces the slope of the dissociation pressure curve derived in section 3 for $T < T_f$. For $T > T_f$, ΔS^{β} is negative, and dP/dT increases. However, as P increases into the kilobar regime, V decreases sharply, while ΔV^{β} increases or decreases only slightly (see numerical evaluations below). Thus $\Delta V^{\beta} - V\nu \rightarrow 0$ and $dP/dT \rightarrow \infty$. At $\Delta V^{\beta} = V\nu$, $dP/dT = \infty$ and the curve of dissociation pressure versus temperature shows a maximum. For higher pressures dP/dT becomes negative, its absolute magnitude decreasing now with increasing pressure. All terms in the numerator are important throughout the pressure range; numerical evaluation (see below) indicates that the numerator remains less than zero throughout this regime. Eventually the dissociation pressure curve crosses the liquid water-high pressure ice phase boundary, and ΔS^{β} is again assumed zero. It is not truly zero, because the enthalpy change in going from ice I to the relevant high pressure phases is nonzero (Eisenberg and Kauzmann, 1969, p. 95). It is, however, much smaller than the ice to liquid enthalpy change, and, hence, is neglected in equation (30). The numerator drops to a small value, and with a large value for the denomenator, dP/dT becomes small, i.e., as T decreases P remains fairly constant.

We calculate the phase diagram explicitly first for pure water,

and CH_4 as the guest molecule, since it likely was the primary clathrate former incorporated in Titan. The effect of pressure dependence of the Langmuir constant, and solubility of methane in water will then be considered, followed by inclusion of an additional clathrate former, N_2. We then calculate the methane clathrate phase diagram with ammonia present.

We construct the phase diagram by evaluating equations (1) and (2) along an isothermal path in pressure. The methane fugacity f given by these equations is compared with the fugacity of the coexisting pure methane phase f_c at each pressure which is calculated essentially from (4) as described below. Where $f_c > f$, the clathrate is stable. Equation (30) is also used to determine the slope of the high pressure phase boundary at each temperature point since uneven quality of the data result in some scatter of this boundary at various temperatures. Above the water-ice field the low and high pressure phase boundaries curve rapidly toward each other with increasing temperature; equation (30) is used to define the slope at the high pressure water-ice phase boundary as well as the ''critical'' pressure at which $dP/dT = \infty$. High temperature clathrate stability data in the $P < 4$ kilobar regime (Marshall et al., 1964) is connected smoothly to the critical pressure point, defining a maximum temperature of clathrate stability. The high pressure end of the diagram, extended through the ice-liquid boundary via (30), (1), and (2), is joined smoothly to the critical temperature-pressure point to complete the clathrate stability region.

To do the calculation, quantitative evaluation of $\Delta\mu^\beta$ and f_c as a

function of temperature and pressure is required. We re-write the pressure dependence of $\Delta\mu^\beta$ as

$$\Delta\mu^\beta(T,P) = \Delta\mu^\beta(T,P_o) + \sum_i \int_{P_{i-1}}^{P_i} \Delta V_i^\beta(T,P)\, dP \qquad (32)$$

where we have broken up the pressure integral into intervals corresponding to phases of water encountered along the isothermal path. Within each phase, however, $\Delta\mu^\beta$ is still a function of pressure. Equations for density as a function of temperature and pressure for water ice are given in Lupo and Lewis (1979); these are fits to data in previous sources. Several of these sources were checked independently (Bridgeman, 1913; Bridgeman, 1937; Dorsey, 1940, p. 212) to verify that at high (~10 kbar) pressure the Lupo and Lewis fits agree with the data to within ~1%. Phase boundaries for the water system were determined from Eisenberg and Kauzmann (1969, p. 93) and Lupo and Lewis (1979).

The compressibility of the clathrate cage, on the other hand, is not well known. The existing data on sound velocity in clathrate give a value within 20% that of ice I and only weakly dependent on type of guest molecule (Pearson et al., 1983; Stoll and Bryan, 1979). Also, the volume thermal expansivity of clathrates has been assumed similar to that of ice I in previous studies (Pearson et al., 1983). We therefore assume

$$K^\beta = \frac{1}{V}\frac{dV}{dP}\Big|_T^{\text{clathrate}} = \frac{1}{V}\frac{dV}{dP}\Big|_T^{\text{ice I}} \qquad (33)$$

where the ice I value is given in Lupo and Lewis (1979). A calculation by Whalley (1980) is consistent with equation (10). We use K^{β} = constant. We also assume that the clathrate undergoes no structural phase transitions in the pressure range under consideration. Although no experimental data exist to justify these assumptions, and there is some weak evidence supporting the existence of a metastable high pressure modification of clathrate (Ross and Andersson, 1982), we adhere to the simplest approximation here. Varying K^{β} for the clathrate (for example setting it equal to that of the coexisting high-pressure form of ice) below 273 K changes $\Delta\mu^{\beta}$ in the high pressure regime by ~1-3% and the pressure of the clathrate phase boundary by 10-20%, which is not crucial. In the liquid water region, however, the phase boundary pressure is very sensitive to the choice of K^{β}. As indicated above, however, data in the ''low'' (<4 kilobar) region as well as the results in the high pressure ice field constrain the clathrate stability boundary in the liquid water field, since the boundary must be continuous across the ice-liquid boundary. Our choice of K^{β} seems to produce the most consistent clathrate stability boundary under the given constraints.

Using the above data and models we calculate ΔV^{β} and write it within each water phase region as linear with pressure. Hence, the form of $\Delta\mu^{\beta}$ is:

$$\Delta\mu^{\beta}(T,P) = \Delta\mu^{\beta}(T,P_{o}) + c + bP + aP^{2}$$

where the constants c, b, and a apply to the particular water ice phase

stable at temperature T and pressure P.

Calculation of the methane fugacity $f_c(T,P)$ differed depending on the temperature because of uneven data coverage and complications in integrating pressure-volume data near the methane critical temperature, 190 K. Figure 9 illustrates the techniques used to evaluate equation (4) on a P-T plot of the pure methane phase diagram. The fugacity at 100 K is calculated by a direct P-V integration up to the region of interest, found by rough calculation to be ~10 kilobars, using Goodwin's (1974) data at pressures up to 700 bars and joining that to high pressure methane ice data fits constructed by Lupo and Lewis (1980), with liquid-solid phase boundary pressure and ΔV data of Cheng et al. (1975). Since the freezing pressure is 377 bar at 100 K, volume data were available continuously throughout the liquid and solid regime. At other temperatures:

$$f_c(T,P) = f_c(T,P_s(T)) \exp \{ \frac{1}{kT} (- \int_T^{100\ K} S(T',P_s)\ dT') + \int_{P_s(T)}^{P} V(100\ K,P')\ dP' - \int_{100\ K}^{T} S(T',P)\ dT') \} \qquad (34)$$

where $P_s(T)$ = vapor pressure (or extrapolated vapor pressure) at T. Normally the calculation was done to two pressures, 5 and 10 kilobar and then a linear fit of log f_c to P constructed for convenience, since the Lupo and Lewis equation of state fit is good to only ~8 kilobar. This approximation turns out to be accurate if the resulting dissociation pressure is not too far above 10 kilobars, as is the case.

Figure 9. Schematic phase diagram of methane, plotted as pressure versus temperature, illustrating thermodynamic paths taken to calculate fugacity. Beginning at point A on the liquid-vapor boundary, fugacity at D was calculated by integrating along A-D, as well as along A-B-C-D.

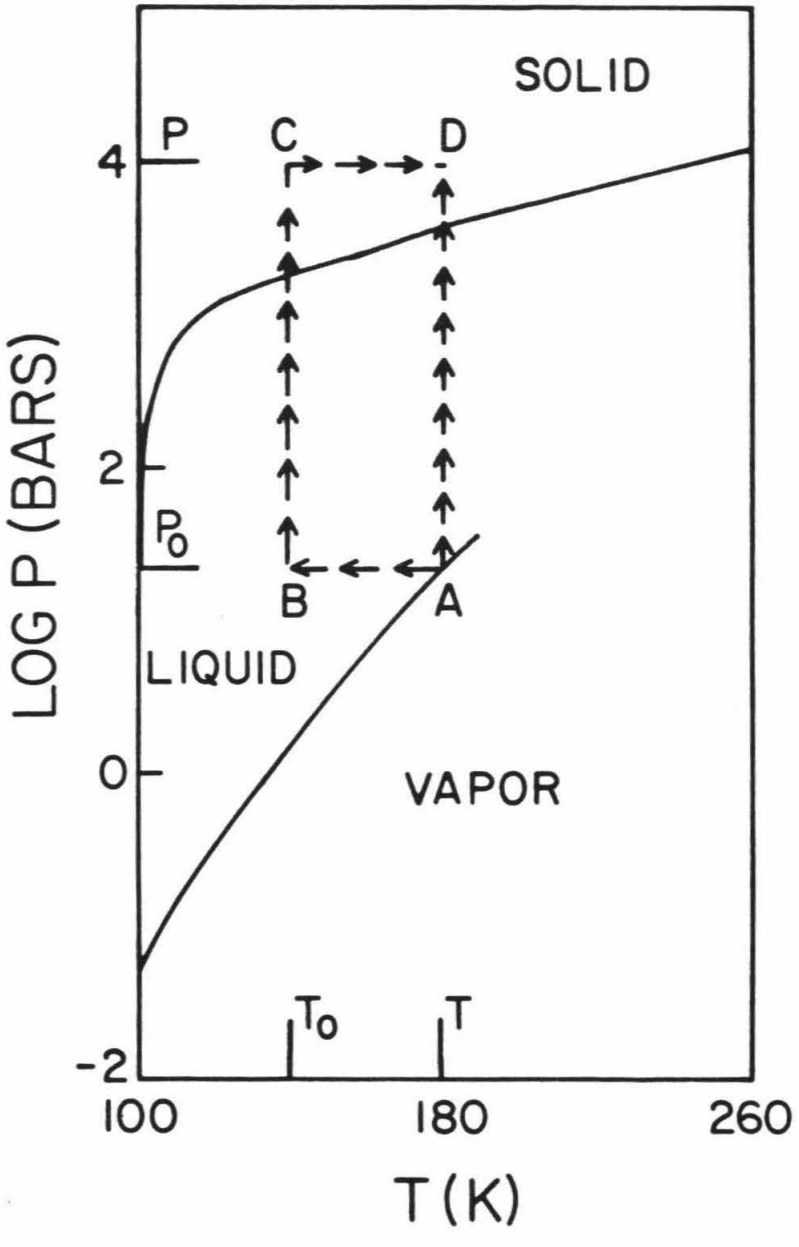
SOLID
P
C
D
4
2
P_o
B
A
LIQUID
0
VAPOR
T_o
T
-2
100
180
260
LOG P (BARS)
T (K)

Low-pressure entropy was evaluated using a linear fit from Goodwin (1974). Entropy at the high pressure end was calculated at each temperature T by

$$S(T,V) = \int_{V_o}^{V} \frac{dP}{dT}\Big|_V dV + S(T,V_o) \qquad (35)$$

$S(T,V_o)$ was read off from Goodwin (1974) at 700 bar in the liquid methane field along with the corresponding volume V_o. $dP/dT|_V$ was then derived from the same source, and in the absence of additional data assumed constant up to the liquid-solid boundary pressure. Here the entropy change of freezing from Cheng et al. (1975) was added, and then the volume integration continued in the solid field using the empirical fit of Lupo and Lewis (1980). The integration was stopped at 10 kilobar at a volume estimated from the Cheng freezing curve data, assuming a negligible coefficient of thermal expansion. Since the additional entropy contribution in the solid field amounted to only a few percent of the total, the small error introduced by estimating the final volume was acceptable.

Because of the uncertainties inherent in the above technique, it was desirable to calculate the entropy difference between T and 100 K at high pressure in an independent fashion. Here S was calculated using the specific heat at constant volume of the methane ice:

$$S(T,P) - S(100\ K,P) = \int_{100}^{T} C_v(T',P) \frac{dT'}{T'} \qquad (36)$$

where the Debye model for solids yields (Reif, 1965, p. 415):

$$C_v = C_v^{\text{lattice}} + C_v^{\text{rotational}} = x\ 3k + \frac{3}{2}k \qquad (37)$$

where the rotational but not vibrational states of the methane molecule are excited at the relevant temperatures (Kerley, 1980). The parameter x in (37) is less than unity since the estimated Debye temperature for methane is in excess of 100 K; we estimate $x \sim 0.8\text{–}0.9$. The Debye model yields ΔS from (36), for T in the range 100–230 K, that is generally within 10% of the value derived above from thermodynamic quantities. The agreement is adequate for our purposes. We then apply a linear fit to S between T and 100 K to calculate $f_c(T,P)$ via (34).

As a check, using available volume data at 180 K from the above sources, we integrated along an isothermal path to compare the resulting fugacity at 10 kilobar with that derived from the above techniques. The two agree to within 35%, which is acceptable considering the uncertainties in the thermodynamic quantities derived above.

At $T \gtrsim 300$ K data from Robertson and Babb (1969) on fluid methane volumes were available to find $f_c(T,P)$ by isothermal V(P) integration. Their data were presented from 2 to 10 kilobar at 308, 373, and 473 K, and were fitted to an isothermal linear function of pressure at 3 and 10 kilobars. At other temperatures, thermal expansion coefficients derived from the data were used to interpolate or extrapolate the volume data to the new temperature. Data in Goodwin (1974) to 700 bar were likewise linearly fitted, and a linear interpolation made between 0.7 and 2

kilobars. Numerical integration by discrete Simpson's approximation of the volume data available showed the linear fits overestimate the $\int V\, dP$ integral by 11% from 700-300 bar and 2% from 2000-10000 bar. The linear fits to volume were thus adjusted slightly to produce a better fit. The fugacities were calculated by equation (4) with P_o = 300 bar at which $\phi \sim 1$. (In this supercritical regime extrapolations from the vapor pressure curve cannot be made accurately; we pick a convenient pressure for which ϕ is roughly = 1 to begin the integration.) Fugacity calculations by Saito et al. (1964) at moderate pressures indicate ϕ (300 K, 300 bar) ~ 0.7, for which our calculation of dissociation pressures at $P < 4$ kilobar fits the Marshall et al. (1964) data more closely than for $\phi = 1$. At the high pressure end (>10 kilobar) the two different values of ϕ alter the derived dissociation pressure by $\lesssim$20%; we use $\phi \sim 0.7$ for consistency. The form of the methane fugacity at $T > 273$ K was expressed as

$$f_c = 0.7 \times 300 \text{ bar} \cdot \exp \frac{1}{kT} (D + EP + FP^2) \qquad (38)$$

with D, E, and F derived from Goodwin (1974) and Robertson and Babb (1969), different in the intervals P = 300-700 bar, 700-2000 bar, >2000 bar. As a check, the Robertson and Babb volume data were extrapolated down to 250 K, f_c calculated at 10 and 12 kilobars and compared with the value calculated using (34). The fugacities disagree by 9% at 10 kilobar, and 18% at 12 kilobars. Since the two techniques primarily use different data sets, this agreement gives confidence in both data and

techniques.

Figure 10 displays the completed phase diagram for the water-methane system. At both the low and high pressure ends, in the water ice field, the magnitude of the slope dP/dT of the stability boundaries is small. A discontinuity in slope at the solid-fluid methane phase boundary (drawn from Grace and Kennedy, 1967) is expected, but is a rather small effect. The computed change in slope and increase in $|dP/dT|$ at the water liquid-ice boundary is seen clearly at the high pressure end; a similar change at the low pressure end is present as well. Recall that the pressure at which $dP/dT = \infty$ is found by setting the denominator of equation (30) equal to zero, and the corresponding temperature (which is the maximum temperature at which methane clathrate is stable) by extrapolating the data of Marshall et al. (1964).

Work by Tamman and Krige (1925) on the high pressure stability of SO_2 clathrate, as described by Davidson (1973), confirms the general shape of the left hand portion of Figure 10 at a mechanical pressure of ~2 kilobars. They found the SO_2 clathrate decomposition temperature hit a maximum with respect to pressure. At that pressure the volume change in going from SO_2 vapor + ice to clathrate was roughly zero, the same criterion by which we found the maximum clathrate stability temperature for the CH_4-H_2O system. Comparable high pressure data for CH_4, CO, or N_2 clathrate do not exist in the literature. (The Marshall et al., (1964) data do not extend to sufficiently high pressure to show the $dP/dT = \infty$ point by itself.) Data of pure xenon clathrate (Aaldijk, 1971) up to 3.7 kilobars do not reach a critical point.

Figure 10. Phase diagram of methane clathrate plotted as temperature versus pressure. Calculated phase boundary between clathrate and water + methane (assuming zero solubility of methane in water) given by heavy solid line; data of Marshall et al. (1964) are plotted as bullets. Vertical arrows indicate estimated critical point; horizontal arrows at 12.5 kilobars show uncertainty in calculated high pressure boundary. Light solid lines are solid-liquid boundaries for water and methane. They are extended into the clathrate stable region but are only relevant there if one of the components (water or methane) is completely depleted in forming clathrate. The low pressure end of the clathrate stability field is indistinguishable from the left-hand axis on this scale.

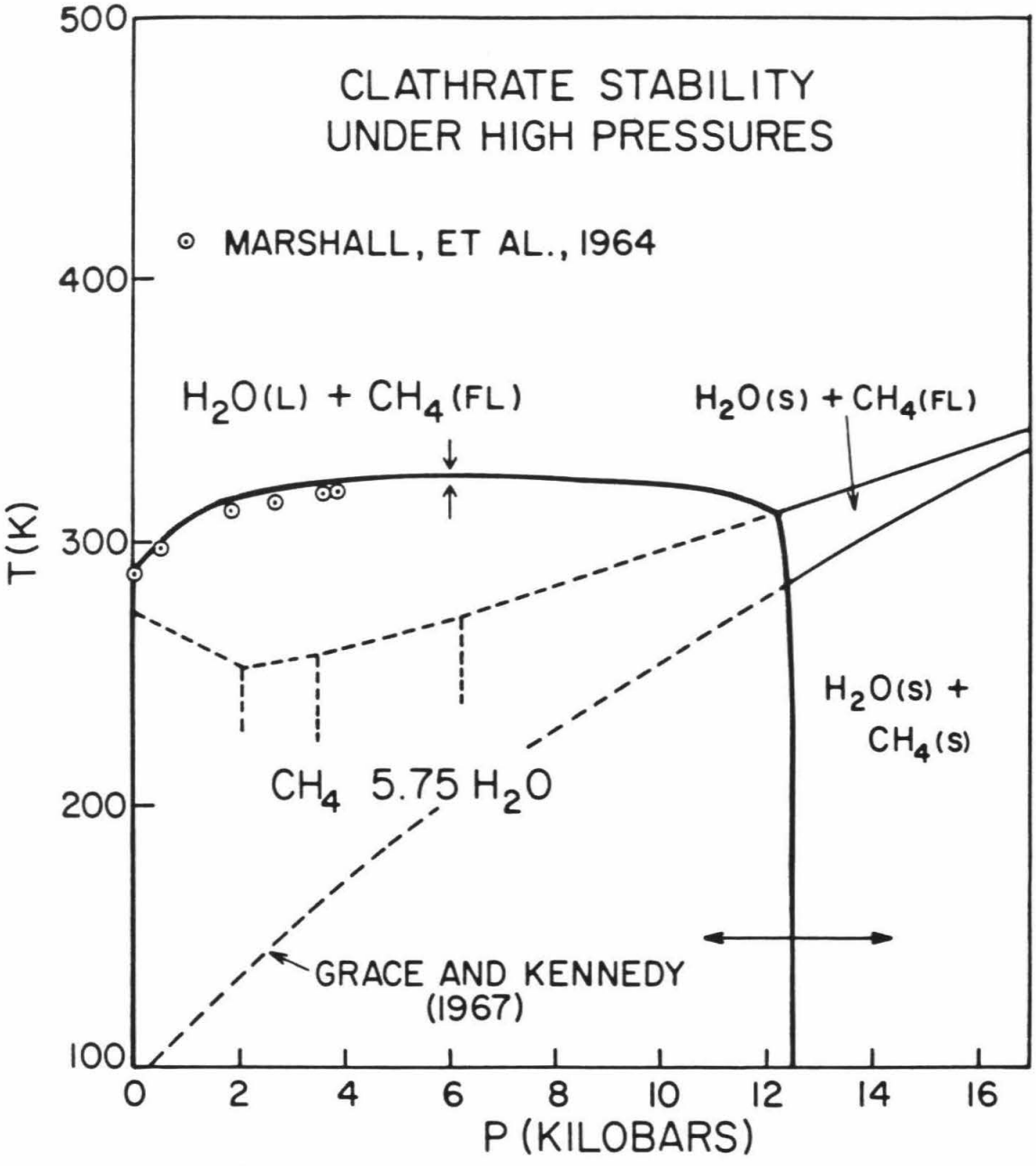
CLATHRATE STABILITY
UNDER HIGH PRESSURES
MARSHALL, ET AL., 1964
$H_2O(L) + CH_4(FL)$
$H_2O(S) + CH_4(FL)$
$H_2O(S) + CH_4(S)$
CH_4 5.75 H_2O
GRACE AND KENNEDY
(1967)
T(K)
P (KILOBARS)
500
400
300
200
100
0
2
4
6
8
10
12
14
16

So far we have neglected the effect of pressure on the Langmuir constant C. To determine the effect of cage compression we assume that the decrease in volume of the clathrate with pressure is taken up by a corresponding decrease in cage volume. We then calculate the Langmuir constant for the large and small cages for cage radii corresponding to the compression. Using $K^{\beta} = 10^{-5}$ the decrease in both cage radii at 10 kilobar is $\simeq$3.7%. Figure 11 plots Langmuir constants for both cages as a function of cage radius at 273 K. The effect is of opposite sign for the large versus small cages. Methane is a sufficiently small molecule that a modest decrease in the large cage radius increases the attractive portion of the guest-host potential without bringing the molecules so close that the repulsive portion of the potential becomes dominant as in the small cage.

Using our formulation of the high pressure case, we solve for the high pressure phase boundary using the altered C's and find that it changes by ~1% from the value based on the low pressure Langmuir constants. (Numerical tests confirm the general insensitivity of the phase boundary P to modest changes in C as can be seen by inspecting equation (1).) The behavior of the Langmuir constants for N_2 (and hence CO) as a function of cage radius is similar to that for CH_4, as expected since these molecules are similar in size.

Very large guest molecules, such as SO_2, may be squeezed out of the cage at rather small reductions in cage radii. Using the fitted Kihara parameters for SO_2, derived in section 3, we find that at low pressures occupancy of the small cage is not possible, whereas large

Figure 11. Langmuir constants for methane clathrate as a function of cage radius at 273 K, for large and small cages, normalized to zero pressure values.

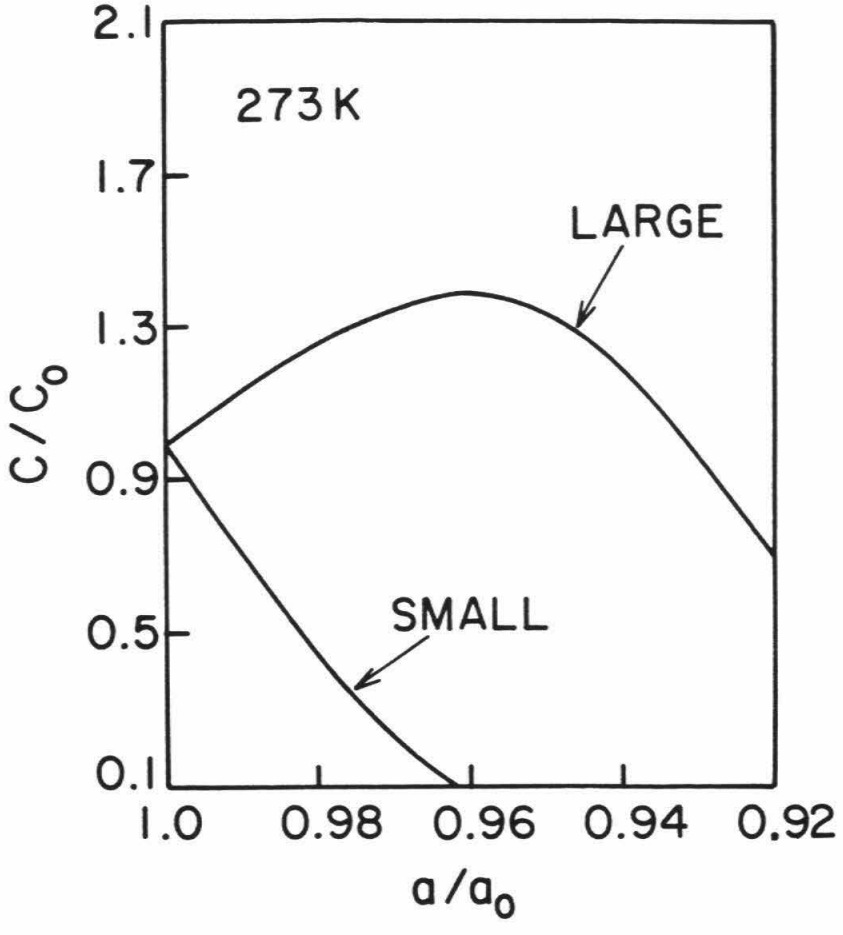
2.1
273 K
1.7
LARGE
1.3
C/C0
0.9
SMALL
0.5
0.1
1.0
0.98
0.96
0.94
0.92
a/a0

cage occupancy is very favorable. A 5% reduction in large cage size results in a decrease of C by a factor of 10^6, effectively preventing SO_2 from incorporating at all. Although the high pressure phase diagram of SO_2 clathrate is not worked out here (see discussion above of experimental data of Tamman and Krige, 1925) such a calculation would have to take dC/dP into account.

5.2. Effect of Methane Solubility in Liquid Water

We now consider the effect of methane solubility in liquid water. We assume in what follows that the solubility of methane in water ice is zero, and that the solubility of water ice in the coexisting methane phase is negligible (Rebiai et al., 1983). Two effects of importance are considered: (1) the presence of a saturated solution of methane in liquid water lowers the chemical potential of the liquid water phase in coexistence with the clathrate, effectively destabilizing the clathrate; (2) stability of clathrate is possible in an unsaturated methane-water solution for which no coexisting pure methane phase is present.

Experimental data on solubility of CH_4 in H_2O extend up to ~680 bar at temperatures down to 298 K (Culberson, 1951). At 310 K and 680 bars, the mole fraction of methane in liquid water, x_2, is 7.8×10^{-3}. We use a modified Henry's law which assumes that the fugacity of solute 2 in liquid solvent 1 is proportional to the mole fraction of 2 in 1 (Prausnitz, 1969, p. 335):

$$f_2^L = H_{2,1}(T,P)\, x_2(T,P) \tag{39}$$

valid over some limited range of x_2.

Using thermodynamic relations in Prausnitz (1969, pp. 30, 357), we find

$$x_2(T_o,P) = \frac{P_o}{H_{2,1}(T_o,P_o)} e^{\frac{1}{kT_o}\int_{P_o}^{P} \left(V(T_o,P') - \bar{V}^{\infty}(T_o,P') \right) dP'} \cdot e^{-\frac{A(T_o,P_o)}{kT_o}\left((1 - x_2)^2 - 1 \right)} \tag{40}$$

where P_o is a reference pressure in the ideal gas regime, $H_{2,1}(T_o,P_o)$ is the Henry's law constant for methane dissolved in water at T_o and P_o, V is the volume of the coexisting pure methane phase, $\bar{V}^{\infty}$ is the volume of methane dissolved in H_2O at infinite dilution, and A is an empirical parameter which characterizes the difference between the H_2O–CH_4 interaction and the H_2O–H_2O interaction. Equation (40) is written in slightly different form in Prausnitz (1969, p. 360). $V(T_o,P)$ is found as described in sub-section 5.1, P_o is chosen to be 300 bars, and $H_{2,1}(T_o,300)$ is taken from Culberson (1951). Since the effect of A is small up to $x_2 \sim 0.1$, the uncertainty in other parameters makes it impossible to estimate A from the Culberson data. Based on data on N_2 in NH_3, an analogous system consisting of a non-polar solute in polar solvent, we estimate A to be negative (net repulsion) and ~1/4 the heat

of vaporization of H_2O. $\bar{V}^{\infty}$ is equally difficult to estimate. The Culberson data up to 600 bar are consistent with $\bar{V}^{\infty}$ fit to a linear function of pressure such that it is 35 cm^3/mole at 300 bar and 30 cm^3/mole at 10 kilobars. The latter value is especially uncertain. Data in Shmulovich et al. (1980) on excess volume of mixing in the H_2O-CH_4 system indicate that the system approaches a critical point above one kilobar pressure and 700 K temperature, where the excess volume of mixing is small ($\lesssim$5 cm^3/mole). However, the excess volume at temperatures of relevance to the present study is not given, and so extrapolation of the Culberson data to derive $\bar{V}^{\infty}$ is necessary.

Our results are given in Figure 12 at 310 K. They indicate a low solubility of 5 x 10^{-3} mole fraction with a small increase from 300 to 10,000 bar, followed by a sharp increase. The behavior of the curve is governed by the ability of the several exponential terms to cancel one another; since two of the terms are poorly known the curve must be regarded as preliminary.

Provided x_2 is small, the dominant correction to the chemical potential of water due to dissolved methane is $kT \ln(1 - x_2) \simeq -kTx_2$. With this correction applied to $\Delta\mu^{\beta}$ in equation (5) we find that at 310 K, the dissociation pressure drops from P = 12,460 bar at $x_2 = 0$ to 12,300 bar at $x_2 = 0.01$, and 10,590 at $x_2 = 0.1$. Thus, if $x_2 < 0.1$, the effect of methane solubility in a <u>saturated</u> solution is small.

Actually, water which is saturated (in the sense that the chemical potential of dissolved methane is equal to that of pure methane at the same T, P) is always supersaturated with respect to clathrate if the

Figure 12. Solubility of methane in water at 310 K plotted as system pressure versus methane mole fraction.

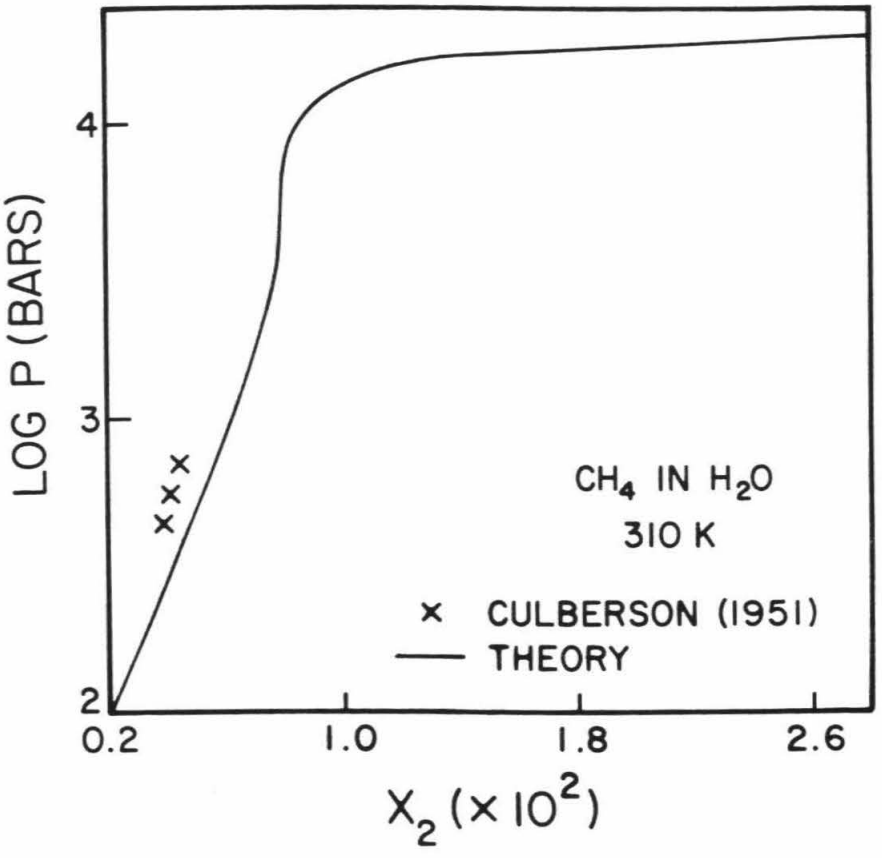
LOG P (BARS)
4
3
2
0.2
1.0
1.8
2.6
X_2 ($\times 10^2$)
CH_4 IN H_2O
310 K
× CULBERSON (1951)
THEORY

T, P conditions lie within the domain of clathrate stability. We can demonstrate the magnitude of this effect as follows. Assume, for simplicity, an ideal solution containing a methane mole fraction x_2 which is less than $x_{2,sat}$, the maximum solubility as obtained above (i.e. Fig. 12). It follows that

$$f_2^{solution}(T,P) = \frac{x_2}{x_{2,sat}(T,P)} f_2^{pure}(T,P) \qquad (41)$$

where $x_{2,sat} << 1$ is the saturated mole fraction of CH_4 at T, P and f_2^{pure} is the fugacity of the pure methane phase at T, P. Using f_2^{pure} as computed in sub-section 5.1 we compute the region of stability of the methane clathrate as a function of degree of saturation of the water $\equiv x_2/x_{2,sat} \leq 1$. This is plotted as a P-x_2 diagram at 310 K in Figure 13. The stability field extends outward from the saturation value to smaller mole fractions of methane with decreasing pressure, as the difference in fugacity between pure methane and methane in clathrate reaches a maximum around 6000 bars. The limiting fraction of saturation for stability then increases again until it equals 1 at the low pressure clathrate stability point at 2000 bars (see Figure 10). There is thus a substantial region of intermediate pressure for which clathrate can coexist with an unsaturated water methane solution. Another way to look at this is to note that clathrate hydrate will continue to form, at some pressures, after all the free methane is exhausted; some additional methane is drawn out of solution.

Figure 13. Calculated stability field of methane clathrate in coexistence with water-methane solution, plotted as system pressure versus methane mole fraction x_2 in water (solid line). Dotted line is value of x_2 for which solution is saturated.

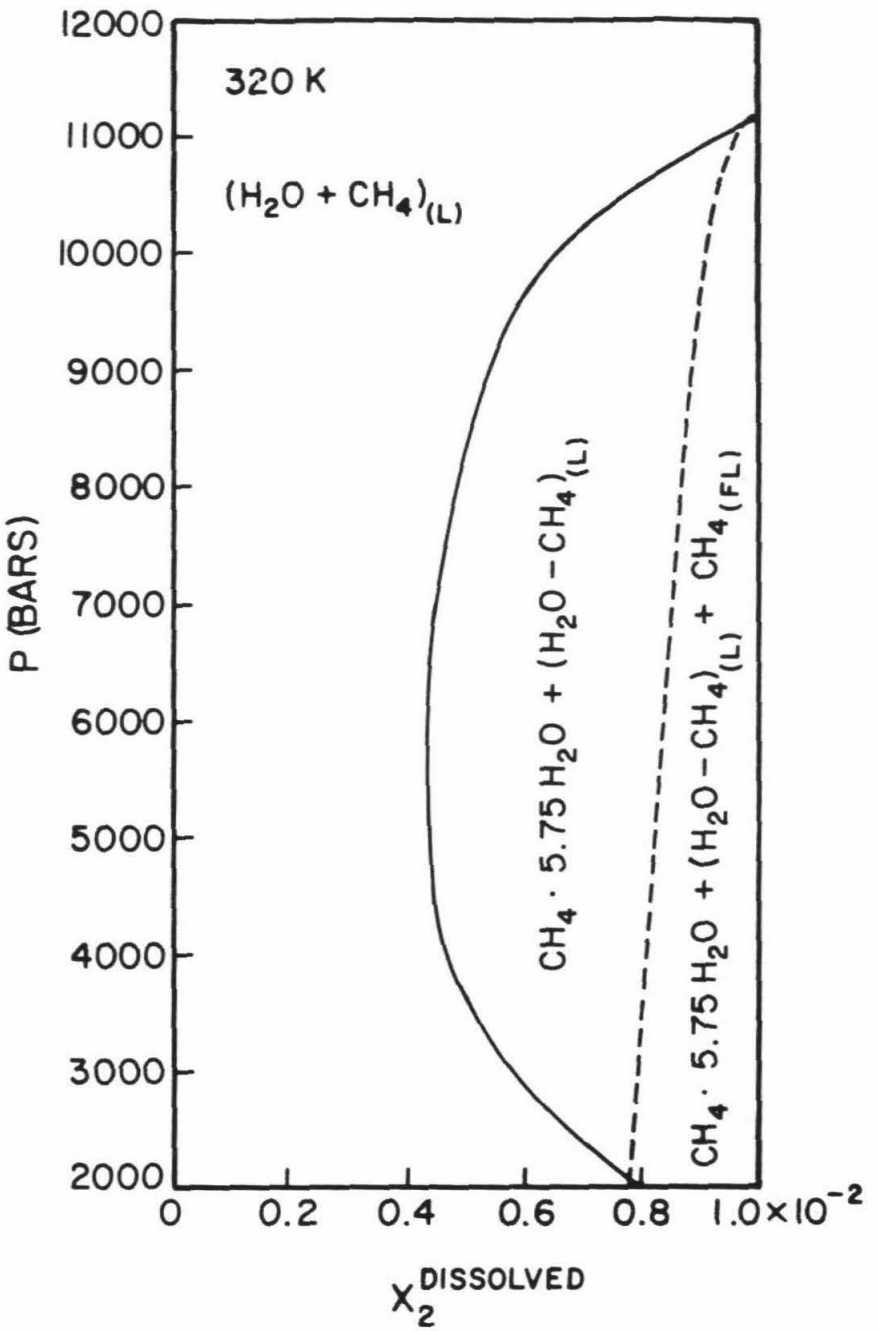
12000
11000
10000
9000
8000
7000
6000
5000
4000
3000
2000
P (BARS)
320 K
$(H_2O + CH_4)_{(L)}$
$CH_4 \cdot 5.75\,H_2O + (H_2O-CH_4)_{(L)}$
$CH_4 \cdot 5.75\,H_2O + (H_2O-CH_4)_{(L)} + CH_{4(FL)}$
0
0.2
0.4
0.6
0.8
1.0×10^{-2}
$X_2^{DISSOLVED}$

5.3. Mixed N_2-CH_4 Clathrate

The analysis in sub-section 5.1 was applied to N_2 using the extensive thermodynamic pressure-temperature-volume data of Jacobsen and Stewart (1973) and Mel'nik (1978). The critical pressure for clathrate stability is 4-5 kilobar; extrapolating the data of Marshall et al. (1964) the corresponding temperature is ~310 K. The shape of the phase diagram is similar to that of methane, the high pressure limit being somewhat less than for methane, about 10 kilobars. Of more interest is the variation in dissociation pressure of the binary clathrate, at a given temperature, due to varying the N_2-CH_4 composition of the co-existing phase. We use equation (1) in its general form, with j = 1, 2 for methane and nitrogen. To determine the fugacities of the methane and nitrogen in the coexisting phase, we consider two alternative models. The simplest assumes CH_4 and N_2 form ideal solid and liquid solutions, i.e.:

$$f_{N_2}^{N_2+CH_4} = (1 - x_{CH_4}) f_{N_2}^{pure}$$

$$f_{CH_4}^{N_2+CH_4} = x_{CH_4} f_{CH_4}^{pure} \qquad (42)$$

where the superscript $N_2 + CH_4$ signifies the mixed phase. Low temperature and pressure studies by Omar et al. (1962) suggest that the solid

and liquid solutions behave more as ''regular'' solutions:

$$f^{reg}_{CH_4} = f^{ideal}_{CH_4} \; e^{\frac{A}{kT}(1 - x_{CH_4})^2}$$

$$f^{reg}_{N_2} = f^{ideal}_{N_2} \; e^{\frac{A}{kT} x^2_{CH_4}} \qquad (43)$$

where A is the energy of exchanging an N_2 molecule for CH_4 in solution, analogous to A for H_2O-CH_4 in sub-section 5.2 above. Here x_{CH_4} is relative to the total CH_4 + N_2 abundance in the pure phase coexisting with clathrate. Based on data in Omar et al. (1962) and Prausnitz (1969, p. 285), $A(N_2, CH_4) \simeq 200$ cal/mole. The effect of A is to increase slightly the pressure at which the binary clathrate destabilizes; at most it is a 3% effect and is not considered further.

Figure 14 plots the stability pressure of the binary clathrate at 180 K versus the mole fraction of CH_4 relative to CH_4 + N_2. As expected, the clathrate composition behaves as a continuous series of ''solid solutions'' (not to be confused with the coexisting solid or liquid N_2-CH_4 solution). The lower curve gives the clathrate composition calculated using equation (2) for the coexisting N_2-CH_4 solution composition indicated by the upper line. Under the ambient conditions the coexisting solution is in the solid field (Grace and Kennedy, 1967), although the qualitative behavior of the phase diagram is not affected if the coexisting solution is fluid. The behavior of the system may be

Figure 14. Phase diagram of binary N_2–CH_4 clathrate at 180 K, displayed as pressure versus CH_4 mole fraction (relative to N_2 + CH_4). The coexisting N_2–CH_4 solution is assumed to be ideal. The lower and upper curves are the composition in the clathrate and coexisting phase, respectively. Letters refer to an isothermal compression of the system discussed in text.

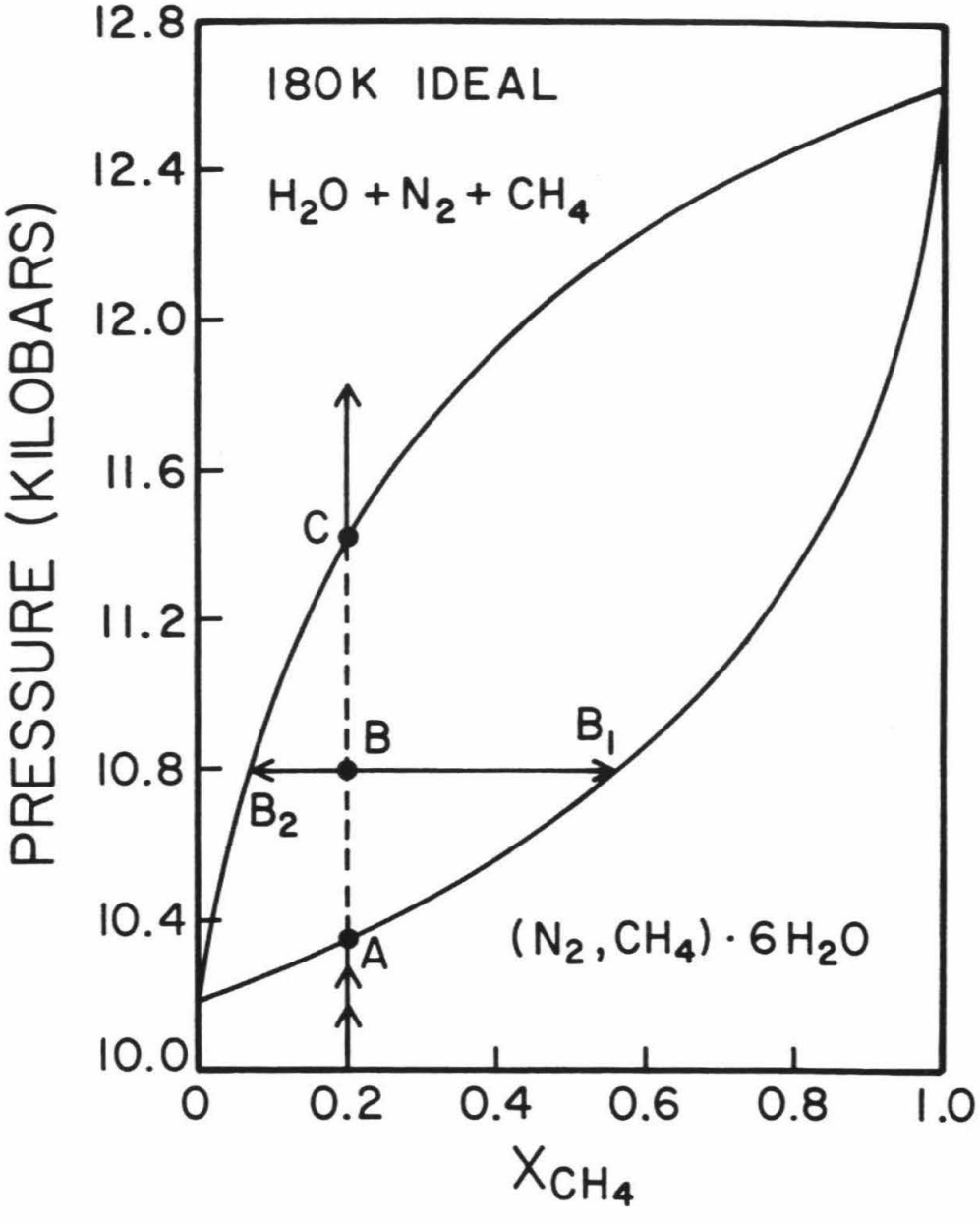
180K IDEAL
$H_2O + N_2 + CH_4$
$(N_2, CH_4) \cdot 6H_2O$
C
B
B_1
B_2
A
PRESSURE (KILOBARS)
12.8
12.4
12.0
11.6
11.2
10.8
10.4
10.0
0
0.2
0.4
0.6
0.8
1.0
X_{CH_4}

seen by choosing an N_2-CH_4 composition in the stability field of the clathrate and increasing the pressure. Let $x_{CH_4}|_{clathrate} = 0.2$, and increase the pressure from 10 kilobars. At point A, pressure 10.3 kilobars, a nearly pure (92%) N_2 solution is evolved from the clathrate (with formation of water ice), which evolves towards more methane rich. As P increases, both clathrate and coexisting solution evolve toward more methane rich, with increasing proportion of water ice + N_2-CH_4 solution to clathrate. At point B, for example, P = 10.8 kilobars, $x_{CH_4}|_{solution} = 0.07$ and $x_{CH_4}|_{clathrate} = 0.55$, with the fraction of N_2 + CH_4 in solution versus clathrate given inversely by the ratio of chord lengths B-B_2 and B-B_1. At C, 11.44 kilobars, all the N_2 and CH_4 has evolved from the clathrate and the stable phase is now N_2-CH_4 solution plus water ice. Thus, in an icy satellite containing binary N_2-CH_4 clathrate, some zoning of coexisting volatile composition is expected, over, however, a rather narrow (~1 kilobar) pressure range. The same behavior is expected for the CH_4-CO binary clathrate. Note also that the closer the stability pressures of the pure clathrate endmembers are, the more similar will be the compositions of the binary clathrate and coexisting phase.

5.4. Clathrate Stability in the Presence of Ammonia

We now calculate the phase diagram for high pressure clathrate stability in the presence of water ice and ammonia-water liquid. Incorporation of NH_3 in cage sites is neglected because the fugacity of NH_3 in the NH_3-H_2O liquid is always low enough compared to that of the guest molecule (e.g. CH_4) phase that NH_3 occupancy relative to CH_4 is $<<1$. As in sub-section 5.1, we calculate $\Delta\mu^{\beta}(T_o,P)$ from $\Delta\mu^{\beta}(T_o,P_o)$ by integrating isothermally using equation (34). $\Delta\mu^{\beta}(T_o,P_o)$ is found from equation (24), where $T_f(P_o)$ for the ammonia water solution is from Haudenschild (1970). The pressure limits on the clathrate stability regime are then calculated as in sub-section 5.1. In the water-ice field, the pressure limits must be unchanged from the pure water results. To define the boundaries of the water ice regime, the freezing curve must be calculated over the entire pressure regime (0-15 kilobars) considered. In the absence of clathratable gases:

$$\mu_{H_2O}^{ice} = \mu_{H_2O}^{solution} = \mu_{H_2O}^{liquid,pure} + RT \ln \gamma_{H_2O} x_{H_2O} \qquad (44)$$

at the freezing curve. Here γ_{H_2O} is the activity coefficient (Prausnitz, 1969, p. 181) of water in the ammonia-water solution, a function of x_{H_2O} but assumed constant with respect to temperature and pressure. Writing $d\mu = VdP - SdT$ and considering the freezing process along an isobar, we find

$$\Delta S_{freeze} \left(T - T_F^o \right) = RT \ln \gamma_{H_2O} x_{H_2O} \qquad (45)$$

where T_F^o is the freezing point of pure water at system pressure P, ΔS_{freeze} is the entropy of freezing at P and is tabulated for the various ice phases in Hobbs (1974, p. 65). For a specified x_{H_2O}, using the melting point data of Haudenschild (1970) equation (45) is solved for γ_{H_2O} in the low pressure field. This value of γ_{H_2O} is then used along with the appropriate ΔS_{freeze} to calculate the freezing curve in the high pressure ice phases. Since $\gamma_{H_2O} \simeq 0.5$ for $x_{H_2O} = 0.70$, the activity coefficient clearly cannot be neglected.

The resulting ice liquid boundary and clathrate stability region for $x_{H_2O} = 0.85$ and 0.75 are plotted in Figure 15. The clathrate stability region has the same general shape as for the pure water case, and is constrained to be identical in the ice field. Note that Figure 8 shows in much more detail the low pressure end of the clathrate stability field of Figure 15; together they display the phase boundaries in the presence of ammonia at all pressures ($0-10^4$ bar) of interest.

Preliminary results of Johnson et al. (1984) suggest that at $x_{H_2O} < 0.85$, an ammonia-dihydrate ($NH_3 \cdot 2H_2O$) phase freezes from the liquid solution at high pressures. A series of temperature-composition plots at several pressures for the ammonia-water system is presented in Appendix B. The resulting freezing boundary at $x_{H_2O} = 0.75$ is shown in Figure 15. Because the volume of the dihydrate phase is not known, we cannot predict the clathrate stability field in the dihydrate region. However, the large $\Delta T/\Delta P$ slope of the dihydrate solidus implies a

Figure 15. Temperature versus pressure of CH_4 clathrate stability field in presence of ammonia for X_{H_2O} = 0.85 and 0.75. Labelling of fields is identical to that in Figure 10, except for the water ice-dihydrate-liquid triple point indicated.

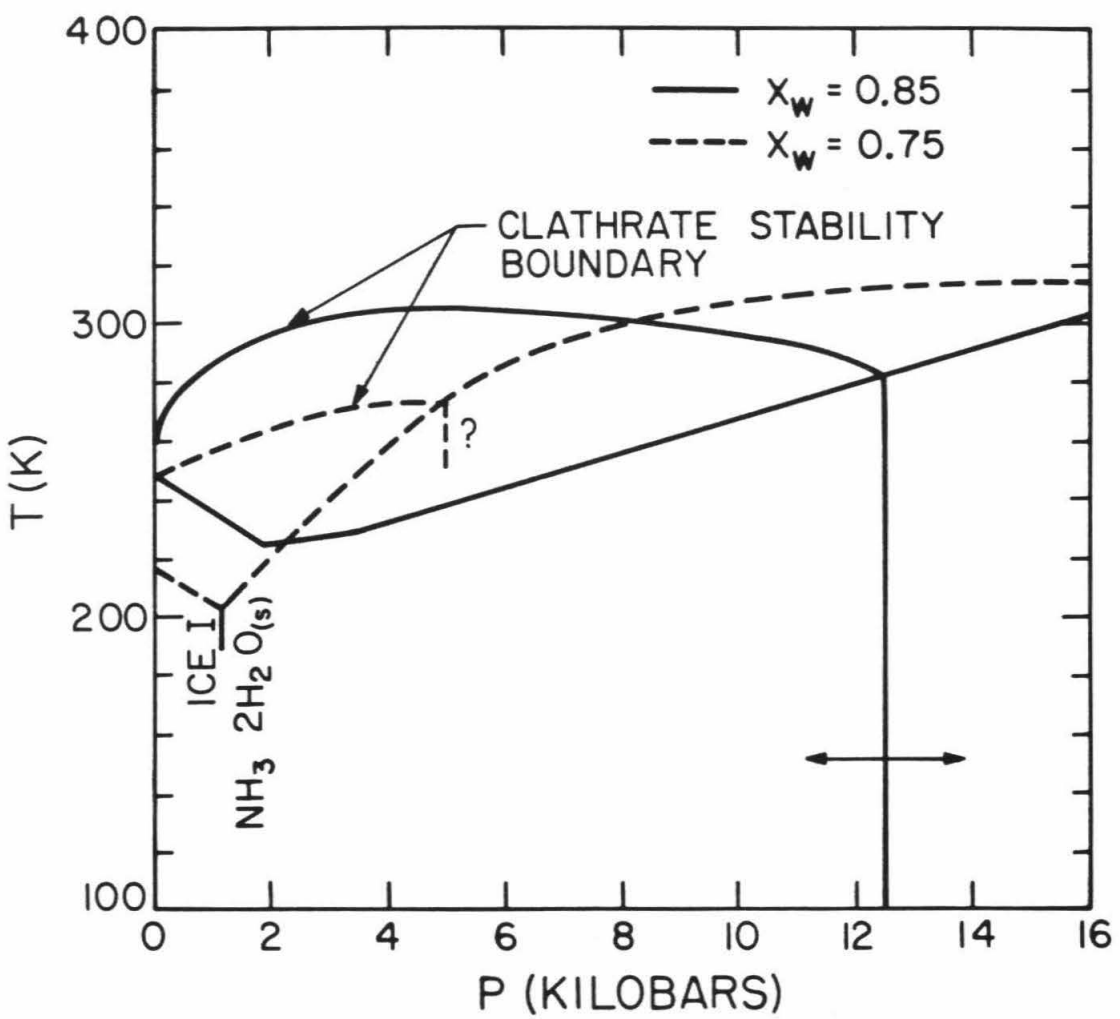
400
300
200
100
T (K)
0
2
4
6
8
10
12
14
16
P (KILOBARS)
X_w = 0.85
X_w = 0.75
CLATHRATE STABILITY BOUNDARY
?
ICE I
NH_3 $2H_2O_{(s)}$

substantial volume decrease upon freezing; hence, the clathrate stability field probably terminates at a lower pressure than it would in the absence of the solidus.

6. Kinetics of Formation

Although in the preceding sections we have been concerned with the thermodynamic aspects of clathrate formation, application to problems of nebular condensation requires consideration of the kinetics of formation. Lewis and Prinn (1980) argue, for example, that formation of clathrate at ''nebular'' temperatures plausible for Uranus and Neptune, i.e., <60 K, may be severely inhibited by the inefficiency of diffusion of large guest molecules (i.e., CO) through water-ice planetesimals. The term ''nebula'' refers to disk-like, primarily H_2 gaseous regions out of which solar system bodies are assumed to have formed. The solar nebula is usually modeled as a low density ($\sim 10^{-12}$ g/cm^3 at Saturn's orbit; Lewis (1974)) disk from which the planets accreted; nebulae around giant planets from which satellites formed could have had densities $\sim 10^{-5}$ g/cm^3 (Prinn and Fegley, 1981; Lunine and Stevenson, 1982). We examine the issue of kinetics below and conclude that while diffusion of gas through the interior of a 10-meter sized planetesimal of high porosity is possible over nebular time scales (10^7 years), diffusion of clathrated layers through the ice grains themselves is too slow to enclathrate most of the ice. However, collisions can expose essentially all the ice to the gas over time scales shorter than or comparable to planetesimal lifetimes in the Saturnian (and perhaps solar) nebula.

If we consider a planetesimal formed by repeated coagulation of smaller grains, we can imagine a rather porous object characterized by a

hierarchy of grain, and, hence, pore sizes, extending perhaps from centimeter-sized particles down to micron-sized. Each size range of particles may itself have pore systems at the next size scale down. Eventually a size (~1 μm) is reached at which porosity is not important; this is the size at which gas phase diffusive growth acted during condensation. For an example of probable morphologies of coagulated grains, see Brownlee (1978), p. 140. One of two diffusional processes thus limits the formation of clathrate: diffusion through the porous volume of the entire planetesimal, or through the smallest scale, non-porous ice particles.

The mean free path of a gas molecule, $kT/\sigma P$, where T = temperature, P = pressure, σ = cross section of molecule, is ~2 cm for H_2 at T = 50 K and P = 10^{-6} bars. Under such conditions, diffusion through centimeter or smaller diameter pores is in the so-called Knudsen regime, i.e., collisions with pore walls dominate over gas-gas collisions (Carman, 1956, p. 63). The Knudsen diffusion coefficient for gas species i is given in Evans et al. (1961):

$$D_i = \frac{4}{3} K_o \left(\frac{8kT}{\pi m_i} \right)^{1/2} \qquad (46)$$

where m_i = mass of molecule of species i, and K_o is a constant with dimensions of length, characteristic of the porous medium, and can be related to the pore diameter d by a ''dusty gas'' model as in Evans et al.:

$$K_o \approx \frac{1}{20} \frac{\varepsilon}{q} d \qquad (47)$$

where ε = porosity, i.e., volume fraction of pore space in the medium, and q = tortuosity which is the square of the ratio of actual distance followed by a gas streamline to the pore length l. The numerical factor in (47) was calculated from the dusty gas model assuming that the average pore size is roughly equal to the ice grain size. We take $\varepsilon \sim 0.5$, and for many porous systems $q \lesssim 3$ (Carman, 1956, p. 48) so $\varepsilon/q \sim 0.1$. Even if d = 1 μm, the diffusion distance is ~10 km over 10^7 years. Hence, H_2 diffuses rapidly through porous bodies.

Diffusion of other nebular gases such as CO, noble gases, etc., is substantially slower due to the formation of clathrate along the ice surfaces of pores. Since, as shown later, diffusion through the solid ice is extremely slow, clathrate formation corresponds to adsorption of gas molecules on the ice.

The one-dimensional diffusion equation for a particular adsorbable gas species is (Barrer, 1967):

$$\frac{\partial c_g}{\partial t} = D \frac{\partial^2 c_g}{\partial x^2} - \frac{\partial c_a}{\partial t} \qquad (48)$$

where c_g is the gas concentration (molecules per unit volume of porous medium) in the pore space, c_a is the concentration of molecules adsorbed on pore walls, D is the Knudsen diffusion coefficient, t and x are the time and space coordinates, respectively. The second term on the right hand side represents the exchange of molecules between the adsorbed and

gas phases. We have neglected the surface diffusion term in (48) as it appears to be less rapid than Knudsen diffusion. Following Fanale et al. (1982) we define an adsorption parameter

$$\alpha = \frac{\partial P_a}{\partial P}\Big|_T \tag{49}$$

Here P is the partial pressure of the gas which is diffusing through the pore and P_a is an effective pressure of the adsorbed or enclathrated molecules: $P_a = \rho_a KT/m$, where ρ_a = adsorbed mass per unit volume of ice. Note that we ignore interaction between different gas species since the gas is in the Knudsen flow regime. Using the ideal gas equation to convert concentrations to pressures, and substituting (49) into (48) we find

$$\frac{\partial P}{\partial t} = D\left(\frac{\varepsilon}{\varepsilon + \alpha}\right)\frac{\partial^2 P}{\partial x^2} \tag{50}$$

So that for substantial adsorption effects from clathration

$$D\left(\frac{\varepsilon}{\varepsilon + \alpha}\right) \sim \frac{D}{\alpha} \qquad \text{for} \qquad \alpha \gg 1 \tag{51}$$

Since α is the slope of the adsorption isotherm, we can calculate it by considering clathration as a limiting case of adsorption wherein the ratio of adsorbate to absorbent molecules is 1/6 and the effective adsorption area A_s is ~5 x 10^6 cm^2/cm^3 ice (Delsemme and Miller, 1970),

~10-100 times larger than for ''normal'' adsorption onto ice. Following Delsemme and Miller (1970), for a single gas species we employ the expression

$$\log_{10} S_a = \log_{10} S_m - aT^2 [\log_{10} (P/e)]^2 \qquad (52)$$

to find α. Here S_a is amount of gas adsorbed in molecules/cm^2, S_m is the monolayer coverage of ice (S_a/S_m = 1/6 at saturation), e is the vapor pressure of the gas species, and a is an empirical constant dependent mainly on the gas species. In their paper, Delsemme and Miller present data on methane adsorption on pyrex glass; since they claim a is not strongly dependent on adsorber we use their value. Writing P_a in terms of A_s and S_a and differentiating with respect to P yields

$$\alpha = -\frac{2S_m A_s akT^3 \log_{10} P/e}{P} 10^{-aT^2[\log_{10} P/e]^2} \qquad (53)$$

For T = 50 K, methane nebular partial pressure 8 x 10^{-10} bar a = 4 x $10^{-6}/°K^2$, S_m = 1.5 x 10^{14} molecules/cm^2, e = 7 x 10^{-6} bar (CRC Handbook, 1970, p. D-146), we find $\alpha \sim 10^8$ or a diffusion distance of 1 meter over 10^7 years if the pore size is 1 μ. A simpler calculation assuming $dP_a/dP = P_a/P$ yields $\alpha \sim 10^9$. In reality, planetesimal architecture probably consists of a hierarchy of pore sizes. Illustrative though exaggerated examples of this sort of architecture are the fractal geom-

etries, discussed by Mandelbrot (1977), especially the Sierpinski sponge (which has dimension 2.7268). Avnir et al. (1984) present experimental evidence that at the molecular scale, the surfaces of most materials exhibit fractal geometries. In most of these hierarchical structures, the diffusion time is not dominated by the smallest pores. This can be demonstrated by examination of the solutions discussed by Carslaw and Jaeger (1959) for (thermal) diffusivities which depend on some power of the spatial coordinate x, say. For example, the diffusivity law $D = \alpha x$ with α = constant, does not inhibit diffusion to or from the point $x = 0$. In a corresponding fashion, we can think of $x \cong 0$ in our problem as corresponding to the position of a deep-seated narrow pore space which is accessible because of connections to progressively larger pore spaces, and is accessed in a time that depends primarily on the diffusivity for large pores.

We conclude that clathratable gases can diffuse on the order of meters over time scales of $\lesssim 10^7$ years. We now examine time scales for diffusion of clathrate gases through the ice grains themselves. That is, given that all grain surfaces are coated with a layer of clathrate, on what time scale can this layer move through the grains?

Experimental data on kinetics of clathrate formation are extremely limited. Delsemme and Wenger (1970) formed methane clathrate hydrate at 82 K by condensing water vapor in the presence of methane gas at appropriate pressures. Barrer and Edge (1967) formed clathrate from ice and rare gases, achieving nearly maximum theoretical incorporation of rare gases at temperatures down to 90 K on time scales of order five hours,

by agitating the ice with steel balls. This procedure allowed exposure of fresh ice to continue until all the ice formed clathrate. Barrer and Ruzicka (1962) studied formation of clathrate from ice, chloroform and rare gases in the absence of shaking. Qualitatively, their plots of gas uptake versus time at constant gas pressure show an initial steep rise over 10 minutes until some fraction of the gas was incorporated, apparently forming a surface layer on the ice grains, followed by a much flatter uptake curve which we interpret as diffusion of the gas through the ice grains to deepen the clathrate layer. The presence of equal parts solid chloroflorm and water ice in the vessel resulted in structure II hydrate formation, in which small cavities are occupied by xenon and the larger by the chloroform according to the formula $\sim CHCl_3 \cdot 2Xe \cdot 17H_2O$. This, coupled with the imprecision of reading small changes in gas uptake from the curve, makes our diffusion coefficient derived from the data at best an order of magnitude estimate for the structure I hydrate.

To derive the diffusion coefficient, we require an expression giving gas uptake as a function of time. Assume the ice grains are spherical. Assuming D is constant

$$\frac{\partial C}{\partial t} = D \left(\frac{\partial^2 C}{dr^2} + \frac{2}{r} \frac{\partial C}{\partial r} \right) \qquad (54)$$

where r is the radial coordinate measured from the center of the sphere, C = gas concentration. Making the substitution u = Cr yields

$$\frac{\partial u}{\partial t} = D \frac{\partial^2 u}{\partial r^2} \qquad (55)$$

We specify the initial boundary conditions for a sphere of radius a:

$$u_1 = 0 \qquad \text{at} \quad r = 0 \qquad \text{for all } t$$

$$u_2 = aC_2 \qquad \text{at} \quad r = a$$

$$u = rC_o \qquad \text{at} \quad t = 0 \qquad \text{for } 0 < r < a$$

which has the solution (Barrer, 1941, p. 29):

$$C = C_2 + \frac{2a}{\pi r} \sum_1^{\infty} \frac{(-1)^n}{n} \sin \frac{n\pi r}{a} \exp \left[\frac{-Dn^2\pi^2 t}{a^2} \right] (C_2 - C_o) \qquad (56)$$

When $C_2 > C_o$, absorption takes place. Since the measured quantity is the total amount of gas Q taken up by the clathrate at time t, we write

$$Q = -\int_0^t D \left(\frac{\partial C}{\partial r} \right)_{r=a} dt$$

$$= \frac{(C_2 - C_o)a}{4} \left(1 - \frac{8}{\pi^2} \sum_1^{\infty} \frac{1}{n^2} \exp\left[\frac{-Dn^2\pi^2 t}{a^2} \right] \right) \qquad (57)$$

The ratio of gas taken up at time t to that at $t = \infty \equiv Q_\infty$ (maximum which can be incorporated) is

$$\frac{Q}{Q_\infty} = 1 - \frac{8}{\pi^2} \sum_{n=1}^{\infty} \frac{1}{n^2} \exp\left[\frac{-Dn^2\pi^2 t}{a^2} \right] \qquad (58)$$

which is given in Carslaw and Jaeger (1959, p. 234) in terms of error functions as

$$\frac{Q}{Q_\infty} = \frac{8}{a} \left(\frac{Dt}{\pi} \right)^{1/2} - \frac{4Dt}{a^2} + \frac{16(Dt)^{1/2}}{a} \sum_{n=1}^{\infty} \text{ierfc} \frac{na}{(Dt)^{1/2}} \qquad (59)$$

For times small compared to those required for substantial uptake we approximate (59) by the first term and solve for D

$$D = \frac{\pi}{64} \left(\frac{Q}{Q_\infty} \right)^2 \frac{a^2}{t} \qquad (60)$$

Recalling that a is the effective radius of the ice spheres, we use the data of Barrer and Edge (1967) and Barrer and Ruzicka (1962) to compute a from the initial portion of the uptake curve. We find a ~ 10^{-5}-10^{-4} cm and hence D ~ 10^{-18} cm^2/s at 200 K. Thus, at 200 K it is possible for clathration to occur throughout micron-sized particles over time scales ~10^3 years. However, since the diffusion process which moves material into the grains involves an activation energy, so that

$$D = D_{T=200\ K}\, e^{-\frac{E}{k}\left(\frac{1}{T} - \frac{1}{200}\right)} \qquad (61)$$

then at 50 K diffusion will be greatly inhibited. If we use an activation energy appropriate to diffusion of hydrogen fluoride through ice,

~4.5 kcal/mole (Haltenhorth and Klinger (1969)) (a severe approximation since the HF and clathrate guest molecule diffusion may proceed by different mechanisms), we find D ~ 10^{-23} cm^2/s at 100 K and ~10^{-33} cm^2/s at 50 K! It is apparent that if the Barrer and Ruzicka data have been correctly interpreted, diffusion of gas into sold grains to form clathrate is negligible at temperatures of interest.

It is important to realize, however, that even in the absence of diffusion and shaking about 1% of the maximum possible amount of xenon gas is incorporated into the ice particles as a monolayer of clathrate, in the experiments of Barrer and Ruzicka. If the ice grains in their experiments are at all representative of those in a porous planetesimal structure then one may conclude that at least ~1% of the available CO or CH_4 (whatever is the predominant carbon species) will be incorporated as clathrate. Thus, we claim that carbon incorporated in clathrate will be <u>at least</u> of the same order of abundance as CO_2 condensate, the latter comprising $\lesssim$1% of the available carbon from the nebular gas (Lewis and Prinn, 1980).

It is possible that enclathrated CH_4 or CO may still be the dominant source of condensed carbon. Experiments by Barrer and Ruzicka (1962), Barrer and Edge (1967) and others indicate essentially complete conversion of the ice to clathrate when the ice is agitated and broken up, suggesting that the clathrate particles are much more likely to be dislodged, exposing fresh ice, than they are to be destroyed by the agitation.

An analogous process in a primordial gaseous nebula is planetes-

imal collision. A porous planetesimal in contact with the gas would consist of ice grains coated with clathrate; upon collision some of the coating would be stripped off, exposing fresh ice. Since laboratory work suggests that the bonding of the clathrate layer to the underlying ice is weaker than the water bonding within the ice, this process is expected to predominate over fracturing of ice itself. Below we develop a crude model to test whether a planetesimal can be eroded completely (i.e., all ice exposed to gas) in a time less than the accretion time, gas drag infall time, etc. of the planetesimals, or the lifetime of the nebula itself.

Consider meter-sized (or larger), porous particles (hereafter referred to as 'planetesimals' although the term is normally reserved in the literature for later, larger objects) composed of micron-sized grains. This is one possible stage for proto-satellite or planet material. We can find the maximum mass of material spalled off of grains during collision as a function of velocity, by equating all of the kinetic energy of colliding planetesimals to the surface bonding energy of the fragment, so that $\Delta m/m = \rho \Delta r v^2/\sigma$, where Δm and m are fragment and grain mass, σ the bonding energy per unit area (probably 0.1-0.01 that of the ice hydrogen bond), ρ the grain density, Δr the fragment thickness (taken to be the thickness of the clathrate layer) and v the collisional velocity. We choose $\rho \sim 1$ g/cm^3, $\Delta r \sim 10^{-7}$ cm, and $\sigma = 10$ erg/cm^3, so $\Delta m/m = 10^{-8} \cdot v^2$, v in cm/s.

We assume v to be due to velocity differences among planetesimals moving through a gaseous disk. The most plausible source of such dif-

ferences is gas drag acting on particles of different radii. From Weidenschilling (1977), we can estimate the radial planetesimal velocity due to gas drag for two drag regimes, that of Saturnian (continuum drag, nebular density $\rho_G = 10^{-5}$ g/cm^3) and solar nebulae (Epstein drag, $\rho_G \simeq 10^{-12}$ g/cm^3). We find $v_R = 100\ r_p^{1/2}\ \rho_p^{1/2}$, and $v_R = 1000\ r_p\ \rho_p$, respectively, where r_p and ρ_p are the planetesimal radius and bulk density, in cgs units. The dependence on r_p implies that the velocity dispersion v is $\sim v_r$ ~100-1000 cm/s for meter-sized objects. To be conservative, we adopt v ~ 10-100 cm/s, hence, $\Delta m/m \sim 10^{-6}$-10^{-4} or at least 10^4-10^6 collisions are required to expose all the ice to clathration.

We calculate the time required for a planetesimal to suffer $m/\Delta m$ collisions as $t = (m/\Delta m)/F$, where the collision frequency F is the ratio of the radial velocity of the planetesimals to their mean free path. The latter is calculated by taking the mass M required to produce a particular planet or satellite and spreading it out as meter-sized planetesimals over a disk of semimajor axis a, and vertical thickness v_z/Ω, Ω the Keplerian angular velocity and v_z the vertical velocity dispersion assumed $\sim v_R$. Then

$$t \sim \frac{m}{\Delta m} \left(\frac{\pi\ \rho_p\ r_p\ a^2}{\Omega M} \right) ,$$

where the density of a planetesimal ρ_p is $\sim 10^{-1}$-10^{-2} for high porosity.

For proto-Titan planetesimals orbiting Saturn, $t \simeq 10$ years; for proto-Saturn planetesimals in the solar nebula $t \simeq 10^6$ years. Note that for the Saturnian nebula case t is independent of r_p, ρ_p; for the solar

nebula $t \propto (r_p \rho_p)^{-1}$, hence, larger or denser planetesimals either do not change t or make it smaller. The former value is short enough that complete clathration of planetesimals is possible prior to accretion as satellites or infall into Saturn (see, e.g., Lunine and Stevenson, 1982b); the latter time scale is marginally short enough that clathration of Saturn forming planetesimals could have occurred. Since $t \propto a^4 \rho_G^2$ for the solar nebula case, out at Neptune only a small fraction of planetesimal material may have clathrated, even over the lifetime of the solar nebula itself.

We also examined the possibility that sublimation and recondensation of water-ice in the nebula is an important mechanism for clathrate formation, since H_2O condensation in the presence of sufficient guest molecule gas pressure produces clathrate as shown by the experiments of Delsemme and Wenger (1970). We write the rate of evaporation f_s over a surface into a vacuum as

$$f_s = \frac{P_v(T)}{\sqrt{2\pi mkT}} \tag{62}$$

where P_v = saturation vapor pressure of water ice (values from Eisenberg and Kauzmann, 1969, p. 60), T is temperature, m is the mass of a water molecule. Assuming the ice to be spheres we calculate the time to evaporate such spheres as a function of radius and temperature and display the result in Figure 16. It is clear that the very low vapor pressure of water ice at the relevant temperatures results in excessively long time scales (i.e., $>10^6$ years) for evaporative formation of

Figure 16. Time to evaporate a water ice sphere in vacuum versus temperature. Numbers on plot refer to radius of sphere.

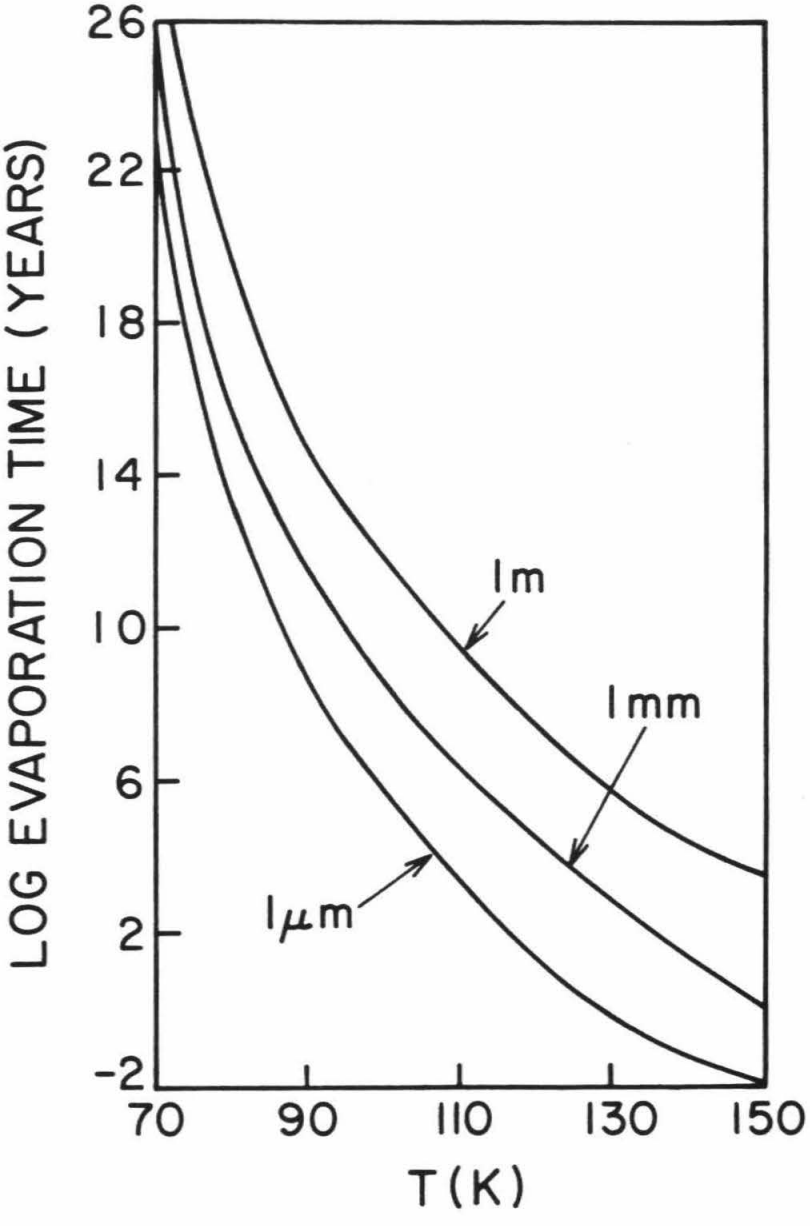
LOG EVAPORATION TIME (YEARS)
26
22
18
14
10
6
2
-2
1m
1mm
1μm
70
90
110
130
150
T(K)

clathrate, even from micron-sized grains. This mechanism may be important, however, in forming clathrate after planetesimal collisions, which produce localized heating and enhanced sublimation in the colliding planetesimals (in addition to disturbing interior ice grains and exposing fresh ice to the gas).

We suggest in conclusion that under plausible conditions in Saturnian and solar nebulae, it is possible that all of the ice could be converted to clathrate. An exception may be the outermost portions of the solar nebula (i.e. the Neptune formation zone) where collisions may have been too infrequent to expose the ice over the life time of the nebula.

7. Applications

7.1. Application to Primordial Nebulae

Having compiled, in section 3, a set of dissociation pressures for clathrate containing single types of guest molecules, we now calculate the relative abundances of guests incorporated in clathrate from a coexisting gas of specified composition. We will see that abundance patterns in the clathrate are strikingly different from that in the coexisting gas, and can lead to distinctive signatures of certain molecules accreted as clathrate into satellites and giant planet atmospheres.

Consider a gas composed of molecules j = 1, 2, ··· each with partial pressure P_j. Equation (2) gives the fraction of cages y_j occupied by species j. We can then determine the relative abundances of species k and ℓ in each type of cage, and sum these to get the abundance ratio of species k and ℓ in clathrate:

$$\mathcal{f}_{k\ell} = \frac{y_{1k} + 3y_{2k}}{y_{1\ell} + 3y_{2\ell}} = \frac{\dfrac{C_{1k}P_k(1 + C_{2k}P_k + C_{2\ell}P_\ell)}{1 + C_{1k}P_k + C_{1\ell}P_\ell} + 3C_{2k}P_k}{\dfrac{C_{1\ell}P_\ell(1 + C_{2k}P_k + C_{2\ell}P_\ell)}{1 + C_{1k}P_k + C_{1\ell}P_\ell} + 3C_{2\ell}P_\ell} \qquad (63)$$

where P_k, P_ℓ are the partial pressure of k and ℓ in the coexisting gas. If the large and small cage Langmuir coefficients are not too different

(both for gases k and ℓ), then the following expression holds:

$$f_{k\ell} = \frac{P_k}{P_\ell} \frac{P_\ell^o}{P_k^o} \tag{64}$$

where P_j^o is the dissociation pressure of clathrate in coexistence with pure gas j. For gases we consider (64) does not strictly hold, and P can differ by as much as a factor of ~10 when computed using (64) vs. (63). Our fits to experimental data on dissociation pressure produce an ambiguity with regard to choice of C_1 and C_2, the small and large cage Langmuir constants. Use of Kihara vs. L-J potentials can produce similar fits to dissociation pressures but different values of C_1 and C_2. L-J fits tend to have larger σ values than the Kihara because they do not possess the hard cores of the latter case. This tends to increase C_2 at the expense of C_1 in the L-J fits. Physically, for medium sized molecules (up to CO, N_2) one expects only small differences between C_1 and C_2; also a hard core or rod is physically reasonable for the guest molecule. Experimental data indicate CH_4 occupies large and small cages equally well (Holder et al., 1980), in agreement with our Kihara calculation. An unreasonably low value of C_1 for CH_4, CO or N_2, for example, allows unrealistically high relative incorporation into small cages by small molecules such as argon. It is thus most physically reasonable for molecules under consideration to use Kihara-derived Langmuir constants in equation (63). Since CO Langmuir constants were derived from an L-J potential, it was necessary to estimate the sensitivity of f to the different potentials by using N_2, for which both

Kihara and L-J parameters were derived. The Ar/CO f ratio was corrected slightly on the basis of this sensitivity test; other noble gas f values relative to CO were not corrected since they are either abundance limited (essentially all gas incorporated) or extremely low. The N_2/CO ratio was calculated using L-J parameters.

We apply equation (63) to models of gaseous nebulae surrounding the sun and giant planets. Abundances of elements are from Anders and Ebihara (1982). Relative abundances of molecules containing these elements (particularly C, O, and N) is controversial; Lewis and Prinn (1980) and Prinn and Fegley (1981) argue that CO and N_2 are the dominant carbon and nitrogen species in the solar nebula while CH_4 and NH_3 dominate in a high-pressure protosatellite nebula. An important assumption implicit in the work of Lewis and Prinn (1980) is that all of the C, N, and O is present in the gas phase or able to participate in gas phase chemistry. Greenberg (1983) and associates suggest that a large fraction of those atoms could be locked up in grains as polymeric compounds, which in the outer-most solar nebula may never be heated sufficiently to return to the gas phase. Such material could comprise comets. Even if most of the C, N, and O is in the gas phase, it is possible that CH_4/CO and N_2/NH_3 ratios in the outer solar system may reflect interstellar abundances rather than nebular processes. We assume that N_2 is present in both solar and giant planet nebulae as it is of interest to determine its maximum degree of incorporation in clathrate for satellite evolution models. Recall that NH_3 does not incorporate primarily in clathrate but binds chemically to water ice.

At low temperatures (T < 170 K) the only effect of NH_3 is to remove $\lesssim$15% of the water ice available for clathrate formation. In what follows, we assume all components are in good thermodynamic contact; the issue of kinetics of clathrate formation in a low temperature/pressure environment was discussed above.

Table III lists the assumed gas phase abundances. Figure 17 plots dissociation pressure versus temperature for major clathrate formers in the absence of other gases. "Major" is here defined as a gas which is capable of tying up most of the available water as clathrate. Plausible P-T regions for solar and protosatellite nebulae are also shown, from Lewis (1974), Prinn and Fegley (1981), Lunine and Stevenson (1982b), and Pollack and Consolmagno (1984). The plot indicates that in a nebula around Saturn,for T $\lesssim$ 100 K and P $\lesssim$ 0.1 bar, most of the available water ice is in the form of clathrate; for the solar nebula T ~ 50-60 K, P ~ 10^{-7}~10^{-6} bar. The dotted lines show formation regions for CH_4 and CO clathrate in the presence of amorphous water ice. The clathrate boundaries are increased in temperature for a given pressure. The metastability of amorphous ice implies, however, that it does not form upon cooling of ice I. Its importance under nebular conditions is therefore uncertain; and we choose T = 60 K and 100 K, respectively, to evaluate abundance patterns in clathrate in solar and giant planet nebulae.

Using Table III, equation (63), and the Langmuir constants derived in section 3 we compute the ratio of various gases incorporated in clathrate. Table IV lists Kihara and L-J derived Langmuir constants at a number of temperatures to facilitate their use in other applications.

Table III

Gas Abundances (Mole Fraction) Relative to H_2 in Nebula

Molecule	X_{CH_4}		X_{CO}
H_2O	1.48×10^{-3}		5.90×10^{-4}
CH_4	8.90×10^{-4}		0
CO	0		8.90×10^{-4}
N_2		9.10×10^{-5}	
Ne		2.83×10^{-4}	
Ar		7.65×10^{-6}	
Kr		3.33×10^{-9}	
Xe		3.20×10^{-10}	

Abundances computed from Anders and Ebihara (1982). X_{CH_4}, X_{CO} refer to nebulae where all carbon is in form of CH_4 or CO, respectively. All nitrogen is assumed to be in form of N_2. Only top three entries differ for the two types of nebulae.

Table IV

Derived Values of Langmuir Constants Used in Text

T	Ne[a,b]		Ar		Kr	
273	4.07(-3)[c]	6.61(-3)	1.58(-1)	3.45(-1)	1.30(0)	1.99(0)
180	2.92(-2)	4.12(-2)	1.79(1)	3.12(1)	4.20(2)	4.23(2)
100	2.45(0)	2.33(0)	1.19(6)	1.06(6)	3.18(8)	1.04(8)
80	2.80(1)	2.09(1)	6.13(8)	3.57(8)	6.43(11)	1.06(11)
	Xe		CH_4		CH_4 (L-J)	
273	4.73(0)	2.78(1)	2.04(-1)	1.80(0)	1.74(-1)	1.92(0)
180	5.61(3)	3.87(4)	5.48(1)	6.65(2)	3.88(1)	7.12(2)
100	1.01(11)	8.81(11)	3.01(7)	6.82(8)	1.40(7)	7.48(8)
80	1.26(15)	1.21(16)	5.27(10)	1.63(12)	1.93(10)	1.83(12)
	N_2		N_2 (L-J)		CO_2	
273	6.19(-2)	2.55(-1)	3.80(-2)	2.94(-1)	1.27(-2)	6.30(0)
180	6.96(0)	2.78(1)	3.27(0)	3.61(1)	2.37(0)	8.96(3)
100	4.76(5)	1.53(6)	1.24(5)	2.80(6)	5.85(5)	2.28(11)
80	2.55(8)	6.89(8)	4.80(7)	1.57(9)	6.59(8)	3.38(15)
	He[b]		H_2 (L-J)[b]		O_2 (L-J)[b]	
273	1.21(-3)	2.07(-3)	3.21(-3)	5.81(-3)	1.38(-1)	4.43(-1)
180	3.54(-3)	5.75(-3)	2.40(-2)	3.82(-2)	1.79(1)	5.34(1)
100	3.50(-2)	4.85(-2)	2.28(0)	2.52(0)	1.66(6)	3.70(6)
80	1.19(-1)	1.49(-1)	2.85(1)	2.49(1)	1.05(9)	1.90(9)
	CO (L-J)[b]		H_2S		PH_3	
273	3.69(-2)	3.78(-1)	2.70(1)	2.86(1)	1.61(1)	1.56(1)
180	3.41(0)	5.70(1)	6.55(4)	3.17(4)	2.28(4)	1.06(4)
100	1.54(5)	7.22(6)	5.81(12)	3.71(11)	5.54(11)	3.83(10)
80	6.57(7)	5.35(9)	1.73(17)	3.33(15)	7.88(15)	1.77(14)

[a]Kihara potential unless (L-J) indicated; noble gases pointlike.

[b]Based on similar molecules and hence approximate.

[c]Small and large Langmuir constants, respectively; a(-b) = a x 10^{-b}.

Figure 17. Condensation temperatures of selected major volatiles in a solar composition gaseous nebula, plotted versus H_2 pressure. The CH_4 and CO clathrate lines apply separately to cases in which each comprises the full solar carbon abundance. Solid and dashed lines for the clathrates refer to formation from hexagonal and amorphous ice, respectively. Shaded areas are plausible pressure-temperature fields for solar and Saturnian nebular models as discussed in text.

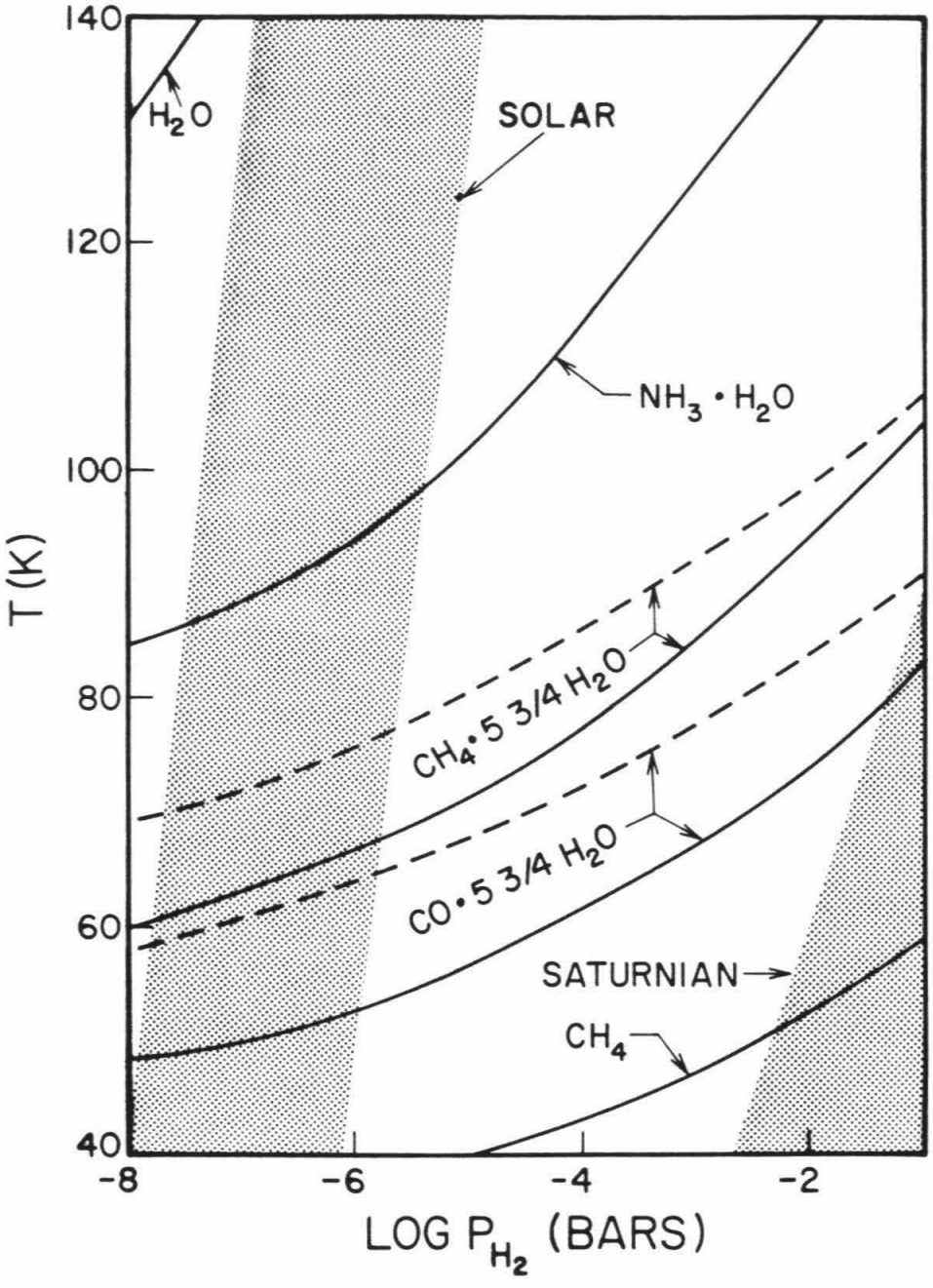
140
120
100
80
60
40
T (K)
-8
-6
-4
-2
LOG P_{H_2} (BARS)
H_2O
SOLAR
$NH_3 \cdot H_2O$
$CH_4 \cdot 5\ 3/4\ H_2O$
$CO \cdot 5\ 3/4\ H_2O$
SATURNIAN
CH_4

Some species incorporate so highly in the clathrate that their presence in the gas is fully depleted; their abundance is then the total initial abundance in the gas. Figures 18a,b depict f for the CH_4- and CO-rich cases, respectively. Figures 19a,b display the abundance of molecules in clathrate relative to initial abundance in the nebula; that is, gases which incorporate completely into clathrate display a value of log(1) = 0 in this figure. Ratios may be taken of the various molecules to determine the altered abundance pattern in clathrate. Of particular interest are (1) the noble gas ratios and (2) the ratios of N_2, CO, and CH_4 in the clathrate.

CO_2 is not shown because of large uncertainties in its gas abundance relative to CO and CH_4. Note also the existence of a ''lower critical decomposition pressure'' for CO_2 at ~120 K (Miller and Smythe, 1970). Below this temperature the vapor pressure of CO_2 condensate is less than the dissociation pressure of pure CO_2 clathrate, and hence the latter is not stable relative to solid CO_2. However, some CO_2 will always be incorporated in the mixed clathrate in the nebula, given the high propensity for CO_2 to do so. We thus expect almost all available CO_2 to be present in condensed material either as pure condensate or in clathrate, the relative proportion of the two being dependent on ambient nebular conditions and CO_2 abundance.

Figure 20 shows the Ne, Kr, and Xe abundances relative to argon in the clathrate relative to these ratios in a solar composition gas, for both a CH_4- and CO-rich gas, as a function of temperature. The striking enhancement of xenon and krypton, and depletion of neon, rela-

Figure 18. Fraction of volatiles from a solar composition gas incorporated in clathrate dominated by CH_4 (top) and CO (bottom) relative to the amount of CH_4 or CO incorporated. All sulfur is assumed to be in H_2S, all P in PH_3 and all N in N_2. Unshaded bars refer to maximum double occupancy by H_2 and Ne.

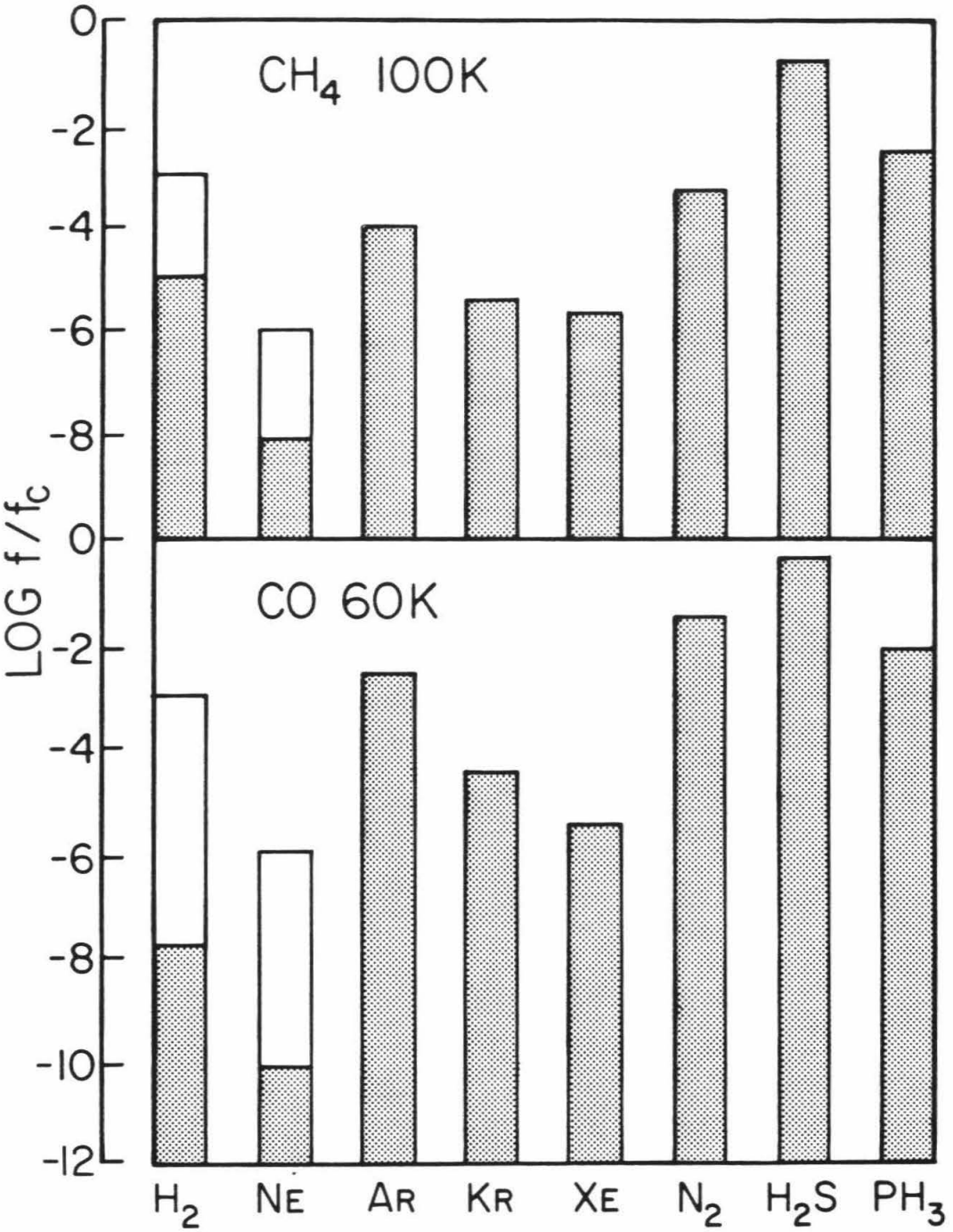
CH4 100K
CO 60K
LOG f/fc
0
-2
-4
-6
-8
0
-2
-4
-6
-8
-10
-12
H2
NE
AR
KR
XE
N2
H2S
PH3

Figure 19. Fraction of volatiles incorporated in clathrate relative to total available in solar composition gas, for CH_4- (top) and CO- (bottom) dominated clathrate. A log value of zero means essentially all of that species is sequestered in clathrate. ''C'' refers to CO or CH_4 as appropriate. Unshaded bars assume double occupancy by H_2 and Ne.

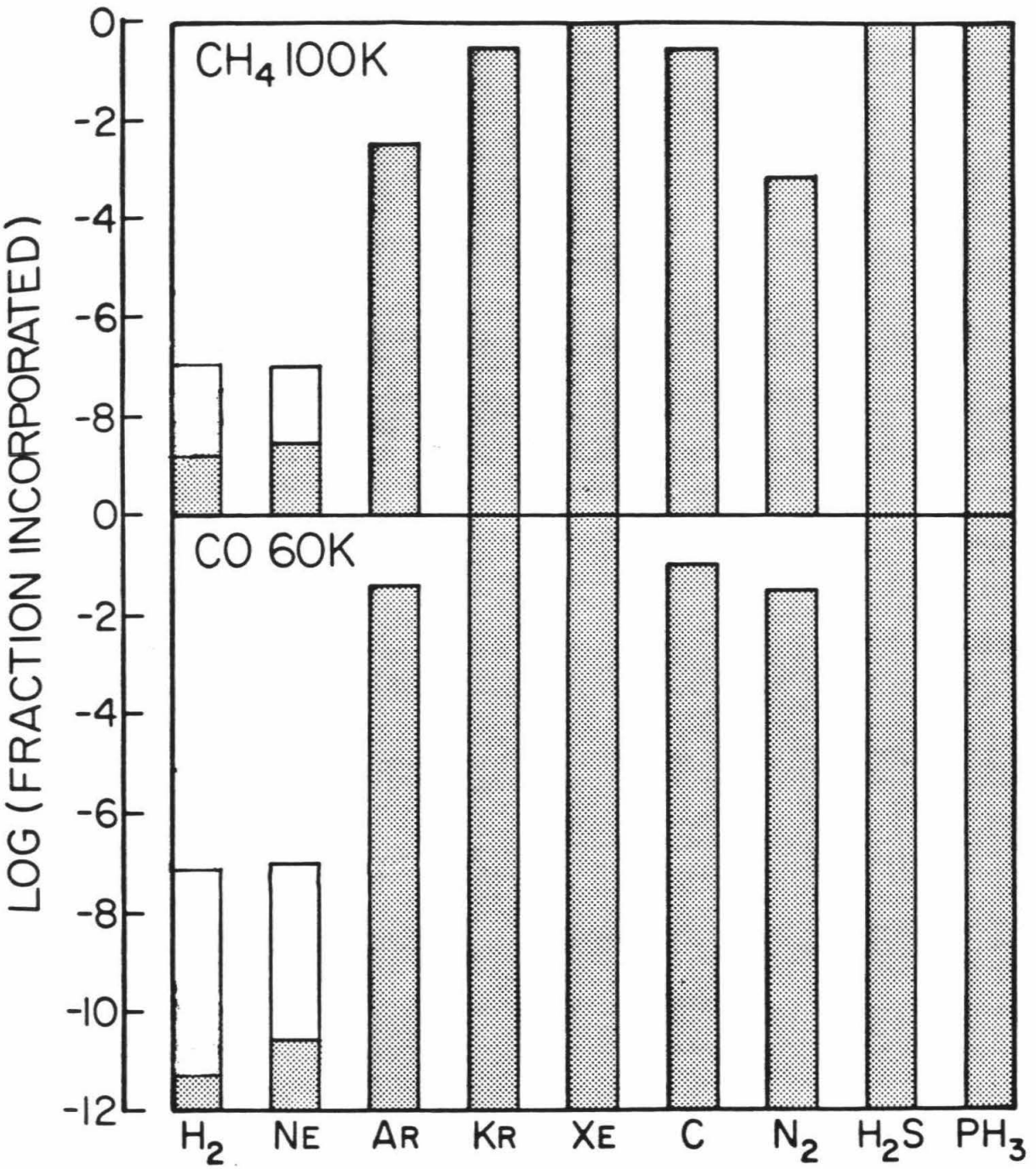
LOG (FRACTION INCORPORATED)
0
-2
-4
-6
-8
0
-2
-4
-6
-8
-10
-12
CH4 100K
CO 60K
H2
NE
AR
KR
XE
C
N2
H2S
PH3

Figure 20. Noble gas abundance ratios in CH_4-dominated clathrate relative to abundance ratios in solar-composition gas, as a function of temperature. Double occupancy by neon is neglected.

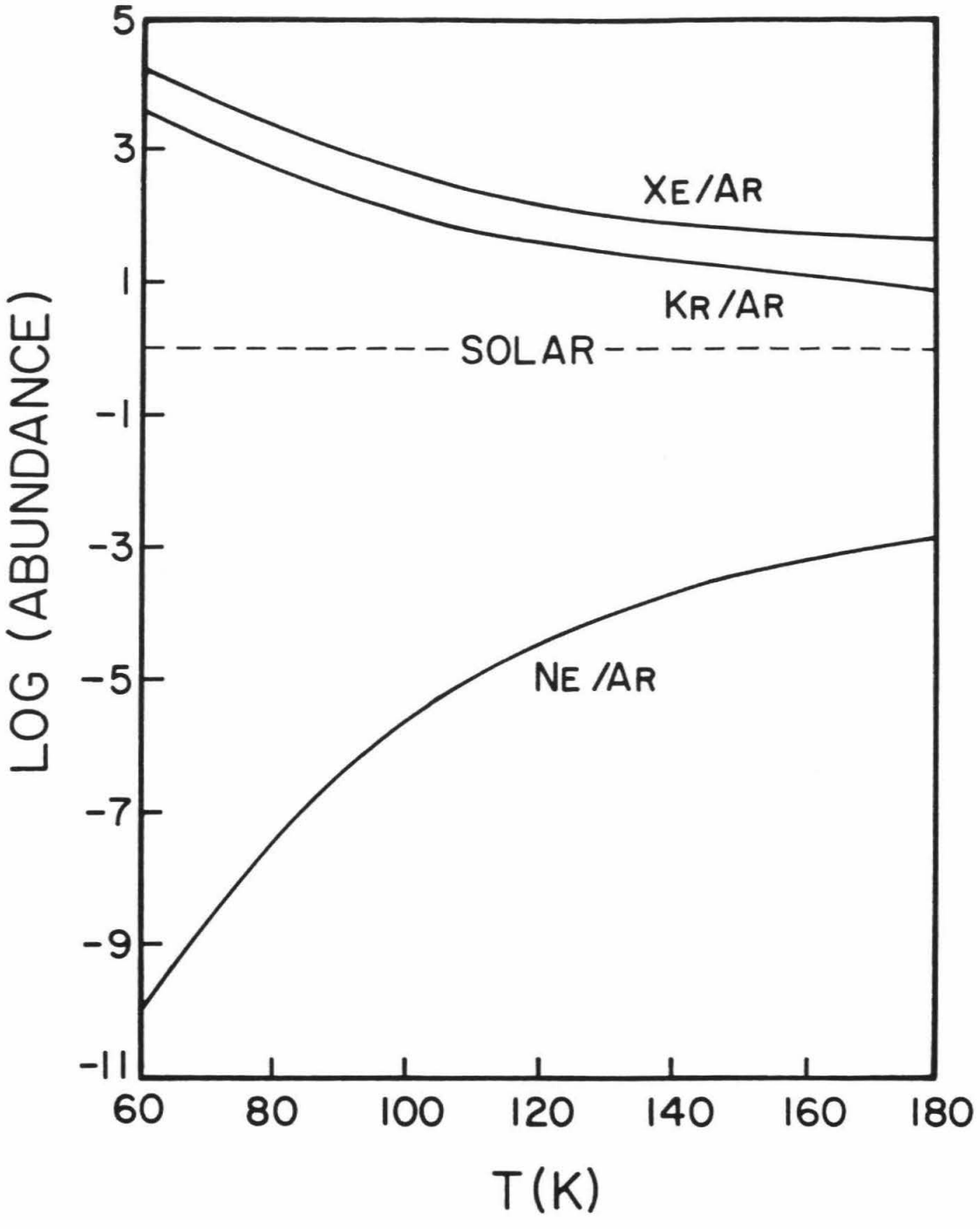
5
3
1
-1
-3
-5
-7
-9
-11
LOG (ABUNDANCE)
XE/AR
KR/AR
SOLAR
NE/AR
60
80
100
120
140
160
180
T(K)

tive to argon is clearly evident. These abundance patterns are similar to, and for neon more pronounced than, those seen in meteorites and terrestrial atmospheres (Fig. 21) (Mukhin, 1983; Donahue and Pollack, 1983). The meteoritical enhancements are likely caused by physical adsorption which, because it involves the same sort of guest-host interaction as clathration (Delsemme and Miller, 1970), would be expected to produce similar partitioning. The maximum uptake possible in surface adsorption processes is, however, much less than in clathration, so in low temperature conditions where water ice is in good thermodynamic contact with surrounding gas, the incorporation and partitioning of molecules in clathrate dominates.

The noble gas enhancement may have observable consequences. It has been suggested (Stevenson, 1982b) that the observed two-fold enhancement of carbon relative to solar in the atmosphere of Jupiter (Gautier et al., 1982) could be due to the accretion of several Earth masses of cometary material onto the planet. This material could contain carbon as CH_4 or CO ices or as these gases enclathrated in water ice. Temperatures and pressures in the environment of the accreting Jupiter (Lewis, 1974) were probably not conducive to the formation of methane clathrate or solid methane; hence, the initial supply of methane in the Jovian envelope would have been gaseous and presumably solar in abundance. Doubling the gaseous methane abundance implies dredging >2 Earth masses of CH_4 from the core, an unreasonable quantity if the core material did not originally contain CO or CH_4 clathrate. Alternatively, if the enhanced carbon were derived from clathrate bearing planetesimal

Figure 21. Abundance (number) ratios of noble gases in clathrate compared with solar abundance, meteorites and terrestrial planet atmospheres. Key: 1) Earth atmosphere, 2) Venus atmosphere, 3) Carbonaceous chondrites, 4) normal chondrites, 5) CO-dominated clathrate, 6) CH_4-dominated clathrate, 7) solar. 1) through 4) from Mukhin (1983), Donahue and Pollack (1983), and Pollack and Black (1982). Dotted extensions of neon abundance in 5) and 6) assume double occupancy.

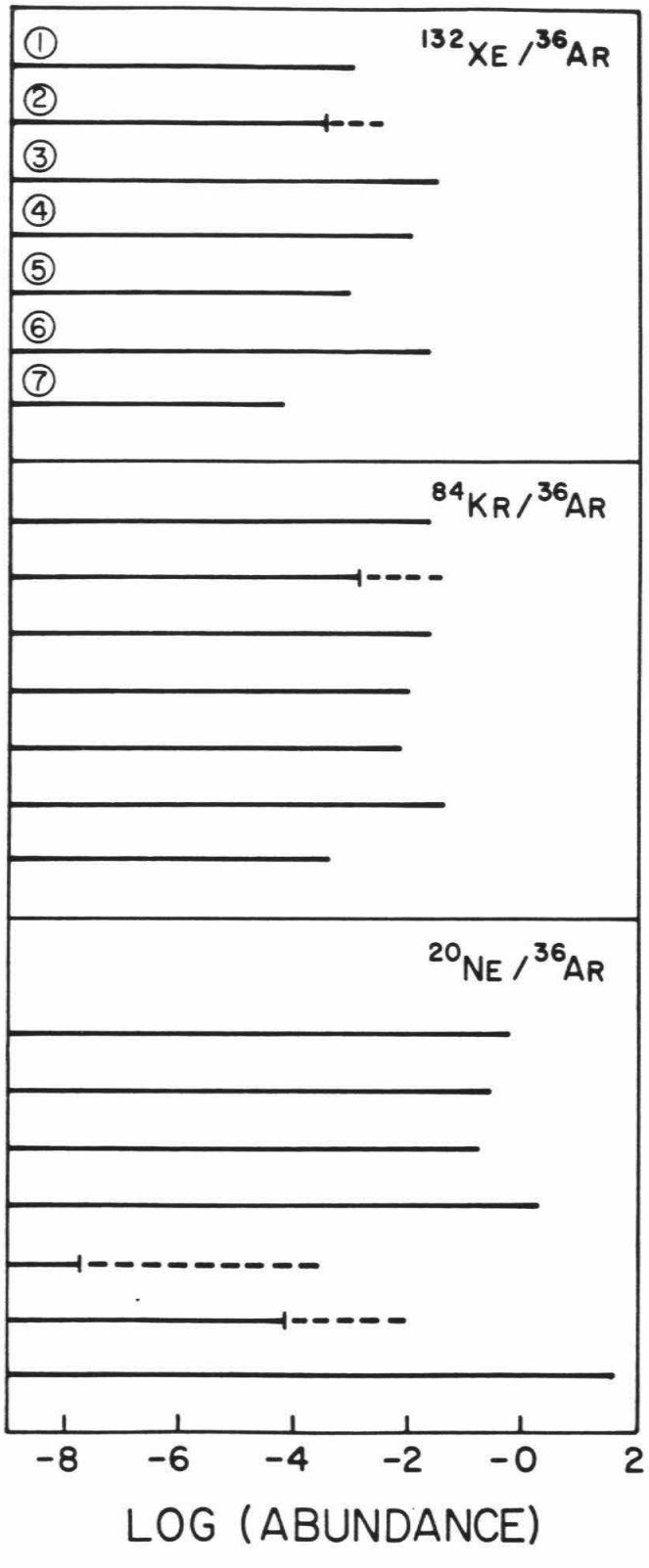
① $^{132}XE/^{36}AR$
②
③
④
⑤
⑥
⑦
$^{84}KR/^{36}AR$
$^{20}NE/^{36}AR$
-8
-6
-4
-2
-0
2
LOG (ABUNDANCE)

debris, the noble gas signature would be distinctive. Figure 22 plots the noble gas abundance ratios as a function of total carbon enhancement in the Jovian atmosphere; the enhancement is assumed due to clathrate dominated by CO (top) or CH_4 (bottom) impacting the initially solar-composition atmosphere. Measurement of noble gas abundances along with methane abundance by the Galileo probe could thus test the above hypothesis against others which do not involve clathrate as the enhanced carbon source.

Uranus and Neptune probably accreted in environments cold enough to allow condensation of methane or carbon monoxide clathrate; Saturn is a marginal case (Lewis, 1974). One currently favored model for giant planet formation, the nucleated collapse scenario (Mizuno, 1980) would lead to incorporation of clathrate volatiles in the core with possibly substantial dissemination in the envelope. Earth-based data hint at a two- to three-fold methane enhancement in Saturn, and as much as twenty-fold in Uranus and Neptune (Lutz et al., 1976). Under the simple assumption that the cores of these planets incorporated clathrate and sufficient mass was then removed to the envelope to produce the observed carbon enhancement, the noble gas enhancements can be calculated. Because of the smaller envelope to core ratio in these bodies, the amount of methane required for dredging from the core to account for the observed enhancement is much smaller than for Jupiter: ~0.6 earth mass of methane for Saturn and $\lesssim$0.4 for Uranus and Neptune. The dredging process likely would not discriminate compositionally, allowing the use of Figure 22 (extrapolated for Uranus and Neptune) to determine noble

Figure 22. Predicted noble gas enhancements over solar as a function of CH_4 enhancement in Jovian atmosphere. Top panel assumes CO-rich clathrate, bottom assumes CH_4-rich. Note essentially all CO brought into Jupiter is assumed converted to CH_4. Formation temperature of CO clathrate set at 60 K and that of CH_4 clathrate 100 K.

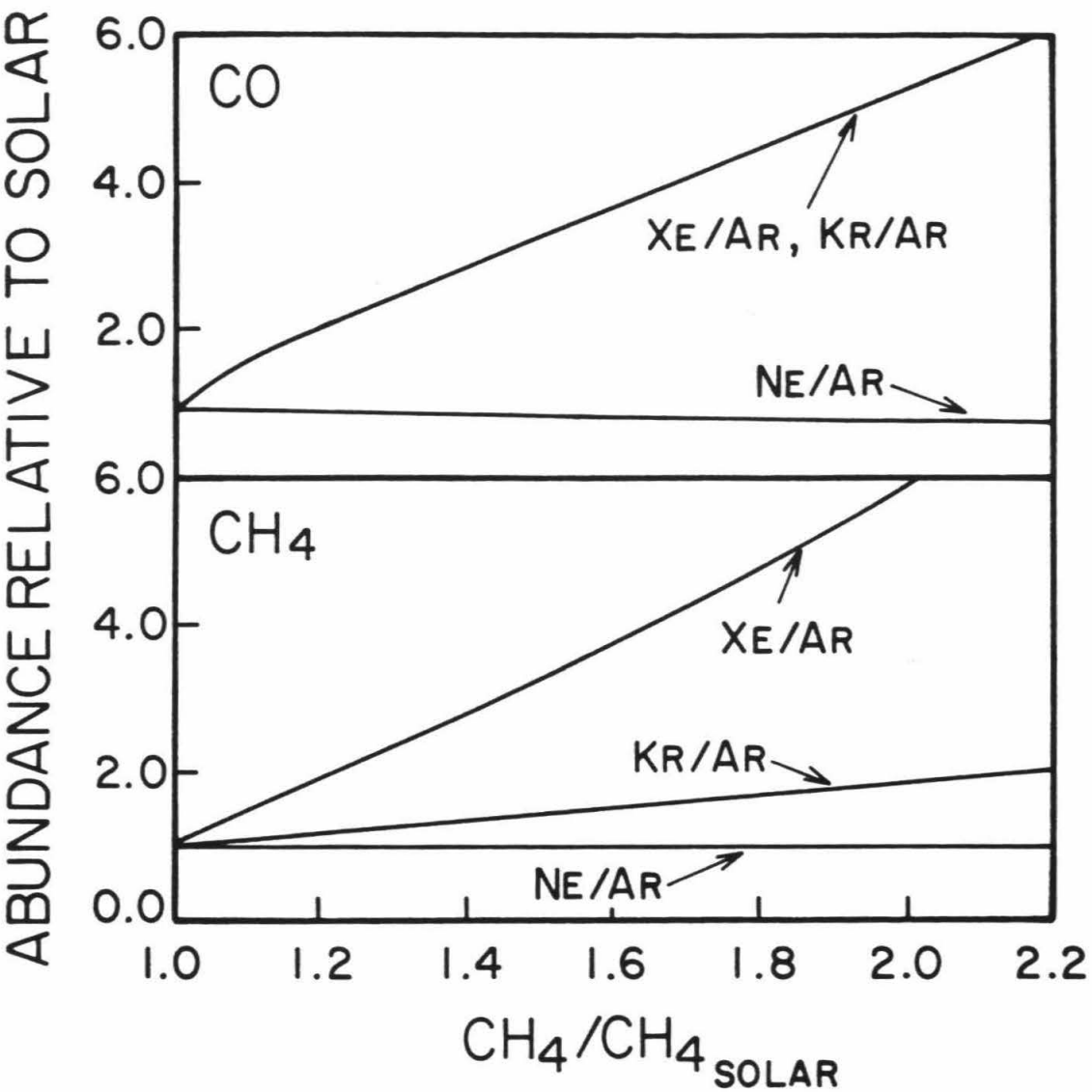
ABUNDANCE RELATIVE TO SOLAR
6.0
4.0
2.0
CO
XE/AR, KR/AR
NE/AR
6.0
4.0
2.0
0.0
CH4
XE/AR
KR/AR
NE/AR
1.0
1.2
1.4
1.6
1.8
2.0
2.2
CH4/CH4 SOLAR

gas enhancements in the envelope as a function of observed methane enhancement. The stability of clathrate under present temperature and pressure conditions in the giant planets was discussed by Miller (1961); in particular, the possibility that the large H_2 pressure and presence of other hydrocarbons might stabilize CH_4 clathrate at the Jovian water cloud level.

Finally, Titan's atmosphere may carry a record of the noble gas pattern calculated above. Since Titan is presumed to have accreted solely from condensed material its volatile components were derived ultimately from the condensed solids or entrapped in clathrate. The latter hypothesis would imply a distinctive noble gas pattern. Tied in with the clathrate hypothesis is the issue of the origin of the 1.5 bar N_2 atmosphere (Lindal et al., 1983); measuring the argon to nitrogen ratio is a potential diagnostic of the competing models.

The primitive N_2 scenario (Owen, 1982) derives the present atmospheric abundance of N_2 directly from clathrate accreted during Titan's formation. The ''secondary N_2'' hypothesis uses the Atreya et al. (1978) photochemical scheme for converting primordial ammonia condensed in the nebula into the N_2 seen at present. The latter scenario requires a warm period early in Titan's history to permit the conversion to occur; an outline of a plausible scenario is given in Lunine and Stevenson (1982a). In either model, the CH_4 and a number of other gaseous nebular constituents accrete as clathrate; up to 10^{25} g of CH_4 can be accreted in this way.

In the secondary N_2 hypothesis, up to 7% of the mass of Titan is

accreted as condensed ammonia (the rock to ice ratio is ~1.5, modestly in excess of solar (Hunten et al., 1984)), and up to several tens of bars of N_2 could be produced photochemically at the surface. From our results above, it is clear that the amount of N_2 brought into Titan in the primitive hypothesis depends on the carbon composition of the nebula, i.e., on the ratio of CH_4 to CO. In the extreme limit where the primary carbon species is CH_4, and all of the water ice is available for clathration (no ammonia), about 1×10^{22} g of N_2 could be brought into Titan by clathrate, or ~1.7 bars equivalent surface pressure. This is just marginally enough to explain the present atmosphere, especially allowing for escape of dissociated N_2 with time (Strobel and Shemansky, 1982). More interesting is the nitrogen to hydrocarbon ratio, which is estimated to be ~0.2 for the present Titan surface and atmosphere. This number includes the amount of hydrocarbons produced over the age of the solar system by photolysis of CH_4, estimated from Yung et al. (1984). The ratio for the CH_4 clathrate is 6×10^{-4}. It is difficult to conceive of atmospheric escape or other processes that would remove (or sequester) >99% of the primitive methane incorporated in Titan while retaining (or outgassing) 90% of the entire primitive N_2 budget in(to) the atmosphere.

More plausible perhaps is a nebula containing a mixture of CO and CH_4. Increasing the CO to CH_4 ratio in the gas decreases the H_2O and CH_4 abundance (the oxygen budget being assumed to remain fixed). Two effects occur: (1) the abundance in clathrate of N_2 and CO relative to CH_4 increases as the CH_4 gas abundance goes down, and (2) the CH_4

abundance eventually drops sufficiently that it is all enclathrated with excess water available to form CO, N_2 clathrate at lower temperatures. Because CH_4 incorporates into clathrate much more readily than CO or N_2, the N_2 abundance in clathrate does not rise sharply until effect (2) occurs, when 90% of the carbon is in the form of CO. The preponderance of oxygen locked in CO implies a water abundance ~0.4 times that in a CH_4 rich nebula. This would lead to an average density for Titan of around 2.1 $g.cm^{-3}$, substantially higher than the observed value of 1.88 $g.cm^{-3}$. It would also lead to densities for the other Saturnian satellites of around 1.7-1.8 $g.cm^{-3}$; their observed values are in the range 1.1-1.4 $g.cm^{-3}$. For this reason, we consider that the required extreme enrichment of CO relative to CH_4 is implausible.

Figure 23 plots N_2/CH_4 and CO/CH_4 ratios in clathrate as a function of CO/CH_4 in the surrounding nebular gas (T = 80 K). For a N_2/CH_4 (number) ratio ~0.25 in clathrate, the CO to N_2 abundance ratio in clathrate could be as high as ~20. The physical chemical properties of CO and N_2 are sufficiently similar that this ratio should have been preserved in the Titan atmosphere. For this model to be viable, then, some mechanism for destroying >tens of bars of CO over the age of the solar system must be invoked. The photochemical mechanism of Samuelson et al. (1983) can destroy 0.2 bars over the age of the solar system; this rate would have to be increased by $\gtrsim$10-100 to derive the present CO/N_2 ratio from that in clathrate.

One potentially diagnostic test of the competing models for N_2 origin is measurement of the argon to N_2 abundance in the present atmos-

Figure 23. Ratio of CO and N_2 to CH_4 incorporated in clathrate as a function of CO to CH_4 ratio in solar composition nebula, at 80 K. All nitrogen is assumed to be in the form of N_2; total carbon to oxygen ratio in H_2O, CO, and CH_4 is solar.

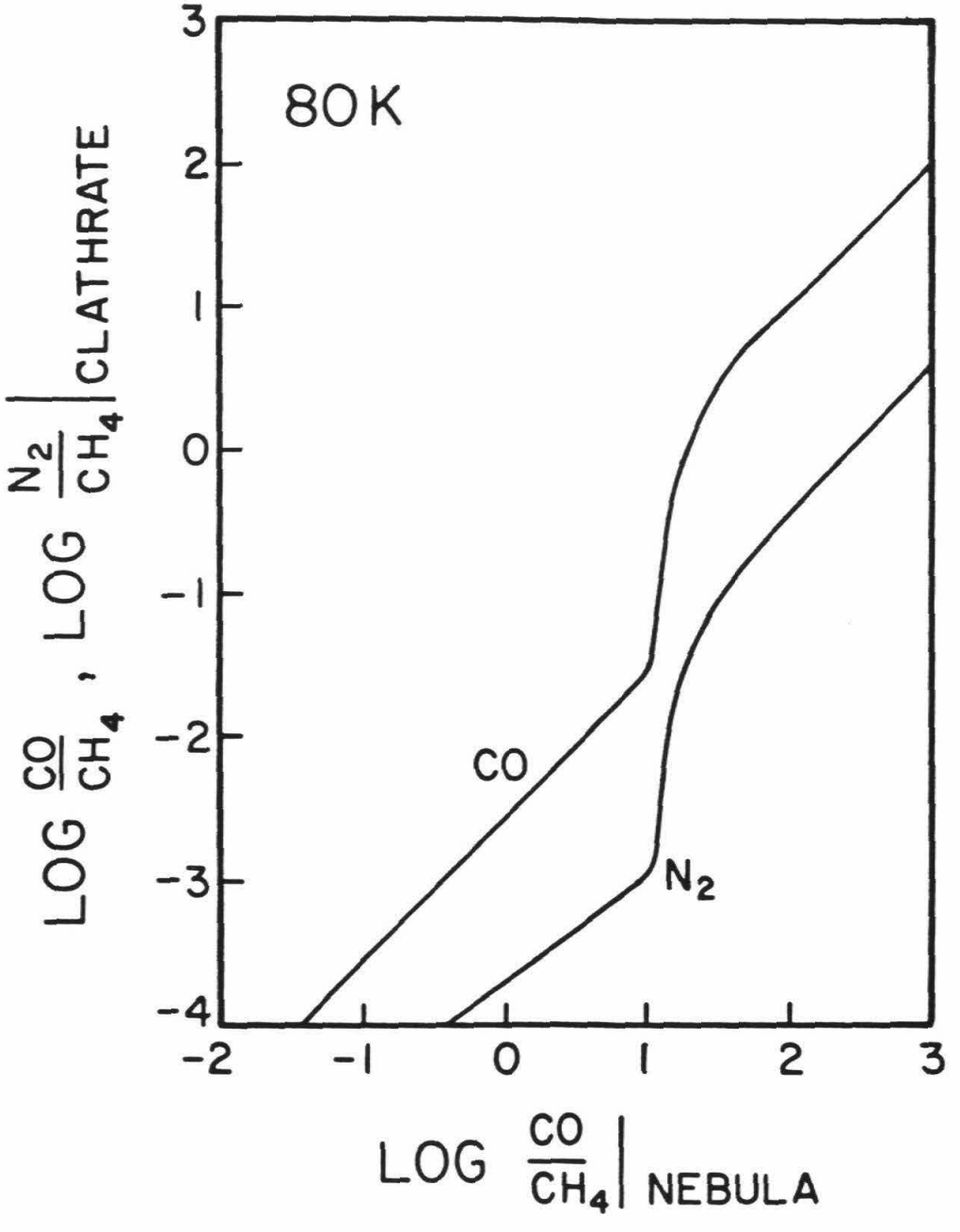
80K
CO
N_2
$\log \frac{CO}{CH_4}$, $\log \frac{N_2}{CH_4}\Big|_{CLATHRATE}$
$\log \frac{CO}{CH_4}\Big|_{NEBULA}$
3
2
1
0
-1
-2
-3
-4
-2
-1
0
1
2
3

phere. If N_2 is derived entirely from clathrate, then the argon to N_2 ratio in Titan's atmosphere would be ~0.1-0.2. The molecular properties of Ar and N_2 are such that their outgassing histories plausibly could be similar; photochemical and charged particle destruction of N_2 in the atmosphere might reduce N_2 by 20% over the age of the solar system (Strobel and Shemansky, 1982; Yung et al., 1984). If the N_2 were photochemically derived, and the primitive N_2 abundance relative to carbon were negligible (as for CH_4 clathrate) then Ar/N_2 would depend on the amount of N_2 produced photochemically and on the argon outgassing and escape history. Define $\chi \equiv$ argon abundance relative to CH_4 (and CH_4 produced hydrocarbons) for the present Titan surface, divided by initial Ar/CH_4 ratio in pure CH_4 clathrate. If all available argon were outgassed and retained in the present atmosphere ($\chi \sim 300$), $Ar/N_2 \sim 0.16$; if the argon and methane-derived hydrocarbon outgassing and loss histories have been similar, $\chi = 1$ and $Ar/N_2 \sim 8.8 \times 10^{-4}$. Thus, a low value of argon in the Titan atmosphere would suggest N_2 derived not from clathrate but from primitive ammonia; a large argon value would be ambiguous. Voyager data require no argon and yield an upper limit of 0.12 (Lindal et al., 1983).

The above test will be affected only slightly by the presence of an ocean on Titan's surface; a kilometer deep ethane-methane ocean has been proposed based on Voyager data (Lunine et al., 1983). Figure 24a plots Ar/N_2 in ocean and atmosphere, assuming the atmospheric Ar/N_2 is fixed at 0.1. Figure 24b plots Kr/Ar in the atmosphere as a function of ocean depth, assuming Kr/Ar in ocean and atmosphere is that expected in

Figure 24. Abundance patterns expected in Titan atmosphere and hypothetical hydrocarbon ocean predicted from solubility considerations, as a function of ocean depth. Top panel plots Ar to N_2 ratio in ocean plus atmosphere assuming atmospheric ratio of 0.1, roughly the Voyager upper limit (Lindal et al., 1983). Bottom panel shows ratio of Kr to Ar abundance in atmosphere assuming ratio in ocean plus atmosphere is 0.1, roughly that predicted from CH_4-rich clathrate model. Arrows indicate solar values (assuming all nitrogen as N_2). Note log scale in bottom panel.

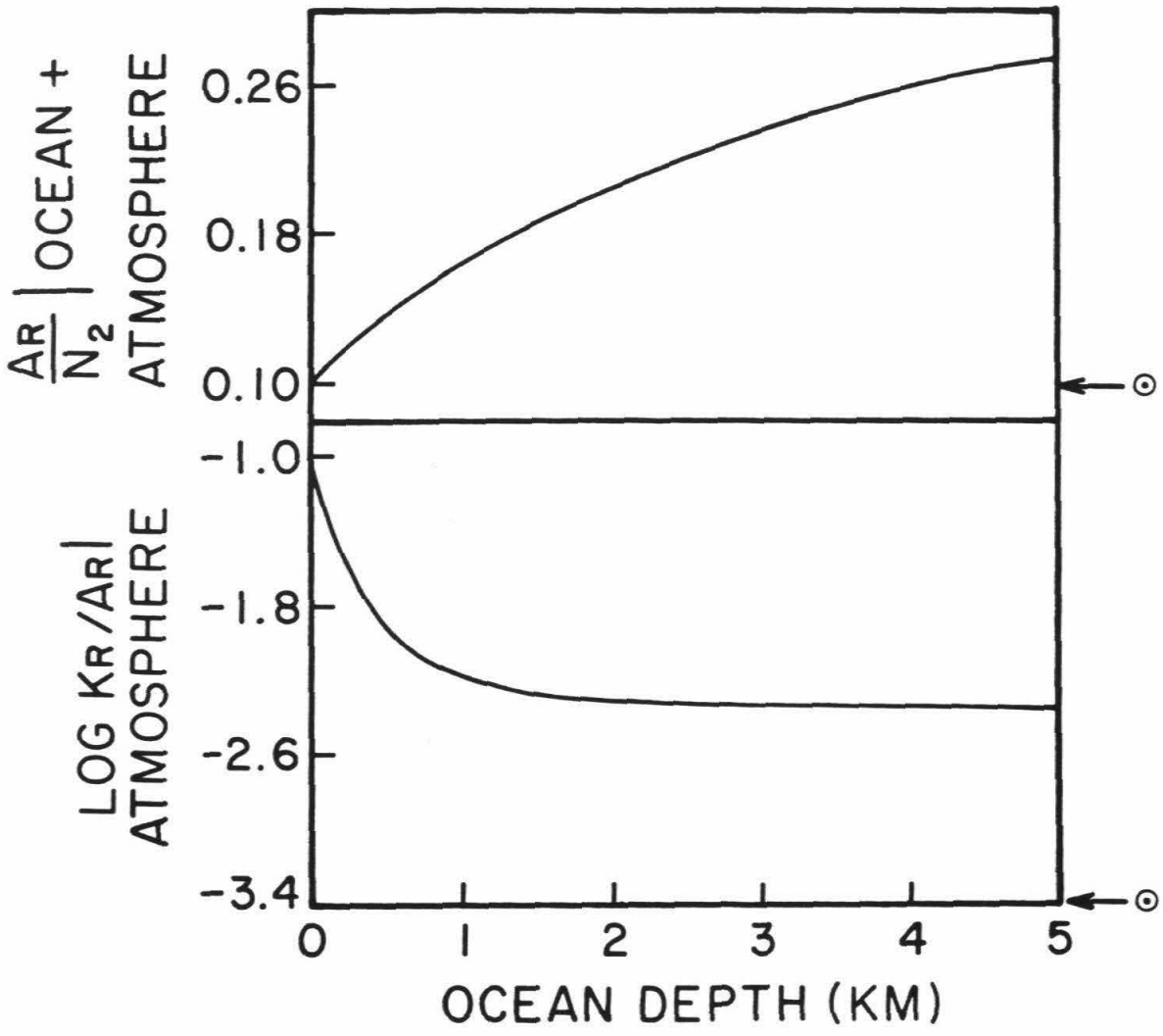
$\frac{Ar}{N_2}$ | OCEAN + ATMOSPHERE
0.26
0.18
0.10
⊙
LOG Kr/Ar| ATMOSPHERE
-1.0
-1.8
-2.6
-3.4
⊙
0
1
2
3
4
5
OCEAN DEPTH (KM)

clathrate, ~0.1. Although the solubility of Kr in hydrocarbons is substantially larger than that of Ar, even a deep ocean would preserve a nonsolar Kr/Ar atmospheric abundance, if the total ocean and atmosphere ratio is nonsolar. Similar results are expected for Xe/Ar although no solubility data on Xe in hydrocarbons apparently exist.

In conclusion, an enhanced heavy noble gas and depleted neon abundance are signatures of primordial incorporation of these constituents in Titan as clathrate. The Ar/N_2 ratio in the present atmosphere is potentially a test of the origin of the N_2 comprising the bulk of the atmosphere. The rather modest enhancement of rock/ice in Titan relative to cosmic, and the current lack of a means for almost completely destroying large amounts of CO in the Titan atmosphere both argue, however, against a primordial, clathrate origin for N_2 in Titan.

We now examine whether double occupancy of cages by H_2 and CH_4 is an important source of H_2 in solar system objects. Double occupancy by H_2 of H_2-occupied cages is not important since the number of cages singly occupied by H_2 is small. The fraction of $\underline{CH_4}$ $\underline{\text{occupied}}$ cages also containing H_2 is

$$d_{M-H} = \frac{q_{MH}\, C_H\, P_H\, C_M\, P_M}{C_M\, P_M} = q_{MH}\, C_H\, P_H \qquad (65)$$

where P_M, P_H are ambient CH_4 and H_2 gas pressures and C_M, C_H are large cage Langmuir constants (the double occupancy probability in the small cages is zero). Plausible Saturnian nebular models give $P_H \sim 0.1$ bar at 100 K (Prinn and Fegley, 1981; see also Lunine and Stevenson, 1982b).

Equation (65) then becomes, with C_H calculated using the L-J potential parameters, $d = 0.3\ q_{MH}$. Hence, $d = 10^{-2} - 0$ for the range of q_{MH} calculated in section 3. The upper bound is potentially a substantial amount of H_2 which, incorporated into icy satellites, may have consequences for subsequent outgassing histories.

For example, if Titan incorporated most of its water ice as methane clathrate, then the total CH_4 mass incorporated would be $\sim 0.06 \times 1.4 \times 10^{26}$ g $\sim 1 \times 10^{25}$ g. If H_2 ''double-occupies'' the cages to the maximum extent calculated above, the total H_2 mass incorporated in Titan would be $\sim 10^{22}$ g, or 10^4 times the inferred amount in the present atmosphere (Hunten et al., 1984). The mass of H_2 which has been produced photochemically over the age of the solar system is $\sim 5 \times 10^{21}$ g (Yung et al., 1984), i.e., comparable to our maximum speculative primordial source.

Neon, lower in solar abundance than H_2 by a factor of 10^4, but with comparable L-J parameters could have $d_{M-Ne} \leq 10^{-6}$. Although still a trace amount, this could be the primary source of neon in clathrate. The double occupancy enhancements of H_2 and Ne in primordial clathrate are shown in Figures 18 and 19. The low Langmuir constant for helium relative to hydrogen yields $d_{M-He} \leq 10^{-5}$, although the smaller value of σ for helium versus hydrogen may increase q_{M-He} and d_{M-He} by ~ 3 or so. Helium is thus substantially depleted relative to solar abundance.

We now briefly consider the relevance of clathrates to cometary composition and phenomena. An extensive literature exists in this area (see e.g., Delsemme, 1983), and two points must be emphasized: (1)

there is no compelling observational data strongly for or against a primordial clathrate component to cometary volatiles, and (2) no physical cometary phenomena observed require (or rule out) the presence of clathrates in comets. Our work adds a theoretical argument against primordial clathrate being a primary component of cometary nuclei, if indeed the formation region of these bodies was in the outer (trans-Neptunian) solar nebula: kinetic inhibition of clathrate formation would be expected under conditions in the outer solar nebula. If comets initially incorporated clathrates, the extremely long time scales for diffusion of gas through ice grains implies that this material may still exist in the nucleus.

The distinctive noble gas systematics predicted above in the scenario for carbon enrichment in Jupiter provides a somewhat indirect and tenuous test of the presence of clathrate in comets, if it is supposed that the source of the enrichment was infalling cometary material from the outer solar system. A more direct test would be mass spectrometric measurements of noble gas abundances in the gas surrounding a comet nucleus.

In closing this section it is worth considering again the work of Sill and Wilkening (1978), with regard to contamination of terrestrial atmospheres by infalling planetesimal debris containing clathrate. They point out the distinctive noble gas signature of clathrates, and the resemblance of Xe/Ar and Kr/Ar to terrestrial atmosphere noble gas signatures (Fig. 21). The terrestrial nitrogen, carbon, neon, and water budget in their model must, however, be augmented by other sources.

This conclusion is not surprising considering the complexity of accretion and evolution processes in large bodies and the requirement to transport clathrate, as solar-orbiting cometary debris, into the inner solar system where temperatures during accretion would have been too high to condense it directly. Clathrate may have been much more important in determining the volatile budget in the outer solar system (with the proviso of kinetic limitations) than in terrestrial planets. It is still necessary to consider carefully physical processes in bodies which may segregate volatiles and further evolve abundance patterns, as illustrated in the next two sections.

7.2. Application to Titan Accretion and Cooling History

In this section, two applications of the phase diagram shown in Figure 8 are outlined: modeling of the primordial atmosphere of Titan during accretional heating and postaccretional cooldown. Both of these applications involve extensive modeling of physical processes which is beyond the scope of this paper. Much of the effort to fully explore these models is work in progress. Here we will emphasize the role of clathrate thermodynamics.

The accretional model is motivated by the need to understand the initial conditions of the atmosphere and volatile budget of Titan. The possible implications of the extreme range of accretion models, from cold (where the impact velocity of planetesimals, and, hence, surface temperatures, are low) to hot (high velocity, high temperature) are

discussed in Hunten et al. (1984). The high mass of Titan, coupled with high gas pressures in Saturnian nebular models motivate the so-called ''gaseous accretion'' model. The physics of this model and its application to the Galilean satellites are given in Lunine and Stevenson (1982b). Briefly, the satellite, forming in a high pressure (~0.1 bar) nebula, gravitationally ''captures'' a solar composition gaseous envelope, which is optically thick in all but the earliest stages of accretion. Planetesimals falling through the envelope are slowed by gas drag, disseminating a portion of their kinetic energy and volatile mass in the envelope. The temperature structure in this optically thick envelope is adiabatic because of the large accretional energy. The highest surface temperatures are obtained under the assumption that the planetesimal mass is disseminated into small pieces, allowing thermal equilibration between the infalling planetesimal mass and atmosphere; this is the limiting case we consider here. The convective temperature structure of the atmosphere is modified by the latent heat release of freezing and condensing volatiles, as given in equation (22) of Lunine and Stevenson (1982b). For Titan, the primary volatiles in the model are ammonia hydrate and methane clathrate. (We assume that the entire solar abundance of nitrogen is in the form of ammonia. The abundance of other volatiles contained in the clathrate is too small to affect the thermodynamics of the system.) So long as the abundance of methane is not a limiting factor (see below), the atmosphere and, hence, surface are constrained to be methane-saturated with respect to clathrate. On a plot of methane pressure versus temperature such as Figure 25 (a portion

Figure 25. Water-ammonia-methane phase diagram, (x_A = 0.15) reproduced from Figure 8, illustrating application to early Titan models. Arrows superimposed show schematically the temperature-pressure path taken by the base of Titan's atmosphere during gaseous accretion, and subsequent cooling driven by rapid, adiabatic escape. The atmosphere is assumed to be in contact with an ammonia-water solid or liquid surface as appropriate. Arrows on the phase boundaries III-IV, and V-VII indicate the base of the atmosphere is saturated with respect to methane clathrate formation; arrowed paths in V and VI imply too little atmospheric methane to form clathrate at the specified temperature.

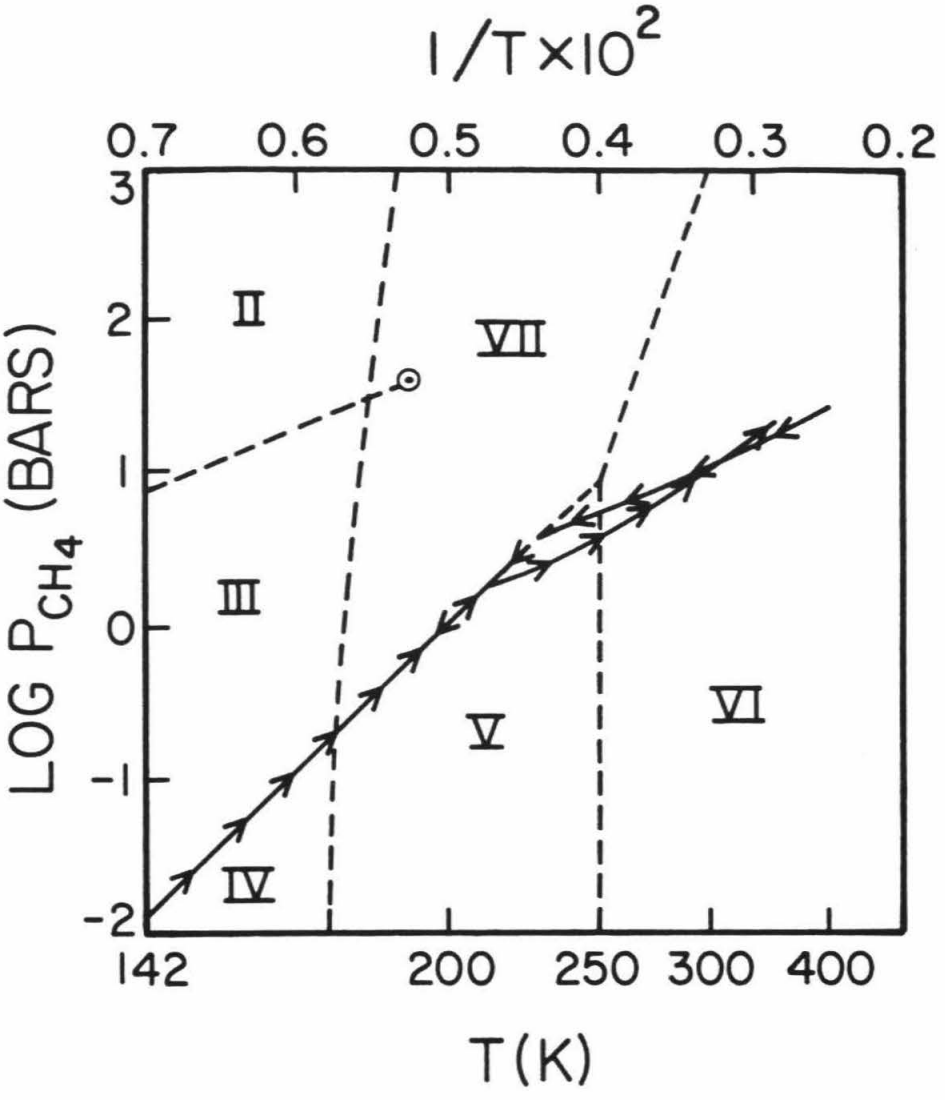
1/T×10²
0.7
0.6
0.5
0.4
0.3
0.2
3
2
1
0
-1
-2
LOG P_CH4 (BARS)
II
III
IV
V
VI
VII
142
200
250
300
400
T(K)

of the phase diagram of Figure 8), methane pressure as a function of temperature through the atmosphere runs along the dissociation pressure curve. Hence, as the satellite mass grows and the atmosphere ''deepens'', the surface temperature must also run along this curve and we can identify the coexisting surface phase assemblages at each point during accretion.

During the late stages of accretion the temperature-pressure curve runs off the clathrate dissociation pressure line at a point in this atmosphere at which incoming planetesimals can no longer supply enough methane mass to maintain the clathrate-saturated pressure. Temperatures increase more rapidly toward the surface because of (a) the absence of the clathrate-saturated adiabat and (b) the low specific heat of the now dominant CH_4 and NH_3 gaseous constituents (as opposed to H_2, He). The point at which the atmosphere departs from the dissociation curve in Figure 25 should be regarded as <u>schematic</u>. This calculation demonstrates that most of the CH_4 accreted onto Titan is liberated into the primordial atmosphere, rather than sequestered as clathrate. The methane affects the subsequent evolution of the atmosphere, as discussed below.

Similarly, application of the phase diagram to the post-accretional cooldown of Titan's atmosphere permits the identification of the effect of surface phase assemblages on the cooling history. Although detailed modeling of mechanisms for loss of gas and cooling has not been done, a simple adiabatic cooling model is adequate to illustrate use of Figure 25. Adiabatic cooling of an atmosphere would

be expected if an energy source (such as solar EUV heating) were available to remove gas rapidly (see Watson et al., 1981); if the lower atmosphere were an optically thick grey medium then an adiabatic temperature profile

$$\frac{T}{T_o} = \left(\frac{P}{P_o}\right)^{\gamma-1/\gamma} \qquad (66)$$

is appropriate in that region. Here γ is the ratio of gas specific heats, T_o and P_o are temperature and pressure at optical depth unity in the atmosphere. We choose $T_o = 90$, $P_o = 0.1$ bar in a pure methane atmosphere for illustrative purposes, and in Figure 25 plot the adiabat given by (66) and values of γ determined from Goodwin (1974). The choice of T_o and P_o would be appropriate for formation of methane clouds as the opacity source along with pressure induced gas opacity, the adiabat moving away from pure methane saturation with increasing temperature. Note also that although water and ammonia vapor are present in the atmosphere as saturated vapor in equilibrium with the surface, their vapor pressures are so small at temperatures of interest that the gas may be considered to be pure methane.

By the above assumptions, the adiabat plotted also represents the change of surface pressure with temperature. If we start the atmosphere at some high temperature and pressure on the adiabat (66), with the methane pressure well below clathrate saturation (i.e., in regions IV, V, or VI) and allow it to cool, the pressure-temperature path must intersect the clathrate dissociation pressure curve and cross into

regions III or VII. Our choice of adiabat crosses into region VII and clathrate begins to form at ~225 K, the surface phases being water ice in coexistence with ammonia water liquid and methane gas. Although higher levels in the atmosphere will also be in the clathrate stable region, the lack of water precludes clathrate formation. The near-surface atmosphere must now move along the dissociation curve in Figure 25, with the production of clathrate from methane gas and surface water-ice causing the gas pressure to drop more sharply with temperature than on the adiabat. (Latent heat release due to clathrate formation may buffer the temperature drop and increase cooling times, but the surface must move along the dissociation curve.) The dropout of the atmosphere as clathrate can continue provided the previously formed clathrate sinks. Although the densities of the ammonia water and methane clathrate are inadequately known (for ammonia-water: International Critical Tables, 1928, p. 59; Hildebrand and Giauque, 1953; for clathrate: Byk and Fomina, 1968; Kvenvolden and McDonald, 1982), the clathrate may be slightly denser, especially if molecules heavier than CH_4, such as N_2, are also incorporated. At 172 K, eutectic freezing of the surface occurs and a layer of clathrate in contact with the atmosphere forms over the ice, kinetically inhibiting further clathrate formation at a methane pressure of 0.18 bars.

The scenario becomes more interesting if, during the warm period after accretion, several tens of bars of N_2 were photolytically produced from gaseous NH_3 (Atreya et al., 1978). An outline of a cooling scenario involving N_2 photolysis is given in Lunine and Stevenson

(1982a). Consideration of the dissociation pressure curve for a mixed N_2-CH_4 clathrate suggests that the near-surface portion of such an atmosphere begins producing clathrate at roughly 200 K. As the surface cools, moving along the dissociation pressure curve, the amounts of N_2 and CH_4 incorporated in the clathrate differ; hence, the composition of the atmosphere changes during the cooling. Using Langmuir constants for N_2 and CH_4 computed in section 3, we calculate gas pressures of the two guest molecules and relative abundances in the clathrate at a given temperature T. Assuming the clathrate sinks, permanently sequestering the encaged N_2 and CH_4, we then self-consistently compute the new equilibrium pressures and incorporation factors of CH_4 and N_2 at a lower temperature $T - \Delta T$, repeating the process until the eutectic temperature of 172 K is reached. To facilitate the calculation we use a convenient expression for the equilibrium pressures P_i derived by Miller (1961) from equations (1) and (2)

$$\sum_i \frac{P_i}{P_i^o} = 1 \qquad (67)$$

where P_i^o is the dissociation pressure for pure species i. For N_2 and CH_4 P_i from (67) agrees with that from the full expression to 20%. The greater propensity for CH_4 to incorporate in clathrate results in enrichment of the atmosphere in N_2 with decreasing temperature. Although results do depend on initial gas abundances, for comparable initial values of N_2 and CH_4 and total pressure of order ~10 bars, the final abundances of N_2 and CH_4 at 172 K are similar to those in the

present atmosphere of Titan, i.e., several bars of N_2 and <1/2 bar CH_4. Figure 26 plots total pressure and methane mole fraction in clathrate and atmosphere as a function of temperature for the model case of equal starting abundances of N_2 and CH_4 in the atmosphere. Although the current atmospheric value of CH_4 (Lindal et al., 1983) may be only a small fraction of the surface hydrocarbon budget (Lunine et al., 1983), it is intriguing that the amount of N_2 corresponds so closely to the present-day value. Additional work must be done to better characterize the physical processes involved in the cooling before firm conclusions can be drawn; in particular, the implications of new data on the ammonia-water phase diagram (Appendix B) must be incorporated in analyzing the effect of the ocean on the atmosphere.

Additional calculations along the above lines have been done including argon and other noble gases as well as N_2 and CH_4. The argon tends to partition with N_2 in the cooling atmosphere while Kr and Xe partition strongly into the ''oceanic'' clathrate. The differing solubilities for various atmospheric constituents, and temperature dependence of the solubility, in the NH_3-H_2O solution also modifies the atmospheric composition and cooling process in such models. Details of ongoing work are beyond the scope of this paper; here we have demonstrated the necessity of understanding clathrate thermodynamics in the presence of ammonia (for methane alone as well as with other guest molecules of cosmochemical interest) in constructing satellite evolution models.

Figure 26. Composition of a cooling N_2-CH_4 gas in coexistence with clathrate as a function of temperature. The gas in contact with water ice is assumed to start at 10 bars total pressure (P_T) and methane fraction $x_{CH_4} = 0.5$; under these conditions at 230 K clathrate formation ensues and the resulting composition and pressure changes as a function of temperature are plotted. f_{CH_4} is CH_4 composition (relative to CH_4, N_2) in clathrate. The calculations are applicable to modeling of a cooling N_2-CH_4 Titan atmosphere in contact with a freezing ammonia-water ocean at the base; the clathrate is assumed to sink allowing further clathrate formation to occur. The temperature decrease is then driven by the loss of atmosphere to clathrate.

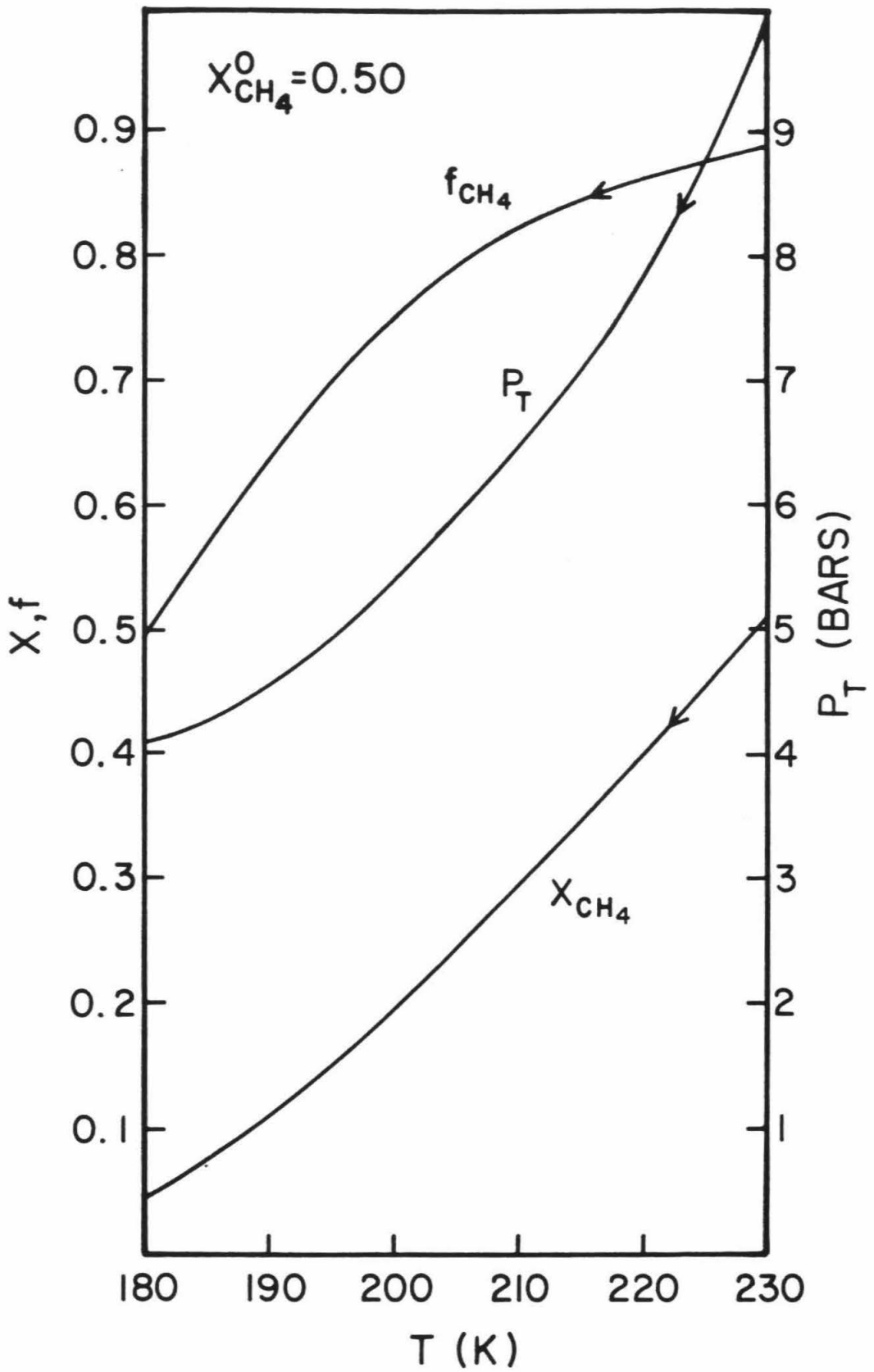
$X^0_{CH_4}$=0.50
f_{CH_4}
P_T
X_{CH_4}
X,f
P_T (BARS)
T (K)
0.9
0.8
0.7
0.6
0.5
0.4
0.3
0.2
0.1
9
8
7
6
5
4
3
2
1
180
190
200
210
220
230

7.3. Application to Satellite Internal Evolution

> ''Oh that delightful engine of her thoughts
> That blabbed them with such pleasing eloquence
> Is torn from forth that pretty hollow cage,
> Where like a sweet melodious bird it sung
> Sweet varied notes, enchanting every ear!''
> (Titus Andronicus, 1968; III.1.26)

We briefly outline application of Figure 15 to the stability of clathrate in Titan and other icy satellites.

Accretion scenarios for large satellites (Lunine and Stevenson, 1982b; Hunten et al., 1984) predict an initially undifferentiated rock-ice core underlying a differentiated mantle, the relative sizes of the regions being dependent on the choice of initial formation conditions, accreting volatiles and details of the accretional model. Figure 27 shows one possible configuration for Titan at the close of accretion, assuming ammonia hydrate and methane clathrate were present in planetesimals. Based on the results of Figure 10, methane clathrate is unstable at $P \gtrsim 11$–14 kilobars, and would dissociate as soon as core pressures exceeded this range during accretion. At the temperatures predicted for the core, methane would likely remain a solid, buoyant relative to water ice, and could move upward during a postulated later overturn of core and mantle (the latter process is described in Friedson and Stevenson, 1983). The subsequent history of the methane is dependent on the amount of methane already in the mantle, temperatures in that region, and the phase relationships derived above. The issue to be addressed is whether the total methane and methane-derived hydro-

Figure 27. Schematic model of the internal structure and atmospheric composition of Titan immediately after accretion. Radii are indicated on the right side of the figure; approximate pressure on the left. Subsequent evolution includes overturn of undifferentiated core which is replaced by overlying rock layer (see Friedson and Stevenson (1983)).

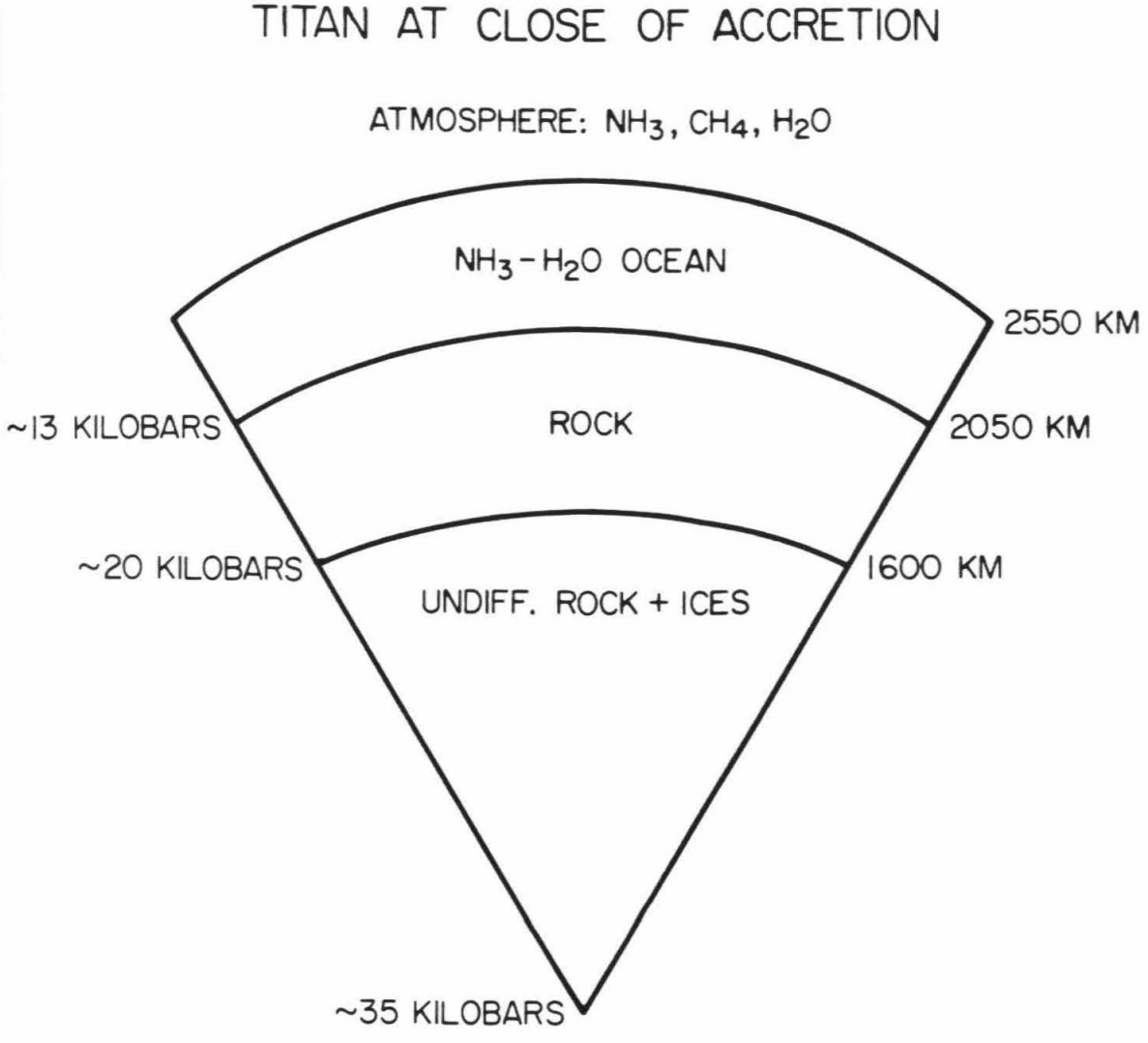
TITAN AT CLOSE OF ACCRETION
ATMOSPHERE: NH_3, CH_4, H_2O
$NH_3 - H_2O$ OCEAN
2550 KM
~13 KILOBARS
ROCK
2050 KM
~20 KILOBARS
1600 KM
UNDIFF. ROCK + ICES
~35 KILOBARS

carbon mass inferred to be on the surface of Titan today (Yung et al., 1984; Lunine et al., 1983) could be derived from an internal source such as a primordial core. Measurement of the volume of the newly identified high-pressure ammonia-dihydrate phase (Johnson et al., 1984 and Appendix B) will allow calculation of the clathrate stability field at $x_{H_2O} < 0.85$, which likely has important implications for the internal evolution outlined above.

Also bearing on this issue is the occupancy factor of clathrate as a function of pressure. At high pressures (T > 100 bar) y as defined in equation (2) is $\simeq 1$. As pressure decreases y decreases; at 230 K and 5.61 bars y = 0.90 in the small cage. Although this is a small effect, the amount of methane and methane derived products inferred to be on Titan's surface is also a small fraction (<1%) of the maximum which could have been incorporated in Titan as clathrate; in fact, it is only ~10% of the amount estimated to be in the primordial core of Figure 27. Whether methane-rich clathrate can work its way to the near-surface environment and release methane requires modeling of physical processes in conjunction with the thermodynamic modeling presented here.

Pressures are $\lesssim$ several kilobars and temperatures <300 K in the icy intermediate-sized Saturnian satellites (Stevenson, 1982a); similar conditions may be obtained in the icy Uranian satellites (Stevenson, 1984). CH_4, N_2, and/or CO clathrate is therefore thermodynamically stable in these satellites according to Figure 10. An important point is that the clathrate is stabilized by confining hydrostatic pressures and not by coexistence of a guest molecule (i.e., CH_4) pure phase (which

could slowly diffuse out of the body). Only in a near-surface, porous regolith would diffusion and escape of guest molecules occur, leading to depletion of clathrate in this outermost, ~kilometer-deep (Hartmann, 1973) regime. The diffusion process is sufficiently slow that impact-generated release of methane from clathrate may be more important. Charged particle bombardment of the surficial methane may then produce dark polymeric material (Cheng and Lanzerotti, 1978).

8. Summary and Conclusions

We have undertaken an analysis of the thermodynamics and kinetics of clathrate formation under conditions of interest to outer solar system studies. In particular, we have used a statistical mechanical model of clathrate formation from Van der Waals and Platteeuw (1959) along with laboratory data to systematically calculate dissociation pressures over a wide range of temperatures for guest molecules of cosmochemical interest. We have predicted the dissociation pressure-temperature curve for CO clathrate, which has not been examined experimentally, as well as calculated the degree of double occupancy of cage sites by small molecules such as H_2. The above results were then used to determine the abundance pattern of volatiles entrapped in clathrate in solar composition gaseous nebulae postulated to be source regions of planet and satellite accretion. Predictions of nonsolar gas abundances in giant planet and satellite atmospheres were made, and are potentially testable (Galileo probe measurements of Jupiter's atmosphere, for example). The issue of kinetics of clathrate formation in such nebulae was addressed and it was concluded that collisional stirring of planetesimals may be required to ensure substantial clathration of the ice.

The phase diagrams of methane clathrate and N_2 clathrate over the entire pressure-temperature range of stability were calculated, and the effect of ammonia considered. A preliminary phase diagram for the high pressure ammonia-water system was constructed (Appendix B) based on

new data of Johnson et al. (1984). Experimental data to verify the predicted diagrams do not exist. The utility of such diagrams in modeling the evolution of large satellites such as Titan was also demonstrated.

We conclude with a list of recommended observations and laboratory investigations which would test our predictions and resolve remaining uncertainties in the work. Such data are of crucial importance in understanding the role of clathrate hydrate in satellite and planetary evolution in the outer solar system.

1. Measure dissociation pressure as a function of temperature of clathrates of CO, N_2, CH_4, Ar, Kr, Xe, Ne, H_2, down to T ~ 50 K. Examine the effect of the presence of amorphous ice on clathrate formation. In the cases of H_2 and Ne, identification of cage double occupancy is useful.
2. Map out phase diagram of clathrate formation at low pressure in presence of ammonia hydrate compounds and ammonia-water solution.
3. Map out stability regions of CH_4, N_2 and CO clathrate up to P $\gtrsim$ 15 kilobars, and T $\gtrsim$ 320 K. Measure the effect of ammonia on the resulting phase diagram. Determination of the solubility of methane in water and ammonia-water solutions at high (10^4 bar) pressures is also crucial to satellite evolution studies.

4. Study the kinetics of clathrate formation in the laboratory, with emphasis on diffusion time scales of gas through ice to form clathrate. Elucidation of the process whereby agitation of ice and gas facilitates clathrate formation would be helpful; i.e., is the exposure of fresh ice, or vaporization and recondensation of water most important for the formation of clathrate?

5. Measure the density of clathrate containing various proportions of CH_4 and N_2 at low pressure; also, the compressibility of clathrate to high (10^4 bar) pressure. Measure the density of high pressure ammonia water phases and map out their regions of stability. These properties are important to satellite evolution studies.

6. Study rheological and thermal properties of clathrate hydrate under a range of pressures. Indirect evidence for a larger number of defects in clathrate structure than in ice I (Davidson and Wilson, 1963) and limited studies of H_2S clathrate (Pinder, 1964) suggest rheology distinct from ice I. The low thermal conductivity reported by Cook and Leaist (1983) and Stoll and Bryan (1979) should be confirmed. These properties are important to thermal models of satellites which may contain clathrate.

7. Study the spectroscopic detectability of clathrate and its products. Smythe (1975) studied near IR reflection spectra of clathrate; study of the visible and IR properties of

polymeric products of CH_4, N_2, CO-rich clathrate produced by particle bombardment of surfaces could be crucial to identifying satellites whose interiors may contain clathrate. (Are the products detectably different from those produced from the pure CH_4, N_2, or CO frosts?)

Acknowledgements: We gratefully acknowledge support from NASA grant NAGW-185.

9. Appendix A

Outline of Derivation of Equations (1) and (2)

based on Van der Waals (1956)

Consider a large number of clathrate cells, consisting of N identical cages. A fraction y of the cages are occupied by guest molecule g. Let m = number of host molecules per cage. Then the partition function for the system is

$$e^{-F/kt} = e^{-F_o/kT} \frac{N!}{(Ny)![N(1-y)]!} \left(h_g(T) \right)^{Ny} \qquad (A1)$$

where F = free energy of system, F_o = free energy of Nm molecules of the host in the empty lattice structure and h_g is the contribution to the partition function of each guest molecule. The combinatorial term on the right expresses the number of distinct ways Ny guest molecules can be distributed over N cavities.

Taking the logarithm of equation (1), and writing the system free energy in terms of chemical potentials $\mu^{cl}_{H_2O}$ and μ^{cl}_g for the host structure and guest, one finds:

$$\frac{\mu^{cl}_g}{kT} = \ln \frac{y}{1-y} - \ln h_g(T) \qquad (A2)$$

$$\frac{\mu^{cl}_{H_2O}}{kT} = \frac{\mu^{B}_{H_2O}}{kT} + \frac{1}{m} \ln (1 - y) \qquad (A3)$$

where $\mu^{B}_{H_2O}$ is the chemical potential of the empty cage structure. Equating the chemical potentials to those of the coexisting phases:

$$\mu^{v}_{g} = \mu^{cl}_{g} \qquad (A4)$$

$$\mu^{i}_{H_2O} = \mu^{cl}_{H_2O} \qquad (A5)$$

where μ^{v}_{g} is the chemical potential of the guest in its coexisting phase and $\mu^{i}_{H_2O}$ is the coexisting phase of water. Equations (A3) and (A5) imply

$$\sum_j \frac{1}{m_j} \ln (1 - y_j) = \frac{\mu^{i}_{H_2O} - \mu^{\beta}_{H_2O}}{kT} \equiv - \frac{\Delta\mu}{kT} \qquad (A6)$$

where we generalized the equation as in Van der Waals and Platteeuw (1959) for j cage sizes. Now

$$\mu^{v}_{g} = kT \left(\ln \frac{f_g}{kT} - \ln \phi_g(T) \right) \qquad (A7)$$

where ϕ_g is the partition function (volume factor removed) of the free molecule. Also

$$h_{gj}(T) = z_{gj}\phi_g(T) \int_0^{a_j/2} e^{-\omega_{gj}(r)/kT} 4\pi r^2 \, dr \qquad (A8)$$

where the factor z_{gj} is 1 for a freely rotating and vibrating encaged molecule. The integral is the volume factor of the encaged-guest partition function, with symbols described in text (equation (3)). Defining

$$C_{gj}(T) \equiv \frac{1}{kT} \left(\frac{h_{gj}(T)}{\phi_g(T)} \right)$$

we combine (A2), (A4), (A7), and (A8):

$$y_{gj} = \frac{C_{gj} f_g}{1 + \sum_i C_{ij} f_i} \qquad (A9)$$

generalized to i guest species; combining (A9) with (A6):

$$\frac{\Delta\mu}{kT} = \sum_j \frac{1}{m_j} \ln \left(1 + \sum_i C_{ij} f_i\right) \qquad (A10)$$

10. Appendix B

Construction of the Ammonia-Water Phase Diagram at High Pressure

Preliminary data of Johnson et al. (1984) indicate the existence of a room temperature transition from ammonia-water solution to an ammonia-dihydrate ($NH_3 2H_2O$) at pressures of relevance to icy satellite interiors. Based on this data, as well as low pressure thermodynamic properties of the dihydrate, we have constructed temperature-composition plots for the NH_3H_2O binary system at a number of pressures.

Data at low pressures on phase transitions of $NH_3 2H_2O$ are in Rollet and Vuillard (1956) and on entropy of freezing in Chan and Giauque (1964); similar data for the NH_3H_2O solid are in Haudenschild (1970) and Hildenbrand and Giauque (1953). Freezing point depression data for water are given in Haudenschild. For an ammonia-water solid compound $zNH_3\ yH_2O$ in equilibrium with a nearly ideal solution containing x mole fraction of water, the freezing point temperature T is given by

$$T = \frac{T_c}{1 - \frac{k}{\Delta s}\left(y \ln \gamma x/x_c + z \ln \frac{1 - x}{1 - x_c} \right)} \qquad \text{(B1)}$$

where Δs is entropy of freezing of a liquid with congruent composition x_c (= y/(z + y)) and T_c is the congruent freezing temperature. Deviations from ideality are incorporated through the activity coeffi-

cient γ which is a function of x, but assumed constant with respect to T and P. γ is found at low pressure for H_2O, $NH_3 \cdot 2H_2O$ and NH_3H_2O by inverting equation (B1). The data of Rollet and Vuillard (1956) for $NH_3 2H_2O$ are extended to metastable temperatures and compositions by fitting to a parabola, since its stability field at low pressures is quite limited in composition and temperature.

The γ values are then used in equation (B1) along with high-pressure freezing point data to construct T-x plots up to 25 kilobars, x from 1 to 0.4. High pressure freezing data for NH_3H_2O were taken from unpublished work by Johnson, Schwake and Nicol. It is implicitly assumed that the low and high pressure dihydrates are the same phase, and likewise for the monohydrate. The resulting phase diagrams at 1 bar, 1, 5, 8, 12, and 24 kilobars are shown in Figure B-1. The form of equation (B1) and assumption $\gamma(x,T,P) = \gamma(x)$ implies that the stability fields of the three solids are described by parabolas of constant shape which move up and down relative to each other for various pressures.

At low pressures the water ice and monohydrate stability fields dominate the diagram; by 5 kilobars the dihydrate stability field overwhelms the monohydrate at x values down to 0.45. The dihydrate continues to be important up to the maximum pressure of 24 kilobars at which a dihydrate-ice VII-liquid triple point was observed by Johnson et al. (1984) at x = 0.85 and 294 K. The data at 24 kilobars require the water ice freezing point to drop ~80-100 K from x = 1 to x = 0.85, twice the drop predicted by low pressure data and equation (B1). Although additional non-ideality at high pressure could arise, it is somewhat

Figure B1. Temperature versus water mole fraction in the binary system NH_3-H_2O, calculated for a number of pressures as described in the text. No data for $2NH_3H_2O$ exist at high pressure; hence, the NH_3H_2O-$2NH_3H_2O$ boundary is shown only at low pressure.

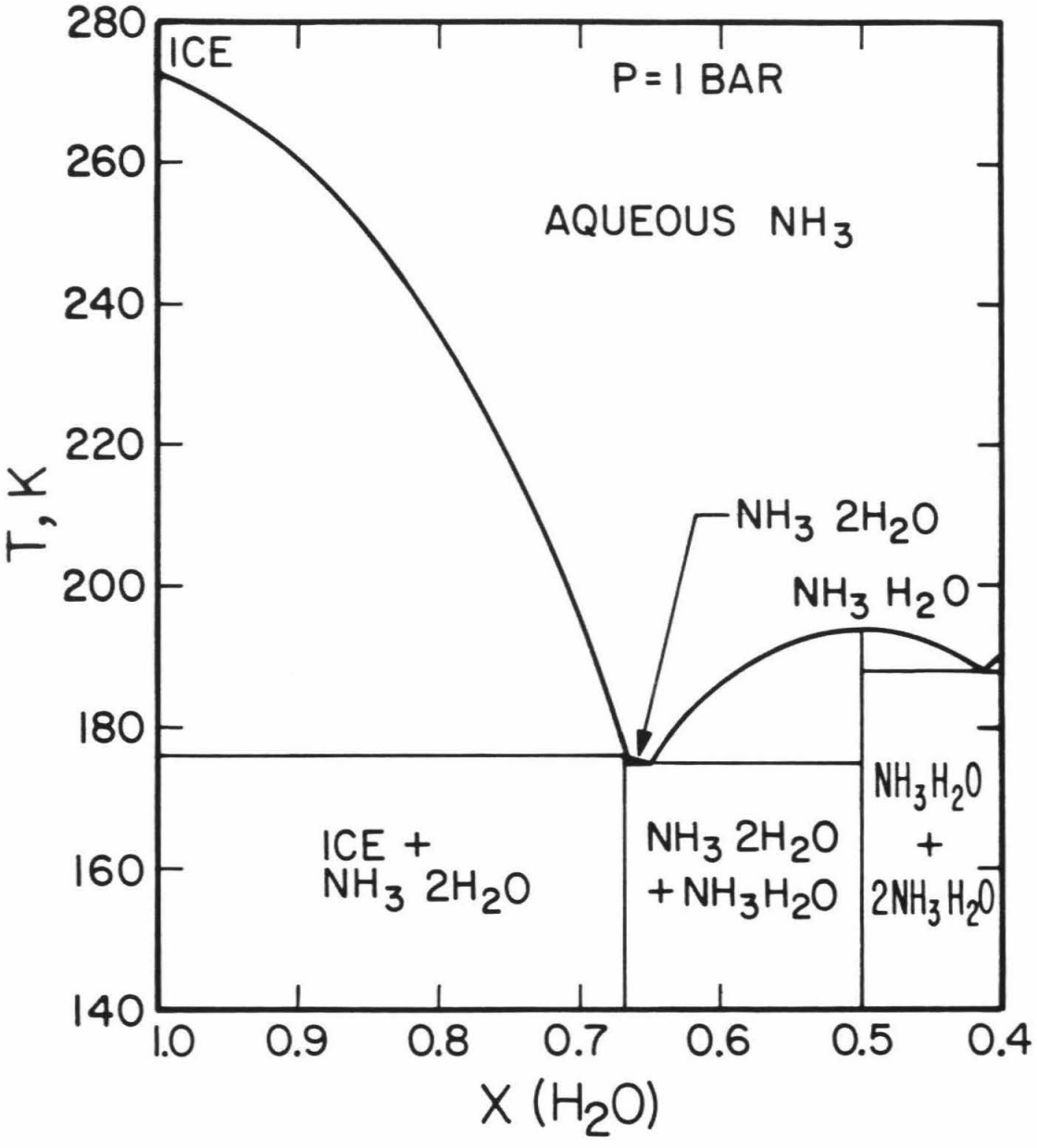
ICE
P = 1 BAR
AQUEOUS NH_3
NH_3 $2H_2O$
NH_3 H_2O
ICE +
NH_3 $2H_2O$
NH_3 $2H_2O$
+ NH_3H_2O
NH_3H_2O
+
$2NH_3H_2O$
T, K
280
260
240
220
200
180
160
140
1.0
0.9
0.8
0.7
0.6
0.5
0.4
X (H_2O)

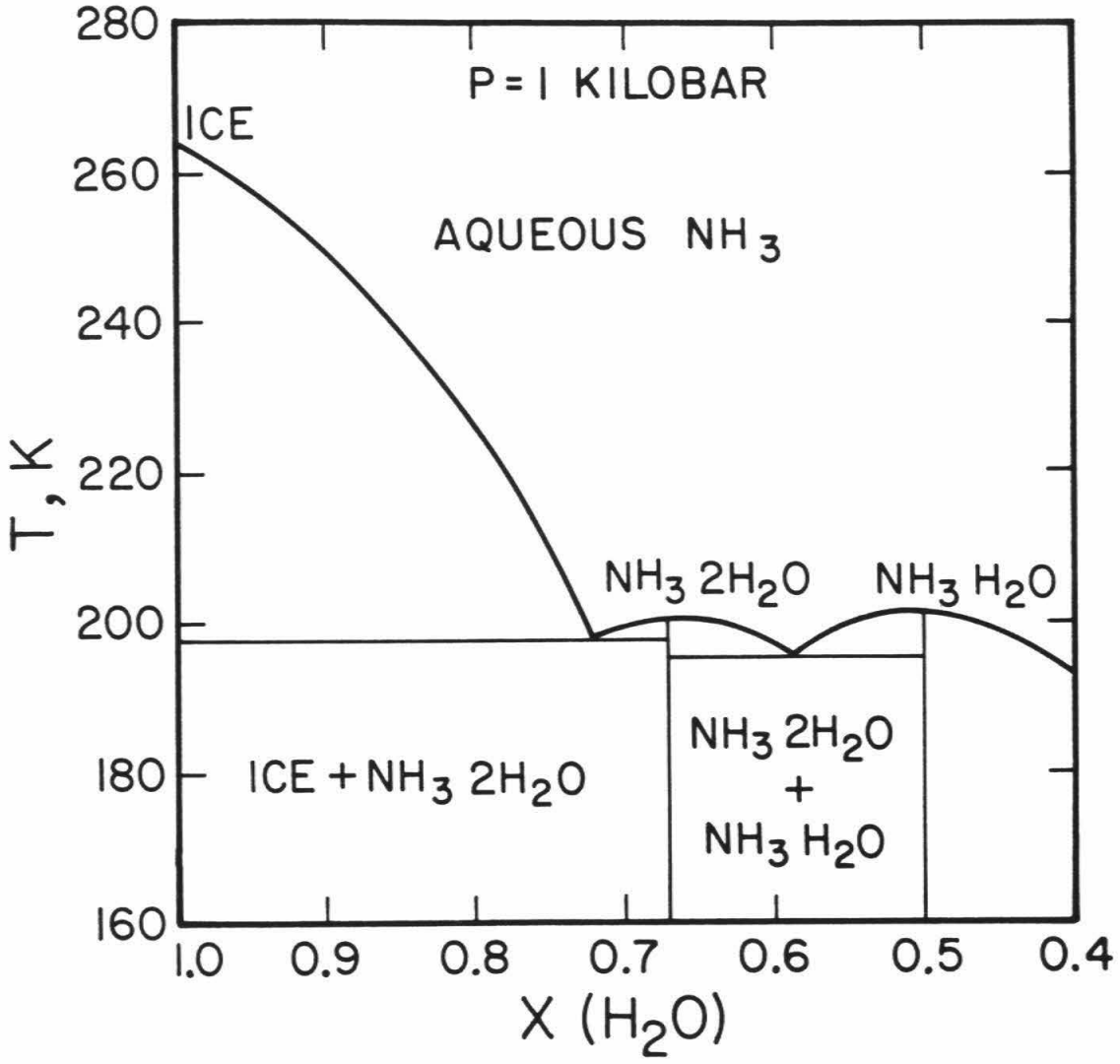
P = 1 KILOBAR
ICE
AQUEOUS NH3
NH3 2H2O
NH3 H2O
ICE + NH3 2H2O
NH3 2H2O
+
NH3 H2O
T, K
280
260
240
220
200
180
160
1.0
0.9
0.8
0.7
0.6
0.5
0.4
X (H2O)

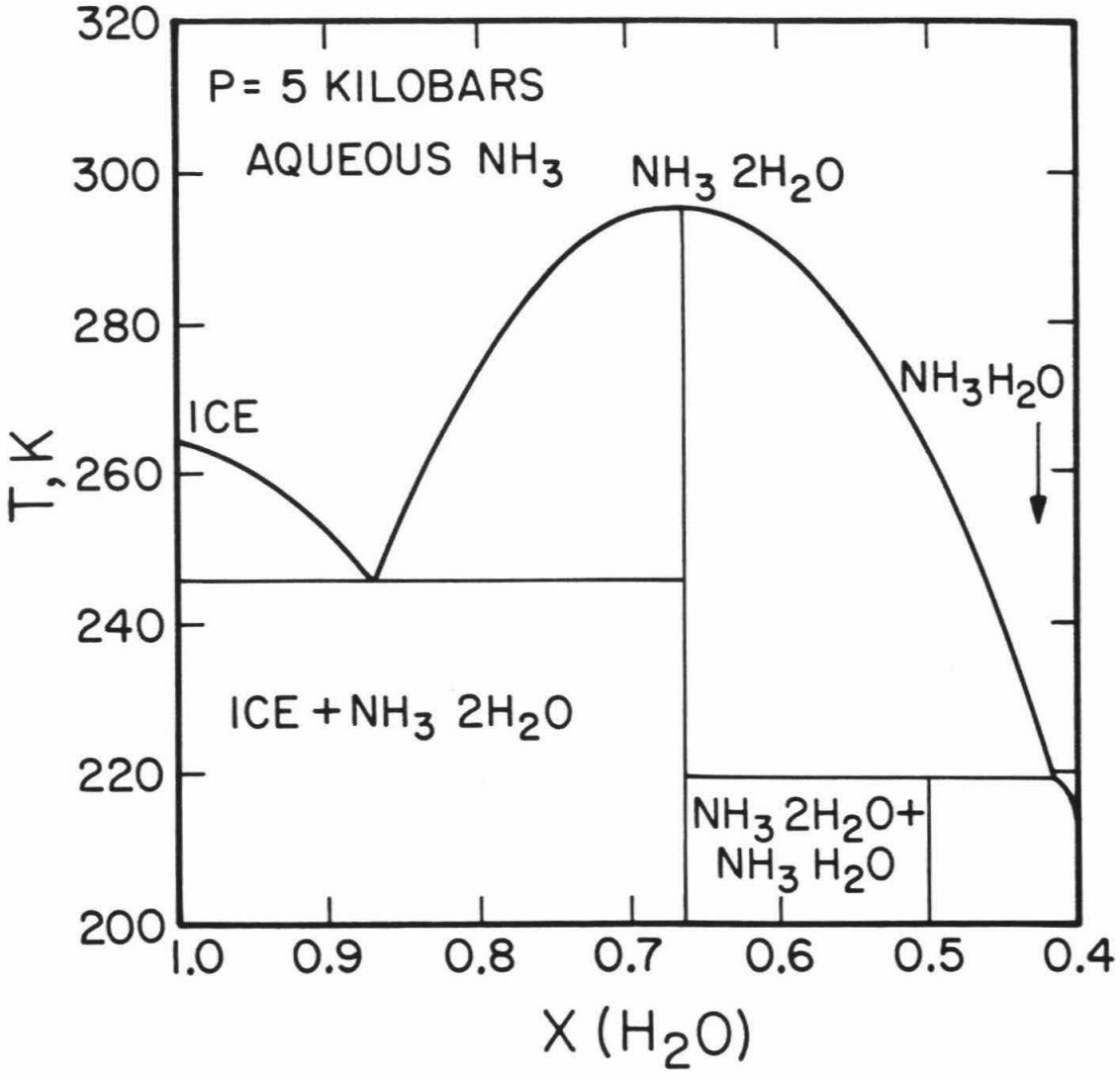
P= 5 KILOBARS
AQUEOUS NH3
NH3 2H2O
NH3H2O
ICE
ICE + NH3 2H2O
NH3 2H2O+
NH3 H2O
T, K
320
300
280
260
240
220
200
1.0
0.9
0.8
0.7
0.6
0.5
0.4
X (H2O)

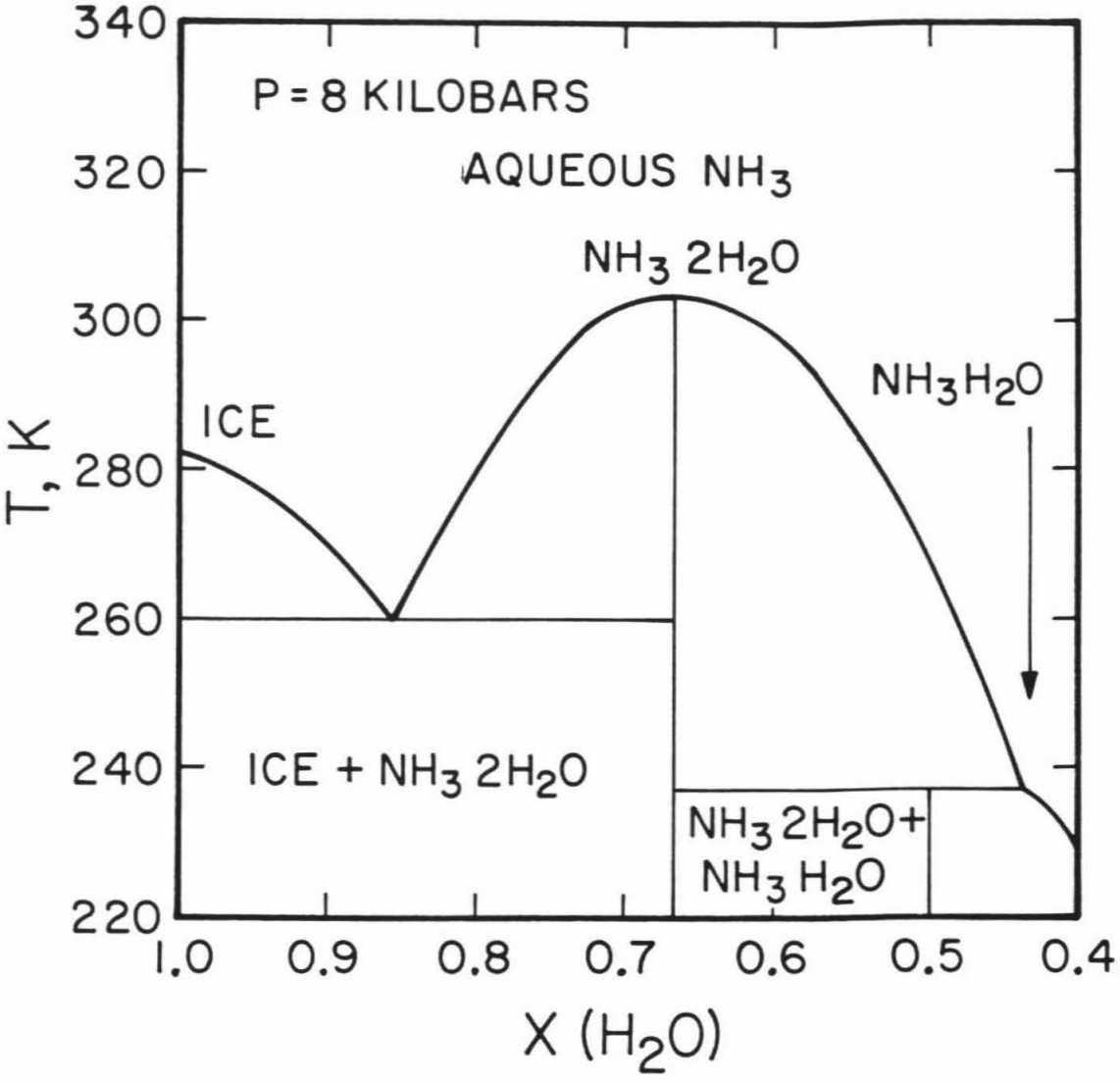
340
320
300
280
260
240
220
T, K
P = 8 KILOBARS
AQUEOUS NH3
NH3 2H2O
NH3 H2O
ICE
ICE + NH3 2H2O
NH3 2H2O+
NH3 H2O
1.0
0.9
0.8
0.7
0.6
0.5
0.4
X (H2O)

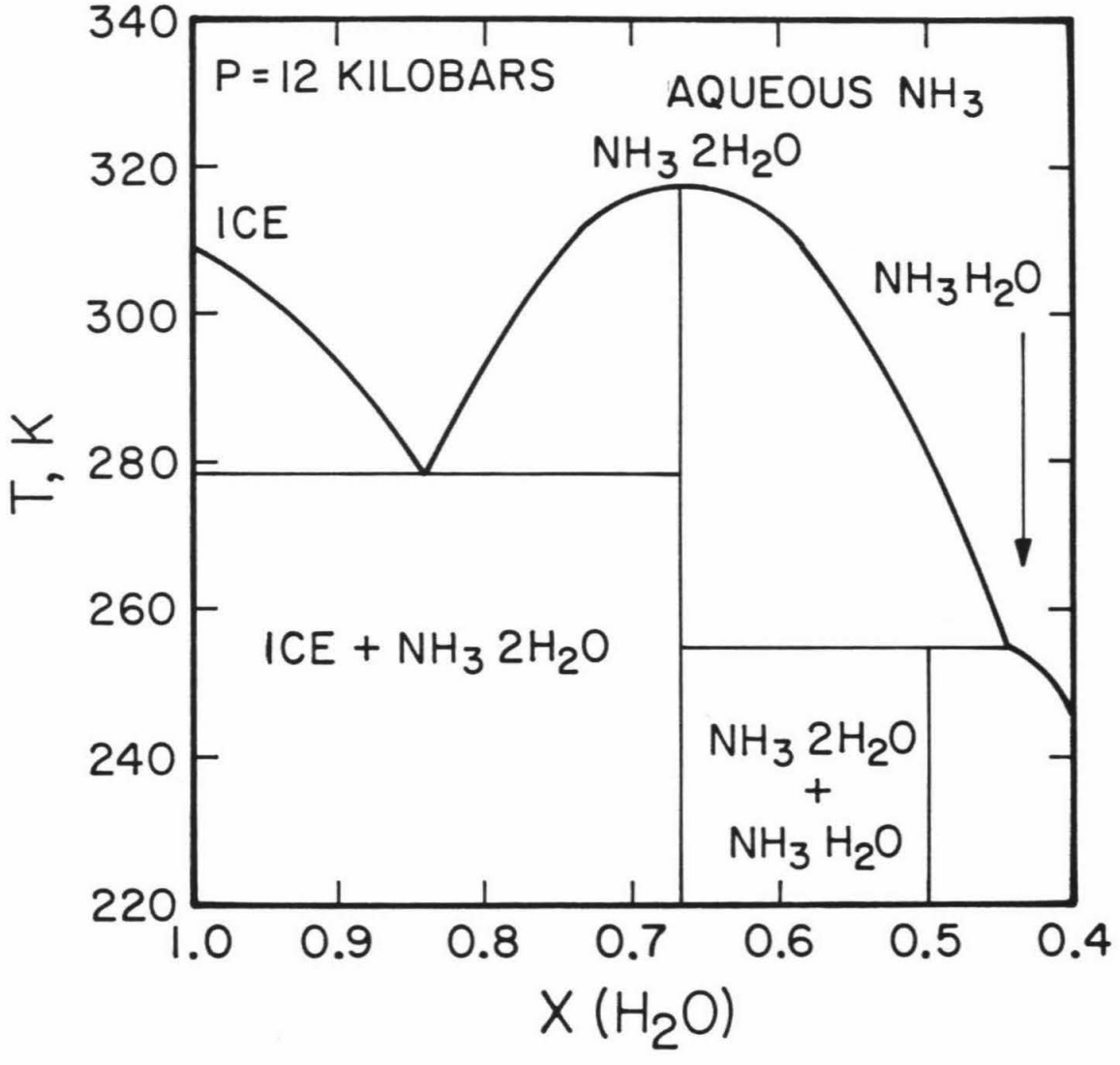
340
320
300
280
260
240
220
T, K
P = 12 KILOBARS
AQUEOUS NH3
NH3 2H2O
ICE
NH3 H2O
ICE + NH3 2H2O
NH3 2H2O
+
NH3 H2O
1.0
0.9
0.8
0.7
0.6
0.5
0.4
X (H2O)

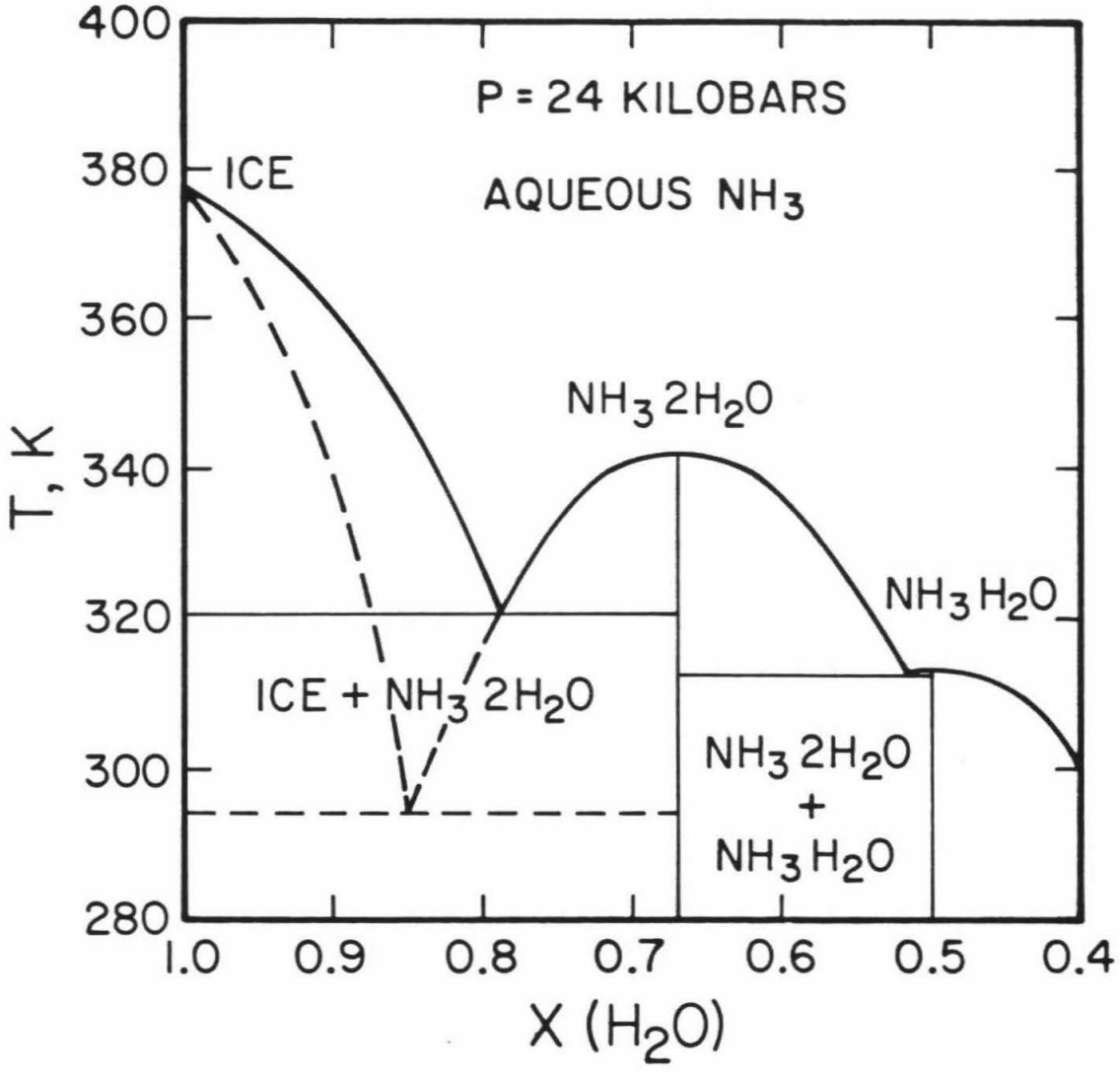
P = 24 KILOBARS
ICE
AQUEOUS NH3
NH3 2H2O
NH3 H2O
ICE + NH3 2H2O
NH3 2H2O
+
NH3 H2O
T, K
400
380
360
340
320
300
280
1.0
0.9
0.8
0.7
0.6
0.5
0.4
X (H2O)

surprising that the effect would be so large; metastability in the experiment cannot be ruled out. Thus, two lines are plotted for $x > 0.8$: the dotted is forced to agree with the experimental triple point, and the solid is based on prediction of equation (B1) and the assumption that the experimental triple point is metastable.

The Clausius-Clapeyron slope $\Delta T/\Delta P$ of congruent dihydrate melting is predicted to be $\simeq +7$ K/kilobar. Using the entropy of freezing in Chan and Giauque (1964) $\Delta V \sim 3$ cm^3/mole which, although the dihydrate density at high pressure is not known, probably corresponds to ~5% volume decrease upon freezing. The dihydrate is thus a denser phase than the corresponding liquid and would sink if formed in a satellite interior.

References

Aaldijk, L. (1971). Dissertation, Woensdag, Rotterdam.

Anders, E. and Ebihara, M. (1982). Geochim. et Cosmochim. Acta, **46**, 2363.

Atreya, S.K., Donahue, T.M., and Kuhn, W.R. (1978). Science, **201**, 611.

Avnir, D., Farin, D., and Pfeifer, P. (1984). Nature, **308**, 261.

Barrer, R.M. and Edge, A.V.J. (1967). Proc. Roy. Soc. London Ser. A, **300**, 1.

Barrer, R.M. and Ruzicka, D.J. (1962). Trans. Far. Soc., **58**, 2262.

Barrer, R.M. (1941). Diffusion in and through Solids (Cambridge: University Press).

Barrer, R.M. (1967). In The Solid-Gas Interface, Vol. 2, ed. E.A. Flood (New York: Marcel Dekker), p. 557.

Bertie, J.E. and Jacobs, S.M. (1977). Can. J. Chem., **55**, 1777.

Bertie, J.E. and Jacobs, S.M. (1978). J. Chem. Phys., **69**, 4105.

Bertie, J.E. and Jacobs, S.M. (1982). J. Chem. Phys., **77**, 3230.

Bridgeman, P. (1913). Proc. Am. Acad. Arts and Sciences, **48**, 307.

Bridgeman, P. (1937). J. Chem. Phys., **5**, 964.

Brownlee, D.E. (1978). In Protostars and Planets, ed. T. Gehrels (Tucson: University of Arizona Press), p. 134.

Byk, S.Sh. and Fomina, V.I. (1968). Russian Chemical Reviews, **37**, 469.

Carman, P.C. (1956). Flow of Gases through Porous Media (New York: Academic Press).

Carslaw, H.S. and Jaeger, J.C. (1959). Conduction of Heat in Solids (Oxford: Clarendon Press).

Chan, J.P. and Giauque, W.F. (1964). J. Phys. Chem., **68**, 3053.

Cheng, A.F. and Lanzerotti, L.J. (1978). J. Geophys. Res., **83**, 2596.

Cheng, V.M., Daniels, W.B., and Crawford, R.K. (1975). Phys. Rev. B, **11**, 3972.

Claypool, G.E. and Kvenvolden, K.A. (1983). Ann. Rev. Earth Planet. Sci., **11**, 299.

Clifford, I.L. and Hunter, E. (1933). J. Phys. Chem., **37**, 101.

Cook, J.G. and Leaist, D.G. (1983). Geophys. Res. Lett., **10**, 397.

CRC Handbook of Chemistry and Physics (1970), ed. R.C. Weast (Cleveland, Ohio: Chemical Rubber Company).

Culberson, O.L. (1951). Petrol. Trans. AIME, **192**, 223.

Davidson, D.W. (1971). Can. J. Chem., **49**, 1224.

Davidson, D.W. (1973). In Water: A Comprehensive Treatise, Vol. 2, ed. F. Franks (New York: Plenum), p. 115.

Davidson, D.W. and Wilson, G.J. (1963). Can. J. Chem., **41**, 1424.

Delsemme, A.H. (1983). In Comets, ed. L. Wilkening (Tucson: University of Arizona Press), p. 85.

Delsemme, A.H. and Miller, D.C. (1970). Planet. Space Sci., **18**, 717.

Delsemme, A.H. and Swings, P. (1952). Annls. Astrophys., **15**, 1.

Delsemme, A.H. and Wenger, A. (1970). Planet. Space Sci., **18**, 709.

Dharma-Wardana, M.W.C. (1983). J. Phys. Chem., **87**, 4185.

Diepen, G.A.M. and Scheffer, F.E.C. (1950). Rec. Trav. Chim., **69**, 593.

Donahue, T.M. and Pollack, J.B. (1983). In Venus, eds. D.M. Hunten, L. Colin, T.M. Donahue, and V.I. Moroz, (Tucson: University of Arizona Press), p. 1003.

Dorsey, N.E. (1940). Properties of Ordinary Water Substance, (Scranton, Pennsylvania: Reinhold).

Eisenberg, D. and Kauzmann, W. (1969). The Structure and Properties of Water (New York: Oxford University Press).

Ellsworth, K. and Schubert, G. (1983). Icarus, **54**, 490.

Evans, III., R.B., Watson, G.M., and Mason, E.A. (1961). J. Chem. Phys., **35**, 2076.

Fanale, F.P., Banerdt, W.B., Saunders, R.S., Johansen, L.A., and Salvail, J.R. (1982). J. Geophys. Res., **87**, 10215.

Fink, U. and Sill, G. (1982). In Comets, ed. L. Wilkening (Tucson: University of Arizona Press), p. 164.

Fowler, R. and Guggenheim, E.A. (1960). Statistical Thermodynamics (Cambridge: Cambridge University Press).

Friedson, A.J. and Stevenson, D.J. (1983). Icarus, **56**, 1.

Gaffney, E.S. and Matson, D.L. (1980). Icarus, **44**, 511.

Gautier, D., Bezard, B., Marten, A., Baluteau, J.P., Scott, N., Chedin, A., Kunde, V., and Hanel, R. (1982). Astrophys. J., **257**, 901.

Giauque, W.F. and Stout, J.W. (1936). J. Am. Chem. Soc., **58**, 1144.

Goodwin, R.D. (1974). NBS Technical Note 653, (Washington, D.C.: U.S. Government Printing Office).

Grace, J.D. and Kennedy, G.C. (1967). J. Phys. Chem. Solids, **28**, 977.

Greenberg, M. (1983). In Comets, ed. L. Wilkening. (Tucson: University of Arizona Press), p. 131.

Hagan, M.M. (1962). Clathrate Inclusion Compounds. (New York: Reinhold Publishing Corp.).

Haltenhorth, H. and Klinger, J. (1969). In Physics of Ice: Proceedings of International Symposium on Physics of Ice, eds. N. Riehl, B. Bullemer, and H. Engelhardt (New York: Plenum Press), p. 579.

Hartmann, W.K. (1973). Icarus, **18**, 634.

Haudenschild, C. (1970). JPL Space Programs Sum. III, 4.

Hildenbrand, D.L. and Giauque, W.F. (1953). J. Am. Chem. Soc., **75**, 2811.

Hirschfelder, J.O., Curtiss, C.F., and Bird, R.B. (1954). Molecular Theory of Gases and Liquids (New York: John Wiley and Sons).

Hobbs, P.V. (1974). Ice Physics (Oxford: Clarendon Press).

Holder, G.D., Corbin, G., and Papadopoulos, K.D. (1980). Ind. Eng. Chem. Fundam., **19**, 282.

Hunten, D.M. (1978). In The Saturn System, ed. D.M. Hunten and D. Morrison (NASA CP 2068), p. 127.

Hunten, D.M., Flasar, F.M., Samuelson, R.E., Strobel, D.F., and Stevenson, D.J. (1984). In Saturn, ed. T. Gehrels (Tucson: University of Arizona Press). In press.

International Critical Tables, Vol. 3, (1928). (New York: McGraw-Hill).

Jacobsen, R.T. and Stewart, R.B. (1973). J. Phys. Chem. Ref. Data, **2**, 757.

Jeffrey, G.A. and McMullan, R.K. (1967). Prog. Inorg. Chem., **8**, 43.

Johari, G.P. and Chew, H.A.M. (1984). Philosophical Mag. B, **49**, 281.

Johnson, M.L., Schwake, A., and Nicol, M. (1984). In Proceedings of NATO Conference Ices in the Solar System, ed. J. Klinger. Submitted.

Kerley, G.I. (1980). J. Appl. Phys., **51**, 5368.

Korvezee, A.E. and Scheffer, F.E.C. (1931). Rec. Trav. Chim., **50**, 256.

Kvenvolden, K.A. and McDonald, T.J. (1982). AGU Trans. EOS, **63**, 1015.

Kvenvolden, K.A. and McMenamin, M.A. (1980). U.S. Geol. Surv. Circ. 825.

Landau, L.D. and Lifshitz, E.M. (1969). Statistical Physics, (Oxford: Pergamon Press).

Lewis, J.S. (1969). Icarus, **10**, 365.

Lewis, J.S. (1971). Icarus, **15**, 174.

Lewis, J.S. (1974). Science, **186**, 440.

Lewis, J.S. and Prinn, R.G. (1980). Astrophys. J., **238**, 357.

Lindal, G.F., Wood, G.E., Hotz, H.B., Sweetnam, D.N., Eshleman, V.R., and Tyler, G.L. (1983). Icarus, **53**, 348.

Lunine, J.I. and Stevenson, D.J. (1982a). Bull. Am. Astron. Soc., **14**, 713.

Lunine, J.I. and Stevenson, D.J. (1982b). Icarus, **52**, 14.

Lunine, J.I., Stevenson, D.J., and Yung, Y.L. (1983). Science, **222**, 1229.

Lupo, M.J. and Lewis, J.S. (1979). Icarus, **40**, 157.

Lupo, M.J. and Lewis, J.S. (1980). Icarus, **42**, 29.

Lutz, B.L., Owen, T., and Cess, R.D. (1976). Astrophys. J., **203**, 541.

Mandelbrot, B.B. (1977). Fractals: Form, Chance, and Dimension, (San Francisco: W.H. Freeman Publishing).

Marion, J.B. (1970). Classical Dynamics of Particles and Systems. (New York: Academic Press).

Marshall, D.R., Saito, S., and Kobayashi, R. (1964). A. I. Ch. E. J., **10**, 202.

Mazo, R.M. (1964). Molecular Physics, **8**, 515.

McKoy, V. and Sinanoglu, O. (1963). J. Chem. Phys., **38**, 2946.

Mel'nik, Yu.P. (1978). Geochem. Intl., **15**(6), 49.

Miller, S.L. (1961). Proc. Natl. Acad. of Sciences US, **47**, 1798.

Miller, S.L. (1973). In Physics and Chemistry of Ice, eds. E. Whalley, S.J. Jones and L.W. Gold (Ottawa: Royal Society of Canada), p.42.

Miller, S.L. (1974). In Natural Gases in Marine Sediments, ed. I.R. Kaplan (New York: Plenum Press), p. 151.

Miller, S.L. and Smythe, W.D. (1970). Science, **170**, 531.

Miller, S.L. (1969). Science, **165**, 489.

Mizuno, H. (1980). Prog. Theor. Phys., **64**, 544.

Mukhin, L.M. (1983). In Venus, eds. D.M. Hunten, L. Colin, T.M. Donahue, and V.I. Moroz (Tucson: University of Arizona Press), p. 1037.

Nagata, I. and Kobayashi, R. (1966). I. and E.C. Fundamentals, **5**. 344.

Omar, M.H., Dokoupil, Z., and Schroten, H.G.M. (1962). Physica, **28**, 309.

Owen, T. (1982). Planet. Space Sci., **30**, 833.

Parrish, W.R. and Prausnitz, J.M. (1972). Ind. Eng. Chem. Process. Des. Develop, **11**, 26.

Pauling, L. and Marsh, R.E. (1952). Proc. Natl. Acad. Sci., **38**, 112.

Pearson, C.F., Halleck, P.M., McGuire, P.L., Hermes, R., and Mathews, M. (1983). J. Phys. Chem., **87**, 4180.

Pinder, K.L. (1964). Can. J. Chem. Eng., 132.

Plummer, P.L.M. and Chen, T.S. (1983). J. Phys. Chem., **87**, 4190.

Pollack, J.B. and Black, D.C. (1982). Icarus, **51**, 169.

Pollack, J.B. and Consolmagno, G. (1984). In Saturn, ed. T. Gehrels (Tucson: University of Arizona Press). In press.

Prausnitz, J.M. (1969). Molecular Thermodynamics of Fluid-Phase Equilibria (Englewood Cliffs, New Jersey: Prentice-Hall).

Prinn, R.G. and Fegley, Jr., B. (1981). Astrophys. J., **249**, 308.

Rebiai, R., Rest. A.J., and Scurlock, R.G. (1983). Nature, **305**, 412.

Reif, F. (1965). Fundamentals of Statistical and Thermal Physics, (New York: McGraw-Hill).

Robertson, S.L. and Babb, Jr., S.E. (1969). J. Chem. Phys., **51**, 1357.

Rollet, A.-P. and Vuillard, G. (1956). Comptes Rend. Acad. Sci., **243**, 383.

Ross, R.G. and Andersson, P. (1982). Can. J. Chem., **60**, 881.

Saito, S., Marshall, D.R., and Kobayashi, R. (1964). A. I. Ch. E. J., **10**, 734.

Samuelson, R.E., Maguire, W.C., Hanel, R.A., Kunde, V.G., Jennings, D.E., Yung, Y.L., Aikin, A.C. (1983). J. Geophys. Res., **88**, 8709.

Selleck, F.T., Carmichael, L.T., and Sage, B.H. (1952). Ind. Eng. Chem., **44**, 2219.

Shipley, T.H. and Didyk, B.M. (1982). Init. Reports Deep Sea Drilling Project, **66**, 547.

Shipley, T.H., Houston, M.H., Buffler, R.T., Shaub, F.J., McMillen, K.J., Ladd, J.W., and Worzel, J.L. (1979). Bull. Am. Assoc. Petrol. Geol., **63**, 2204.

Shmulovich, K.I., Mazur, V.A., Kalinichev, A.G., and Khodorevskaya, L.I. (1980). Geochem. Intl., **17**(6), 18.

Shoji, H. and Langway, Jr., C.C. (1982). Nature, **298**, 548.

Sill, G.T. and Wilkening, L.L. (1978). Icarus, **33**, 13.

Smythe, W.D. (1975). Icarus, **24**, 421.

Stevenson, D.J. (1982a). Nature, **298**, 142.

Stevenson, D.J. (1982b). Lunar Planet. Sci. Conf. Abstract XIII, 770.

Stevenson, D.J. (1984). Paper presented at Uranus Neptune Workshop, Pasadena, California, February 6-8.

Stoll, R.D. and Bryan, G.M. (1979). J. Geophys. Res., **84**, 1629.

Strobel, D.F. and Shemansky, D.E. (1982). J. Geophys. Res., **87**, 1361.

Tamman, G. and Krige, G.J.R. (1925). Zeitschrift fur Anorganische und Allegemeine Chemie, **146**, 179.

Tester, J.W., Bivins, R.L., and Herrick, C.C. (1972). A. I. Ch. E. J., **18**, 1220.

Titus Andronicus (1968), ed. J.D. Wilson, (Cambridge: University Press).

Tse, J.S., Klein, M.L., and McDonald, I.R. (1983). J. Phys. Chem., **87**, 4198.

Tsiklis, D.S., Linshits, L.R., and Goryunova, N.P. (1965). Russian J. Phys. Chem., **39**, 1590.

van Cleef, A. and Diepen, G. (1965). Rec. Trav. Chim., **84**, 1085.

Van der Waals, J.H. (1956). Trans. Far. Soc., **52**, 184.

Van der Waals, J.H. and Platteeuw, J.C. (1959). Adv. Chem. Phys., **2**, 1.

van Kasteren, P.H.G. (1973). Bull. Inst. Int. Froid Annexe, **4**, 81.

von Stackelberg, M. and Meinhold, W. (1954). Zeitschrift fur Elektrochemie, **58**, 40.

von Stackelberg, M. and Muller, H.R. (1954). Zeitschrift fur Elektrochemie, **58**, 25.

Watson, A.J., Donahue, T.M., and Walker, J.C.G. (1981). Icarus, **48**, 150.

Weidenschilling, S.J. (1977). Mon. Not. R. Astron. Soc., **180**, 57-70.

Whalley, E. (1980). J. Geophys. Res., **85**, 2539.

Wiebe, R. and Gaddy, V.L. (1937). J. Am. Chem. Soc., **59**, 1984.

Yung, Y.L., Allen, M., and Pinto, J. (1984). Astrophys. J. Suppl. Ser., in press.

PART II

A. ETHANE OCEAN ON TITAN

B. EVOLUTION OF TITAN'S COUPLED OCEAN-ATMOSPHERE SYSTEM AND INTERACTION OF OCEAN WITH BEDROCK

Ethane Ocean on Titan

Jonathan I. Lunine, David J. Stevenson and Yuk L. Yung

Division of Geological and Planetary Sciences

California Institute of Technology

Pasadena, California 91125

Published in condensed form in

Science, **222**, 1229-1230, 1983

Abstract

We propose a global Titanic ocean, one to several kilometers deep, the modern composition of which is predominantly ethane. If the ocean is in thermodynamic equilibrium with an atmosphere of 3% (mole fraction) methane then its composition is roughly 70% C_2H_6, 25% CH_4, and 5% N_2. Photochemical models predict that C_2H_6 is the dominant end-product of CH_4 photolysis so that the evolving ocean is both the source and sink for ongoing photolysis. The coexisting atmosphere is compatible with Voyager data.

The Voyager 1 IRIS experiment (Hanel et al., 1981) verified that methane is the predominant hydrocarbon molecule above the tropopause of Titan. The Voyager 1 radio-occultation experiment placed a probable upper limit on the abundance of CH_4 in the lower atmosphere of 3 mole % (Lindal et al., 1983), well below the 12% obtained by assuming an atmosphere in equilibrium with a pure methane liquid surface at 94 K. The near-surface temperature gradient inferred from the data is 1.38 ± 0.1 K/km, essentially that of an unsaturated N_2 adiabat over a solid surface. For these reasons a predominantly methane ocean is very unlikely (Flasar, 1983; Eshleman et al., 1983). However, the present abundance of CH_4 in the atmosphere will be consumed by photochemical processes in a time of order 10^7 years. Alternatively, an almost pure N_2 atmosphere is still compatible with the presence of an ocean provided the dominant oceanic constituent is less volatile than CH_4, and substantially depresses the CH_4 vapor pressure. Photochemical modeling provides a natural candidate: ethane. An ethane-rich ocean containing ~25% CH_4 is shown below to be consistent with the occultation data, as well as providing a long-lived ($\gtrsim 10^9$ year) source for methane photolysis. The essential new idea presented here of an ocean in which the CH_4 vapor pressure is depressed by the presence of higher hydrocarbons has been suggested independently by F. Flasar and J. Pearl (Flasar, 1983; Eberhardt, 1983).

The essential aspects of mesospheric chemistry of CH_4 were due to Strobel (1973; 1974). Laboratory studies by Lasaga et al. (1971) Scattergood and Owen (1977), Chang et al. (1979), Bar-Nun and Podolak

(1979), and Gupta et al. (1981) have produced substantial amounts of C_2 and C_3 hydrocarbons from CH_4 dissociation. We present here, in outline form, the photochemical model of Yung et al. (1984). Methane is readily photolyzed in the mesosphere of Titan by absorption of sunlight shortward of 1450 Å to yield the reactive radicals $^1CH_2$, CH_2, and CH, which can further react to produce C_2H_4 and C_2H_2. The net result can be schematically summarized as

$$2CH_4 \rightarrow C_2H_4 + 2H + H_2$$

$$2CH_4 \rightarrow C_2H_2 + 3H_2 \text{ (or } H_2 + 4H)$$

With the rapid loss of hydrogen via escape, the conversion of CH_4 into the heavier hydrogen-poor hydrocarbons is extremely efficient (>95% per CH_4 dissociation) and irreversible. The most likely fate for C_2H_4 in the mesosphere is dissociation to C_2H_2. Since there are no effective permanent sinks for C_2H_2 in the mesosphere, the molecule flows downward to the stratosphere, and is ultimately removed by condensation at the tropopause.

Photochemistry in the stratosphere is initiated by absorption of photons between 1450 and 2000 Å by C_2H_2, resulting in the photosensitized dissociation of CH_4, and ultimately the production of C_2H_6. The possibility of photosensitized dissociation of CH_4 and subsequent stratospheric chemistry was first proposed by Allen et al. (1980), and supported by laboratory investigators of Okabe (1981;

1983). The net result can be summarized as

$$2CH_4 \rightarrow C_2H_6 + H_2$$

$$2CH_4 \rightarrow C_2H_6 + 2H$$

where C_2H_2 plays the role of a catalyst. With the formation of C_4H_2 (diacetylene) it is possible to drive the photosensitized dissociation of CH_4 using photons as soft as 2300 Å. Since the solar flux increases drastically from 1450 to 2300 Å, the rate of C_2H_6 production in the atmosphere can be much larger than that of C_2H_2. Once it is formed, C_2H_6 is stable against photolysis in part due to shielding by CH_4 and C_2H_2. The primary loss mechanism for stratospheric C_2H_6 is condensation at the tropopause.

The column-averaged mixing ratios for stratospheric H_2, C_2H_6, C_2H_4, C_2H_2 and C_3H_8 predicted by the model are, respectively, 2.1×10^{-3} (2×10^{-3}), 1.7×10^{-5} (2×10^{-5}), 3.3×10^{-8} (4×10^{-7}), 4×10^{-6} (2×10^{-6}), and 7.9×10^{-7} ($2\text{-}4 \times 10^{-6}$), and compare favorably with the observed values enclosed in parentheses (Hanel et al., 1981; Maguire et al., 1981; Kunde et al., 1981; Samuelson et al., 1981; Smith et al., 1982). The column averaged mixing ratio is defined as the ratio of the column integrated abundance of a given species to the same column of N_2 above the tropopause. Integrated production rates and fluxes refer to the surface. In the current epoch, the atmosphere is destroying CH_4 at the rate of 1.5×10^{10} cm^{-2} s^{-1} and converting it into C_2H_6, C_2H_2, and

C_3H_8 at the rates 5.8×10^9, 1.2×10^9, and 1.4×10^8 cm^{-2} s^{-1}. H and H_2 escape from the exosphere at the rates 5.5×10^9 and 7.2×10^9 cm^{-2} s^{-1}. Over the age of the solar system then, a primarily ethane liquid surface layer of order one kilometer deep in coexistence with methane and molecular nitrogen has accumulated. The depth is compatible with limits derived by Sagan and Dermott (1982) from a study of the tidal damping of Titan's orbital eccentricity.

Existing thermodynamic data for C_2H_6-CH_4-N_2 system is restricted to temperatures above 110 K (Ellington et al., 1959; Chang and Lu, 1967); however, lower temperature data exist for binary end-members of this ternary (Miller and Staveley, 1976) and we have thereby estimated equilibrium abundances of the three components for the present conditions at the surface of Titan. In the C_2H_6-CH_4 binary, the ethane vapor pressure at 94 K, Titan's surface temperature, is only $\sim 10^{-5}$ bars. The binary system is nearly ideal so that the mole fraction X_{CH_4} of CH_4 in the liquid is given by

$$X_{CH_4} = P_{CH_4} / P^{o}_{CH_4}$$

where P_{CH_4} is the partial pressure of CH_4 in the atmosphere and $P^{o}_{CH_4}$ is the saturation vapor pressure of CH_4 over the pure liquid at the surface temperature. If we require that the methane mixing ratio at the base of the atmosphere is constrained to between 1.6% and 3%, as suggested by Voyager data, then the methane mole fraction of the liquid is between 13% and 25%. If the CH_4 is not perfectly mixed, its surface mixing

ratio could be as high as 9% (Flasar, 1983) yielding an ocean with as much as 70% CH_4. Figure 1 plots CH_4 mole fraction in the ocean versus its pressure in the atmosphere. For a given CH_4 mole fraction, the ocean depth may be calculated using the C_2H_6 production rate given above. Figure 2 plots depth versus X_{CH_4} assuming ideal mixing. The nitrogen content of the ocean has been estimated using N_2-CH_4 and N_2-C_2H_6 solubility data (Cheung and Wang, 1964) to estimate the Henry's law constant for N_2 in the C_2H_6-CH_4 mixture as (Prausnitz, 1969, p. 373):

$$\log K_{N_2,C_2H_6\text{-}CH_4} = X_{CH_4} \log K_{N_2,CH_4} + (1 - X_{CH_4}) \log K_{N_2,C_2H_6}$$

where $K_{N_2,y}$ is the Henry's law constant for N_2 dissolved in component y, and the system is assumed ideal. Figure 1 plots the mole fraction of N_2, X_{N_2}, as a function of X_{CH_4} in the ocean for an N_2 surface pressure of 1.5 bars. For $X_{CH_4} \simeq 0.25$, $X_{N_2} \simeq 0.05$. A miscibility gap is possible with an N_2-CH_4 layer separating above a primarily C_2H_6-CH_4 layer (Ellington et al., 1959; Chang and Lu, 1967). An approximate extrapolation of the 111 K data down to 94 K suggests that the miscibility gap requires $X_{N_2} \gtrsim 0.15$. The presence of at least several percent propane dissolved in the liquid, implied by the Voyager data, does not alter substantially the CH_4 and N_2 mixing ratios derived above.

At the present temperature of Titan's surface, acetylene is a solid. We estimate its solubility in the ocean at 94 K to be $\lesssim 3.1 \times 10^{-4}$, using regular solution theory presented in Prausnitz (1969, p. 398) and data in Presten and Prausnitz (1970). The density at 94 K of

Figure 1. Partial pressure of CH_4 (bars) at base of atmosphere and mole fraction of N_2 dissolved in CH_4–C_2H_6 liquid as a function of CH_4 mole fraction in liquid, at 94 K. To convert right-hand scale to methane mole fraction divide by 1.5 bars.

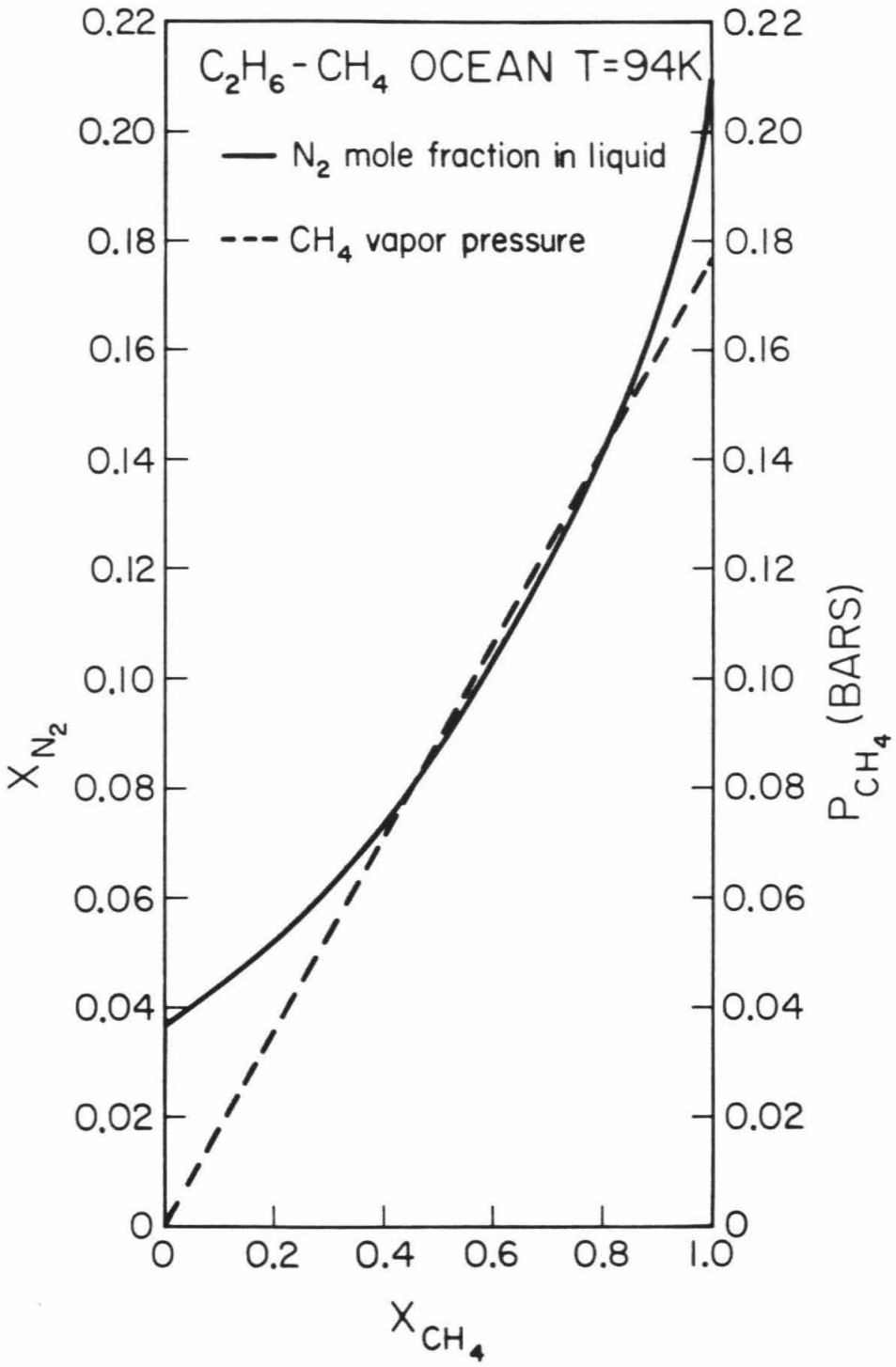
C_2H_6 - CH_4 OCEAN T=94K
N_2 mole fraction in liquid
CH_4 vapor pressure
X_{N_2}
P_{CH_4} (BARS)
X_{CH_4}
0.22
0.20
0.18
0.16
0.14
0.12
0.10
0.08
0.06
0.04
0.02
0
0.2
0.4
0.6
0.8
1.0

Figure 2. Ocean depth in kilometers as a function of methane mole fraction in ocean, assuming remainder of ocean is ethane produced photochemically over the age of the solar system at rate given in text. Volumes of pure constituents from Goodwin (1974) and Goodwin et al. (1976).

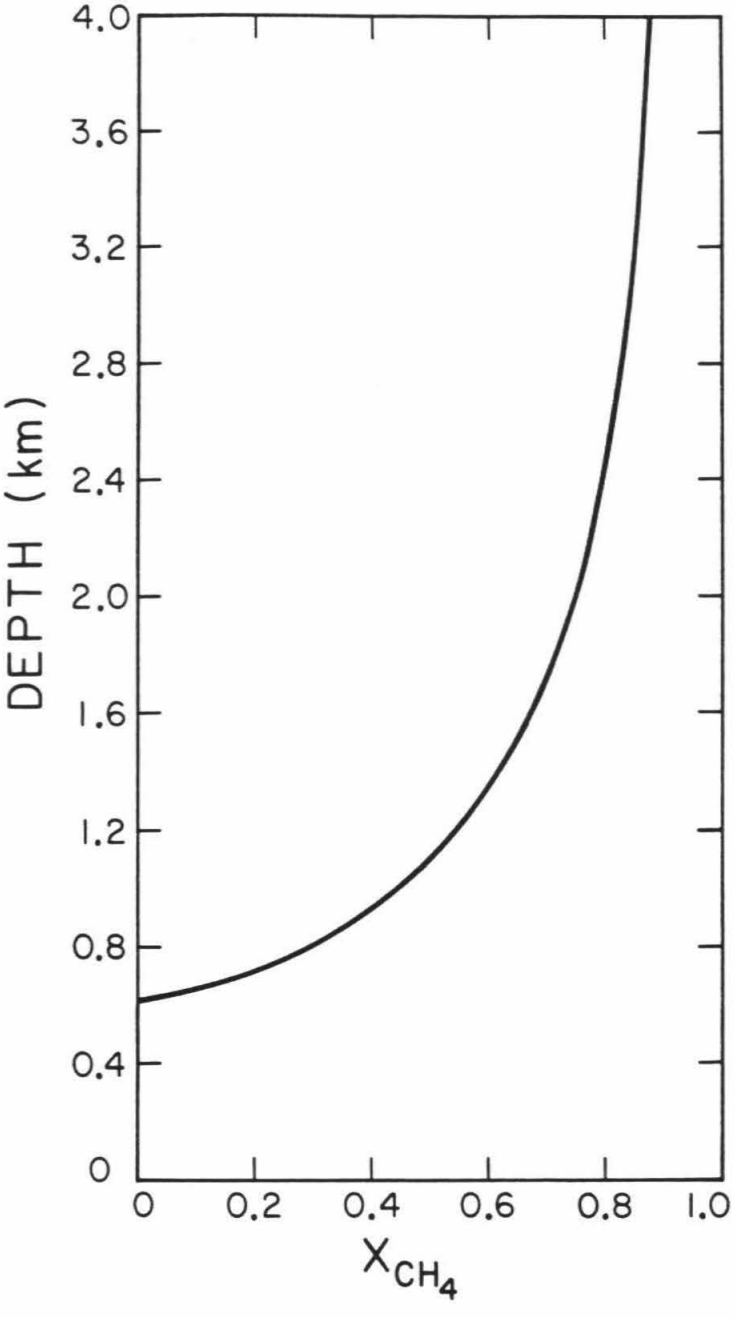
4.0
3.6
3.2
2.8
2.4
2.0
1.6
1.2
0.8
0.4
0
DEPTH (km)
0
0.2
0.4
0.6
0.8
1.0
X_{CH_4}

solid acetylene is 0.78 g/cm^3, extrapolated from Amamchyan and Moroz (1965); that of the liquid ocean is 0.61 g/cm^3 (Goodwin et al., 1976, p. 64; Goodwin, 1974, p. 136; Jacobsen and Stewart, 1973). The ocean floor should be covered with a layer 100-200 meters thick, consisting of acetylene mixed with heavier polymeric debris manufactured from the acetylene both in the upper atmosphere (Hunten et al., 1984) and after deposition on the ocean floor.

We have also examined the solubility of minor constituents in the ocean. CO_2 is sufficiently soluble than an amount equal to the inferred atmospheric abundance of CO (Lutz et al., 1983) may be dissolved. CO and H_2 are relatively insoluble. Because the ocean is capable of dissolving large amounts of Ar and Kr it will control their atmospheric abundances. The ratio of Kr/Ar over the ocean can be predicted and may be diagnostic of the evolution of Titan (see part I of thesis).

We turn now to the atmospheric structure and meteorology above an ethane-methane ocean. A rising parcel of gas, expanding adiabatically, forms ethane-rich droplets and follows a temperature path defined by a ''wet'' adiabat. The adiabatic temperature gradient in an atmosphere of temperature T and pressure P, containing a condensable with vapor pressure e, is (Houghton, 1977, p. 19):

$$\frac{dT}{dz} = \left.\frac{dT}{dz}\right|_{dry} \frac{1 + \frac{Le\ M_V}{PRT}}{1 + \frac{Le\ M_V}{PRT}\frac{\varepsilon L}{cT}}$$

where L = latent heat of condensation, M_v = molecular weight of condensable, ε = ratio of molecular weight of condensable to that of dry gas, R = gas constant, c = specific heat of dry gas. $dT/dz|_{dry}$ is 1.40 K/km for the near surface of Titan (Lindal et al., 1983). This expression is valid to about 15% for $e/p \lesssim 0.1$. Using values of L for methane (Goodwin, 1974, p. 12) and c for nitrogen (Jacobsen and Stewart, 1973), dT/dz as a function of e/p is plotted in Figure 3. Because dT/dz is only weakly dependent on M_v, and L is similar for CH_4 and C_2H_6 (Goodwin et al., 1976, p. 73), the figure is valid for either C_2H_6 or CH_4 as the major condensable. Since the relevant vapor pressure predominantly is that of ethane, $e/p \sim 10^{-5}$, and the resulting lapse rate is found to be about 1.4 K/km, essentially indistinguishable from the dry N_2 adiabat or the radio occultation result of 1.38 ± 0.1 K/km (Lindal et al., 1983). This should be contrasted with the expected wet adiabatic lapse rate of 0.6 K/km for a methane ocean, for which $e/p \sim 0.12$. (Lindal et al. (1983), in computing the saturated adiabat for methane, used an expression which omitted a term involving the change of vapor pressure with temperature and found a value of 0.3 K/km.) Despite the small amount of condensation, it is possible to have significant scattering optical depth: the condensation of a few tens of microbars of C_2H_6 into 0.1 μ droplets gives an optical depth in excess of unity. This may affect the radiative-convective transport in the lower atmosphere which could be relevant to understanding the transition from adiabatic to subadiabatic conditions at 3.5 km as inferred from the radio occultation data.

At successively higher levels in the atmosphere, droplet con-

Figure 3. Adiabatic temperature gradient (K/km) as a function of condensable gaseous mixing ratio e/p at the base of Titan's atmosphere. Horizontal bars bracket Voyager radio occultation measurements (Lindal et al., 1983). Calculation is valid for log e/p $\lesssim -1$; the curve is connected smoothly to dT/dz value for a pure methane atmosphere (log e/p = 0).

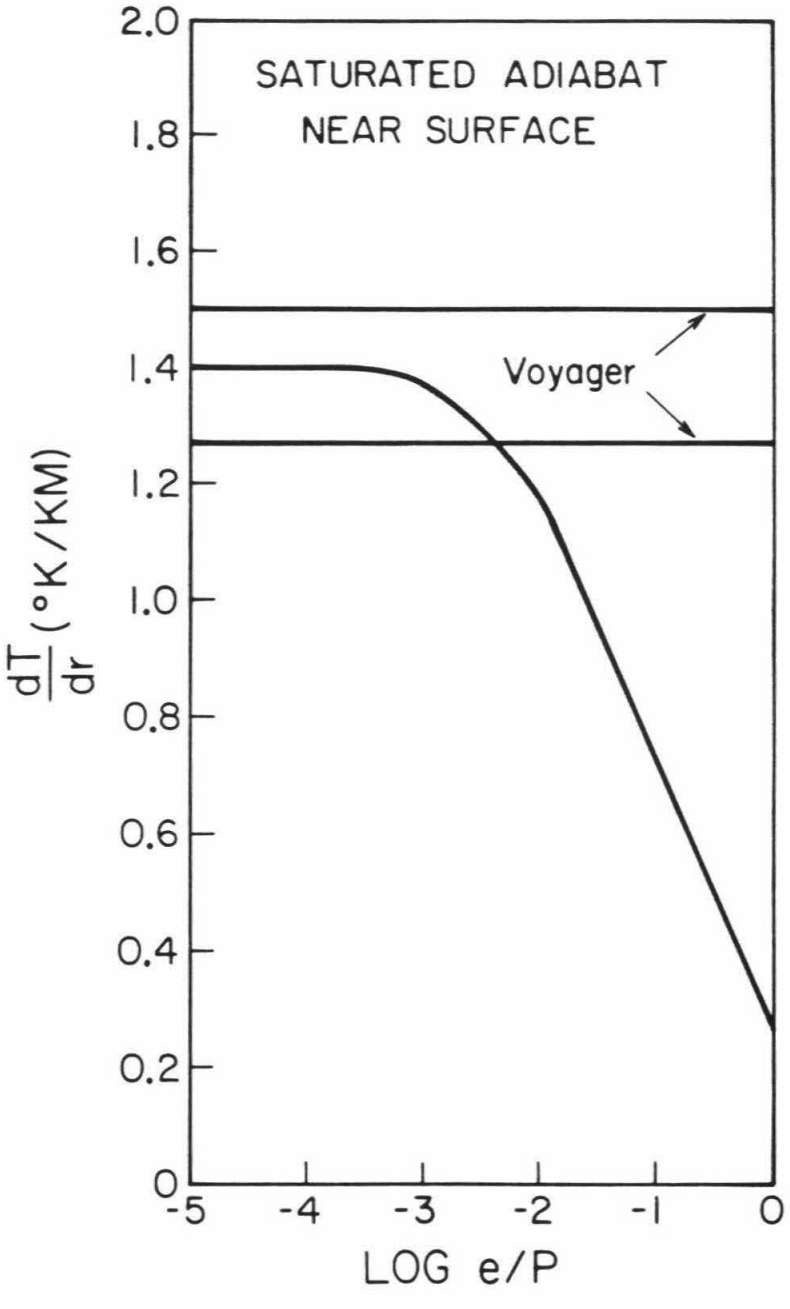
SATURATED ADIABAT
NEAR SURFACE
Voyager
2.0
1.8
1.6
1.4
1.2
1.0
0.8
0.6
0.4
0.2
0
-5
-4
-3
-2
-1
0
dT/dr (°K/KM)
LOG e/P

densation still occurs with the composition of the droplets becoming more methane rich, as dictated by the assumed constant methane mixing ratio and rapidly decreasing ethane vapor pressure. Eventually, a solid condensate forms, primarily methane, in coexistence with liquid droplets. Data from Moran (1959) indicate that the temperature at which the mixed solid forms is only slightly above the temperature at which the methane itself saturates out to form a pure solid condensate. Thus, assuming droplets remain suspended, the condensate sequence with increasing altitude is: ethane-rich mist grading to methane rich mist, coexisting solid haze and mist over a narrow altitude regime, and finally massive methane haze. The last defines the primary region of condensation in the troposphere and for 3% methane mixing ratio occurs at 16 km, as shown in Figure 4.

The structure of ocean and atmosphere are illustrated schematically in Figure 5. The ocean contains the equivalent of at least one Titan atmosphere of CH_4, sufficient to maintain photolysis for $\gtrsim 10^9$ years, and at least 0.2 Titan atmosphere of N_2, a significant buffer of the present atmosphere. The most important observational tests of our model are (i) Verification of the presence of methane clouds as an opacity source in the lower atmosphere (Courtin, 1982; Samuelson, 1983); (ii) Detection of C_2H_6 saturation or near saturation in the lower troposphere; (iii) Evidence (radar or otherwise) of an essentially global ocean, since the expected depth exceeds nearly all probable elevation differences for an icy satellite (c.f. Ganymede).

Figure 4. Altitude and temperature versus CH_4 pressure in Titan atmosphere, for various gaseous mixing ratios of CH_4 assumed constant with altitude, using data of Lindal et al. (1983). Also shown is saturation vapor pressure curve for solid CH_4 from Trafton (1980). Intersection of dashed curve with saturation line defines region of pure methane condensation. Shown displaced for clarity is line defining region of mixed ethane-methane solid condensate, which actually would be almost coincident with pure methane saturation line on this scale.

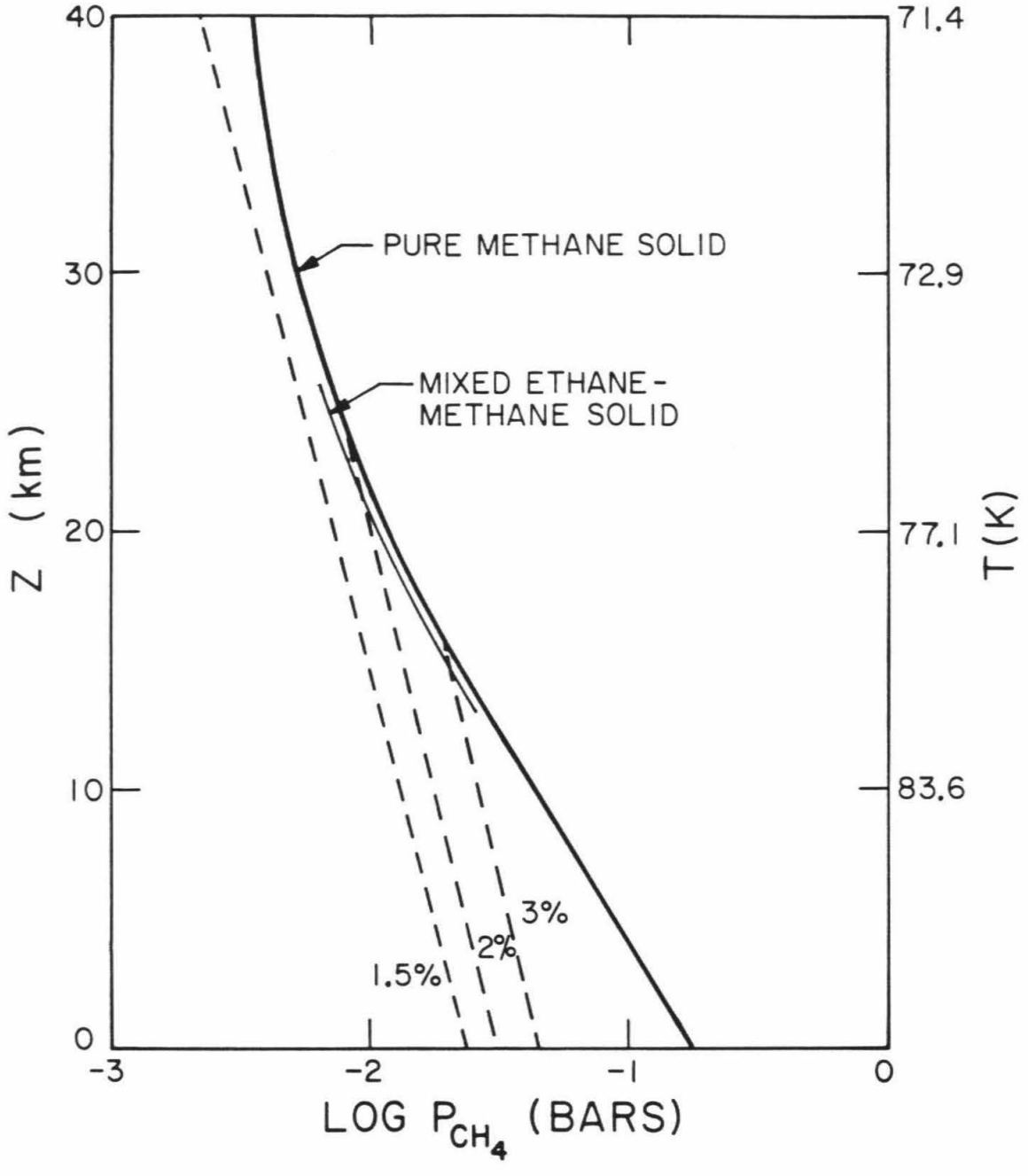
40
30
20
10
0
Z (km)
71.4
72.9
77.1
83.6
T(K)
PURE METHANE SOLID
MIXED ETHANE-
METHANE SOLID
3%
2%
1.5%
-3
-2
-1
0
LOG P_{CH_4} (BARS)

Figure 5. Model of Titan's near surface and atmospheric structures. Plotted is altitude versus temperature from reference (1). Below surface the temperature in the ocean is assumed to follow an adiabat. The mass of ethane-rich mist decreases with altitude in accordance with its vapor pressure relation; above 15-20 km an essentially pure methane haze may condense out. Note the change in altitude scale below 0 km.

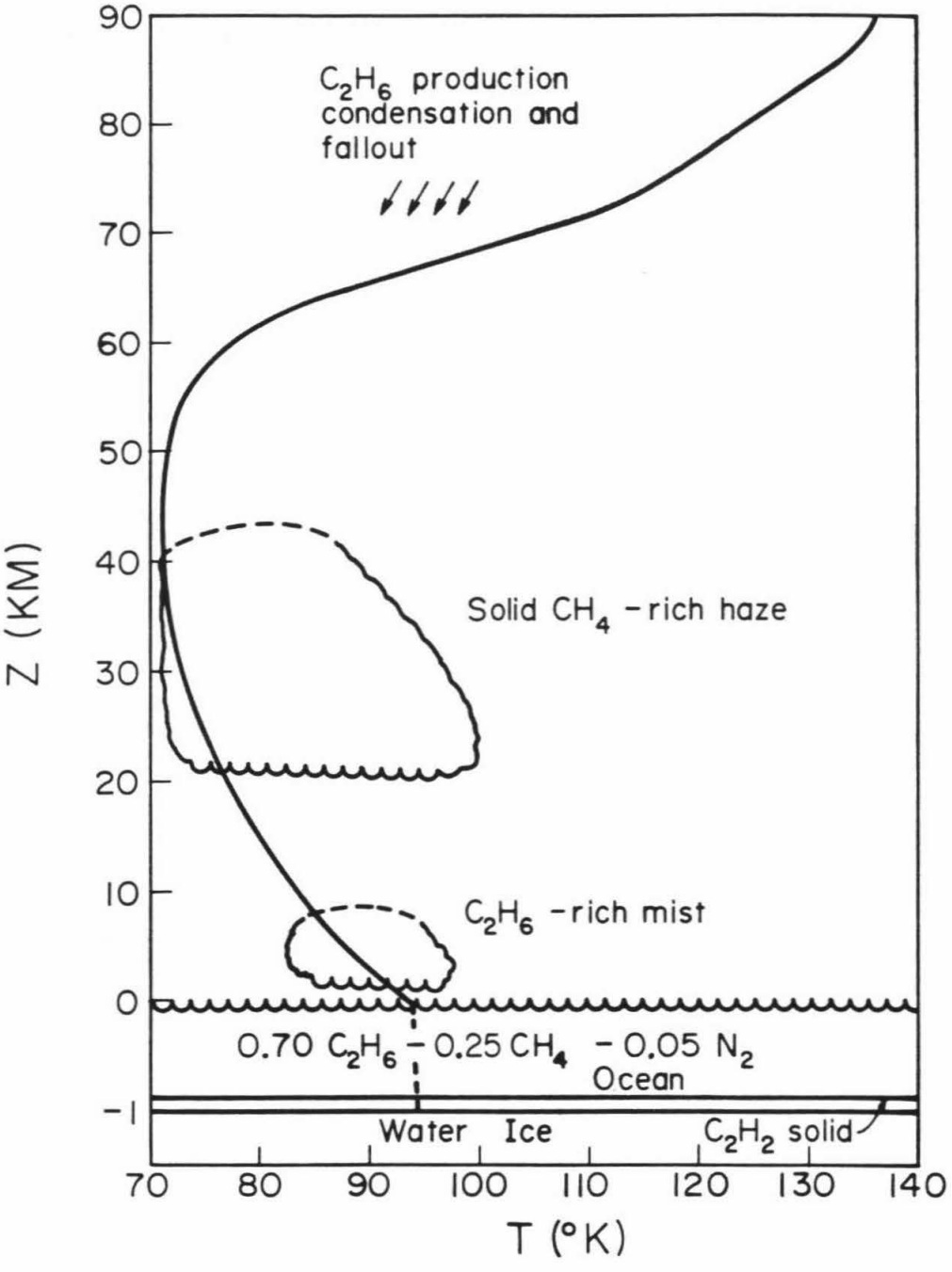
90
80
70
60
50
40
30
20
10
0
-1
Z (KM)
C_2H_6 production
condensation and
fallout
Solid CH_4 - rich haze
C_2H_6 - rich mist
0.70 C_2H_6 - 0.25 CH_4 - 0.05 N_2
Ocean
Water Ice
C_2H_2 solid
70
80
90
100
110
120
130
140
T (°K)

References

Allen, M., Pinto, J.P., and Yung, Y.L. (1980). Astrophys. J. Lett., **242**, L125.

Amamchyan, R.G. and Moroz, A.I. (1965). Tr Vses Nauchn-Issled Inst. Kislorodn Mashinostr., **10**, 150.

Bar-Nun, A. and Podolak, M. (1979). Icarus, **38**, 115.

Chang, S.-D. and Lu, B.C.-Y. (1967). Chem. Engng. Progr. Symp. Ser., **63**, 18.

Chang, S., Scattergood, T., Aronowitz, S., and Flores, J. (1979). Rev. Geophys. Space Phys., **17**, 1923.

Cheung, H. and Wang, D.I.-J. (1964). I and EC Fundamentals, **3**, 355.

Courtin, R. (1982). Icarus, **51**, 466.

Eberhardt, J. (1983). Science News, **124**, 28.

Ellington, R.T., Eakin, B.E., Parent, J.D., Gami, D.C., Bloomer, O.T. (1959). In Thermodynamic and Transport Properties of Gases, Liquids and Solids, Y.S. Toloukian, ed. (New York: McGraw-Hill), p. 180.

Eshleman, V.R., Lindal, G.F., and Tyler, G.L. (1983). Science, **221**, 55.

Flasar, F.M. (1983). Science, **221**, 57.

Goodwin, R.D., Roder, H.M., Straty, G.C. (1976). National Bureau of Standards Technical Note 684.

Goodwin, R.D. (1974). National Bureau of Standards Technical Note 653.

Gupta, S., Ochiai, E., and Ponnamperuma, C. (1981). Nature, **293**, 725.

Hanel, R., Conrath, B., Flasar, F.M., Kunde, V., Maguire, W., Pearl, J., Pirraglia, J., Samuelson, R., Herath, L., Allison, M., Cruikshank, D., Gierasch, P., Horn, L., Koppany, R., and Ponnamperuma, C. (1981). Science, **212**, 192.

Houghton, J.T. (1977). The Physics of Atmospheres. (Cambridge: University Press).

Hunten, D.M., Tomasko, M.G., Flasar, F.M., Samuelson, R.E., Strobel, D.F., and Stevenson, D.J. (1984). In Saturn, T. Gehrels, ed. (Tucson: University of Arizona Press), in press.

Jacobsen, R.T. and Stewart, R.B. (1973). J. Phys. Chem. Ref. Data, **2**, 757.

Kunde, V.G., Aikin, A.C., Hanel, R.A., Jennings, D.E., Maguire, W.C., and Samuelson, R.E. (1981). Nature, **292**, 686.

Lasaga, A.C., Holland, H.D., and Dwyer, M.J. (1971). Science, **174**, 53.

Lindal, G.F. Wood, G.E., Hotz, H.B., Sweetnam, D.N., Eshleman, V.R., and Tyler, G.L. (1983). Icarus, **53**, 348.

Lutz, B.L., deBergh, C., and Owen, T. (1983). Science, **220**, 1374.

Maguire, W.C., Hanel, R.A., Jennings, D.E., Kunde, V.G., and Samuelson, R.E. (1981). Nature, **292**, 683.

Miller, R.C. and Staveley, L.A.K. (1976). In Advances in Cryogenic Engineering Vol. 21, K.D. Timmerhaus and D. H. Weitzel, eds. (New York: Plenum Press), p. 493.

Moran, D.W. (1959). Dissertation, University of London.

Okabe, H. (1981). J. Chem. Phys., **75**, 2772.

Okabe, H. (1983). J. Chem. Phys., **78**, 1312.

Prausnitz, J.M. (1969). Molecular Thermodynamics of Fluid Phase Equilibria (Englewood Cliffs, New Jersey: Prentice-Hall).

Presten, G.T. and Prausnitz, J.M. (1970). Ind. Eng. Chem. Proc. Des. Develop., **9**, 264.

Sagan, C. and Dermott, S.F. (1982). Nature, **300**, 731.

Samuelson, R.E., Hanel, R.A., Kunde, V.G., and Maguire, W.C. (1981). Nature, **292**, 688.

Samuelson, R.E. (1983). Icarus, **53**, 364.

Scattergood, T. and Owen, T. (1977). Icarus, **30**, 780.

Smith, G.R., Strobel, D.F., Broadfoot, A.L., Sandel, B.R., Shemansky, D.E., and Holberg, J.B. (1982). J. Geophys. Res., **87**, 1351.

Strobel, D.F. (1973). J. Atmos. Sci., **30**, 489.

Strobel, D.F. (1974). Icarus, **21**, 466.

Trafton, L. (1980). Icarus, **44**, 53.

Yung, Y.L., Allen, M., and Pinto, J.P. (1984). Astrophys. J. Suppl. Ser., in press.

Evolution of Titan's Coupled Ocean-Atmosphere System and Interaction of Ocean with Bedrock

Jonathan I. Lunine and David J. Stevenson

Division of Geological and Planetary Sciences
California Institute of Technology
Pasadena, California 91125 USA

Proceedings NATO Conference ''Ices in the Solar System'', Nice, France, January 16-19, 1984.

March, 1984

Contribution number 4057 from the Division of Geological and Planetary Sciences, California Institute of Technology, Pasadena, 91125 USA.

Abstract

A recent model for the surface state of Titan proposes a liquid ethane-methane-molecular nitrogen layer of order one kilometer thick which because of stratospheric methane photolysis has become increasingly ethane-rich with time (Lunine et al., 1983). We explore the interaction of such an ocean with the underlying ''bedrock'' of Titan (assumed to be water-ice or ammonia hydrate) and with the primarily nitrogen atmosphere. It is concluded that although modest exchange of oceanic hydrocarbons with enclathrated methane in the bedrock can in principle occur, it is unlikely for reasonable regolith depths and probably physically inhibited by the presence of a layer of solid acetylene and complex polymeric hydrocarbons a couple of hundred meters thick at the base of the ocean. However, the surprisingly high solubility of water ice in liquid methane (Rebiai et al., 1983) implies that topographic features on Titan of order 100 meter in height can be eroded away on a time scale $\lesssim 10^9$ years; ''Karst'' topography could be formed. Finally, the large solubility difference of N_2 in methane versus ethane implies that the ocean composition is a strong determinant of atmospheric pressure; a simple radiative model of the Titan atmosphere is employed to demonstrate that significant surface pressure and temperature changes can occur as the oceanic composition evolves with time. The model suggests that the early methane-rich ocean may have been frozen; scenarios for evolution to the present liquid state are discussed.

1. Introduction

Recently a model for a liquid hydrocarbon ocean on Saturn's satellite Titan was proposed (Lunine et al., 1983) to reconcile Voyager data on the lower atmosphere with current understanding of methane photochemical cycles in the upper atmosphere. The spacecraft and ground-based data sets bearing on Titan are reviewed thoroughly in Hunten et al. (1984).

The primary goal of this paper is to explore the coupled evolution of the ocean and atmosphere, and the interaction of this ocean with the underlying material. In the remainder of this section we review the basic model. For details the reader is referred to Lunine et al. (1983). Section 2 examines two possible interactions of the ocean and water ice + ammonia hydrate bedrock beneath: exchange of hydrocarbons between ocean and clathrate hydrate and erosion of bedrock topography. Section 3 presents a simple model for the coupled evolution of ocean and atmosphere, as the former becomes more ethane rich with time.

The model for the surface state of Titan is shown in Figure 1a, superimposed on a plot of temperature versus altitude in the atmosphere from Lindal et al. (1983). The atmosphere is essentially pure N_2 at a surface pressure of 1.5 bars and temperature 95 K (the possible presence of 12 mole percent argon in the atmosphere does not affect any of the arguments presented in the paper). The ocean methane composition of 25 mole percent is chosen to be consistent with the Voyager radio-occultation upper-limit of 3% methane in the atmosphere. More detailed modeling by Flasar (1983) permits $\lesssim$9% methane in the lowermost

atmosphere which would correspond to a 70% methane ocean. The calculation of the amount of dissolved nitrogen is described in section 3. The low vapor pressure of ethane ($\sim 10^{-5}$ bars at 95 K) allows the atmosphere above to follow an essentially dry adiabat as required by Voyager data (Lindal et al., 1983). A nearly pure methane liquid is not consistent with the data.

The source of the oceanic ethane and the underlying solid acetylene sediment is stratospheric photolysis of methane. The depth of the ocean and sediment are calculated from the inferred rate of ethane and acetylene production (Yung et al., 1984) integrated over the age of the solar system. A 25% methane ocean has a depth of ~800 meters; a 70% methane ocean corresponds to 1.8 kilometers depth. The sediment layer is ~100-200 meters thick. (The relative production rates of ethane and propane are somewhat uncertain; the two are sufficiently similar thermodynamically that we do not distinguish between them in this paper). The ocean is thus the source and sink of methane photolysis and becomes more ethane-rich with time, as illustrated schematically in Figure 1b. In the absence of an ocean, the maximum methane retainable by the atmosphere would be destroyed by photolysis in $\sim 10^7$ years; our model provides sufficient methane for $\gtrsim 10^9$ years. The ultimate source of the methane forms the basis for another study and is not discussed here.

We note here two details which are of relevance to calculations in later sections. Referring to Figure 1b, two methane molecules are photolytically destroyed for each ethane molecule produced. This decrease in number of molecules in the ocean with time, coupled with the

Figure 1. (a) Model of Titan's near-surface and atmospheric structure from Lunine et al. (1983), with altitude versus temperature data from Lindal et al. (1983). Below the surface the ocean temperature is assumed to follow an adiabat. (b) Schematic model of evolution of ocean due to methane photolysis. Methane evaporated from the ocean is photolyzed in the stratosphere, producing hydrogen and ethane, acetylene and other products observed by Voyager IRIS (Hunten et al., 1984). Hydrogen escapes from the atmosphere; the supersaturated ethane condenses and falls to the ocean. As the ocean enriches in ethane, N_2 comes out of solution. Note one molecule of ethane (or acetylene) is produced for every two methane destroyed. Only the methane-ethane-N_2 portion of the cycle is shown for clarity.

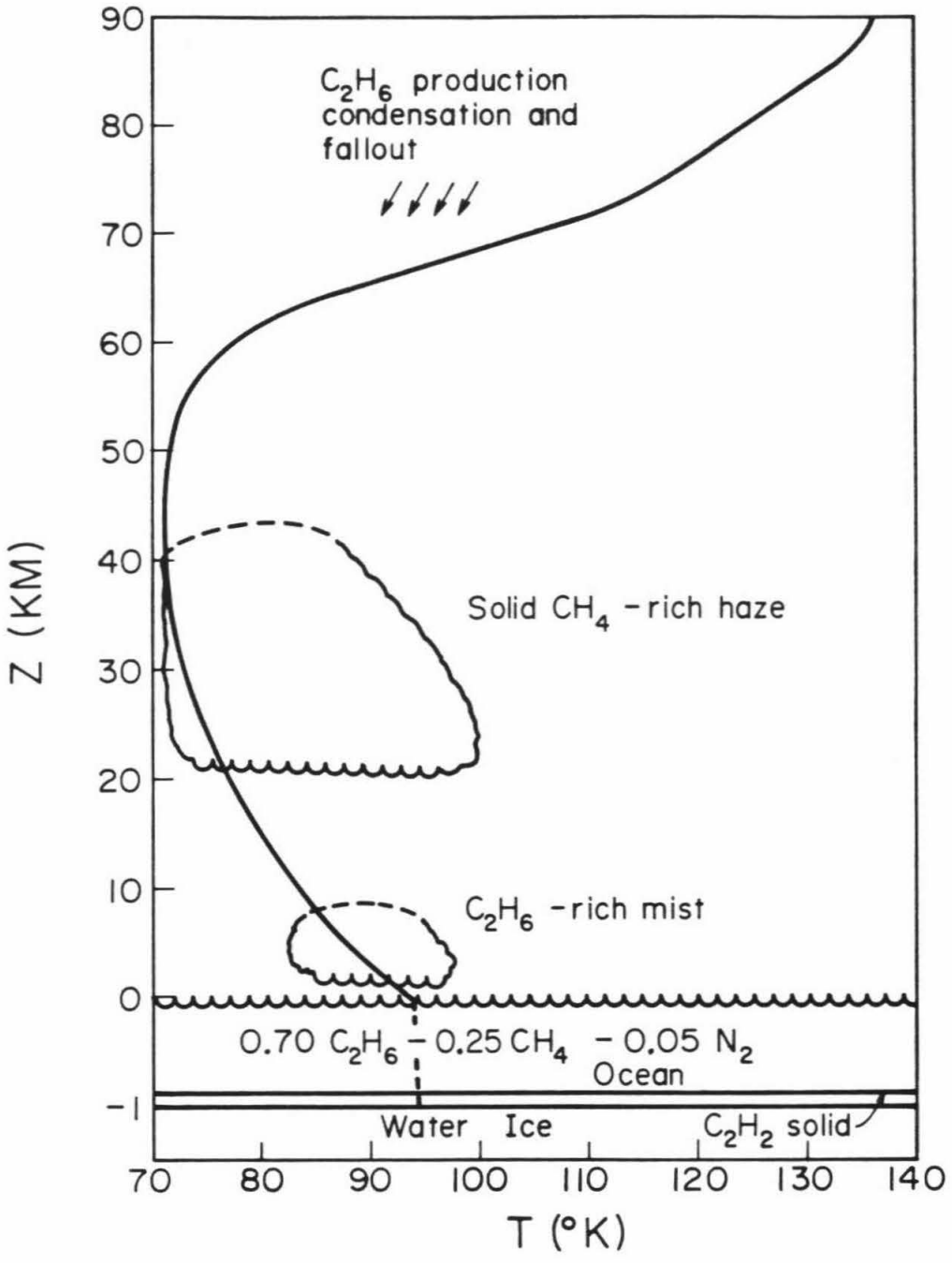
90
80
70
60
50
40
30
20
10
0
-1
Z (KM)
C_2H_6 production
condensation and
fallout
Solid CH_4 - rich haze
C_2H_6 - rich mist
0.70 C_2H_6 - 0.25 CH_4 - 0.05 N_2
Ocean
Water Ice
C_2H_2 solid
70
80
90
100
110
120
130
140
T (°K)

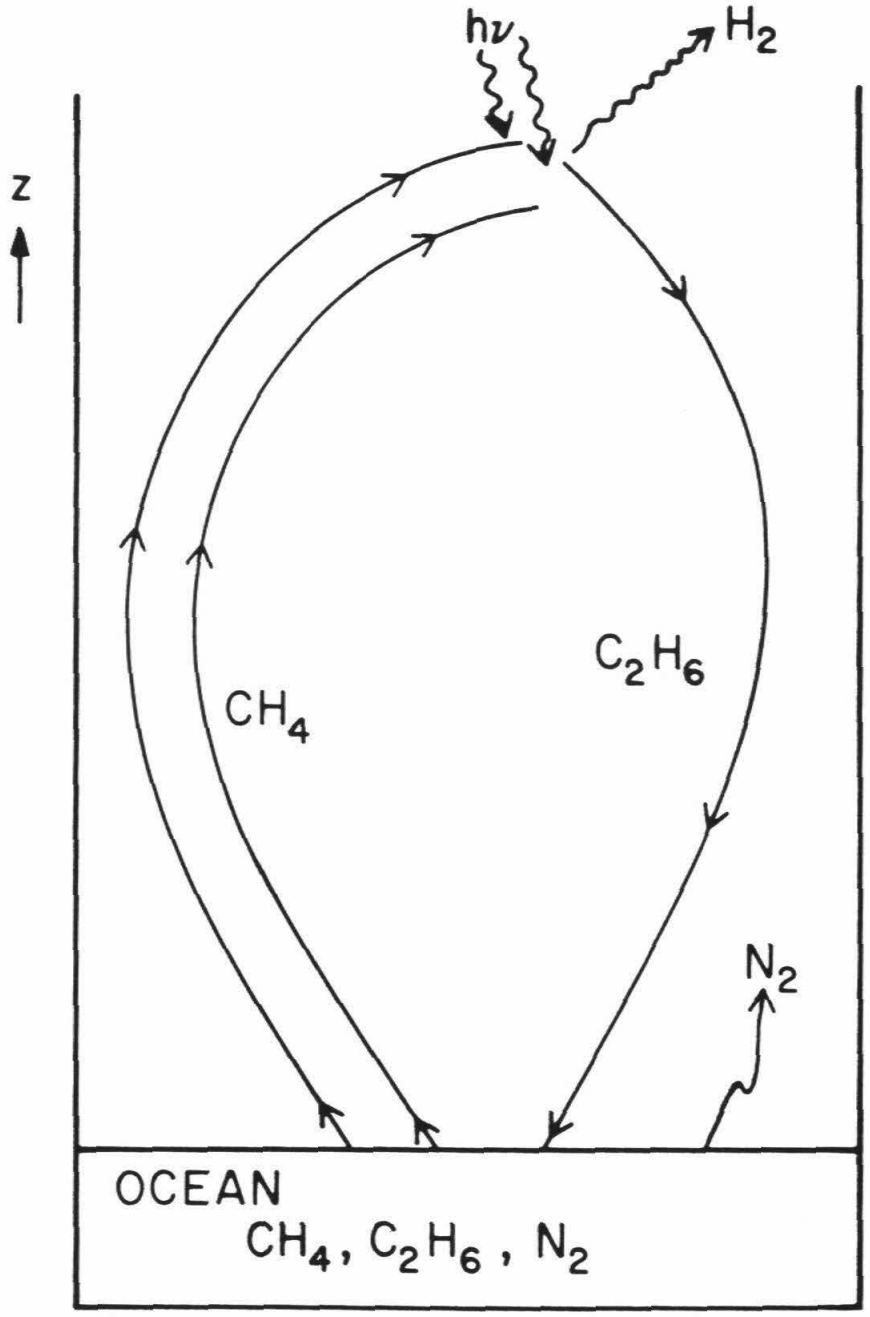
hν
H2
z
C2H6
CH4
N2
OCEAN
CH4, C2H6, N2

rather different solubilities of N_2 in methane and ethane, forms a strong driver for atmospheric evolution as described in section 3. With regard to the acetylene layer, there is some disagreement in the literature as to the relative amounts of acetylene versus higher complex hydrocarbons (and HCN polymers) produced in the stratosphere. The polymeric material is thought to comprise the haze layers seen in the stratosphere. The model in Figure 1a assumes efficient condensation and removal of acetylene and ethane from the region of photolysis and does not include the formation of heavier polymers. In fact, some of the material comprising the sediment is likely to be polymeric. The physical properties of this material at relevant conditions are not well enough known to predict whether a flaky sediment or more coherent ''blacktop'' should be expected at the ocean base. Finally, about 1 meter worth of solid CO_2 may also be present in the layer from a CO-CO_2 photochemical chain (Samuelson et al., 1983); this amount is sufficiently small that we do not consider it further. It is also possible that some of the particulate sedimentary material remains suspended in the ocean indefinitely. For example, spherical particles of radius r (measured in microns) have a Stokes falltime through the ocean of roughly $10^2\ r^{-2}$ years. Ocean flows due to tides, winds and temperature differences are larger than Stokes velocities for small ($\lesssim$100 micron-sized) particles, so the magnitude of the suspension load depends on the poorly known sticking capabilities of the particles with each other.

Beneath the sediment lies the crust of Titan, referred to here as ''bedrock.'' The bulk density of the satellite and cosmochemical

considerations predict water ice probably at least partially transformed into clathrate, and perhaps ammonia hydrate, as the primary bedrock material (Hunten et al., 1984). A small amount of silicate material may be present but does not affect any of our considerations because it is chemically inert at ~100 K.

2. Interaction of Ocean and Bedrock

In this section we consider two types of interaction between the ocean and water ice bedrock: (1) exchange of hydrocarbons between ocean and clathrated bedrock, and (2) erosion of water-ice topography by solution in the ocean.

The possibility of enclathrated methane present on the Titan surface has been previously considered (Lewis, 1971, for example) but never in connection with an ocean. Clearly, a significant exchange of photochemically produced ethane in the ocean with methane in underlying clathrate can only occur if the ocean can establish thermodynamic equilibrium with a substantial thickness of the underlying ice. This thickness is estimated to be >100 meters.

The methane (or ethane) clathrate is a modified water ice lattice enclosing guest molecules and with an approximate formula $X \cdot 6H_2O$ where X is methane and/or ethane. A full description of the thermodynamics of clathrate hydrates and application to solar system bodies is presented in Lunine and Stevenson (1984) the results of which are used here.

At ambient conditions on Titan's surface, ethane, methane and N_2 should fully incorporate in clathrate hydrate, with the result that no ocean could be present and the N_2 atmospheric pressure would be $\sim 10^{-3}$ bars. This situation is prevented by the inability of these species to come into contact with large quantities of water ice. Such contact requires that the ice not only have substantial permeability but that the fluid channels (fissures, cracks, etc.) penetrate the ice to the submicron level, since diffusion of methane or ethane into water ice is

extremely slow even over a distance of one micron (Lunine and Stevenson, 1984). The existence of porosity (and methane-ethane ''aquifers'') is certainly possible since the hydrostatic head and temperature may not be sufficient to deform the ice and squeeze out enclosed methane, even at 10 km depth (temperature ~120 K?, pressure ~200 bars; pressure difference between methane and ice columns of ~100 bars). Fluid penetration to a submicron scale is unlikely, however, since the ice is likely to have undergone annealing at some stage in its history. (It might have formed by freezing from a primordial NH_3-H_2O ocean, for example, or been subjected to impact. In either case, porosity would not extend to the submicron level.) Impact causes formation of a regolith as deep as a kilometer (Hartmann, 1973) which consists of an extreme diversity of particle sizes (Kawakami et al., 1983); only the uppermost 100 meters (or less) is likely to be stirred sufficiently frequently to allow efficient conversion to clathrate. We thus conservatively assume the equivalent of a 100 meter, finely fragmented ice layer. The relative fraction y of C_2H_6 to CH_4 incorporated in the clathrate is given by the rough formula

$$y \sim \frac{P^c(CH_4)}{P^c(C_2H_6)} \frac{f(C_2H_6)}{f(CH_4)} \qquad (1)$$

where f(q) is the fugacity of species q in the ocean and $P^c(q)$ the dissociation pressure of clathrate containing pure species q. $P^c(q)$ is calculated from molecular properties of q in Lunine and Stevenson (1984). f(q) is very nearly $X(q) \cdot P(q)$, X(q) the mole fraction of q in

the ocean, P(q) the vapor pressure of pure q at system temperature. Inserting values from Lunine and Stevenson (1984) equation (1) becomes

$$y \sim \frac{1}{3} \frac{X(C_2H_6)}{X(CH_4)} \quad .$$

Thus, as the ocean C_2H_6 composition is increased with time due to CH_4 photolysis, the underlying clathrate becomes progressively enriched in C_2H_6.

Consider now a starting state consisting of a pure methane ocean, depth ~1.4 km (calculated from a present ocean of 25% CH_4 and 0.8 kilometer depth), overlying a 100 meter regolith of methane clathrate hydrate. We assume for now the acetylene sediment layer does not prevent ocean-regolith contact and is kinetically inhibited from enclathrating because it is in the solid phase. Also, N_2 can be neglected because it is a poor incorporator in clathrate compared to CH_4 or C_2H_6. As the ocean composition becomes more ethane rich, some of the ethane exchanges with the methane in the clathrate producing a negative feedback on ocean composition. Figure 2 plots the fraction of oceanic methane derived from clathrate as a function of the ethane mole fraction in the ocean. By the time the present ocean composition is reached, only 20% of the methane in the ocean is derived from clathrate. Only ~6% of the ethane produced has been incorporated in the clathrate; the remainder resides in the ocean. Arguments presented above suggest that this is an upper limit to the amount of methane and ethane exchanged between ocean and regolith. Moreover, the basal sediment layer of

Figure 2. Logarithm of the fraction of oceanic methane derived from clathrate as a function of ethane mole fraction in the ocean. Starting state is pure methane ocean underlain by 100 meters of methane clathrate hydrate.

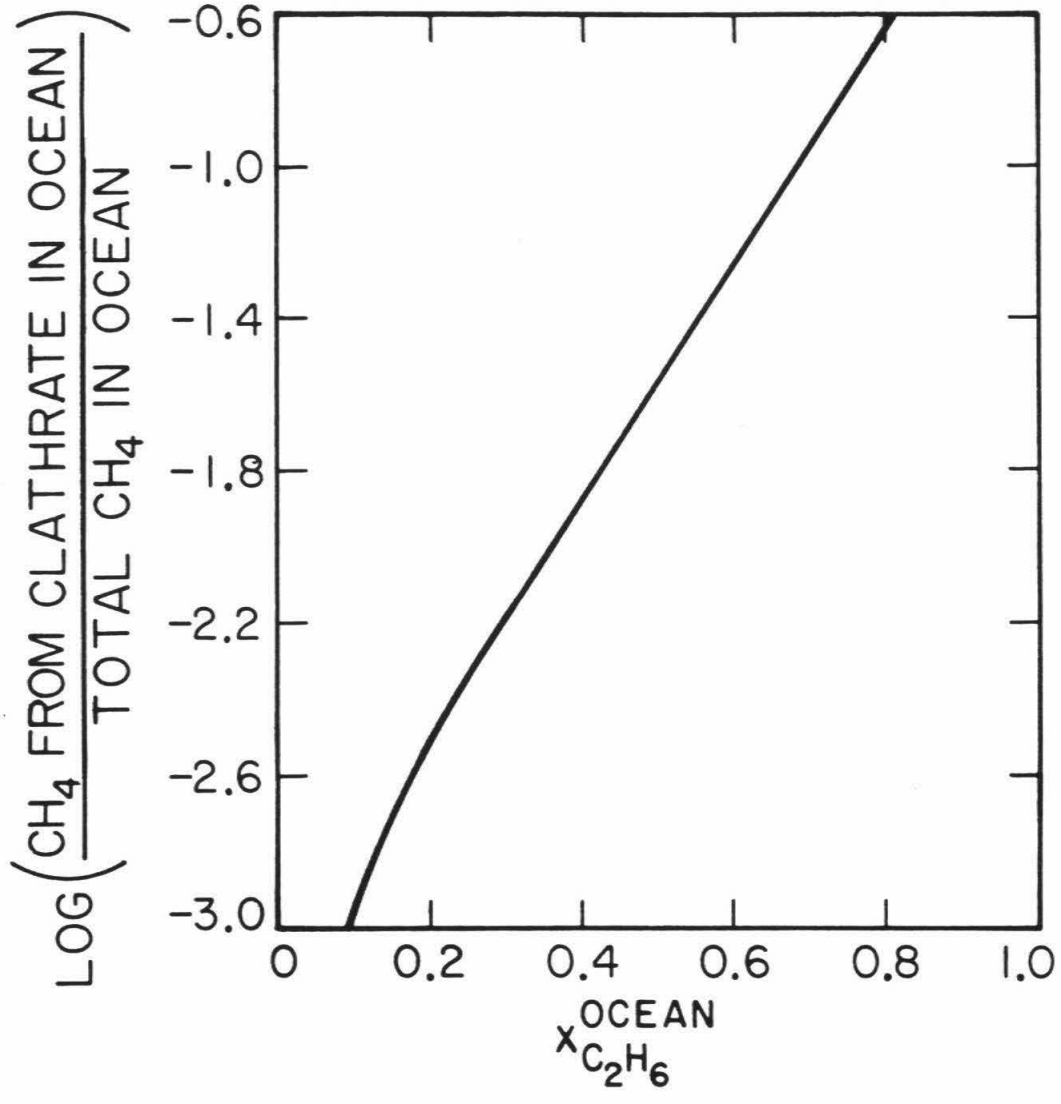
LOG(CH4 FROM CLATHRATE IN OCEAN / TOTAL CH4 IN OCEAN)
-0.6
-1.0
-1.4
-1.8
-2.2
-2.6
-3.0
0
0.2
0.4
0.6
0.8
1.0
X OCEAN C2H6

acetylene and polymeric material could severely inhibit ocean-regolith contact. We conclude that transfer of oceanic and regolith hydrocarbons is probably not an important control on ocean evolution, and may be neglected in what follows.

We next examine the ability of the ocean to erode bedrock topographic features. Such a process could be particularly efficient for newly formed features created by impact or ammonia-water volcanic processes and which are not yet covered with a layer of sediment. The surprisingly high solubility of water ice in non-polar cryogenic liquids (6×10^{-5} mole fraction in methane at 112 K; Rebiai et al., 1983) permits substantial removal of ice from topographic highs, provided saturation of the entire ocean is avoided. Tidal currents generated by Titan's non-zero free eccentricity (Sagan and Dermott, 1982) may provide a mechanism for dissolving and removing water.

Consider a topographic feature ("mound") of height h and length L, encountering an ocean current of velocity v (Figure 3a). Assume, for this example, that the fluid is highly undersaturated in H_2O. At the ocean-mound interface a diffusional boundary layer of thickness δ develops. If the boundary layer remains laminar then $\delta \simeq (Dy/v)^{1/2}$, where y is the distance measured downstream from the upstream tip of the mound. Since a saturated layer of thickness $\sim(DL/v)^{1/2}$ detaches from the mound and flows downstream at velocity v, it follows that the erosion time scale is:

$$\frac{h}{\dot{h}} = \frac{hL}{v\delta X} = \frac{hL}{v[D(L/v)]^{1/2}X} = \frac{h}{X}\left(\frac{L}{Dv}\right)^{1/2} \qquad (2)$$

where X is the saturation mole fraction of water ice in the ethane-methane liquid and D is a diffusion coefficient. For a dissolved constituent moving through the liquid we estimate $D \sim 10^{-4}$ cm^2/s; X at 95 K is conservatively estimated from the methane-water ice data to be $\sim 10^{-8}$. The flow velocity v ~ 1 cm/s is taken from the tidal model of Sagan and Dermott (1982); the scale length of a topographic feature is estimated by analogy with large impact structures on Galilean satellites to be 10 km.

Figure 3b plots $h/\dot{h}$ versus h. Note that a 100 meter-high feature could be eroded over the age of the solar system. Unless the topographic feature is small, turbulence is likely to be important. In this case, one might argue that the boundary layer ''breaks'' and is assimilated into surrounding fluid once it achieves a downstream extent ~l where $vl/\nu \sim 10^3$, a critical Reynolds number. This leads to an enhancement of the erosion rate by a factor $\sim(L/l)^{1/2}$. For the predicted l ~ 1-10 cm and L ~ 10 km, this is an enhancement factor of several hundred. More realistically, the solution and dissolution of water and accumulated hydrocarbon sediment in the CH_4-C_2H_6 liquid depends on the details of the ocean circulation and temperature structure. One could imagine cavernous chemical erosion, similar to Karst topography on Earth (Karst derives its name from the northeastern shore of the Adriatic Sea where Yugoslavia and Italy meet, and is characterized by an irregular limestone terrain with many small

Figure 3. (a) Water ice topographic feature of height h and extent L submerged in ocean with current velocity v. δ is boundary layer thickness over which water mole fraction decreases from saturation to dilute value. Schematic plot shows decrease in mole fraction of dissolved water in boundary layer as a function of distance from feature. Vertical scale of feature and boundary layer thickness (the latter increasing in downstream direction) are schematic. (b) Time in seconds to erode a feature of height h versus h in centimeters. Parameter values given in text. Stippled area is t > age of solar system. As argued in text, the plotted erosion time may be a substantial overestimate.

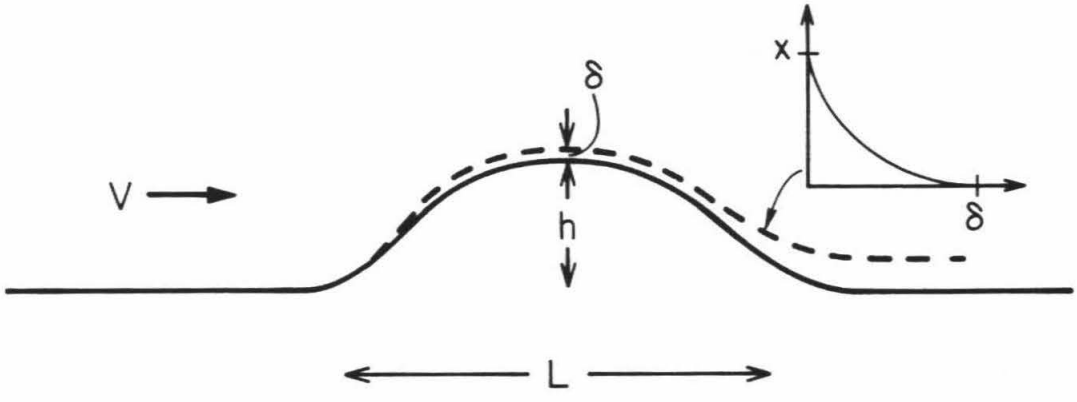
x
δ
V
h
δ
L

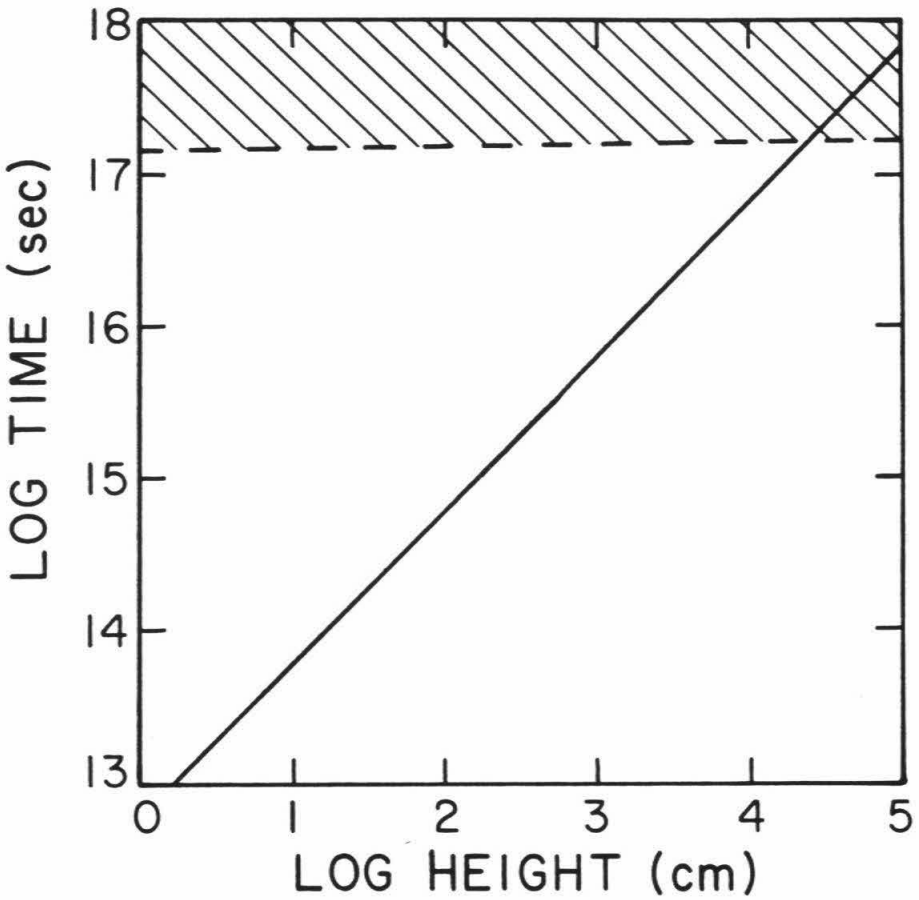
18
17
16
15
14
13
LOG TIME (sec)
0
1
2
3
4
5
LOG HEIGHT (cm)

depressions, which evolved from the dissolving power of the groundwater). The equivalent of stalactites or stalagmites might also form.

The vertical scale of impact and tectonic features on large icy satellites is ~1 km (Squyres, 1981); this scale may apply to volcanic edifices if their height is determined by isostasy as suggested for terrestrial volcanoes by Ben-Avraham and Nur (1980). It is thus possible that significant modification of submerged crater- and tectonic-forms has occurred on Titan. Radar profiling of the submerged ice structure, taking advantage of the low microwave absorption characteristics of hydrocarbons and significant difference in ice and hydrocarbon dielectric constants could reveal such degradation and would be a fascinating experiment.

3. Coupled Evolution of Ocean and Atmosphere

Lunine et al. (1983) compute the solubility of N_2 in their nominal (25% methane) ocean under 1.5 bars N_2 pressure to be ~5 mole percent, implying a dissolved N_2 mass ~1/4 of the atmospheric mass. A pure methane ocean of similar mass under the same conditions would contain >20% N_2 or ~ twice the atmospheric mass of N_2. Clearly the relatively high solubility of N_2 in methane, and low solubility in ethane implies that the ocean composition must exert a strong control on the N_2 atmospheric pressure, and as we show below, temperature. Titan's ocean-atmosphere interaction is thus intermediate between that of Earth's, for which the dissolved oceanic N_2 is <1% of the atmospheric mass (solubility data from International Critical Tables, 1928, p. 256) and Triton, which may possess large amounts of N_2 (Cruikshank et al., 1984) as either liquid or solid, and which would then be overlain by a N_2 saturated vapor atmosphere. In this section we construct a model for the evolution of Titan's surface temperature and pressure as the ocean becomes more ethane-rich with time, and discuss the implications for the original composition and timing of surficial emplacement of the ocean.

The model assumes the ocean and atmosphere to be a closed system as far as the total carbon and nitrogen budgets are concerned. Conversion of methane to ethane and acetylene proceeds at the rates given in Yung et al. (1984); two molecules of methane are converted to one molecule of ethane or acetylene, with loss of hydrogen from the atmosphere. The ocean mass decreases with time, primarily because methane photolysis leads to the formation of insoluble acetylene.

Hydrogen is also formed and escapes, but is less important for the mass balance. The solubility of N_2 in CH_4 and C_2H_6 separately is assumed to obey Henry's law (a valid assumption so long as the mole fraction of N_2 $\equiv X(N_2) \lesssim 0.1 - 0.2$):

$$P(N_2) = K(q)\, X(N_2) \tag{3}$$

where K(q) is the Henry's law constant for N_2 dissolved in component q and $P(N_2)$ is the partial pressure of N_2 ($\simeq$ total pressure). The Henry's law constant at a given temperature for the mixed CH_4-C_2H_6 liquid is (Prausnitz, 1969, p. 373):

$$\log K \sim X(CH_4) \log K(CH_4) + [1 - X(CH_4)] \log K(C_2H_6) \tag{4}$$

since the cryogenic ethane-methane system is roughly ideal (Miller and Stavely, 1976). Then the relationship between atmospheric pressure P and total N_2 mass $M(N_2)$ (ocean + atmosphere) is:

$$P = \frac{M(N_2)}{\frac{4\pi R_T^2}{g} + \frac{M_o}{(K - P)} \frac{\mu(N_2)}{\mu_o}} \tag{5}$$

where R_T = radius of Titan's surface, g = gravitational acceleration at R_T, M_o = mass of the ethane + methane component of the ocean, and μ_o = mean molecular weight of ethane-methane ocean mixture. $M(N_2)$ is computed from the inferred present-day ocean composition (25% methane) given in Lunine et al. (1983) and the observed 1.5 bar atmospheric

pressure; we also do a calculation for a 60%-methane ocean. The ocean mass is a decreasing linear function of ethane mole fraction tied to the present state for which ~20% of the converted methane is in the form of acetylene, and the presumed primordial state consisting of 100% methane.

The compositional and temperature dependences of the Henry's law constant K require some comment. If N_2 dissolves in the ocean in an ideal sense, $K = P_s$, the saturation vapor pressure over pure condensed N_2 at the given temperature. At 92 K, P_s = 4.3 bars (Jacobsen and Stewart, 1973) while $K(CH_4) \simeq 7.0$ bars and $K(C_2H_6) \simeq 45$ bars (Cheung and Wang, 1964). The N_2-CH_4 and N_2-C_2H_6 systems both exhibit positive deviations from ideality; however, the different sizes of the N_2 and C_2H_6 molecules in particular strongly inhibit solution of the N_2 in C_2H_6. It is the difference in solubility of N_2 in CH_4 and C_2H_6 and the changing number of moles of hydrocarbon in the ocean which drive the evolution of the atmosphere with changing ocean composition in the model presented below.

If the solutions were ideal, the temperature dependence of K would follow that of the N_2 vapor pressure curve, $\sim 10^{-|A|/T + B}$, A and B constants. Data for N_2-CH_4 from 105 to 92 K (Cheung and Wang, 1964; Chang and Lu, 1967) suggest this dependence, with a somewhat smaller $|A|$ than for pure N_2 vapor, but a linear fit would do just as well. Moreover, at very low temperatures near the solidus, the temperature dependence may become very weak, since the data show increasing non-ideality with decreasing temperature. Hence we adopt two extreme temperature dependences for K, one going as $10^{-|A|/T + B}$ and the second constant with T at the 95 K value. As shown below, the two extremes

predict somewhat different relationships between T and ocean composition; the qualitative implications for our nominal ocean model, however, are similar. Thus, case ''A'' involves the following equation for K:

$$\log_{10} K = -\frac{140}{T} + 3.16 - X(CH_4) \cdot \left(\frac{52}{T} + 0.22\right) \qquad (6)$$

where due to the lack of N_2-C_2H_6 solubility data at more than one temperature point below 100 K, the temperature dependence of the N_2-C_3H_8 system from Cheung and Wang (1964) was used, C_3H_8 being very similar thermodynamically to C_2H_6. For case ''B'', a temperature-independent K was used:

$$\text{Log}_{10} K = 1.66 - 0.719\ X(CH_4) \qquad (7)$$

Both case A and case B yield $X(N_2) = 0.05$ for present atmospheric conditions and the nominal ocean model.

The ocean evolution model is coupled to a conceptually simple model of the Titan atmosphere. This atmosphere may be broadly divided into three regions according to the mode of energy absorption and emission (Samuelson, 1983). Haze particles in the stratosphere absorb essentially all the violet end of the visible solar spectrum, heating altitudes above 50 kilometers (see Figure 1a). The red spectral end is primarily scattered to the ground; hence an optically thick troposphere in radiative equilibrium is present. A thin convective region also

occurs below 3.5 kilometers. As Samuelson (1983) notes, the atmosphere is dominated by radiative processes; we consider the lower atmosphere to be grey and in radiative equilibrium with an effective temperature T_e fixed by ambient surface conditions. Hence the temperature at the surface, $T(R_T)$, is

$$T^4(R_T) = \frac{1}{2} T_e^4 \left(1 + \frac{3}{2} \tau (R_T) \right) \qquad (8)$$

where τ, the optical depth, is assumed due primarily to pressure-induced N_2 opacity:

$$\tau = \frac{\bar{A}}{2} \frac{1}{k_B m_p \mu(N_2) g} \frac{1}{\eta^2} \frac{p^2}{T} \qquad (9)$$

$\bar{A}$ = absorption coefficient in cm^{-1} $amagat^{-2}$, η = Loschmidt's number, m_p= mass of proton, and k_B= Boltzmann constant. Pressure-induced N_2 opacity is considered to be the primary tropospheric opacity source (Samuelson, 1983); the importance of clouds remains controversial. Using the cloud-free value for $\bar{A}$ in Hunten (1978), we find

$$\tau = 141 \frac{p^2}{T} \qquad (10)$$

or an effective temperature of 72 K for the present surface conditions (95 K, 1.5 bars). T_e is low compared to the global value of 86 K given in Hunten et al. (1984) since most of the solar energy is absorbed and radiated by the upper stratospheric haze. The haze does re-radiate some

energy to the lower atmosphere (Samuelson, 1983) but to first order we can decouple the lower atmosphere and determine its evolution as the ocean composition changes using the simple model of equations (5), (6) or (7), (8), and (10). This approach may not be valid for the earliest ocean compositions (high methane), when the atmosphere is nearly optically thin according to our results, and backwarming by the haze could be important. Note that radiative equilibrium dictates the ground temperature to be larger than the atmospheric value just above it given by equation (8). In practice, convection redistributes the heat and narrows the discontinuity to $\lesssim$ several degrees (Lindal et al., 1983). Here we make the simplifying assumption that the ocean temperature is given by (8).

Figure 4 presents results for the nominal ocean model, plotted as surface temperature versus oceanic methane mole fraction. The associated surface pressure and time before present are plotted as auxiliary scales. Both solubility cases A and B (equations (6) and (7)) are plotted. Superimposed on the figure is the ethane-methane solid-liquid phase diagram from Moran (1959). The N_2 mole fraction in the ocean is $\lesssim$15% throughout the evolution and hence lowers the phase boundaries at most ~5 K.

Both cases exhibit monotonic decreases in temperature as the ocean is changed from the present state back to more methane-rich compositions. The strong positive temperature feedback for case A results in a more rapid evolution. The calculation becomes invalid as the curves cross the liquidus. This occurs for case A at ~ 0.55 mole fraction methane; using the photolysis rate of Yung et al. (1984) this

Figure 4. Surface temperature versus mole fraction of methane in ocean, nominal model. Two cases are shown: A, $K(N_2) \propto 10^{-1/T}$ and B, $K(N_2)$ constant with temperature. Two auxiliary scales are plotted: atmospheric pressure in bars corresponding to temperature and time before present corresponding to methane mole fraction, assuming constant photolysis rate. Time is nonlinear in $X(CH_4)$ due to decrease in number of moles of oceanic hydrocarbon with ethane and acetylene production. Arrow points to present state. Dotted lines are ethane-methane solid-liquid phase diagram from Moran (1959), with L = all liquid, S + L = coexisting liquid + solid and S = all solid. Total N_2 mass for this model = 1.1×10^{22} g, total present day ocean mass = 3.7×10^{22} g.

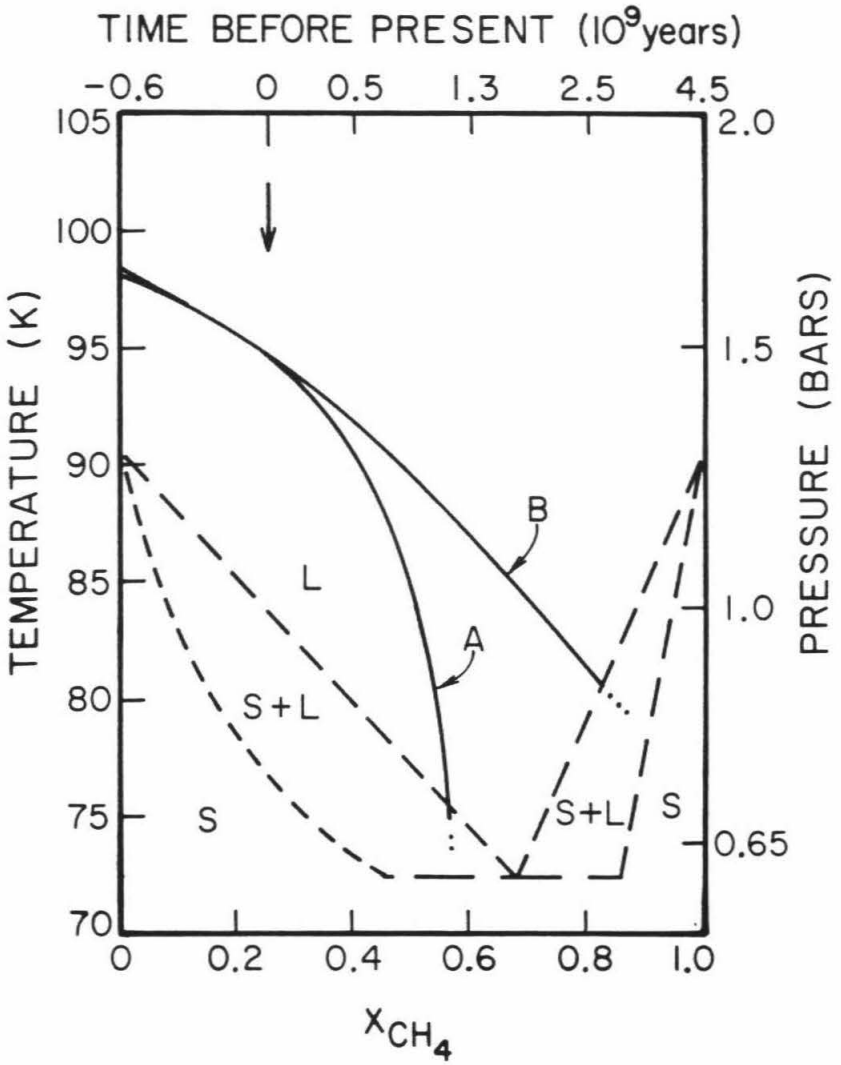
TIME BEFORE PRESENT (10^9 years)
-0.6
0
0.5
1.3
2.5
4.5
105
100
95
90
85
80
75
70
2.0
1.5
1.0
0.65
TEMPERATURE (K)
PRESSURE (BARS)
B
A
L
S+L
S
S+L
S
0
0.2
0.4
0.6
0.8
1.0
X_{CH_4}

corresponds to a time before present of $\Delta t \sim 1.1 \times 10^9$ years. Case B crosses the liquidus at $X \sim 0.8$ corresponding to $\Delta t \sim 2.5 \times 10^9$ years (note Δt assumes constant photolysis rate, initial ocean is pure methane, and no bulk injection of methane or ethane from sources other than photolysis).

Figure 5 plots N_2 pressure and oceanic mole fraction versus temperature for case A along with the N_2 saturation vapor pressure. At $T < 75$ K, the atmospheric pressure begins to approach the saturation vapor pressure value. Since polar surface temperatures even at present may be several degrees below the equatorial value (Hunten et al., 1984), our model could require some pure N_2 condensation in the polar regions at high methane ocean concentrations, until the global pressure is reduced below the saturation pressure at the poles.

We examined the sensitivity of our results to the variation of several parameters. Modeling of N_2 escape processes suggests that ~20% of the present N_2 atmosphere could have been lost over the age of the solar system (Hunten et al., 1984). Using a value of $M(N_2)$ 20% higher than for the Figure 4 calculation pushes the temperature up for a given oceanic methane composition, but the shape of the T-X evolution curve and the Δt needed to reach optically thin conditions is roughly unchanged. Comparable modification of the starting ocean mass has the opposite effect, but similar magnitude. Lowering the N_2 absorption coefficient in the opacity calculation makes the surface temperature less sensitive to changing methane mole fraction as expected, but even a 50% change has a rather minor effect on the curves in Figures 4 and 5.

Figure 6 shows model runs for a present day ocean containing 60%

Figure 5. Surface pressure in bars and oceanic N_2 mole fraction versus temperature in Kelvin for nominal model. Arrow points to present state. Pure N_2 saturation vapor pressure from Jacobsen and Stewart (1973) is also plotted.

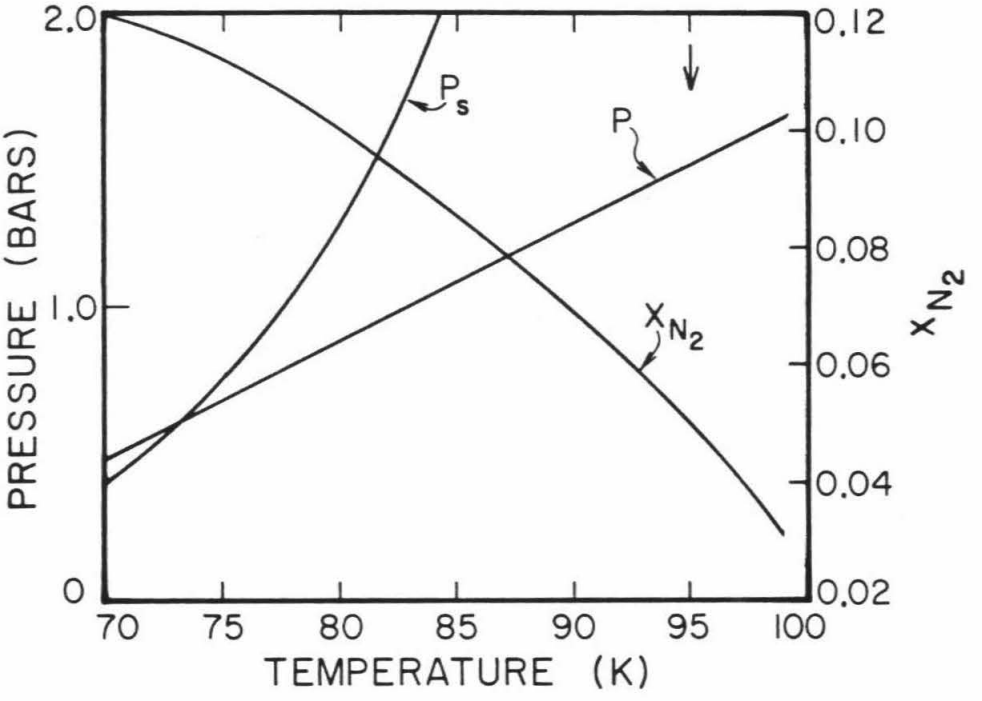
2.0
1.0
0
PRESSURE (BARS)
0.12
0.10
0.08
0.06
0.04
0.02
X_{N_2}
P_s
P
X_{N_2}
70
75
80
85
90
95
100
TEMPERATURE (K)

Figure 6. Same as Figure 4, high methane model. Total N_2 mass 1.6 x 10^{22} g, total present day ocean mass 5.8 x 10^{22} g.

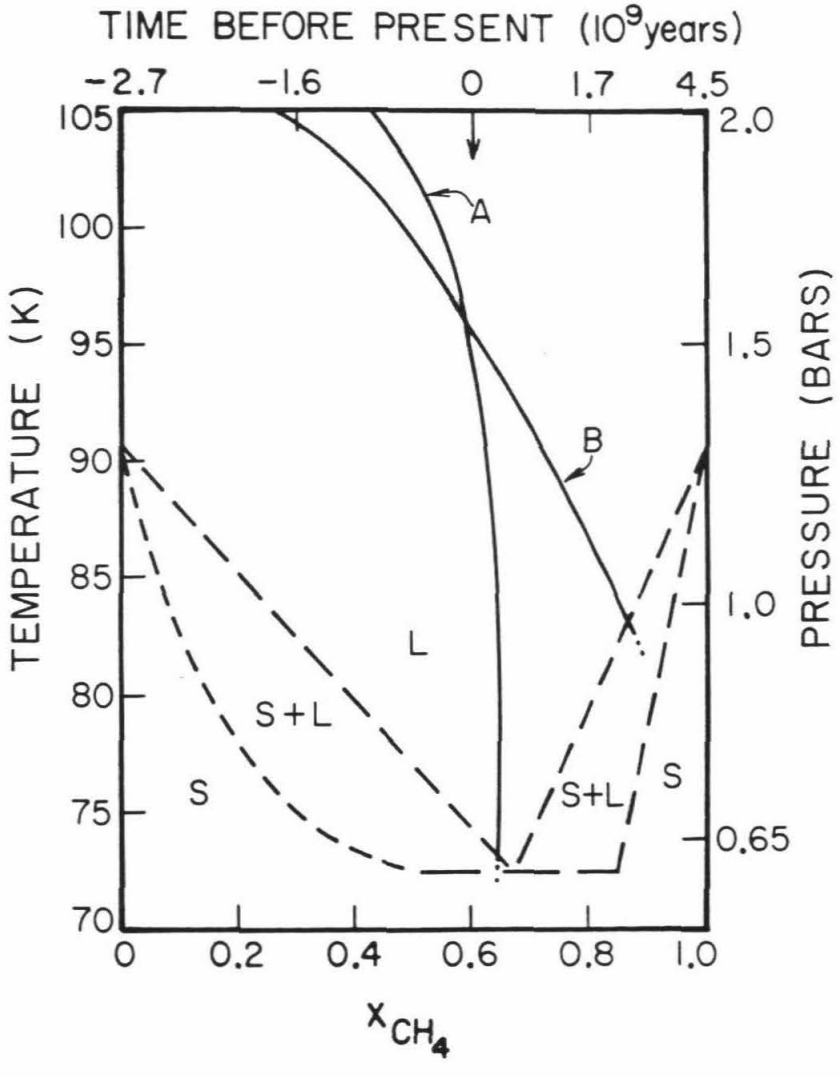
TIME BEFORE PRESENT (10^9 years)
-2.7
-1.6
0
1.7
4.5
105
100
95
90
85
80
75
70
TEMPERATURE (K)
2.0
1.5
1.0
0.65
PRESSURE (BARS)
A
B
L
S+L
S
S+L
S
0
0.2
0.4
0.6
0.8
1.0
X_{CH_4}

methane. Case B yields results roughly similar to the nominal case, with the pure solid field crossed at $X(CH_4) \sim 0.85$. Case A, however, shows a dramatically more rapid evolution. The large mass of CH_4 and N_2 in the ocean relative to the N_2 in the atmosphere, coupled with the strong temperature dependence of solubility, yields an unstable situation: a slight increase in oceanic methane strongly increases the amount of N_2 which can be drawn out of the atmosphere, decreasing T and further increasing the solubility so that the temperature drops. The same effect is seen in Figure 4 case A at $X(CH_4) = 0.6$. We consider, however, the 60% methane ocean to be somewhat of an extreme case, as far as present-day surface conditions are concerned.

With the exception of the high methane case A result, the models explored evolve from low temperature states to the present-day over long time scales, $\sim 10^9$ years. Continuing the evolution to a pure ethane ocean composition leads to a modest temperature and pressure rise from the present day state (Figure 4). The nominal model would completely exhaust its methane on a time scale of $\simeq 6 \times 10^8$ years, implying Titan's atmosphere-ocean system is and has been in a long term, slowly evolving condition.

The earliest evolution of the system is of great interest; however, we are limited at present to rather qualitative speculations. Two complications prevent us from using the above model to trace the evolution back past the point at which the liquidus is crossed: (1) the behavior of the ternary N_2-CH_4-C_2H_6 solid-liquid system is sufficiently uncertain that we cannot reliably predict, for example, the partitioning of N_2 between solid, liquid and gaseous phases, and (2) at $T \lesssim 75$ K, the

atmosphere in our model becomes optically thin, and significant radiative contribution from the stratospheric haze may dominate. A further complication is that some N_2 could have been frozen out at the poles at $T \lesssim 75$ K, controlling the global atmospheric pressure, as indicated in Figure 5. Clearly more involved atmospheric and thermodynamic modeling is required.

We speculate briefly on some possible starting points for the ocean-atmosphere system. N_2 and CH_4 volatiles, extruded together from the interior could have coated the surface as a high albedo material, maintaining a low temperature. Production of dark (albedo ~0.2) haze material which subsequently covered the surface could have raised the temperature above 85 K, allowing N_2 to vaporize and regions containing methane and photochemically produced ethane ice to liquify and initiate an ocean in places. A complex trade-off between the albedo and emissivity properties of haze-covered and ocean-covered regions would have ensued, with a global ocean eventually forming and the atmosphere-ocean system running onto an evolution curve similar to those calculated above.

Other calculations (Lunine and Stevenson, 1982) suggest a hot formation scenario for an ammonia-hydrate rich Titan which could have allowed several bars of N_2 to be produced photochemically. As the surface temperature dropped below ~200 K, and a solid surface formed, most of the N_2 would have remained in the atmosphere. The subsequent extrusion of methane from the interior could have had two effects: if all of the methane inferred to be the source of the present ocean were suddenly outgassed, and temperatures were low enough to allow it to

condense, most of the atmosphere would dissolve into the ocean and freezing would ensue, with subsequent evolution as suggested above. If the extrusion were slow or episodic, so that photolytic conversion of CH_4 to C_2H_6 moderated the N_2 solubility, the atmosphere could have slowly merged onto an evolution curve similar to Figure 4's as the mass of methane extruded reached the inferred present amount. As yet we cannot distinguish between the various options, including the possibility that some ethane or propane was also extruded from the interior. Further modeling of the ocean evolution process, application of tidal constraints (Sagan and Dermott, 1982) and predictions of atmospheric abundances of noble gases (Lunine and Stevenson, 1984) which could ultimately be measured and are diagnostic of satellite formation and early history may constrain mechanisms for the origin of the ocean.

As for Triton, the apparent detection of both condensed CH_4 and N_2 on the surface (Cruikshank et al., 1984) along with the high solubility of CH_4 in N_2 liquid or solid (Omar et al., 1962) suggests that photochemical conversion of CH_4 to heavier hydrocarbons could also strongly couple atmospheric and surface evolution. Uncertainties regarding relative and absolute abundances of CH_4 and N_2 on the surface and in the atmosphere, the phase of condensed N_2 (liquid or solid) and degree of areal mixing of those constituents renders modeling a poorly constrained venture at present. The possibility that Triton could represent a permanent analog for the frozen early state of Titan's surface is an exciting one which should be borne in mind as the Voyager close flyby of Triton (1989) draws near.

References

Ben-Avraham, Z. and Nur, A. (1980). The elevation of volcanoes and their edifice heights at subduction zones. J. Geophys. Res., **85**, 4325-4335.

Chang, S.-D. and Lu, B.C.-Y. (1967). Vapor-liquid equilibria in the nitrogen-methane-ethane system. Chem. Eng. Progr. Symp. Ser., **63**(81), 18-27.

Cheung, H. and Wang, D.I.-J. (1964). Solubility of volatile gases in hydrocarbon solvents at cryogenic temperatures. I and EC Fundam., **3**, 355-361.

Cruikshank, D.P., Brown, R.H., and Clark, R.N. (1984). Nitrogen on Triton. Icarus, in press.

Flasar, F.M. (1983). Oceans on Titan? Science, **221**, 55-57.

Hartmann, W.K. (1973). Ancient lunar mega-regolith and subsurface structure. Icarus, **18**, 634-636.

Hunten, D.M. (1978). A Titan atmosphere with a surface temperature of 200 K. In The Saturn System, D.M. Hunten and D. Morrison, eds. (NASA CP 2068), p. 127-40.

Hunten, D.M., Tomasko, M.G., Flasar, F.M., Samuelson, R.E., Strobel, D.F., and Stevenson, D.J. (1984). Titan. In Saturn, T. Gehrels, ed. (University of Arizona Press, Tucson), in press.

International Critical Tables (1928), Volume III (McGraw-Hill, New York).

Jacobsen, R.T. and Stewart, R.B. (1973). Thermodynamic properties of nitrogen including liquid and vapor phases from 63 K to 2000 K with pressures to 10000 bar. J. Phys. Chem. Ref. Data, **2**, 757-922.

Kawakami, S.-I., Mizutani, H., Takagi, Y., Kato, M., and Kumazawa, M. (1983). Impact experiments on ice. J. Geophys. Res., **88**, 5806-5814.

Lewis, J.S. (1971). Satellites of the outer planets: Their physical and chemical nature. Icarus, **15**, 174-185.

Lindal, G.F., Wood, G.E., Hotz, H.B., Sweetnam, D.N., Eshleman, V.R., and Tyler, G.L. (1983). The atmosphere of Titan: An analysis of the Voyager 1 radio occultation measurements. Icarus, **53**, 348-363.

Lunine, J.I. and Stevenson, D.J. (1982). Post-accretional evolution of Titan's surface and atmosphere. Bull. Amer. Astron. Soc., **14**, 713.

Lunine, J.I., Stevenson, D.J., and Yung, Y.L. (1983). Ethane ocean on Titan. Science, **222**, 1229-1230.

Lunine, J.I. and Stevenson, D.J. (1984). Thermodynamics of clathrate hydrates at low and high pressures with application to the outer solar system. Submitted to Astrophys. J.

Miller, R.C. and Stavely, L.A.K. (1976). Excess enthalpies for some binary liquid mixtures of low-molecular-weight alkanes. Adv. Cryogenic Eng., **21**, K.D. Timmerhaus and D.H. Weitzel, eds. (Plenum Press, New York), p. 493-500.

Moran, D.W. (1959). Low temperature equilibria in binary systems, including the solid phase. Dissertation, University of London.

Omar, M.H., Dokoupil, Z., and Schroten, H.G.M. (1962). Determination of the solid-liquid equilibrium diagram for the nitrogen-methane system. Physica, **28**, 309-329.

Prausnitz, J.M. (1969). Molecular Thermodynamics of Fluid-Phase Equilibria (Prentice-Hall, Englewood Cliffs, New Jersey).

Rebiai, R., Rest, A.J., and Scurlock, R.G. (1983). The unexpectedly high solubility of water in cryogenic liquids. Nature, **305**, 412-413.

Sagan, C. and Dermott, S.F. (1982). The tide in the seas of Titan. Nature, **300**, 731-733.

Samuelson, R.E. (1983). Radiative equilibrium model of Titan's atmosphere. Icarus, **53**, 364-387.

Samuelson, R.E., Maguire, W.C., Hanel, R.A., Kunde, V.G., Jennings, D.E., Yung, Y.L., and Aikin, A.C. (1983). CO_2 on Titan. J. Geophys. Res., **88**, 8709-8715.

Squyres, S.W. (1981). The topography of Ganymede's grooved terrain. Icarus, **46**, 156-168.

Yung, Y.L., Allen, M.A., and Pinto, J.P. (1984). Photochemistry of the atmosphere of Titan: Comparison between model and observations. Astrophys. J. Suppl. Ser., in press.

PART III

COMPOSITIONAL AND THERMAL EVOLUTION OF PRIMORDIAL TITAN ATMOSPHERE

Abstract

A simple convective cooling model of a primordial, CH_4-NH_3-N_2 Titan atmosphere is constructed, in an effort to understand the fate of volatiles accreted from a gaseous disk (''nebula'') surrounding Saturn and released from accreting planetesimals during the satellite's formation. Near-surface temperatures are initially $\gtrsim$400 K consistent with the large amount of energy supplied to the atmosphere during accretion. As a consequence of accretional heating, the upper mantle of the satellite consists of an ammonia-water liquid, extending to the surface. This ''magma ocean'' is the primary buffer of atmospheric cooling because it is $\gtrsim$10 times as massive as the atmosphere. The radiative properties of the atmosphere are assumed independent of frequency and the resulting temperature profile is found to be adiabatic; if the atmosphere contains dark particulates surface temperatures could be lower than calculated here. Three major processes drive the cooling: (1) hydrodynamic escape of gas from the top of the atmosphere, which determines the cooling time scales, (2) atmospheric ablation by high velocity impacts (not modeled in detail here), and (3) formation of clathrate hydrate at the ocean-atmosphere interface, at $T \leq 250$ K. Cooling time scales driven by escape are sufficiently long (10^8-10^9 years) to allow ~10 bars of N_2 to be produced photochemically from NH_3 in the gas phase (Atreya et al., 1978); however, the abundance of NH_3 at temperatures $\lesssim$150 K (where the intermediate photochemical products condense out) is optically thick to the dissociative UV photons. Thus, N_2

formation may proceed primarily by shock heating of the atmosphere during large body impacts, as well as by photochemistry (1) at T < 150 K if intermediate products supersaturate, or (2) in a warm stratosphere, with NH_3 abundance fixed by its tropopause value. The clathrate formed during late stages of cooling sequesters primarily CH_4, with some N_2, and forces surface temperatures and pressures to drop rapidly. The clathrate is only marginally buoyant relative to the coexisting ammonia-water liquid. If it sinks, the atmosphere is driven to an N_2-rich state with most of the methane sequestered in clathrate when the ocean surface freezes over at ~180 K. Implications of this scenario for the present surface state of Titan are contrasted with those obtained if the clathrate forms a buoyant crust at the surface.

1. Introduction

The origin and early evolution of the atmospheres of terrestrial planets has been the subject of extensive study for decades (Pollack and Yung, 1980; Walker et al., 1983; Lewis and Prinn, 1984); the formation and early evolution of the Galilean satellites of Jupiter has also attracted substantial interest in the last ten years (reviewed in Stevenson et al., 1984). Saturn's satellite Titan has been largely neglected on both counts (but see Owen, 1982), because of its uniqueness to the Saturn system and, until very recently, the lack of compositional data on its atmosphere. Because Titan's bulk properties are so similar to the icy Galilean satellites, while its atmospheric and inferred volatile constituents are similar to those currently, or thought originally to have been present, in terrestrial atmospheres, the satellite's origin and evolution is of potential relevance to both areas. Indeed, its atmosphere may hold clues to satellite formation processes as well as to the origin and evolution of ''terrestrial-type'' atmospheres in general. (Here the term terrestrial implies an atmosphere comprising a negligible fraction of the mass of the body, with a well-defined interface between planetary or satellite surface and gas; hence, the giant planets are excluded.)

In this paper a model is constructed for the earliest evolution of Titan's atmosphere. Starting conditions are obtained from fairly general considerations of energy input during satellite accretion; initial composition is consistent with current thinking on the composi-

tion of gaseous formation regions (''nebulae'') around giant planets (Prinn and Fegley, 1981) as well as constraints provided by the inferred rock-to-ice ratio of the satellite. The evolution of the atmosphere is driven by escape processes made energetically possible by early enhanced EUV solar radiation and possibly late heavy bombardment, both of which may have been important for evolution of primordial terrestrial atmospheres.

The cooling is buffered by the presence of a massive liquid ammonia-water mantle (''magma ocean'', in analogy with molten outer layers postulated for the terrestrial planets; see e.g., Hofmeister, 1983). The radiative cooling time Δt_R for an atmosphere buffered by such an ocean is

$$\sim \frac{T_s \, c \, \rho \, \ell}{\sigma(T_e^4 - T_o^4)} \quad , \qquad (1)$$

where T_s, T_e, T_o are temperatures at the surface, at optical depth unity and in equilibrium with solar insolation, c, ρ, and ℓ are specific heat, density, and depth of the magma ocean, and σ is the Stephan-Boltzmann constant. For parameter values $c = 4.2 \times 10^7$ erg/g K, $\rho = 0.95$ g/cm^3, $\ell = 500$ km, $T_e \gtrsim 100$ K, and $T_o \sim 86$ K, $\Delta t_R \sim 10^7$ years. The atmosphere-ocean system tends to approach equilibrium with solar insolation during cooling ($T_e \rightarrow T_o$) and so the time scale Δt_E for evolution of a massive atmosphere to the present state is dictated by the mass loss rate due to escape. In section 2 energy sources for escape are considered and it is concluded that $\Delta t_E \sim 10^8$–10^9 years,

substantially longer than Δt_R. Of order 10 bars of N_2 may be produced from NH_3 during cooling by photochemical (Atreya et al., 1978) or impact processes. At surface temperatures $\lesssim$250 K conditions at the base of the atmosphere permit the formation of clathrate hydrate, which produces two divergent evolutions depending upon the clathrate density relative to the magma ocean: (1) If the clathrate is more dense, the CH_4 in the atmosphere is largely sequestered in clathrate until temperatures drop to 180 K and the ocean itself freezes over. (2) The clathrate if buoyant may form an impermeable layer at the surface, isolating ocean from atmosphere and leaving most of the CH_4 and N_2 in the atmosphere. Neither extreme reproduces the present state, but the model is useful in illustrating the sensitivity of the evolution of the atmospheric volatiles to various physical processes.

Part II examines satellite formation scenarios and post-accretional processes to provide constraints on atmospheric composition and escape rates used in the model. Part III formulates the model. Part IV presents results of models for various input parameters. Part V discusses the implications of our results for the present Titan as well as issues which are not directly addressed by the model (e.g., emplacement of surficial methane).

2. Constraints Based on Accretion, Escape, and N_2 Production Processes

In this section we place limits on accretional heating of Titan, as well as review existing literature on processes and energetics of escape and production of N_2 from NH_3 in the primordial atmosphere. Essentially no published accretion models of Titan exist; a general review of satellite accretion models is given in Stevenson et al. (1984). We use the Galilean satellite accretion scenario of Lunine and Stevenson (1982), extended to include the effects of materials more volatile than water ice, as described below. We then apply existing studies of escape processes to early Titan evolution and address critically the issue of whether sufficient energy is available to remove a massive primordial envelope around the satellite.

2.1. Accretion

A rough measure of the temperature rise possible during accretion is given by equating the gravitational energy of planetesimal infall to the resulting heating

$$\Delta T = \frac{GM}{Rc_p}$$

where M, R are mass and radius of satellite, c_p = specific heat per gram

at constant pressure of the material into which energy is deposited, and G is the gravitational constant. Using M and R for Titan, c_p for an ice-rock mix, $\Delta T \sim 1100$ K. This is an overestimate of the temperature rise because (1) latent heat effects of phase changes are neglected, and (2) energy deposition could occur in a gaseous envelope bound to the satellite, which would buffer the surface temperature. To quantify these effects we must ascertain the likely components and their phases in accreting planetesimals.

Two extreme formation regions for Titan can be envisioned: (1) a low pressure ($<10^{-6}$ bars) gaseous disk surrounding the sun in which CO and N_2 are the primary carbon and nitrogen species (Lewis and Prinn, 1980), and (2) a high pressure (~0.1 bar), gaseous disk surrounding Saturn in which CH_4 and NH_3 predominate (Prinn and Fegley, 1981). The quoted pressures are derived from physical models of solar and giant planet nebulae reviewed in Stevenson et al. (1984). The predominance of one carbon or nitrogen species over another depends on detailed assumptions about reaction and mixing rates, as well as quench temperatures; such modeling is sufficiently uncertain that the ratios of CO versus CH_4 and N_2 versus NH_3 under various primordial conditions remains controversial. We assert, however, that a nebula in which CO was the dominant carbon species is an unlikely source of material for Titan for two reasons: (1) the resulting water ice to rock ratio would give an average density for Titan of ~2.1 g/cm^3 instead of the observed 1.88 g/cm^3, and (2) the resulting CO to N_2 ratio incorporated in clathrate (the only plausible way to bring these constituents into Titan), is ~1-

20 (Lunine and Stevenson, 1984a); $CO/N_2 \sim 10^{-4}$ in the present atmosphere. The physical chemistry of these two molecules is very similar; only photochemical processes are likely to distinguish between the two. Samuelson et al. (1983) claim that ~0.2 bars of CO could be destroyed photochemically over the age of the solar system; this rate would have to be increased by 10-100 to derive the present CO/N_2 ratio from that in clathrate. We thus consider a CH_4-rich gaseous nebula. In contact with such a gas, the predominant molecule incorporated in clathrate is CH_4, and very little N_2 is sequestered (Lunine and Stevenson, 1984a). We thus claim that the most likely source of condensed nitrogen accreted into Titan is the ammonia hydrate stoichometric compound, $NH_3 \cdot H_2O$. If the predominant C and N compounds are CH_4 and NH_3, respectively, then $NH_3/H_2O \sim 0.15$ as assumed in the remainder of the paper. For a gas pressure in the Saturnian nebula of~0.1 bar, $NH_3 \cdot H_2O$ condenses out at ~160 K and $CH_4 \cdot 6H_2O$ (clathrate) at 100 K. Temperatures at the orbit of Titan in nebular models are ~50-100 K (Prinn and Fegley, 1981; Lunine and Stevenson, 1982); hence, both solid compounds are stable.

Although we consider only gaseous accretion in detail here, gas-free planetesimal accretion is a viable alternative. If material originally condensed in a gaseous environment, trapping volatiles such as NH_3, CH_4, N_2, etc., and aggregated into larger bodies after the gas was dissipated, an atmosphere would be raised on the accreting satellite by impact and release of volatiles. The efficiency of retention of such an atmosphere during accretion has never been examined; however, based on calculations by O'Keefe and Ahrens (1982) the impact velocities must be

low ($\lesssim$5 km/s) to prevent net loss of material (including volatiles) from the satellite. Such velocities are plausible for Saturn-orbiting debris impacting Titan, since Titan's orbital velocity is ~5 km/s. Solar orbiting debris, however, would impact Titan at velocities $\gtrsim$10 km/s, the escape velocity from the Saturn system at Titan's orbit. For this reason, post-accretional addition of a volatile rich veneer, from solar orbiting comets, onto a water ice-rock Titan is not plausible. Such a ''late-heavy bombardment'' phase may have played a role in atmospheric escape. The cooling model described in section 3 is potentially applicable to the evolution of an atmosphere formed during gas free accretion as well as to one formed in the gaseous accretion scenario outlined below. The major difference (and uncertainty) between the two scenarios is the total mass of atmosphere retained during the formation process, which is an input to the cooling model.

The physics of accretion in a gas-rich environment is given in Lunine and Stevenson (1982); we briefly outline it here. As a body accretes material in a gaseous environment it forms a gravitationally bound envelope of nebular gas around itself. Although the full extent of the envelope is given by the balance between the gravitational field of the accreting satellite and that of the nebula plus parent body, the high density portion is more restricted in extent, given by the level at which the escape velocity exceeds the gas sound speed. Planetesimals encountering the envelope spiral in due to gas drag, depositing much of their energy of infall in the envelope. Here we consider one extreme case, in which the planetesimal disseminates completely and deposits

essentially all of its energy in the envelope. This gives a maximum to the accretional temperature at the satellite surface; the alternative of incomplete dissemination of planetesimal material can produce lower surface temperatures (Lunine and Stevenson, 1982).

The surface temperature during accretion is therefore dictated primarily by the gaseous envelope. This envelope contains sufficient H_2 to be optically thick to infrared radiation, and the rate of accretional energy input is sufficient to force the envelope to be convective. The temperature structure of the envelope is thus adiabatic, modified by the latent heat effects of saturated volatiles at the surface. The surface temperature is given by equation (22) of Lunine and Stevenson (1982) (note in that equation $\bar{\rho}(r)$ should be defined as the volume averaged density of satellite and envelope at radius r from the center); this is a generalization of the meteorological ''moist adiabat.''

For Titan the plausible volatiles are NH_3-H_2O solid (and subsequently liquid) and clathrate hydrate; we have argued above that the clathrate contains mainly CH_4. Initially surface temperatures during accretion are low, and the body accretes as a solid mixture of rock and ice. As T increases above 172 K, the ammonia-water system becomes liquid and a rock layer separates from the ammonia water liquid in the growing body. The envelope, initially H_2-He with a large specific heat capacity ($\sim 10^8$ erg/g) becomes NH_3 and CH_4 dominated, lowering the specific heat capacity and further increasing temperature (the latent heat of volatile condensation moderates the temperature somewhat, but the specific heat effect dominates). Final surface temperatures can get as high

as 600 K in such a model. (Models in which the highly volatile methane clathrate is not abundant give T ~ 300 K.) The complexity of the accretion process makes these values of T rather uncertain. At issue is whether we can constrain T sufficiently well to predict initial abundances of NH_3 and CH_4 in the immediate post-accretional atmosphere. The H_2O and NH_3 atmospheric mass is constrained by the vapor pressure in coexistence with the surface, which at T > 172 K is an ammonia-water liquid. The CH_4 atmospheric abundance, which at low temperatures is in equilibrium with clathrate hydrate, is constrained only by abundance considerations above ~320 K because CH_4 clathrate is unstable relative to CH_4 and water above this temperature (Lunine and Stevenson, 1984a). A maximum to the amount of methane in the atmosphere derived from clathrate can be estimated by taking the total mass of methane accreted as clathrate (~0.15 that of H_2O) and subtracting the amount in an undifferentiated core of material accreted at T < 172 K; this yields $\simeq 8 \times 10^{24}$ g. A more extreme upper bound assumes methane ice condensed in the nebula and accreted onto Titan; if all of it volatilized into an atmosphere the mass would be 3×10^{25} g. The upper bounds are probably a substantial overestimate since the CH_4-rich gas envelope is in convective contact with the comparatively CH_4-poor nebula. For the clathrate upper bound, the surface pressure of methane at 600 K is estimated, using equations for an adiabatic atmosphere given in section 3 to be of order 100 bars. The ammonia-water vapor pressure, near the critical point of the 15% NH_3-H_2O system is 200 bars (Tsiklis et al., 1965). Figure 1 illustrates schematically the interior and atmosphere of Titan

Figure 1. Schematic model of the interior structure and atmospheric composition of Titan immediately after accretion. Radii are indicated on the right side of the figure; approximate pressure on the left. Subsequent evolution of the interior would plausibly involve overturn of the core and replacement by the rock layer above (Schubert et al., 1981).

TITAN AT CLOSE OF ACCRETION

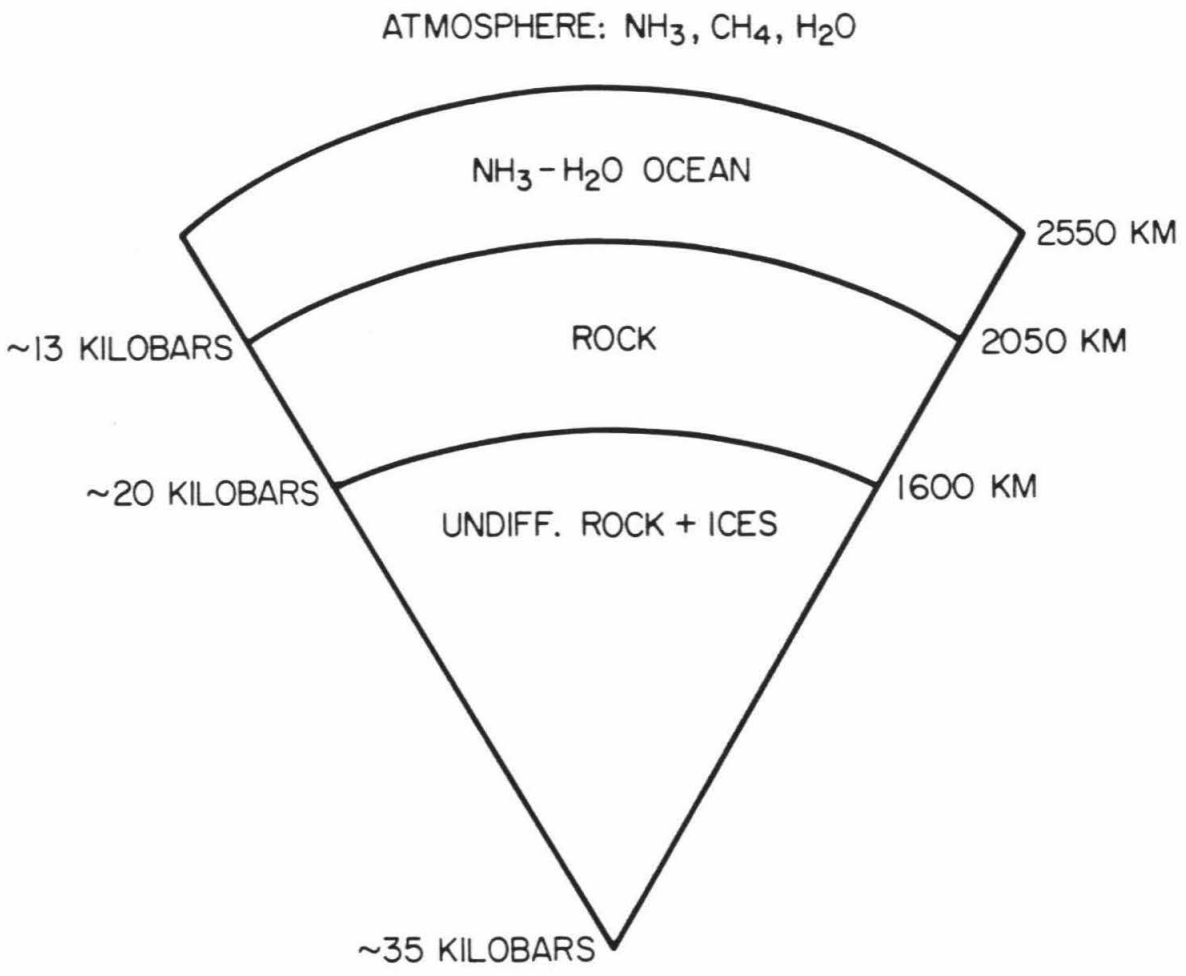

immediately after accretion.

2.2. Escape Processes

The atmospheric model of section 3 is largely independent of the particular mechanism of accretion (i.e. gaseous or gas-free) of the satellite, since only general constraints of energy input, volatile composition and maximum total abundance are applied from the accretion model discussed in the previous section. Lewis and Prinn (1984, p. 37) argue that an atmosphere captured from the surrounding nebula and in convective contact with it must be dissipated with the nebula, since the gas capture process is thermodynamically reversible. This conclusion does not strictly hold if compositional gradients are introduced in the atmosphere during accretion, as occurs for water and methane accreting as clathrate in the gasous formation scenario. We therefore assert that a substantial fraction of a methane rich primordial atmosphere, formed in a gaseous nebula, would remain gravitationally bound to Titan after dissipation of the nebula; we have not, however, quantified this fraction. In the gas-free case the argument of Lewis and Prinn is not relevant. Our cooling models span a range of two orders of magnitude in the atmospheric mass retained after nebular dissipation. We now examine what energy sources are available to drive escape of such an atmosphere.

Rapid escape of primordial terrestrial atmospheres has been analyzed by Hunten (1979), Sekiya et al., (1980), Watson et al. (1981), and Walker (1982). The primary energy source for escape is presumed to

be an enhanced solar extreme ultraviolet flux (EUV) in analogy with the observed T-Tauri phase in stars (Zahnle and Walker, 1982; Canuto et al., 1982). Enhancements relative to present of 10^4 in the EUV flux at a stellar age of 10^6 years, dropping to 30 at 10^8 and 4 at 10^9 are possible (Canuto et al., 1982). Watson et al. (1981) present an analytic model for rapid escape of the atmosphere due to EUV heating. The efficiency of the escape of gas is primarily limited by the conduction of heat from the level of EUV absorption r_1 to the region r_o where most of the atmospheric mass is located. This constrains the level at which radiation is absorbed and, hence, the escape flux $\dot{M}$. Because the gas is cooled by adiabatic expansion the temperature profile between these levels displays a minimum T_m; as $\dot{M}$ increases, T_m decreases. If $T_m = 0$, then the escape flux must be a maximum, since if $\dot{M}$ or r_1 are increased $T_m < 0$. Hunten and Watson (1982) applied this model to escape of CH_4 from Pluto; we apply it here to escape of a primitive Titan atmosphere. We assume $r_o = R$, the surface of the planet. This will underestimate $\dot{M}$ since much of the mass of this distended atmosphere is at higher levels, although below the level at which the EUV radiation is absorbed. Methane is assumed to be the dominant gaseous constituent at the level of EUV absorption; the temperature profile for the lower atmosphere given in section 3 indicates NH_3 would be cold-trapped at the tropopause. Using nomenclature of the above two papers we solve

$$\xi = \frac{2}{s+1} \left[\frac{(\lambda_1/2)^{(s+1)/2} + 1}{\lambda_s - \lambda_1} \right]^2 \qquad (2)$$

$$\lambda_1^2 = \frac{\beta}{\lambda_s \xi - (2\xi/(s+1))^{1/2}} \qquad (3)$$

where $\lambda_s = GMm/kT_sR$, $\beta = \mathcal{F}_{EUV}\lambda_s R/K_o T_s$, $\xi = \dot{M}(k/K_o\lambda_s 4\pi Rm)$, m = mass of methane molecule, T_s = surface temperature, $\mathcal{F}_{EUV}$ = solar EUV flux, K_o = thermal conductivity of methane, and k = Boltzmann's constant. Using an efficiency factor of 1/2, present EUV rate and CH_4 conductivity from Hunten and Watson (1982) the limiting escape flux and heating level are shown in Figure 2 as a function of enhancement over present EUV rate, for T_s = 400 K. The maximum flux, 10^{15} g/year is achieved at an EUV enhancement of ~100; however, r_1 -> R which violates an assumption of the model. Also, the currently inferred mass loss rate of N_2 from Titan is ~2 x 10^{11} g/yr (Strobel and Shemansky, 1982) most of which is due to magnetospheric electrons, implying an escape efficiency due to EUV absorption <<1. (The extended nature of the primitive atmosphere could increase the efficiency.) We thus do not expect an enhanced escape flux in excess of 10^{14}-10^{15} g/yr, over $\lesssim 10^8$ years (Canuto et al., 1982), during which time 10^{22}-10^{23} grams of material may be lost.

We thus have a mismatch between the maximum post-accretional methane mass in the Titan atmosphere, and the mass loss driven by EUV heating of that atmosphere over a time < age of the solar system. One of two conclusions may be drawn (1) Titan never possessed a massive atmosphere, or (2) other processes, less well quantified than EUV heating, removed almost all of the primordial Titan atmosphere. These processes could include enhanced solar/Saturnian wind, enhanced Saturn

Figure 2. Mass flux (gram/year) and level of EUV heating (in units of Titan radii) as a function of EUV heating (relative to present heating rates). An EUV heating efficiency factor of 1/2 is used.

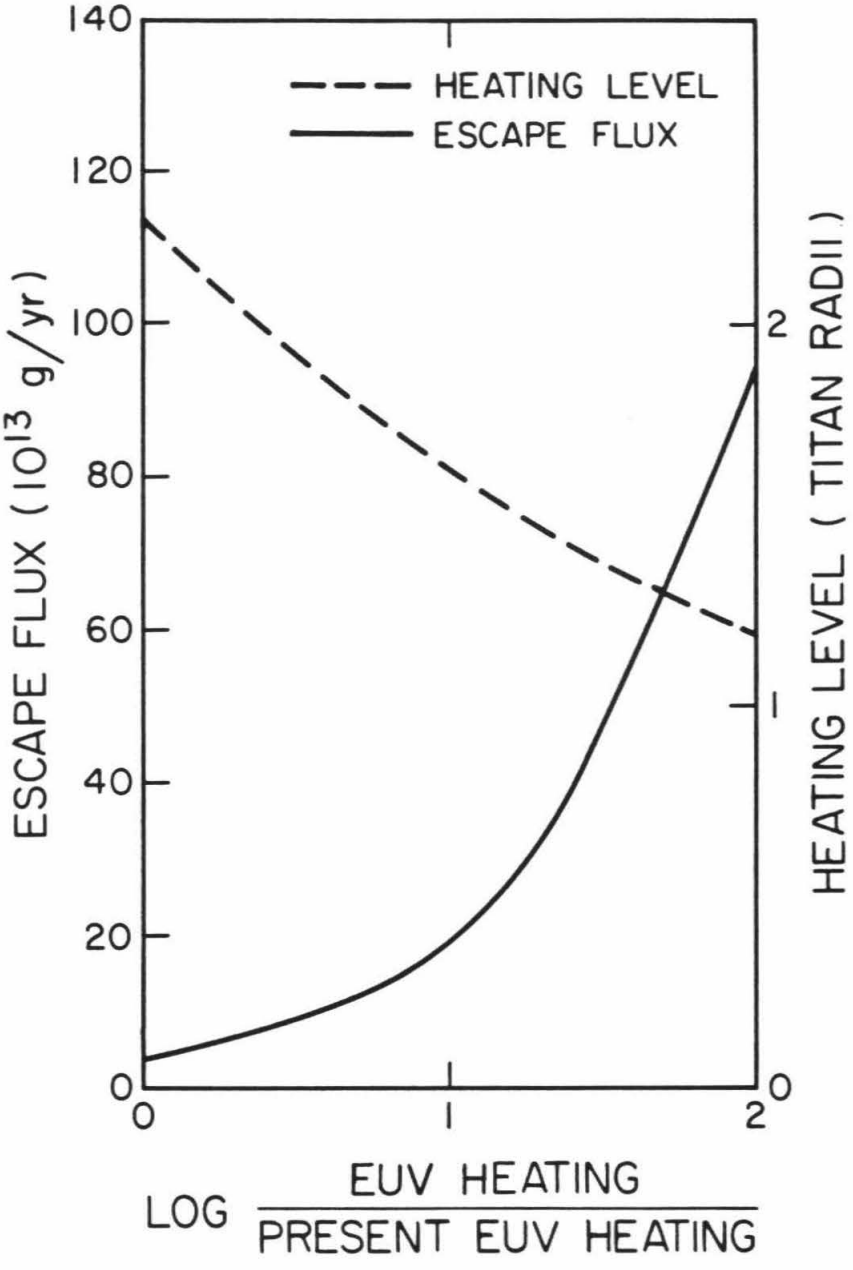
HEATING LEVEL
ESCAPE FLUX
ESCAPE FLUX (10^{13} g/yr)
HEATING LEVEL (TITAN RADII)
140
120
100
80
60
40
20
0
2
1
0
0
1
2
LOG EUV HEATING / PRESENT EUV HEATING

luminosity or magnetic field, or outward transport of angular momentum due to viscous coupling. The latter process is described in Lynden-Bell and Pringle (1974); its effect on a bound primordial atmosphere embedded in the nebula has not been modeled. Horedt (1978) argued that an augmented solar wind accompanying the T-Tauri phase could dissipate a 0.1 solar mass nebula in 10^7 years; potentially marginally enough energy in the form of solar wind particles could be intercepted by an extended Titan envelope to dissipate it in 10^7 years. The physics of the interaction between wind and nebula in Horedt's model is so simplified, however, that it is probably invalid for bound atmospheres. Detailed modeling of such a process for a planetary atmosphere has not been done. A ''Saturn wind'' is also possible during an enhanced luminosity phase of Saturn's evolution (Pollack and Consolmagno, 1984), but is even more speculative. The enhanced Saturn luminosity phase itself could heat the atmosphere below the EUV absorption level and augment escape, but the enhancement is not sufficiently large nor prolonged to allow a significant fraction of the atmosphere to escape. An enhanced Saturnian magnetic field would increase loss of gases by electron bombardment and formation of hot atoms (Strobel and Shemansky, 1982); the process is complex and requires knowledge of the early particle environment in the magnetosphere at Titan's orbit as well as how the efficiency of the process scales (up or down) with increased B-field strength. The simplest assumption is that the escape rate scales as the square of the B-field, and is similar for N_2 and CH_4-derived atoms; then loss of a primordial atmosphere over 10^7 years requires a 300-fold increase in B-

field strength during this time. Until the scaling of this process can be made more quantitative its application to early atmospheric escape remains speculative.

In what follows, we focus on the later stages of cooling, M ~ 10^{23} g, and will argue that our results are not very sensitive to particular earlier conditions (i.e., immediate post-accretional T, P). Thus, it may not be necessary (or possible) to distinguish between conclusions (1) and (2). One additional, previously neglected escape energy source requires some attention, however: high velocity impacts of planetesimals.

During accretion of Saturn-orbiting planetesimals, planetesimal encounter and impact velocities on Titan are small ($\lesssim$several km/s). After accretion, high velocity impact of solar-orbiting debris may cause net loss of gas. The impact process and net loss of solid target debris have been quantified by O'Keefe and Ahrens (1982) as noted above but atmospheric loss has not been quantitatively modeled. Because large impactors will deposit most of their energy in the lower portion of a massive atmosphere (i.e., over a column integrated mass of order the planetesimal mass), the energy transport limitation on the escape flux applicable to EUV heating is probably not relevant. If the atmosphere is too thin, most of the impact energy will be deposited in solid debris, although some gas may be entrained with the ejecta. Escape by large body impact is thus likely to be most efficient in a massive atmosphere such as that envisioned for primordial Titan. Cameron (1983) argues that impacts would have dominated early terrestrial atmospheric

escape. Stevenson (1982a) concludes that the observed carbon enhancement in Jupiter and Saturn was most likely acquired by impact of several earth masses of condensed material. In conjunction with the Saturnian satellite cratering record and other evidence (Shoemaker and Wolfe, 1984), the implication is that a post-accretional bombardment of the Saturnian system by >several earth masses of material occurred. This event may have been of singular importance to the earliest evolution of Titan's atmosphere, as a primary driver of escape.

Based on the above considerations, we choose a range of mass loss rates $\dot{M} \sim 10^{14}$-10^{15} g/year and a starting atmospheric mass ~10^{23}-10^{24} g in the models presented below. We also consider, however, models with higher mass loss (10^{16} g/year) and initial mass (10^{25} g) to investigate evolution during catastrophic escape due perhaps to impacts.

2.3. Production of N_2

If arguments presented above that the earliest atmosphere was primarily CH_4 are correct, N_2 must have been produced from other constituents. Atreya et al. (1978) developed a photochemical scheme for conversion of NH_3 to N_2. To first order, the process is independent of CH_4 abundance, since the molecule absorbs photons shortward of 1600 Å wavelength and NH_3 photolysis can be initiated at wavelengths as long as 2300 Å. The crucial requirement for photolysis to form N_2 is that photons be available to NH_3 molecules at T > 150 K, below which temperature hydrazine (N_2H_4), an intermediate product, condenses out under

Atreya et al.'s model conditions. Using near UV absorption coefficient data from Thompson et al. (1963) and a vapor pressure relation shown in Table I for NH_3 in coexistence with a 15% NH_3 magma ocean, we conclude the gaseous NH_3 is optically thick to photons shortward of 2250 Å at an altitude corresponding to T = 150 K, i.e., few photons shortward of that limit are available below that altitude. However, our NH_3 vapor pressure curve probably overestimates P_A since it assumes ideality and in fact the NH_3-H_2O activity coefficient is <1 (Haudenschild, 1970). Also N_2H_4 may be modestly supersaturated if the atmosphere contains few particulates. Above the cold trap (86 K) the mixing ratio of NH_3 is sufficiently high that the integrated optical depth to absorption of 2000 Å photons is ~0.1; if T increases rapidly enough to 150 K above the cold trap some photolysis of NH_3 to N_2 may occur there as well. This requires detailed model of stratospheric temperature profiles, beyond the scope of the present models. As an upper limit to the N_2 production rate we take Atreya et al.'s (1978) value of $\sim 10^{14}$ g/year. Since near UV radiation is not likely to have been enhanced after the first 10^6 years (Zahnle and Walker, 1982), this rate is probably nearly constant.

An additional means of forming N_2 may be shock heating of NH_3. Unpublished calculations by D.J. Stevenson suggest that impacts, in addition to causing escape of gas, can convert NH_3 to N_2 during the shock process. The efficiency of this process (N_2 retained versus N_2 formed) has not been quantified. Most of the conversion is likely to have occurred over $\sim 10^8$ years during the speculative post-accretional heavy bombardment discussed above.

3. Formulation of Model

Consider a hot, optically thick atmosphere containing both 'dry' or unsaturated gases (CH_4, N_2) and saturated vapor (NH_3, H_2O), in good thermal contact with a massive NH_3-H_2O magma ocean surface which is heated by sunlight. This scenario is illustrated in Figure 3a and is intended to represent the surface and atmospheric state of Titan after accretion. Because of accretional heating, the effective radiating temperature T_e at optical depth unity in the atmosphere is higher than T_o, the effective temperature defined by the flux of incident sunlight. The atmosphere thus cools on a time scale given by equation (1). As atmospheric cooling ensues, $T_e \rightarrow T_o$ and Δt_R increases, as shown in Figure 4. Eventually $\Delta t_R > \Delta t_e$, the cooling time defined by loss of gas from the atmosphere due to escape processes discussed in section 2. Δt_e is shown in Figure 4 for an atmospheric mass M of 10^{23} g and $\dot{M} = 10^{14}$ g/year. This phase of atmospheric evolution, ''steady-state'' phase, is depicted in Figure 3b. As M decreases, surface temperature and pressure decrease to keep the atmosphere/ocean system in equilibrium with sunlight.

As T drops below ~250 K, the CH_4 and/or N_2 in contact with the ocean may become supersaturated with respect to the clathrate hydrate $(CH_4, N_2)\cdot 6H_2O$ (Lunine and Stevenson, 1984a). The uptake of gas by clathrate, shown in Figure 3c, results in a pressure drop ∂P for a given ∂T_s which is much larger than that given by adiabatic adjustments to the

Figure 3. Illustration of phases of atmospheric evolution, described in text. Temperature-altitude profile is schematic; time scales are typical for a model with $\dot{M} \sim 10^{14}$ g/year and starting mass 10^{23}-10^{24} g. Minor constituents are indicated in parentheses. Although some processes may occur in all panels, only those important to the particular stage are shown in a given panel. (a) Hot, post-accretional atmosphere with $T_e > T_o$ cools down at a rate given by equation (1) which is greater than that due to escape. A small fraction of the mass of the atmospheric constituents is dissolved in the ocean, but does not affect evolution. (b) Atmosphere has achieved steady state with $T_e \sim T_o$; cooling rate now determined by mass loss rate. Photochemical and impact-induced $NH_3 \rightarrow N_2$ conversion may occur. (c) Base of atmosphere has entered clathrate stability field, dropping surface pressure rapidly and forcing $T_e > T_o$, increasing cooling rate. (d) Ocean freeze-over terminates clathrate formation, atmosphere returns to steady-state ($T_e \sim T_o$).

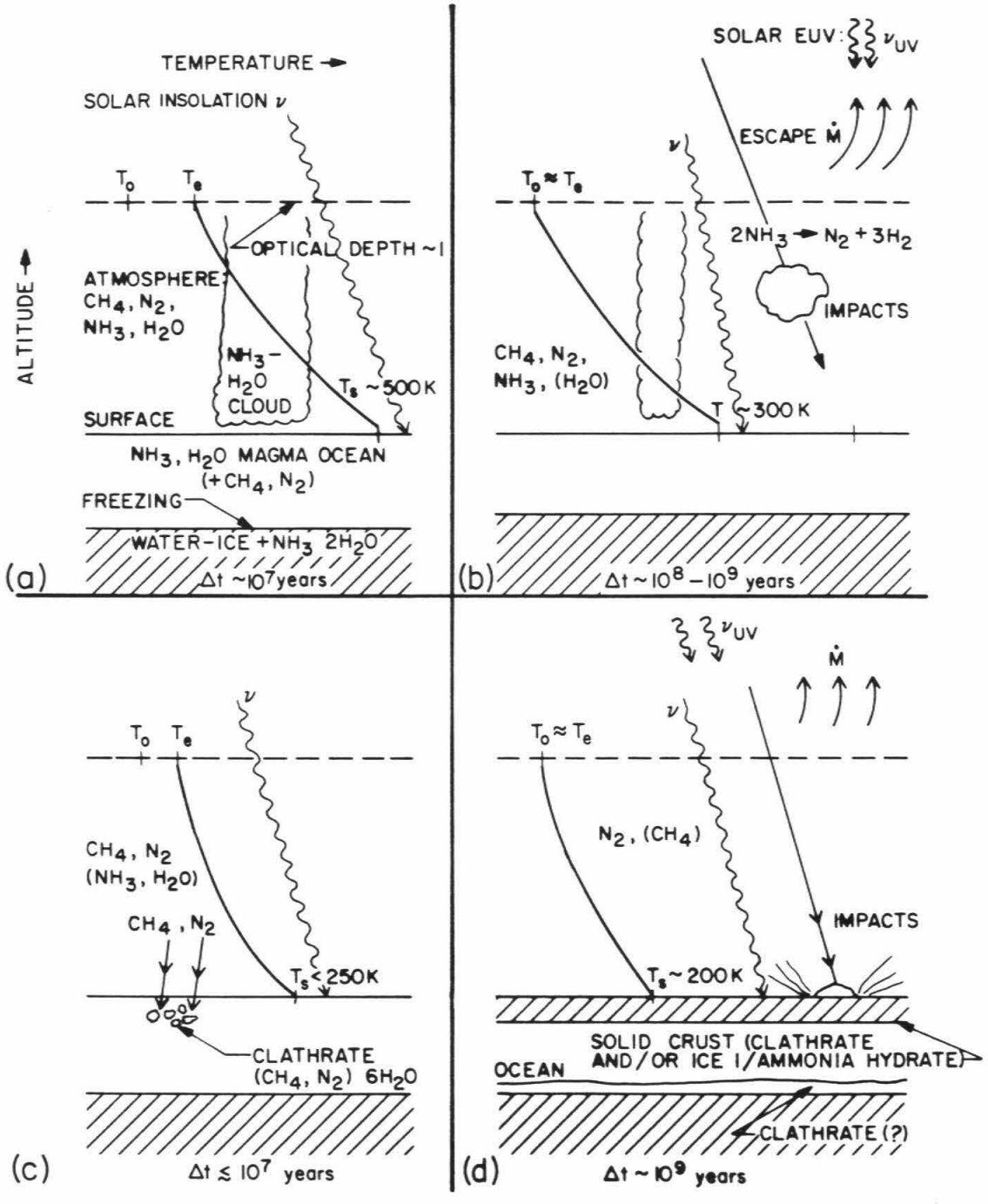
TEMPERATURE →
SOLAR INSOLATION ν
ALTITUDE →
T₀
Tₑ
OPTICAL DEPTH ~1
ATMOSPHERE:
CH₄, N₂,
NH₃, H₂O
NH₃ – H₂O CLOUD
Tₛ ~ 500 K
SURFACE
NH₃, H₂O MAGMA OCEAN
(+CH₄, N₂)
FREEZING
WATER-ICE + NH₃ 2H₂O
(a)
Δt ~ 10⁷ years
SOLAR EUV: ν_UV
ESCAPE Ṁ
ν
T₀ ≈ Tₑ
2NH₃ → N₂ + 3H₂
IMPACTS
CH₄, N₂,
NH₃, (H₂O)
T ~ 300 K
(b)
Δt ~ 10⁸ – 10⁹ years
ν
T₀
Tₑ
CH₄, N₂
(NH₃, H₂O)
CH₄, N₂
Tₛ < 250 K
CLATHRATE
(CH₄, N₂) 6H₂O
(c)
Δt ≲ 10⁷ years
ν_UV
Ṁ
ν
T₀ ≈ Tₑ
N₂, (CH₄)
IMPACTS
Tₛ ~ 200 K
SOLID CRUST (CLATHRATE
AND/OR ICE I/AMMONIA HYDRATE)
OCEAN
CLATHRATE (?)
(d)
Δt ~ 10⁹ years

Figure 4. Cooling time Δt_R (years) versus T_e (K), for an NH_3-H_2O ocean of depth 500 km. The effective temperature due to solar insolation is set at 86 K. Dotted line is Δt_e, cooling time defined by atmospheric escape as described in text.

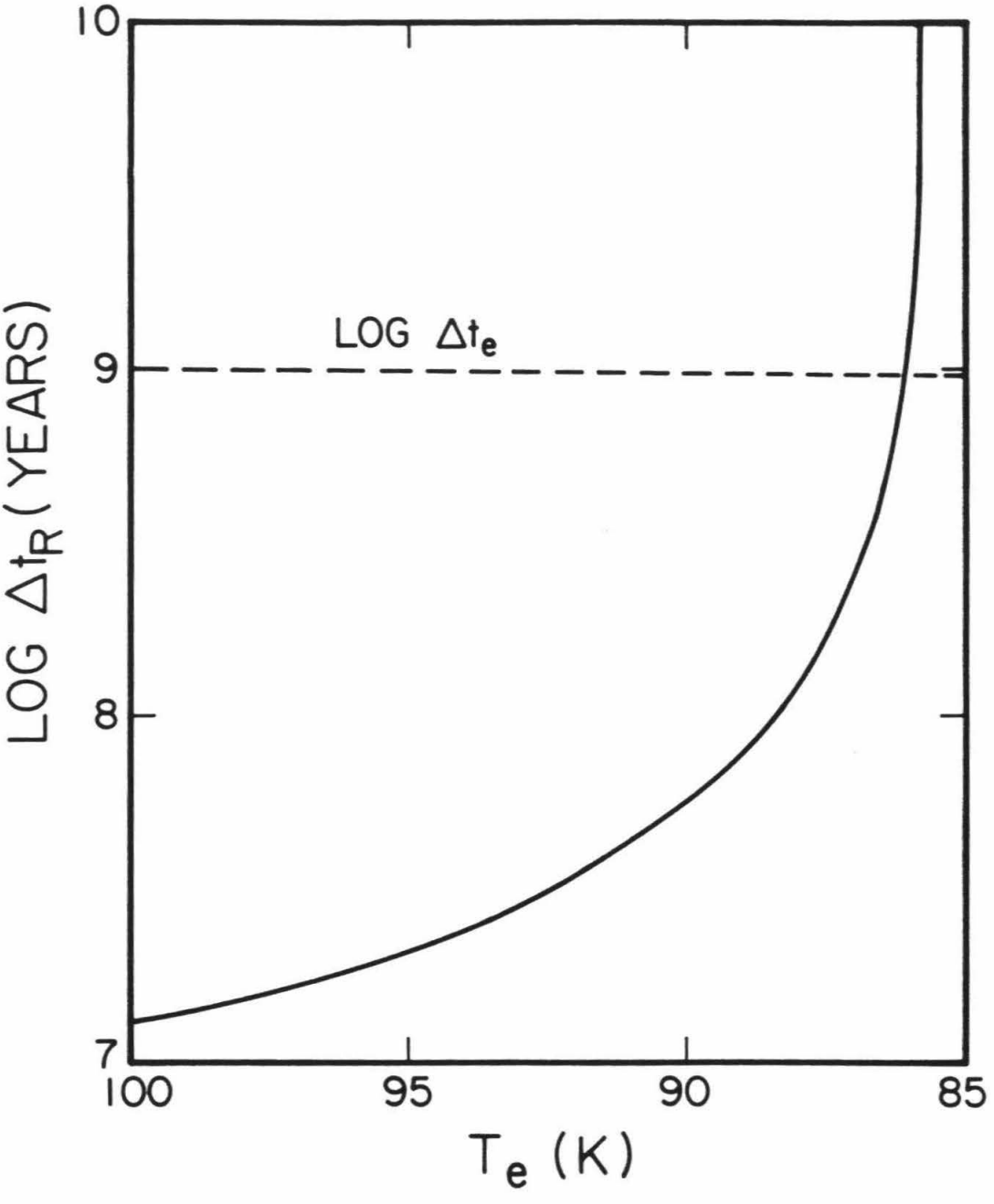
10
9
8
7
LOG Δt_e
LOG Δt_R (YEARS)
100
95
90
85
T_e (K)

''slow'' escape processes operative to this point. Hence, $T_e > T_o$, and T_s must drop further, resulting in catastrophic loss of atmosphere to clathrate so long as H_2O is available from the ocean. This continues until the ocean freezes over (Figure 3d) and the atmosphere returns to steady state.

We now outline the model which incorporates these processes. By balancing the heat content of the ocean (including latent heat of freezing at depth) and atmosphere against heat lost due to radiation we find

$$c\rho\ell\ \frac{dT_s}{dt} = -\sigma(\ T_e^4 - T_o^4\ ) - L\ \rho\ \frac{d\ell}{dt} \qquad (4)$$

where L is the latent heat of freezing of water (3.3×10^9 erg/g), and we assume that both frozen and liquid portions of the ocean buffer the atmosphere; hence,

$$c\rho\ \frac{d\,\ell\,T_s}{dt} = c\rho\ell\ \frac{dT_s}{dt} \quad .$$

The surface and effective radiating level are linked by a moist adiabat:

$$\frac{T_s}{T_e} \simeq \left(\frac{P_s}{P_e}\right)^{(\gamma-1)/\gamma}\ e^{-L_A q_A/c_g T_s} \qquad (5)$$

with P_s, P_e the total pressure at the surface and effective radiating level, γ the ratio of specific heats of the gas, L_A, q_A the latent heat

and mixing ratio of NH_3 and H_2O in the atmosphere, and c_g the specific heat of the dry gas. Note only the NH_3-H_2O is assumed to be saturated; CH_4 and N_2 are unsaturated in the model (except at the effective radiating level, where CH_4 may saturate; this is neglected). q_A is determined from the saturation vapor pressure of the ammonia-water magma ocean (15% NH_3) and except at temperatures $\gtrsim$500 K is primarily NH_3. The exponential term in equation (5) is valid only for $q \lesssim 0.05$; to correct the expression approximately we define an effective specific heat $C_g^1 = C_g + 2L_A q_A/(T_s + T_e)$ which roughly accounts for a term neglected in the derivation (Fleagle and Businger, 1980, p. 78). During terminal stages of cooling ($T_s < 250$ K), $q < 0.05$. Also, (5) assumes ideal gas, roughly true for CH_4 and N_2 for much of the evolution. The NH_3 is highly nonideal, however, and hence, the equation is roughly correct for $T_s \lesssim 300$ K ($q_s < 0.1$) only. The CH_4 and N_2 pressures are determined by the total mass of each in the atmosphere and ocean and their solubilities in the ammonia-water ocean:

$$P_i = \frac{M_i}{\frac{4\pi R^2}{g_s}\frac{\mu_i}{\bar{\mu}} \cdot \delta + \frac{M_o}{K_i}\frac{\mu_i}{\mu_o}} \qquad (6)$$

where $i = CH_4$ or N_2, M_i = total mass of i in atmosphere and ocean, μ_i = molecular weight of i, K_i = Henry's law constant for i, μ_o and $\bar{\mu}$ are, respectively, mean molecular weight of the ocean (= 18 g/mole) and dry component of the atmosphere, M_o = mass of ocean and g_s is the gravitational acceleration at the surface. δ is a factor which approximately

corrects the pressure for the non-isothermality of the atmosphere: , for an adiabatic ideal gas atmosphere δ is:

$$\delta = \frac{(R_c - R)\ \bar{\mu}\ m_p\ g_s}{kT_s} \tag{7}$$

where

$$R_c = \left(\frac{1}{R} + \left(T_e - T_s \right) \frac{c_g}{GM} \right)^{-1} \tag{8}$$

Here m_p = proton mass, k = Boltzmann's constant, G = gravitational constant. The correction factor δ is of order 1 for the present Titan atmosphere, and is $\tilde{}5$ for the earliest atmospheres in our models. Equation (8) is derived for a dry adiabat; a further correction $\lesssim 2$ is applied for the wet adiabat which does not significantly affect the model results.

To fix P_e, as well as to test whether a convective profile is appropriate, the radiative properties of the atmosphere must be specified. We assume a grey atmosphere (opacity independent of frequency), in which pressure-induced opacity of N_2 and CH_4 predominate. Hence, optical depth $\tau \sim A\ P_{CN}^2/T$, where A depends on relative N_2 abundance and P_{CN} is total $N_2 + CH_4$ pressure. In the lowermost atmosphere NH_3 gas and cloud opacity become important; to first order the same expression for τ may be used with a term involving the ammonia vapor pressure P_A.

Thus, at the effective radiating level:

$$P_e = \left(\frac{2/3\ T_e}{A} \right)^{1/2} \qquad (9)$$

where A as a function of methane mole fraction X is given as {140(1 + $10x - 6x^2$)/(1 - 3/7 x)}, based on data in Hunten (1978) and Courtin (1982). The value of T_e for a radiative temperature profile is

$$T_{eR} = T_s \Big/ \left\{ \frac{1}{2} + \frac{3}{4} \left(AP_{CN}^2 + BP_A^2 \right) \frac{1}{T_s} \right\}^{1/4} \qquad (10)$$

where the Eddington approximation is assumed to hold (Mihalas, 1978, p. 61); B for NH_3 gas + cloud is arbitrarily taken to be ~ twice the pure CH_4 value of A. If $T_e > T_{eR}$ for a given T_s, the adiabatic profile is used. This condition is generally satisfied through most of the evolution.

Two approximations require mention. Equation (10) is derived strictly for a plane-parallel atmosphere, rather than the somewhat extended spherical atmosphere of our model. Based on the discussion in Mihalas, 1978, p. 245 this approximation is adequate so long as we are not concerned with frequency distribution of outgoing flux. The assumption of greyness is of more concern. The assumption that optical depth to incoming visible solar radiation τ_v is negligible compared to outgoing infrared radiation τ_{IR} could be violated if substantial amounts of dark particulate material, for example, were present in the lower atmosphere. Then $\tau_{vis} \gtrsim \tau_{IR}$ and convection would be inhibited, with $T_s \rightarrow T_e$. Such an atmosphere would achieve clathrate supersaturation (phase 3) at a much higher mass (i.e., earlier on) than the grey models.

A photochemical source of such haze would not produce $\tau_V \gtrsim \tau_{IR}$ within the troposphere of our model since photolysis of CH_4 should predominate at altitudes above the tropopause; in the present Titan troposphere $\tau_V < \tau_{IR}$ (Samuelson, 1983). It would, however, reduce the effective temperature at the tropopause from 86 K to a substantially lower value as in the present Titan atmosphere. We assert that our grey atmosphere treatment gives a maximum T_S for a given atmospheric mass, and hence, a <u>maximum</u> for the evolution time in phases (1) and (2) of Figure 3.

Freezing of water at the base of the ocean under pressure is calculated using thermodynamic data from Haudenschild (1970) and Eisenberg and Kauzmann (1969, p. 93). A high pressure phase diagram is constructed from these data in Lunine and Stevenson (1984a). By assuming a fixed depth of 500 km for the initial ammonia-water ocean (see Figure 1) we derive the change in depth due to cooling from T_S' to T_S

$$\Delta \ell = \left(R^2 - \frac{R}{\rho g} P(T_S') \right)^{1/2} - \left(R^2 - \frac{R}{\rho g} P(T_S) \right)^{1/2} \qquad (11)$$

where the ocean is assumed isothermal (roughly correct for the ocean adiabat) and

$$P(T_S) = 65.96\ T_S - 6717. \qquad (12)$$

is the pressure level in bars at which freezing occurs. The mole fraction of ammonia in the ocean as a function of temperature is then

$$X_A = \frac{0.15(R^3 - r^3)}{R^3 - r'^3} \qquad (13)$$

where r = depth of ocean at $X_A = 0.15$ and r' = new ocean depth at T_s. Figure 5 illustrates the path of the freezing level of the ocean on a T-P plot, superimposed on water freezing curves for varying ammonia concentrations. Freezing at the top will begin to occur at ~220 K, as the low pressure solidus is reached. This introduces additional latent heat into the ocean but also steepens the dotted curve in Figure 5 (i.e., the lower boundary of the ocean moves up more slowly with temperature). These two effects oppose each other somewhat and are neglected.

Recent data on the ammonia water phase diagram at room temperature and high pressure (Johnson et al., 1984) indicate that for $X_A \gtrsim 0.15$, an ammonia dihydrate ($NH_3 2H_2O$) freezes out in preference to water ice. A preliminary set of temperature-composition phase diagrams based on the data has been constructed in part I of the thesis (Figure B1). These imply that the ocean composition would remain near $X_A \sim 0.15$ during freezing at the base, also shown in Figure 5, since the ice-dihydrate eutectic remains near this composition over a range of pressures. The effect of the data on the models is three-fold: (1) the effective specific heat of the ocean due to latent heat contribution is larger, (2) clathrate formation is initiated at a higher temperature for a given atmospheric composition and pressure, and (3) the ocean is denser. Effect (1) is only significant during phase I of the evolution ($T_e > T_o$) which involves a small fraction of the total evolution time for most models run, and, hence, does not affect our conclusions.

Figure 5. Temperature versus pressure at which freezing of ammonia-water solution occurs, for various mole fractions of water as marked on the figure, from Lunine and Stevenson (1984a). Superimposed on the plot is the T-P-composition path of the lower ocean boundary shown as a dotted line, as it freezes in response to cooling. Initial ocean depth assumed to be 500 km. Approximate freezing curve incorporating preliminary data of Johnson et al. (1984) is also shown.

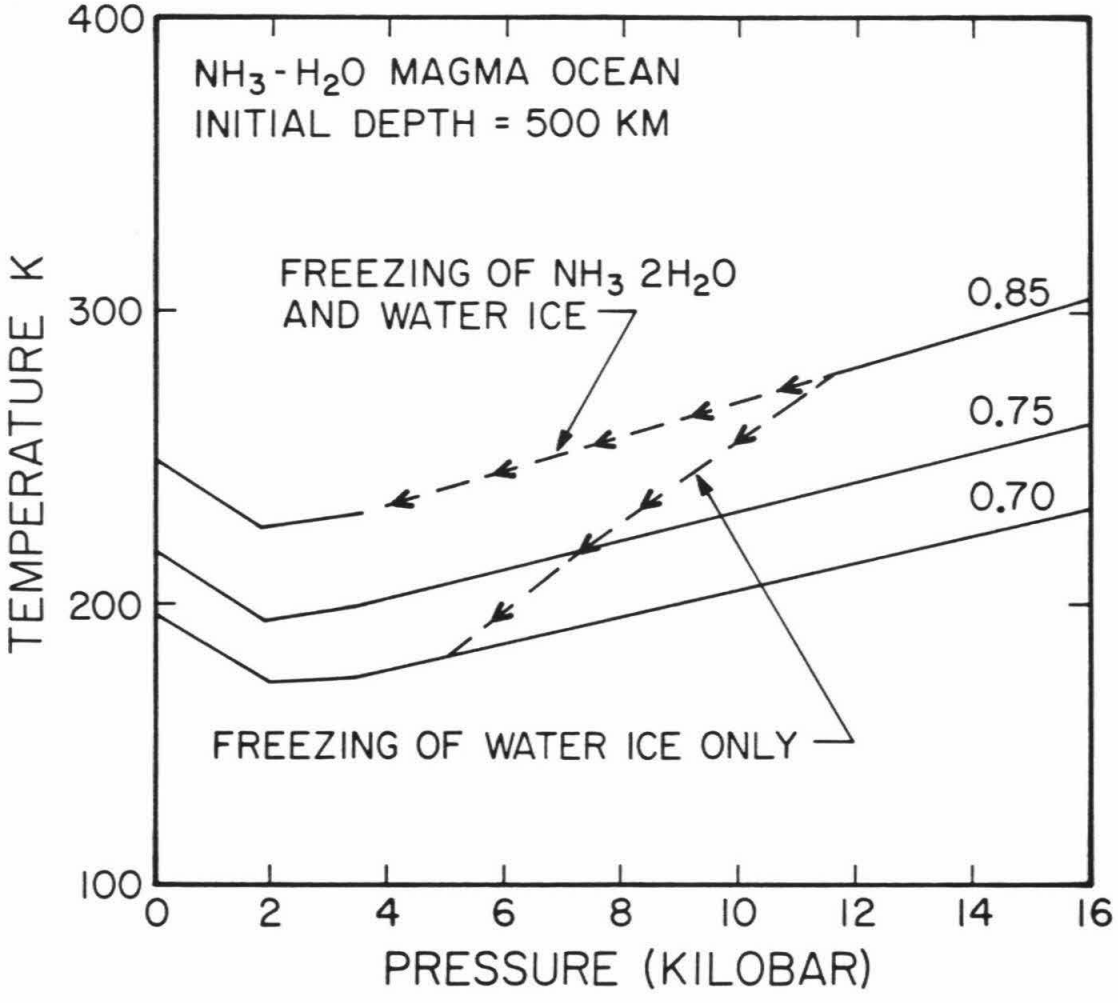
400
300
200
100
TEMPERATURE K
NH3 - H2O MAGMA OCEAN
INITIAL DEPTH = 500 KM
FREEZING OF NH3 2H2O
AND WATER ICE
0.85
0.75
0.70
FREEZING OF WATER ICE ONLY
0
2
4
6
8
10
12
14
16
PRESSURE (KILOBAR)

Points (2) and (3) are discussed as they arise below.

As temperatures at the base of the atmosphere decrease below 250 K, the possibility of clathrate hydrate formation, with atmospheric CH_4 and N_2 as the guest molecules and the ocean as the source of H_2O, must be examined. Only the base of the atmosphere forms clathrate, as the vapor pressure of H_2O in the atmosphere is much smaller than P_{CN} at temperatures of interest. The thermodynamics of clathrate hydrate is analyzed in Lunine and Stevenson (1984a); those results are used here without derivation. For clathrate formation to occur:

$$\frac{P_C}{P_C^{cl}(T_s)} + \frac{P_N}{P_N^{cl}(T_s)} \geq 1 \qquad (14)$$

where P_C, P_N are the partial pressures of CH_4 and N_2 at the surface, P_C^{cl} and P_N^{cl} are the pressures above the clathrate for pure CH_4 or N_2 at temperature T_s. Adequate approximations for P_C^{cl} and P_N^{cl} are:

$$P_C^{cl} = \frac{10^{-\frac{2873}{T_s} + 11.91}}{q^{5.75}}$$

$$T_s > T_F \qquad (15)$$

$$P_N^{cl} = \frac{10^{-\frac{2462}{T_s} + 11.20}}{q^{5.75}}$$

$$P_C^{cl} = 10^{-\frac{939}{T_S} + 4.83}$$

$$T_S < T_F \qquad (16)$$

$$P_N^{cl} = 10^{-\frac{680}{T_S} + 4.65}$$

where

$$q = a(X_A)\cdot(1 - X_A) \qquad (17)$$

and

$$T_F = 273 \; / \; (\; 1 - 0.385 \; \mathrm{Ln}(q) \;) \qquad (18)$$

Here T_F is the low pressure water ice freezing point, a function of X_A, and a is the activity coefficient of water in the NH_3-H_2O solution; $a \approx 1.32\text{-}2.67\ X_A$. Thermodynamic data used to calculate q, a, and T_F are from Haudenschild (1970) and Eisenberg and Kauzmann (1969, p. 95). Figure 6 illustrates the T-P path of the atmosphere superimposed on a phase diagram of CH_4-NH_3-H_2O from Lunine and Stevenson (1984a); we assume in the figure only CH_4 (and no N_2) for simplicity. Once the clathrate stability field is reached, P_C and P_N are determined by requiring equality in equation (14) and calculating the relative amounts of N_2 and CH_4 incorporated in clathrate:

$$P_{CN}(T_s) = \frac{P_N(T_s) - (f - X(T_s + \Delta T_s)) \cdot P_{CN}(T_s + \Delta T_s)}{1 - f} \quad (19)$$

where X and f are the CH_4 mole fraction relative to $N_2 + CH_4$ in the atmosphere and sequestered in clathrate, respectively. f is averaged between T_s and $T_s + \Delta T_s$ by iteration.

The program solves for the decrease in T_s with time using equation (4) written as a difference equation, with a variable time step adjusted by specifying the range of acceptable ΔT_s between time steps. At each step an amount of CH_4 and N_2 mass is removed to simulate escape; the rate of mass loss is input initially and decreases with time as $\dot{M}_o(\lambda/t)$ or $\dot{M}_o(\lambda/t)^{1/2}$ where λ is a time constant. The dependence of $\dot{M}$ on time is consistent with the model presented in section 2 for rapid escape driven by EUV radiation, and the inferred decrease in solar EUV output with time (Zahnle and Walker, 1982). Results are not sensitive to the power of t. NH_3 is assumed to be cold-trapped at T_e and, hence, does not participate in escape. Similarly N_2 mass can be augmented (simulating photochemistry or other N_2 production processes) at each step. P_C, P_N, T_e, X, and P_e are solved for using (6), (7), (8), (9), (5) or (10), with T_e iterated once so an average between time steps is used in (4). At ocean freezing $d\ell/dt$ becomes non-zero and (4) must be numerically solved by bisection since then $\ell = \ell(T_s)$ via (11) and (12). As the lower atmosphere enters the clathrate stability field P_C and P_N are determined by (13), (14), (15) or (16), (17), (18), and (19). Inputs are T_s, M_C, M_N, $\dot{M}$, λ, and $\dot{M}'_N$ the rate of production of N_2. Outputs as a function of time are T_s, P_{CN}, P_A, T_e, X, and f. Table I

gives values for thermodynamic and physical parameters fixed in the program.

Table I

Physical and Thermodynamic Parameters for Atmosphere Models

	CH_4	N_2	NH_3	Reference
$\text{Log}_{10} K_i$ (bars)	$-727/T_s + 7.01$	$-550/T_s + 6.75$		1
C_g (erg/gK)	2.5×10^7	1.0×10^7		2, 3
$\text{Log}_{10} P_A$ (bars)			$-1190/T_s$ 4.17	4
L_A (erg/g)			$2.6 \times 10^{10} - 3 \times 10^7 T_s$	5
$\gamma/(\gamma - 1)$	4.1	3.1	4.0	2, 3, 4

1. International Critical Tables (1928, III, pp. 256, 260).
2. Goodwin (1974).
3. Jacobsen and Stewart (1973).
4. Haar and Gallagher (1978) and ideal solution assumed.
5. Scatchard et al. (1947).

4. Model Results

Table II lists input parameters for selected model runs, grouped according to the initial N_2 and CH_4 masses. Sets I through III represent cooling of a low mass ($M_{CN} \sim 10^{23}$-10^{24} g) atmosphere; as discussed earlier, these models could represent terminal stages of evolution of a more massive primordial atmosphere. Model IV is a massive primordial atmosphere cooled by a highly energetic process. In all cases, starting surface temperature is chosen within a range allowed by plausible accretion models, ~400-500 K, for which $T_e > T_o$.

Model results are summarized in Table III, in terms of time for the atmosphere to reach phase 3 (clathrate formation), temperature at which phase 3 is reached, and the final N_2 and CH_4 masses in the atmosphere and in clathrate at ocean freeze-over. Figures 6 and 7 verify that the model atmospheres evolve in the manner described qualitatively in section 3. Figure 6 plots the temperature pressure path of a pure methane atmosphere (case IV) superimposed on the CH_4-NH_3-H_2O phase diagram constructed by Lunine and Stevenson (1984a). As the clathrate stability field is reached, the slow cooling evolution driven by escape is replaced by more rapid evolution because the large value of dP_s/dT_s along the clathrate stability boundary, compared to dP_s/dT_s for the adiabat, forces T_e to be $>T_o$ and, hence, T_s to decrease more rapidly. This unstable situation rapidly drives the atmosphere to low temperatures along the clathrate phase boundary if the ammonia-water liquid can

Table II

Input Parameters

Case	M_C[1]	M_N[2]	$\dot{M}$[3]	λ[4]	$\dot{M}'_N$[5]
I A	1×10^{24}	1×10^{21}	1×10^{14}	1×10^{9}	1×10^{13}
B	1×10^{24}	1×10^{21}	1×10^{14}	1×10^{9}	5×10^{13}
II A	3×10^{23}	3×10^{23}	1×10^{14}	1×10^{9}	1×10^{13}
B	3×10^{23}	3×10^{23}	1×10^{15}	1×10^{8}	1×10^{13}
C	3×10^{23}	3×10^{23}	1×10^{14}	1×10^{8}	1×10^{13}
D	1.5×10^{23}	1.5×10^{23}	1×10^{14}	1×10^{9}	1×10^{13}
III	1×10^{22}	2×10^{23}	1×10^{14}	1×10^{9}	1×10^{13}
IV	1×10^{25}	1×10^{21}	3×10^{16}	1×10^{9}	3×10^{13}

1. Starting CH_4 mass, g.

2. Starting N_2 mass, g.

3. Mass loss rate due to escape, g/year.

4. Time constant for loss, years.

5. Production rate of N_2, g/year.

Table III

Selected Output Parameters

Case	$\tau^{(1)}$	$T^{(2)}$	$M_N^{cl(3)}$	$M_C^{cl(3)}$	$M_N^{A(4)}$	$M_C^{A(4)}$
I A	4×10^9	248	4×10^{22}	7×10^{23}	5×10^{21}	3×10^{21}
B	(clathrate saturation never reached: T = 260 K at 4.5×10^9 years)					
II A	3×10^9	235	2×10^{23}	2×10^{23}	6×10^{22}	2×10^{21}
B	2×10^8	238	2×10^{23}	2×10^{23}	5×10^{22}	2×10^{21}
C	(clathrate saturation never reached: T = 249 K at 4.5×10^9 years)					
D	2×10^6	234	1×10^{23}	1×10^{23}	4×10^{22}	2×10^{21}
III	8×10^8	191	2×10^{22}	2×10^{21}	9×10^{22}	1×10^{21}
IV	3×10^8	246	---	7×10^{23}	---	4×10^{21}

1. Time in years from start of model to reach clathrate saturation at base of atmosphere.

2. Temperature (K) at time τ.

3. Masses in grams of N_2 and CH_4 sequestered in clathrate at 180 K.

4. Masses of N_2 and CH_4 in atmosphere at 180 K.

Figure 6. Illustrative temperature-pressure path (dots) of CH_4 atmosphere during cooling, superimposed on a portion of the H_2O-NH_3-CH_4 phase diagram from Lunine and Stevenson (1984a). Above the solid lines clathrate is stable; labeled lines delineate phase boundaries for ammonia-water solution concentrations $\gtrsim$20%, which is the ocean concentration at which the atmosphere crosses the clathrate stability field in this case. Assuming unlimited methane available, regions are: I. solid ammonia hydrate + clathrate + CH_4, II. solid ammonia hydrate + ice I + CH_4, III. ammonia-water solution + ice I + CH_4, IV. ammonia-water solution + CH_4, V. ammonia-water solution + clathrate + CH_4.

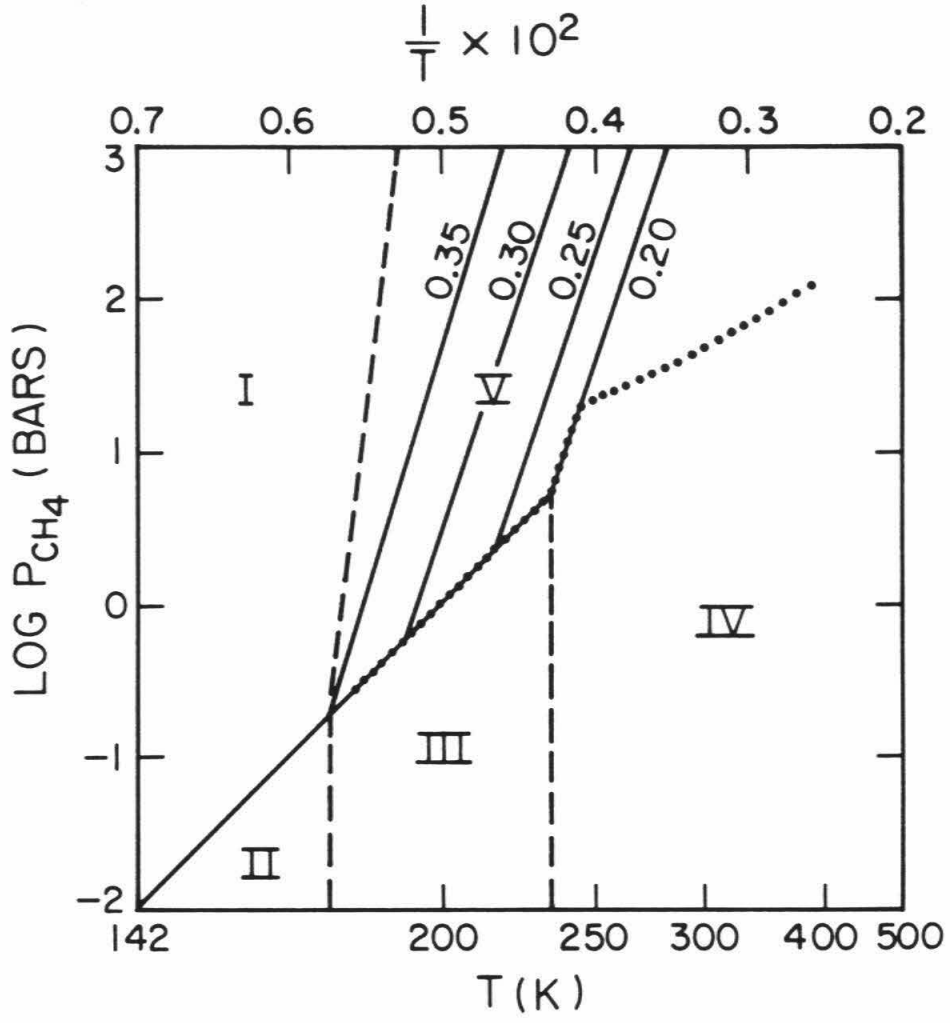
1/T × 10²
0.7
0.6
0.5
0.4
0.3
0.2
3
2
1
0
−1
−2
LOG P_CH4 (BARS)
0.35
0.30
0.25
0.20
I
II
III
IV
V
142
200
250
300
400
500
T(K)

remain in contact with the atmosphere, i.e., if the clathrate sinks in the ocean. Data on density of ammonia water solutions are given in International Critical Tables (1928, III, 59) and Hildenbrand and Giauque (1953); extrapolation to other temperatures and pressures is possible assuming ideal mixing and a constant thermal expansion coefficient. Clathrate density data are scarce and reviewed in Lunine and Stevenson (1984a). At clathrate formation in model set II, the clathrate is $\lesssim$4% less dense than the coexisting ocean liquid. As T decreases and the clathrate incorporates more N_2, the density difference shrinks. The ammonia water data are accurate to 2%, the clathrate data are less accurate. Hence, we consider below two end states of the coupled ocean atmosphere evolution: (1) clathrate sinks upon formation, and the atmospheric uptake into clathrate continues until the ocean freezes over at ~180 K; (2) clathrate floats upon formation, eventually producing an impermeable layer which isolates ocean from atmosphere. The results in the final four columns of Table III assume end state (1); the mass of the gas remaining in the atmosphere at freeze-over in end state (2) is given by adding M^A and M^{cl} in Table III. This is a maximum estimate since the buoyant clathrate layer will have some finite thickness, perhaps as much as a kilometer, and can sequester ~10^{22} grams of CH_4 and/or N_2. The temperature at freeze-over in case 2 is between 180 K and that given by column 2 of the table.

If the phase diagram (Figure B1, part 1 of thesis) based on the Johnson et al. (1984) data is employed, the ocean composition is 85% water at clathrate formation, and hence, the clathrate is likely to be

buoyant. Clathrate formation then occurs at 257 and 249 K for cases IV and IIA, respectively. The mass of atmospheric CH_4 and N_2 in the latter case at clathrate formation is ~3 x 10^{23} g each, similar to that in Table III. Implications of end states (1) and (2) for the subsequent evolution of Titan are discussed in section 5.

The clathrate formation drastically modifies the atmospheric composition, particularly if it sinks, since CH_4 incorporates in the clathrate structure to a much higher degree than N_2 (Lunine and Stevenson, 1984a). To illustrate the dependence of this effect on initial atmospheric composition, Figures 7a and b show atmospheric methane mole fraction X and total pressure P_{CN} as a function of decreasing temperature for starting X values of 0.9 and 0.3. Here it is arbitrarily assumed that the clathrate field is entered at 230 K. The atmosphere is driven to an N_2 rich state relative to the starting N_2 abundance. In addition to CH_4 and N_2, minor constituents such as noble gases were undoubtably present in Titan's primordial atmosphere (Owen, 1982; Lunine and Stevenson, 1984a), Figure 8 shows Ar/N_2 and Kr/Ar ratios in the atmosphere during clathrate formation and cooling from 230 to 180 K. Argon tends to partition in a manner similar to N_2 in the atmosphere and clathrate, while Kr (and Xe) incorporate primarily in clathrate along with CH_4. It is thus necessary to model explicitly the fate of noble gases during Titan's evolution, if measurement of their present day abundance pattern is to be used to infer primordial conditions.

Of interest then, in looking at the results in Table III, are the

Figure 7. Methane mole fraction in atmosphere X, in clathrate f and total pressure P as a function of temperature during clathrate formation. (a) Starting X = 0.9 at 230 K. (b) Starting X = 0.30 at 230 K.

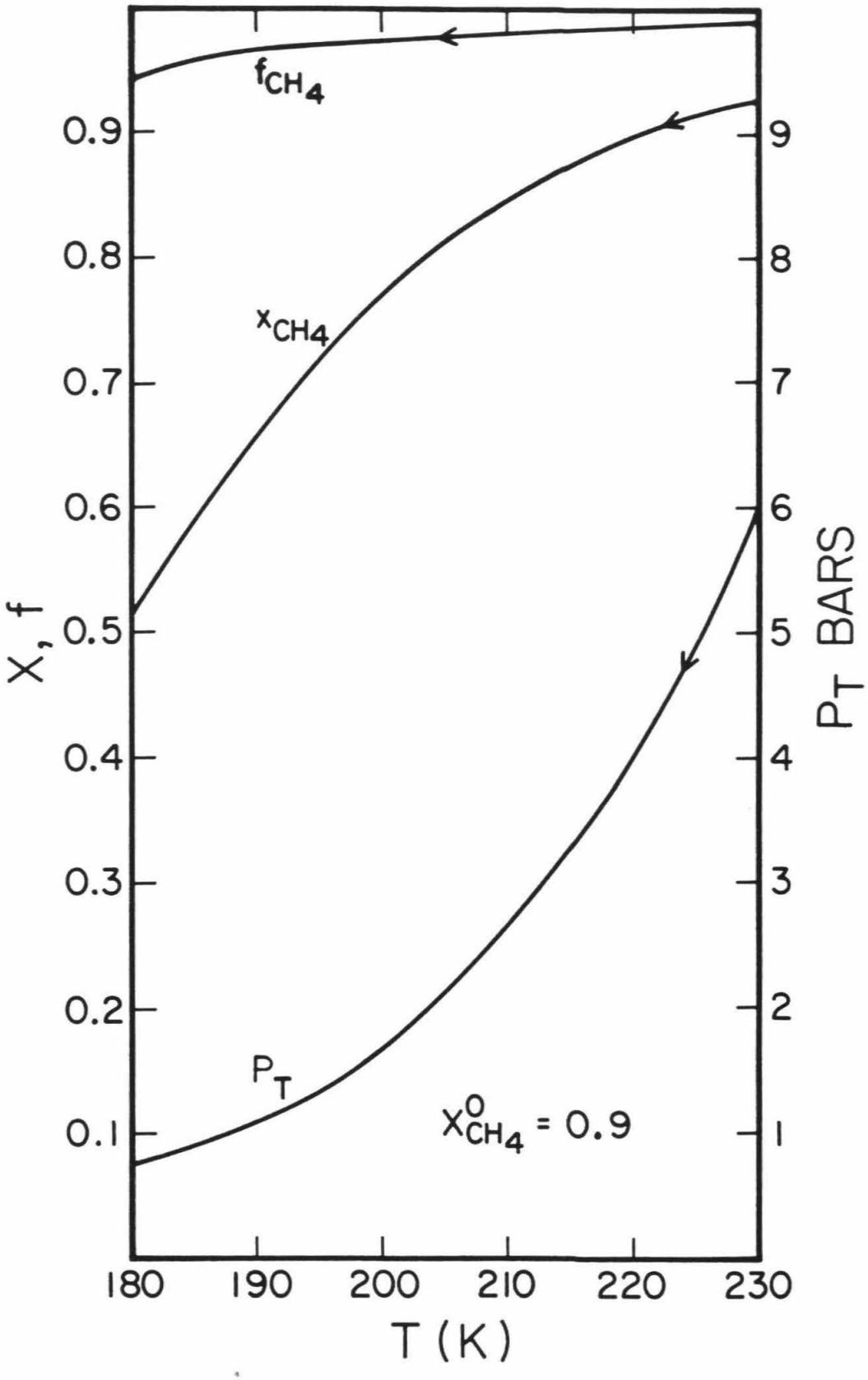
f_{CH_4}
x_{CH_4}
P_T
$X^0_{CH_4} = 0.9$
X, f
P_T BARS
T (K)
0.1
0.2
0.3
0.4
0.5
0.6
0.7
0.8
0.9
1
2
3
4
5
6
7
8
9
180
190
200
210
220
230

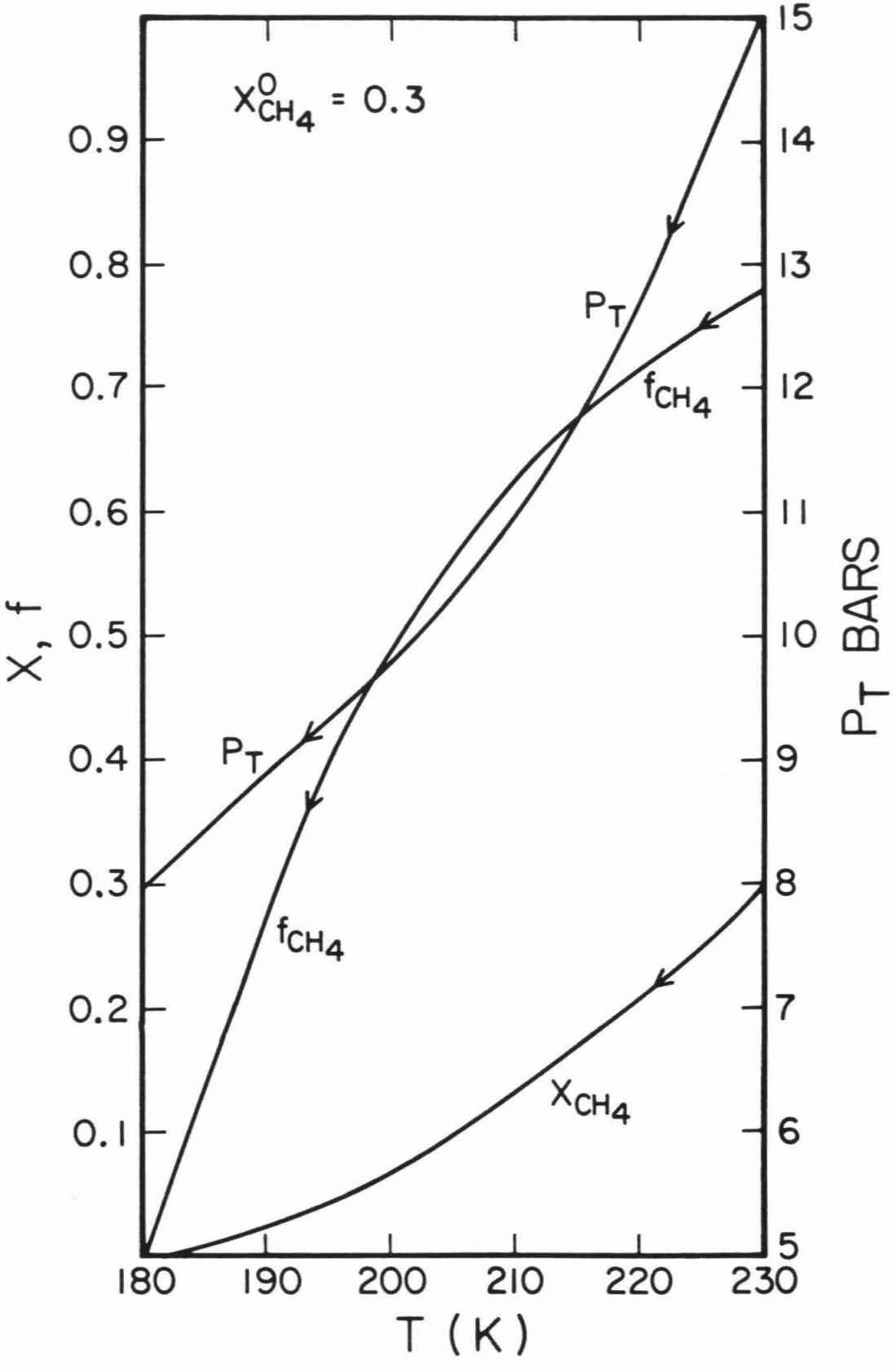
$X^0_{CH_4}$ = 0.3
P_T
f_{CH_4}
P_T
f_{CH_4}
X_{CH_4}
X, f
P_T BARS
T (K)
0.9
0.8
0.7
0.6
0.5
0.4
0.3
0.2
0.1
15
14
13
12
11
10
9
8
7
6
5
180
190
200
210
220
230

Figure 8. (a) Argon mole fraction f in clathrate (top) and atmosphere X (bottom) as a function of temperature during clathrate formation, for initial X of 0.01. (b) Same for Kr/Ar; initial ratio = 1.

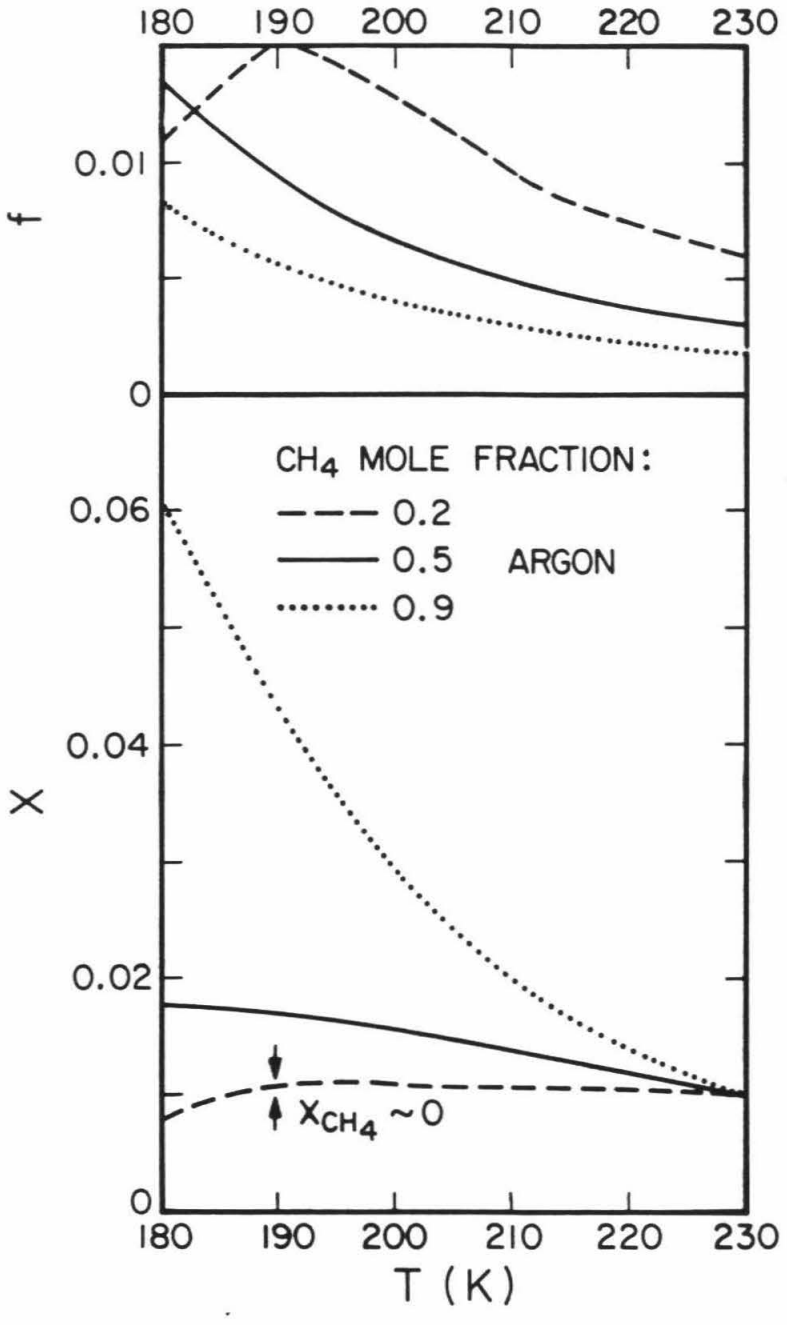
180
190
200
210
220
230
0.01
0
0.06
0.04
0.02
0
f
X
CH4 MOLE FRACTION:
0.2
0.5
0.9
ARGON
XCH4 ~ 0
T (K)

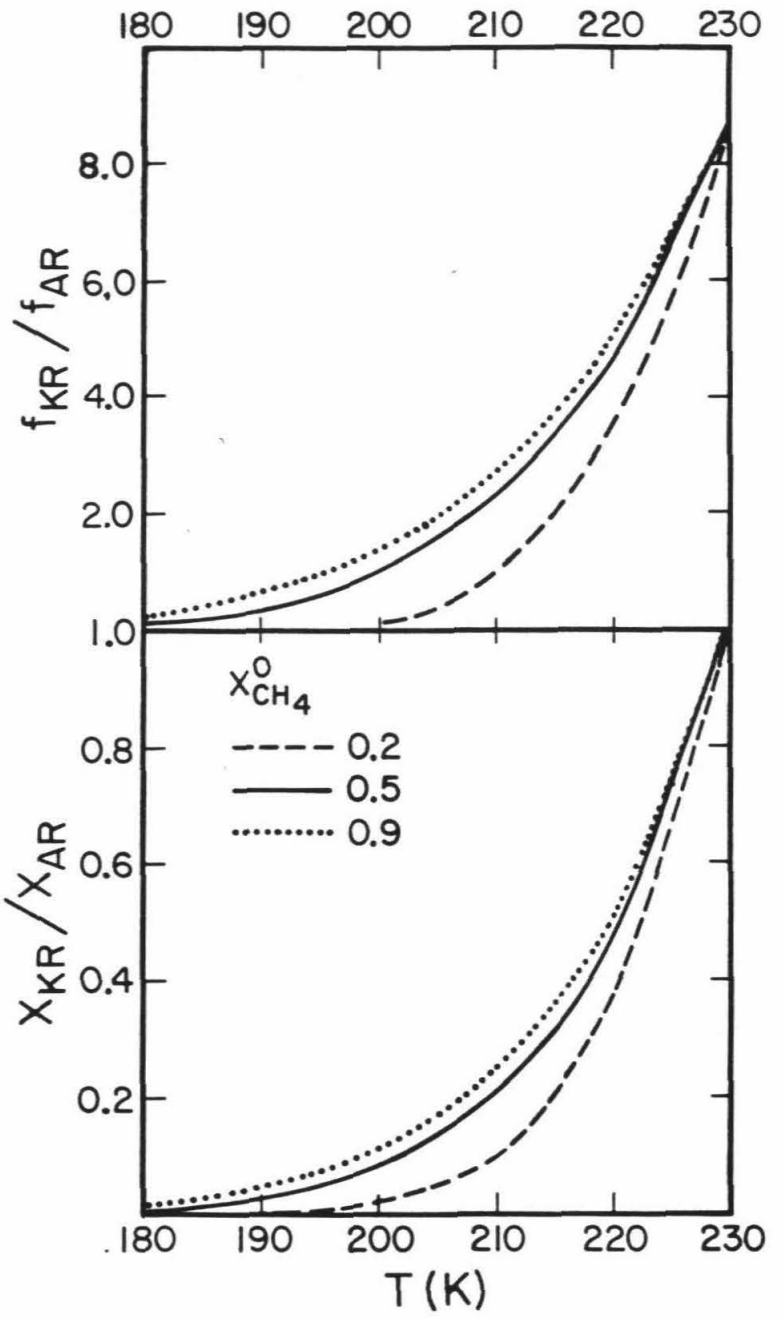
180
190
200
210
220
230
8.0
6.0
4.0
2.0
1.0
f_{KR}/f_{AR}
$X^0_{CH_4}$
0.2
0.5
0.9
0.8
0.6
0.4
0.2
X_{KR}/X_{AR}
T (K)

following issues: (1) What is the time scale for reaching the clathrate stability field (and, hence, ocean freeze-over)? and (2) how much N_2 and CH_4 are sequestered in clathrate versus that remaining in the atmosphere at freeze-over? Because the atmosphere cools adiabatically in response to decreasing mass, and the adiabats are very roughly comparable for N_2 and CH_4-rich cases, the surface total pressure as a function of temperature is fairly insensitive to starting conditions. The cooling time is primarily dependent on initial mass, escape rate, and N_2 production rate.

The models presented are illustrative of the interplay of composition, mass loss and N_2 production rate. A much wider range of starting conditions could be chosen, within the constraints of section II, but the selected cases illustrate the range of behavior exhibited by the model atmosphere. Case I begins with a methane rich composition, building N_2 slowly by photolysis. The rate of photolysis strongly influences the atmospheric evolution prior to clathrate formation: a low rate produces a methane rich atmosphere, while a rate higher by a factor of five causes the atmospheric mass to build up irreversibly, since the slowly decreasing escape rate cannot keep up with the N_2 production. Case II starts with a 50-50 mix of N_2 and CH_4, and the evolution is less sensitive to N_2 production rate. Models A and B illustrate the effect of changing the loss rate and decay constant proportionally; the results are identical except τ changes appropriately. Model C uses Model A parameters with the decay constant λ decreased by a factor of 10; now N_2 production rate overtakes loss at

~10^9 years and the atmospheric mass builds. Model IID is identical to IIA, but with half the starting mass. The mass is sufficiently low that the atmosphere relaxes to clathrate saturation before $T_e \rightarrow T_o$; hence, the atmospheric evolution is extremely rapid. We cannot constrain the initial mass sufficiently well to rule out Model D as too low in starting mass; based on gaseous accretion models, however, such a state would have been possible only if the bulk of the accreted methane had been removed with the nebula. Figure 9 plots results of Models IIA and IIC.

Case III is an N_2 rich model; because the CO and N_2 thermodynamic properties are similar it also simulates an N_2–CO rich case. This would correspond to the CO rich nebula discussed in section 2 (but with sufficient ammonia to allow a massive depressed-freezing point ocean). Note that the lack of CH_4 inhibits clathrate formation until ~190 K, and, hence, little gas is incorporated in clathrate. Finally case IV is a massive methane atmosphere driven by extremely rapid escape. The resulting composition at clathrate formation is similar to case IA, confirming the concept that the lower mass atmospheres may be thought of as the end product of high mass atmospheres driven initially by a very high escape rate.

Figure 9. (a) Total pressure P, methane mole fraction X and temperature T as a function of time in models II A and C. Clathrate formation stage is not shown on this plot. (b) Pressure and composition as a function of temperature during clathrate formation for model IIA.

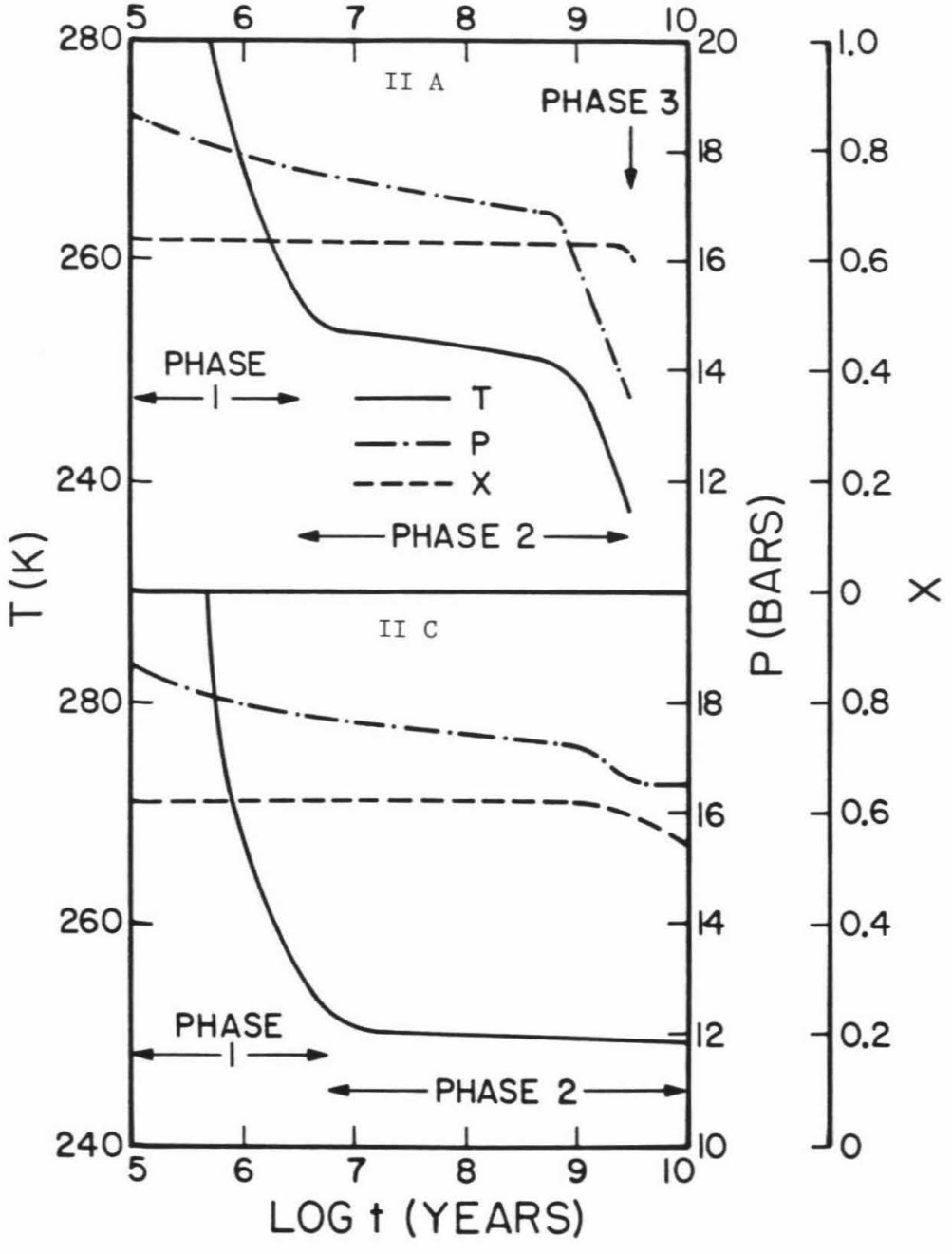
II A
PHASE 3
PHASE 1
PHASE 2
T
P
X
II C
PHASE 1
PHASE 2
T (K)
P (BARS)
X
LOG t (YEARS)
280
260
240
5
6
7
8
9
10
20
18
16
14
12
1.0
0.8
0.6
0.4
0.2
0

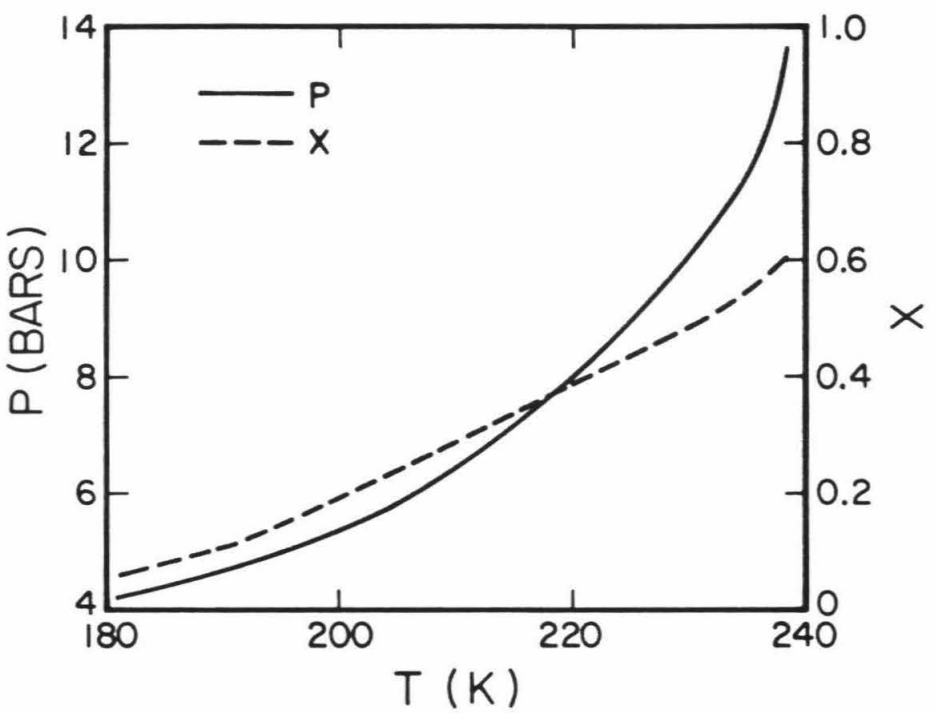
14
12
10
8
6
4
P (BARS)
P
X
1.0
0.8
0.6
0.4
0.2
0
X
180
200
220
240
T (K)

5. Analysis and Conclusions

The models described above illustrate the coupling between rapid escape of gas, N_2 production, and clathrate formation in a cooling atmosphere in contact with a massive ammonia-water ocean. What can such models say about evolution to the present state as we understand it? The most direct comparisons with the present-day atmosphere are the N_2 mass and total reservoir of CH_4 and CH_4-derived hydrocarbons in the atmosphere and surface. The present N_2 mass, augmented by 20% to account for HCN production and escape at current rates (Strobel and Shemansky, 1982; Yung et al., 1984) is 1.1×10^{22} g; if the N_2 is in equilibrium with dissolved N_2 in the ethane-methane ocean proposed by Lunine et al. (1983) it is $\sim 1.3 \times 10^{22}$ g. The total hydrocarbon budget is less certain; based on photochemical modeling (Hunten et al., 1984) it could be $\sim 6 \times 10^{22}$ g of CH_4 and CH_4-derived products.

If end state (1) of section 4 is assumed, then most of the CH_4 mass remaining at ocean freeze-over is locked up in clathrate, along with, for set II models of Tables II and III, a substantial amount of N_2, about 10 times the present abundance. The amount of N_2 in the atmosphere is comparable to the present abundance; the CH_4 atmospheric mass is insufficient to account for the present surficial reservoir. It is thus tempting to argue that subsequent outgassing of the interior released the CH_4 (and N_2) from clathrate to form the present atmosphere and surface volatile budget, especially since escape processes would

likely have continued after freeze-over, diminishing the remaining N_2 in the atmosphere. If the solid crust contained ammonia, photolysis of NH_3 to N_2 in the atmosphere could have continued until surface temperatures dropped below 150 K.

Alternatively, the formation of a buoyant clathrate layer during cooling would have stranded most of the N_2 and CH_4 in the atmosphere, which would continue to be depleted by escape. The present abundances would then be those remaining as energetic escape processes tailed off.

As yet we cannot distinguish between these options. The results do suggest the necessity of very energetic escape processes early in the history of Titan to remove large quantities of gas volatilized during accretion. EUV heating is unlikely to have persisted over 10^8-10^9 years at the intensity required to remove a massive primordial Titan atmosphere. Loss of gas by impact of solar orbiting debris is at least a promising mechanism and bears study. In particular, it can be a ''self-limiting'' loss mechanism in the sense that as the atmosphere thins, loss of gas (as opposed to loss of surface material) due to large impacts may become less efficient. Whether the impact efficiency for gas loss would have dropped off as the present N_2 and CH_4 mass was reached requires quantitative study.

In summary, accretion of a volatile-rich Titan produces a massive, hot atmosphere over an ammonia-water magma ocean. Simple models of the evolution of such an atmosphere suggest that highly energetic escape processes were required to cool the atmosphere toward its present state; impact induced loss of gas and/or shock heating con-

verting NH_3 to N_2 may have been important processes. Photolysis of NH_3 to N_2 would have been difficult due to high optical depth in the warmer regions of the atmosphere. Clathrate formation is important during later stages of cooling in the models since it drives the atmosphere toward an N_2-rich state; eventually a buoyant layer of clathrate may have separated the atmosphere from the magma ocean.

Further modeling of the evolution of Titan's surface and atmosphere require: (1) better data on densities of clathrate and ammonia-water solutions, (2) additional data on the ammonia-water phase diagram at high pressures, (3) quantitative modeling of impact-induced loss of gas and chemistry in the shock-heated regions. Mechanisms for outgassing of volatiles locked in clathrate also bear examination; the possible participation in later resurfacing events of volatiles originally trapped in the core of Titan should be considered. Finally, the coupled evolution of the atmosphere and proposed hydrocarbon ocean on the present satellite surface (Lunine et al., 1984) has been modeled (Lunine and Stevenson, 1984b); tying that evolution to the earlier evolution of the satellite is an intriguing future challenge.

References

Atreya, S.K., Donahue, T.M., and Kuhn, W.R. (1978). Science, **201**, 611-613.

Cameron, A.G.W. (1983). Icarus, **56**, 195-201.

Canuto, V.M., Levine, J.S., Augustsson, T.R., and Imhoff, C.L. (1982). Nature, **296**, 816-820.

Courtin, R. (1982). Icarus, **51**, 466-475.

Eisenberg, D. and Kauzmann, W. (1969). The Structure and Properties of Water. Oxford: University Press.

Fleagle, R.G. and Businger, J.A. (1980). An Introduction to Atmospheric Physics, New York: Academic Press.

Goodwin, R.D. (1974). NBS Technical Note 653. Washington: U.S. Government Printing Office.

Haar, L. and Gallagher, J.S. (1978). J. Phys. Chem. Ref. Data, **7**, 635-792.

Haudenschild, C. (1970). In JPL Space Programs Summary 37-64, **III**, 4-9.

Hofmeister, A.M. (1983). J. Geophys. Res., **88**, 4963-4983.

Horedt, G.P. (1978). Astron. Astrophys., **64**, 173-178.

Hunten, D.M. (1978). In The Saturn System, D.M. Hunten and D. Morrison, eds. (NASA CP 2068), p. 127-140.

Hunten, D.M. (1979). Icarus, **37**, 113-123.

Hunten, D.M. and Watson, A.J. (1982). Icarus, **51**, 665-667.

Hunten, D.M., Tomasko, M.G., Flasar, F.M., Samuelson, R.E., Strobel, D.F., and Stevenson, D.J. (1984). In Saturn, T. Gehrels, ed. (Tucson: University of Arizona Press), in press.

International Critical Tables (1928). Volume III. New York: McGraw-Hill.

Jacobsen, R.T. and Stewart, R.B. (1973). J. Phys. Chem. Ref. Data, **2**, 757-922.

Johnson, M.L., Schwake, A., and Nicol, M. (1984). In Proceedings NATO Workshop Ices in the Solar System (J. Klinger, ed.), submitted.

Lewis, J.S. and Prinn, R.G. (1980). Astrophys. J., **238**, 357-364.

Lewis, J.S. and Prinn, R.G. (1984). Planets and Their Atmospheres: Origin and Evolution. New York: Academic Press.

Lindal, G., Wood, G.E., Hotz, H.B., Sweetnam, D.N., Eshleman, V.R., and Tyler, G.L. (1983). Icarus, **53**, 348-363.

Lunine, J.I. and Stevenson, D.J. (1982). Icarus, **52**, 14-39.

Lunine, J.I. and Stevenson, D.J. (1984a). Submitted to Astrophys J.

Lunine, J.I. and Stevenson, D.J. (1984b). In Proc. NATO Conference Ices in the Solar System, (J. Klinger, ed.). Submitted.

Lunine, J.I., Stevenson, D.J., and Yung, Y.L. (1983). Science, **222**, 1229-1230.

Lynden-Bell, D. and Pringle, J.E. (1974). M.N.R.A.S., **168**, 603-637.

Mihalas, D. (1978). Stellar Atmospheres, San Francisco: W.H. Freeman and Company.

O'Keefe, J.D. and Ahrens, T.J. (1982). J. Geophys. Res., **87**, 6668-6680.

Owen, T. (1982). Planet. Space Sci., **30**, 833.

Pollack, J.B. and Consolmagno, G. (1984). In Saturn, T. Gehrels, ed. (Tucson: University of Arizona Press). In press.

Pollack, J.B. and Yung, Y.L. (1980). Ann. Rev. Earth Planet. Sci., **8**, 425-487.

Prinn, R.G. and Fegley, B. (1981). Astrophys. J., **249**, 308-317.

Samuelson, R.E., Maguire, W.C., Hanel, R.A., Kunde, V.G., Jennings, D.E., Yung, Y.L., and Aikin, A.C. (1983). J. Geophys. Res., **88**, 8709-8715.

Samuelson, R.E. (1983). Icarus, **53**, 364-387.

Scatchard, G., Epstein, L.F., Warburton, Jr., J., and Cody, P.J. (1947). J. Am. Soc. Ref. Eng., (May), 413.

Schubert, G., Stevenson, D.J., and Ellsworth, K. (1981). Icarus, **47**, 46-59.

Sekiya, M., Nakazawa, K., and Hayashi, C. (1980). Prog. Theoret. Phys., **64**, 1968-1985.

Shoemaker, E.M. and Wolfe, R.F. (1984). Lunar Planet. Sci. Conf. Abstract XV, 780-781.

Stevenson, D.J. (1982a). Lunar Planet. Sci. Conf. Abstract XIII, 770-772.

Stevenson, D.J., Harris, A.W., and Lunine, J.I. (1984). In Planetary Satellites (J. Burns and D. Morrison, eds.), Tucson, University of Arizona Press, in preparation.

Strobel, D.F. and Shemansky, D.E. (1982). J. Geophys. Res., **87**, 1361-1368.

Thompson, B.A., Harteck, P., and Reeves, Jr., R.R. (1963). J. Geophys. Res., **68**, 6431-6436.

Tsiklis, D.S., Linshits, L.R., and Goryunova, N.P. (1965). Russ. J. Phys. Chem., **39**, 1590-1592.

Walker, J.C.G. (1982). Precambrian Res., **17**, 147-171.

Walker, J.C.G., Klein, C., Schidlowski, M., Schopf, J.W., Stevenson, D.J., and Walter, M.R. (1983). In Earth's Earliest Biosphere: Its Origin and Evolution (J.W. Schopf, ed.). Princeton: University Press, 260-289.

Watson, A.J., Donahue, T.M., and Walker, J.C.G. (1981). Icarus, **48**, 150-166.

Yung, Y.L., Allen, M.A., and Pinto, J.P. (1984). Astrophys. J. Suppl. Ser., in press.

Zahnle, K.J. and Walker, J.C.G. (1982). Rev. Geophys. Space Phys., **20**, 280-292.